GOVERNMENT OF INDIA
MINISTRY OF EARTH SCIENCES
INDIA METEOROLOGICAL DEPARTMENT

IMD Met. Monograph :
MoES/IMD/Synoptic Met/01(2023)/28

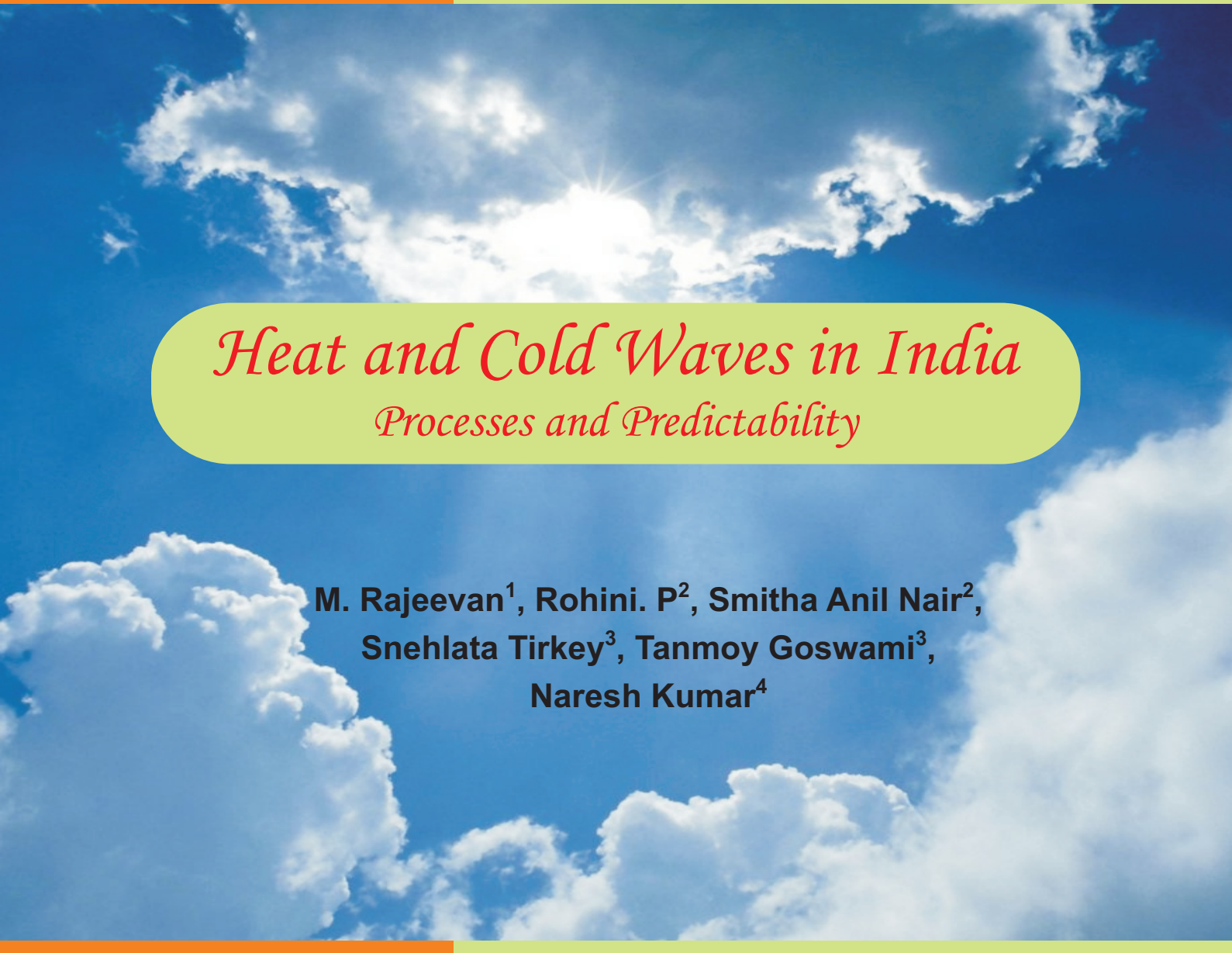

Heat and Cold Waves in India

Processes and Predictability

M. Rajeevan[1], Rohini. P[2], Smitha Anil Nair[2], Snehlata Tirkey[3], Tanmoy Goswami[3], Naresh Kumar[4]

April 2023

1. Ministry of Earth Sciences
2. India Meteorological Department, Pune
3. Indian Institute of Tropical Meteorology, Pune
4. India Meteorological Department, New Delhi

Government of India
Ministry of Earth Sciences
India Meteorological Department

Meteorological Monograph

Heat and Cold Waves in India

Processes and Predictability

M. Rajeevan[1], Rohini.P[2], Smitha Anil Nair[2],

Snehalata Tirkey[3], Tanmoy Goswami[3]

Naresh Kumar[4]

1. Ministry of Earth Sciences
2. India Meteorological Department, Pune
3. Indian Institute of Tropical Meteorology, Pune
4. India Meteorological Department, New Delhi

April 2023

Table of Contents

Foreword

Heat waves and cold waves are extreme weather events that can have significant impacts on human health, infrastructure and the environment. Heat waves occur when temperatures rise above average for an extended period of time, while cold waves occur when temperatures fall below average for an extended period of time.

Heat waves can lead to heat exhaustion, heat stroke and other heat-related illnesses, especially in vulnerable populations such as the elderly, young children and people with pre-existing health conditions. Heat waves can also worsen air pollution and cause power outages as the need for air conditioning increases. They can also negatively impact agriculture and ecosystems by damaging crops and causing droughts.

On the other hand, cold waves can lead to hypothermia and other cold-related illnesses, especially among people who are not properly dressed for the cold weather. Heat and cold waves can also lead to increased energy consumption as people rely on heating systems to keep warm, which can strain power grids and cause power outages.

As extreme weather events become more frequent and severe due to climate change, it is increasingly important to understand the impacts of heat and cold waves and develop strategies to mitigate their effects. These include improving infrastructure to withstand extreme temperatures, implementing heat warning systems and emergency plans.

In this meteorological monograph titled "Heat and Cold Waves in India: Processes and Predictability", the authors discuss the scientific basis, physical mechanisms and predictability of heat and cold waves. The impacts and adaptability issues are also briefly discussed. This monograph is thus an excellent reference book for students, researchers and policy makers to learn about heat and cold waves in India with up-to-date information and statistics.

I congratulate the authors for bringing out this useful monograph published by the India Meteorological Department (IMD), Ministry of Earth Sciences.

(M Ravichandran)

Acknowledgements

We are grateful to Dr M Ravichandran, Secretary, Ministry of Earth Sciences, Dr M. Mohapatra, DGM, IMD and Dr Gopal Iyengar for their support and encouragement to complete this monograph. MR also is grateful to the Director, NCESS, MoES for providing all support to complete this monograph. Prof R.R. Kelkar, former DGM, IMD and Dr Prashanth Pillai, IITM Pune provided very useful comments on the first draft of the monograph to improve its quality.

We also thank Dr J.V. Ratnam, JAMSTEC Japan and Dr Raju Mandal, IITM Pune for providing their original figures and images to include in the monograph.

Chapter-1

Introduction

Anthropogenic activities such as industry, construction, transport and deforestation have caused concentrations of greenhouse gases such as carbon dioxide, methane and nitrous oxide to increase over the last 150 years, even faster than since the Industrial Revolution. The increase in greenhouse gas concentration in the atmosphere has ultimately led to global warming with a trend of about 1.1°C over the period from 1880 to 2022. Annual surface temperatures over India have also recorded a similar increase over the period 1901-2022. In recent years, minimum (night time) temperatures have increased more than day time temperatures, suggesting the possible role of moisture and greenhouse gases.

An increase in the mean or coefficient of variation (CV) of temperatures increases the probability of extreme temperature events, as shown in Fig. 1.1. This can lead to an increase in the frequency of heat waves as well as cold waves. Extreme weather events have become increasingly common globally in recent decades (IPCC 2012; IPCC 2014). India is also feeling the effects of climate change as extreme weather events such as heavy rainfall, heat waves and intense tropical cyclones are occurring more frequently every year. The increasing frequency and intensity of these extreme events causes great damage to crops and rural economies.

Heat waves are anomalous episodes with extremely high surface air temperatures, lasting for several days with serious consequences. Similarly, cold waves are anomalous episodes of extremely low surface air temperatures lasting several days. There is no universal definition of a heat wave or a cold wave. Heat waves are usually defined as events in which certain temperature thresholds are exceeded for a minimum number of consecutive days.

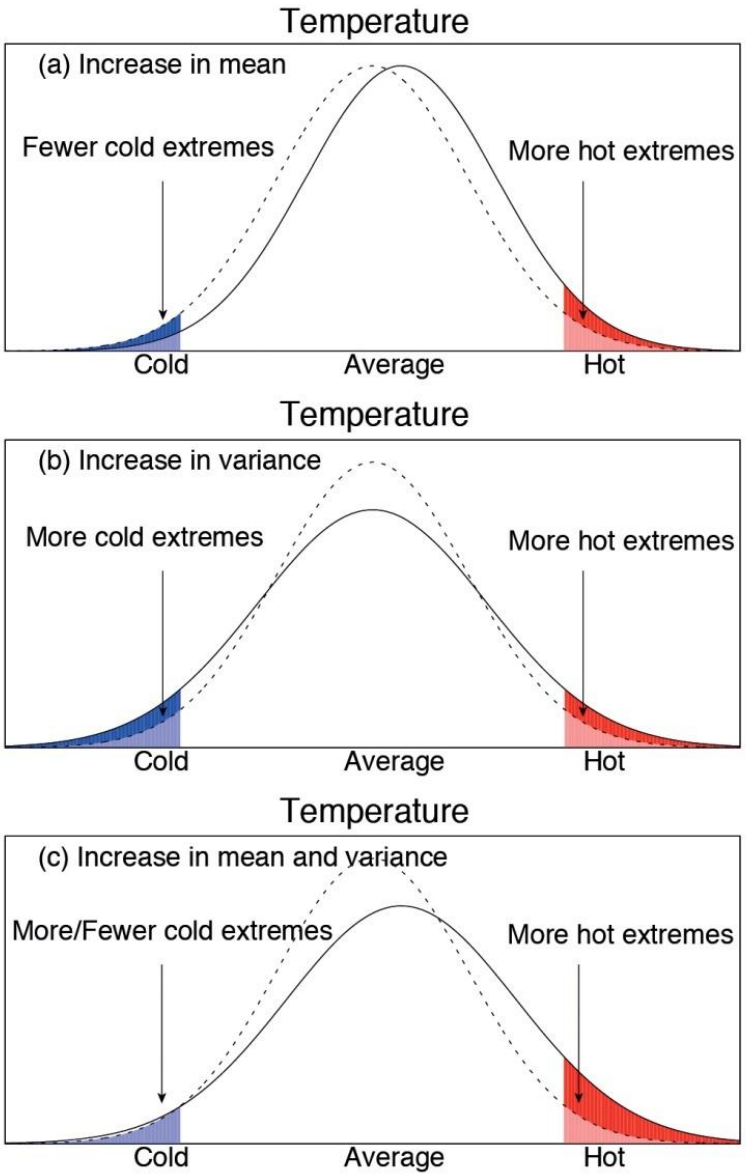

Fig. 1.1. Schematic representations of the probability density function of daily temperatures. Dashed lines represent a previous distribution and solid lines a changed distribution. The probability of occurrence, or frequency, of extremes, is denoted by the shaded areas. In the case of temperature, changes in the frequencies of extremes are affected by changes (a) in the mean, (b) in the variance or shape, and (c) in both the mean and the variance (Source: IPCC, 2014).

Heat waves are not uniform across the world and there is a lack of a common index to identify the heat extremes (Perkins et al. 2012). The thresholds used for defining heat wave are different for different regions. Thresholds may be absolute or statistical and the absolute thresholds depend on the region and its geography. World Meteorological Organization (WMO) defines heat wave as "when the daily maximum temperature exceeds the average maximum temperature by 5 °C for more than five consecutive days, the normal period being 1961-1990".

Heat waves are a major concern globally and regionally due to their catastrophic impact on society (Coumou and Rahmstorf 2012; Coumou et al. 2013; Cowan et al. 2014; Meehl and Tebaldi 2004; Perkins et al. 2012; Perkins 2015; Pai et al. 2013; Trenberth and Fasullo 2012; Rohini et al. 2016; Ratnam et al. 2016 a). The mortality rate due to heat waves is higher than any other natural hazard in different parts of the world (De et al. 2005). In 2003, an intense heat wave occurred over western Europe, causing about 70,000 deaths (Coumou and Rahmstorf 2012). On the other hand, the Russian heat wave in 2010 reportedly claimed 54,000 lives. The severe heat wave over the southeastern parts of India in May 2015 claimed the lives of more than 2500 people. This heat wave was triggered by the delayed onset of the southwest monsoon and persistent anomalous atmospheric conditions. The IPCC Fifth Assessment Report (IPCC 2014) states that the major climate risk for south Asian countries will be the rising mortality rate due to the impending heat waves. A moderate increase in average temperatures or a slight increase in the duration of heat waves will lead to a significant increase in the mortality rate in India.

Heat waves are considered silent killers because of their direct impact on human health (Patz et al. 2005; Hondula et al. 2014, Heo et al., 2019). Heat waves have immense impacts on human health, causing heat cramps, heat exhaustion, heat stress and heat stroke (Oldenborgh et al. 2018) and very severe heat waves even lead to death (Steffen et al. 2014). Children and the elderly are particularly affected, but also people

who already suffer from illnesses such as heart and respiratory diseases, kidney diseases and psychiatric disorders (Nitschke et al. 2007; Hansen et al. 2008; Wilker et al. 2012; Steffen et al. 2014).

Another serious impact of heat waves is on agriculture (both crop and livestock). Extreme periods of high temperatures can lead to a significant reduction in crop yields and cause reproductive failure in many crops (Chaudhuri et al. 2000; Attri and Rathore 2003; Chakraborty et al., 2019, Dash and Mamgain 2011; Siebert et al. 2014; Steffen et al. 2014). Extreme temperatures increase water stress in plants, which can lead to plant death due to the cessation of photosynthesis (Schlenker and Roberts 2009; Steffen et al. 2014). In animals, heat stress leads to reduced appetite, lower productivity, adverse effects on the immune system and sometimes death (Lefcourt and Adams 1996; Steffen et al. 2014). A decline in agricultural productivity leads to lower food production, which in turn leads to an increase in food prices. Chakraborty et al. (2019) examined the impact of heat waves on wheat crop production over India and found a negative impact. Their study revealed the wheat crop yield decreased by 4.9 %. 4.1 % and 3.5% over Punjab, Haryana and Uttar Pradesh respectively.

Heat waves also cause damage to infrastructure such as the transport system, electricity supply, railways, etc. Heat waves affect the economy through lower labour productivity during extreme temperature periods (Kjellstrom and McMichael 2013; Steffen et al. 2014), agricultural failure, damage to infrastructure, etc. All these catastrophic impacts highlight the need for more studies on heat waves, their impacts and their predictive capabilities.

In India, heat waves (HW) usually occur in the pre-monsoon months from March to June. There are two areas in India where heat waves are prevalent. One is central and northwestern India, called the heat wave zone, and the other is on the east coast of India (Andhra and Odisha). The frequency of heat waves is higher in the heat wave zone

than on the east coast of India. Different physical mechanisms are responsible for the heat waves in the heat wave zone and on the east coast of India.

In India, cold waves (CWs) usually occur during the period from November to March in association with the incursion of cold winds into north-western and central India when westerly disturbances (WDs) pass over the region (Bedekar et al. 1974). WDs are transient disturbances of mid-latitude westerly winds followed by the occurrence of cold waves, mostly over the areas north of 20^0 N and rarely in areas south of this latitude. There are many previous studies that have investigated various climatological features of CWs in India (Bedekar et al. 1974; Subbaramayya and Surya Rao, 1976; Chaudhury et al. 2000; De et al. 2005; Pai et al. 2004). Most of these studies have used threshold criteria based on minimum temperature anomalies to define CWs. Pai et al. (2004) studied the decadal changes in the various characteristics of CWs over India by using daily CW information over all meteorological sub-areas of India (the country was then divided into 35 meteorological sub-areas by the IMD) for the period 1971-2000 based on the minimum temperature deviation.

Bedekar et al. (1974) published the first India Meteorological Department (IMD) forecast manual on heat and cold waves, covering both climatological and forecasting aspects in detail. This publication is the first comprehensive documentation of the various aspects of heat and cold waves. Since then, many research papers have been published, especially in recent years when global warming has attracted the interest of researchers. However, a comprehensive compilation of the different aspects of heat and cold waves with updated information has not been produced. Since 1974, there has been tremendous progress in the understanding and predictive ability of heat and cold waves over India. The present monograph aims to compile and present the latest findings on various aspects of heat and cold waves over India. This monograph is intended as a reference book on heat and cold waves for researchers, students and forecasters.

In the next few paragraphs, a brief review of the recent studies on heat and cold waves in India is provided.

Most recent observational studies suggested an increasing trend in heat waves over India (Pai et al. 2013; Jaswal et al. 2015; Pai et al. 2017; Rohini et al. 2016). The recent study of Ratnam et al. (2016 a) identified the two prominent areas of heat waves over India which is maintained by two different physical processes. The trends of heat waves are significant both over the north western parts of India and southeastern coast of India (Ratnam et al. 2016 a; Rohini et al. 2016). Variability of heat waves over India is linked to El Nino/Southern Oscillation (ENSO) and the Indian Ocean SST anomalies (Ratnam et al. 2016 a; Rohini et al. 2016). These studies suggested that occurrence of heat waves over northwestern part of India is associated with anomalous persistent high along with depleted soil moisture and its variability is strongly influenced by tropical ocean SST anomalies. Frequency, duration and spatial extent of heat waves over India are found to be more in the succeeding year of El Nino (Pai et al. 2013; De and Mukhopadhyay 1998; Rohini et al. 2016).

In March and April 2022, large parts of South Asia including India and Pakistan experienced prolonged hot weather. The month of March was the hottest in India since 1901. Temperatures were consistently 3°C-8°C above average, breaking many records in several parts of the country (Zachariah et al., 2022). The states of Odisha, Madhya Pradesh, Gujarat, Chhattisgarh, Telangana and Jharkhand also experienced heatwaves. In Pakistan many individual weather stations recording monthly all-time highs in March. The heatwave conditions continued into April, reaching its preliminary peak towards the end of the month. Around 300 large forest fires occurred in the country on April 28, a third of these in Uttarakhand (Zachariah et al. 2022). In Pakistan, temperatures above 49°C were recorded in Jacobabad in Sindh. The 2022 heatwave is estimated to have led to at least 90 deaths across India and Pakistan, and to have triggered an extreme Glacial Lake Outburst Flood in northern Pakistan and

forest fires in India. The heat reduced India's wheat crop yields, causing the government to reverse an earlier plan to supplement the global wheat supply that has been impacted by the war in Ukraine (Zachariah et al. 2022).

Pai et al. (2004) studied the decadal variations of cold and heat waves using the data of 1971-2000. A significant increase was noticed in the frequency, persistency and spatial coverage of both of these high frequency temperature extreme events (heat and cold waves) during the decade (1991-2000). These changes might be the manifestation of regional impact of highest ever decadal scale global warming recorded during the period (1991-2000). A part of these changes might also be caused by local factors such as deforestation, urbanization etc. The Cold Wave (CW)/Severe cold wave (SCW) activity over north India showed increase from the decade of seventies to eighties and then to nineties. Pai et al. (2013) examined the occurrence of heat waves over India in detail using the data of 1961-2010. It was observed that many areas of the country (north, northwest, central and northeast peninsula) have experienced HW days of more than 8 days on an average per season. The severe heat waves were mainly experienced over north, northwest and central parts of the country. Significant long-term increasing trends in HW days was also observed over India during the analysis period. In general, the frequency, persistency and area coverage of the HW/SHW days were found to be more than average during the years succeeding El Nino (El Nino +1) years.

Recently, Pai et al. (2017), have summarized the results related to heat and cold waves over India. During the hot weather season (AMJ), stations from the north, north-west, central, east India and north-east Peninsula (together called Core Heat wave Zone) are most prone for HW/SHW days with relatively highest frequency experienced during May. During the cold weather season (DJF), stations from CCZ that is nearly same as CHZ but includes Jammu and Kashmir and excludes coastal Andhra Pradesh are most prone for CW/SCW days with the highest frequency during January.

Satyanarayana and Bhaskara Rao (2020) studied the phenology of heat waves over India using the data from 1951-2015. Their study revealed three localized regions of heat wave vulnerability in the north, northeast and southeast parts of India, which are different from the three maximum temperature zones. Dodla et al. (2017) analyzed the 2015 catastrophic heat wave over the east coast of India, which claimed about 2500 lives. Analyses revealed that isolated region of Andhra Pradesh (AP) had experienced severe heat wave conditions during May 23–27, 2015, with temperatures above 42°C and the sudden escalation by 7–10°C within a short span of 2–3 days. Short-range weather predictions with Advanced Research Weather Research and Forecasting model at 3-km resolution, up to 72-h lead time, have been found accurate with statistical metrics of small mean absolute error and root-mean-square error and high index of agreement confirming the predictability of the heat wave evolution.

Kishore et al (2022) studied the human influence on the changing patterns of heat waves in India using the Heat Wave Magnitude Index daily (HWMId). Their study found that anthropogenic factors have increased the probability of occurrence of severe heat waves in central and central-southern India by two times during the twentieth century. The risk of heatwaves is projected to increase tenfold in the 21st century. More than 70% of the land area in India is expected to be affected by heat waves with a magnitude of more than 9. Mazdiyasni et al. (2017) suggested that future climate warming will lead to a significant increase in heat-related mortality, especially in lower-latitude developing countries like India, where heat waves will be more frequent and the population is particularly vulnerable to these extreme temperatures. The study also shows that even a moderate increase in average temperatures can lead to a sharp rise in heat-related mortality and supports the efforts of governments and international organizations.

The study by Murari et al. (2015) using CMIP data suggests that heat waves are projected to be more intense, have longer durations and occur at a higher frequency

and earlier in the year. Southern India, currently not influenced by heat waves is expected to be severely affected by the end of the 21st century. Projections indicate that a sizable part of India will experience heat stress conditions in the future.

Vittal et al. (2020) examined the role of Atlantic Ocean SST anomalies on Indian heat waves. They used observations and climate model experiments to show that Indian heat waves during the period 1961-2010 period were only weakly driven by Indian Ocean SST, but were instead strongly tied to SST in the Atlantic Ocean. The conditions in the Atlantic that drove those heat waves were exacerbated by greenhouse emissions rather than natural forcing.

Pai and Smitha (2022) examined the impact of extreme phases (El Nino and La Nina) of El Nino-Southern Oscillation (ENSO) on the frequency, duration, magnitude and spatial coverage of heat waves (HWs). It was observed that there is an appreciable increase (decrease) in the number of HW days during El Nino (La Nina) events. Severe Heat waves were more prominent (longest and hottest) in El Nino years. Exactly opposite association was observed in case of CW days. El Nino event mostly inhibits cold wave activities over India. Nageswara Rao et al. (2020) examined the heat waves occurring over the east coast of India (Odisha, Andhra Pradesh and Telangana). The study revealed the continued increase in maximum temperature and its variability as the hot weather season progresses. In the recent period, a notable increase in the weekly Tmax and its variability has been observed.

Earlier studies (Bedekar et al. 1974) showed that cold waves occur mostly due to the intrusion of cold air from northern latitudes into the northwestern parts of India. The cold wave conditions over the northern parts of India are often associated with the passage of western disturbances, which manifest as an eastward moving well marked troughs in the upper tropospheric westerlies north of 20°N and often seen extending to the lower troposphere, transport cold air from northern latitudes into India. There are also few instances of occurrence of cold waves due to a low-pressure system over the

North Arabian Sea. In these cases, the easterlies to the north of the low-pressure system transport cold air from higher latitudes.

Jaswal et al (2017) studied increased trends in temperature and moisture induced heat index and its effect on human health in climate change scenario over the Indian sub-continent. Using dry bulb temperature and relative humidity records from 283 surface meteorological stations over India, they analyzed the heat index (HI) during summer and monsoon seasons. Averaged over the country, HI is increasing during summer and monsoon seasons at the rate of $+0.56^0$ C/decade and $+0.32^0$ C/decade respectively, which is statistically significant at 95% level. The increasing HI indicates high level of discomfort in both the seasons which is primarily due to increase in humidity in summer season and maximum temperature in monsoon season. Spatial distribution of HI indicates greater chances of heat related illness in India, more prominently in the southeast coastal regions (Andhra Pradesh, Orissa and Tamil Nadu) in summer and over northwest India (Rajasthan and Indo-Gangetic plains) in monsoon season.

Srivastava et al (2022) conducted a heat weather hazard analysis over India, attempting to quantify the impact of different meteorological parameters on heat waves in different regions of India for different summer months (March, April, May and June). The impact of different meteorological parameters is determined for different months and regions of the country. The cumulative values are calculated for different regions considering different meteorological parameters to make an initial analysis of the heat wave and zonation for the entire country.

Narkhede et al (2022) developed an empirical model-based framework for operational monitoring and forecasting of heat waves based on temperature data. In this study, they proposed an operationally applicable empirical model that uses a set of indices to monitor and forecast heat waves on the short-term time scale. The model consists of two main components: a) index-based monitoring over a spatial domain and

b) temporal prediction over different locations. Three heat wave indices are calculated, the heat stress index, the heat stress index and the heat stress factor. They have also considered the effects of meteorological parameters such as wind and humidity on the intensity and duration of heat waves. For the prediction component, they have used a simple machine learning based method for predicting the overheating factor index. The study shows that the heat wave indices can be predicted with this simple model up to a lead time of 2-3 days for most regions of India.

Sharma and Mujumdar (2017) studied the impacts of concurrent droughts and heat waves that could have more serious impacts. Meteorological drought condition, which is characterized by low rainfall can be amplified with simultaneous occurrence of heat waves. The study found significant changes in concurrent meteorological droughts and heat waves. There is substantial increase in the frequency of concurrent meteorological droughts and heat waves across whole India. Statistically significant trends in the spatial extent of droughts are observed in Central northeast India and west central India. However, the spatial extend affected by concurrent droughts and heatwaves is increasing across whole India.

Dubey et al. (2021) addressed the hot weather dynamics and variability. The seasonal composites for extreme temperature years show that hot season over North India (NI) occurs mainly due to blocking high in upper atmospheres. Similarly, daily temperature anomalies for the heatwave days during hot years exhibit stationarity of such blocks centered over the region. Two global teleconnections have been found to be responsible for the NI seasonal anomaly, (i) a continuous anomalous low over Europe cause anomalous high across the region, (ii) the subtropical jet stream and the polar jet stream help to maintain stationarity of anticyclonic blocks over the region. Sinking of air due to an upper atmospheric high over NI causes adiabatic warming near the surface.

The cold waves are known to increase mortality rate owing to the socio-economic conditions of people of the northern parts of India. For example, the cold wave that

occurred in January 2003 resulted in death of about 900 people. During 1978–1999, a total number of 3264 deaths were reported due to cold waves in the northern parts of India (Ratnam et al. 2016 b). The cold waves also affect Rabi crops, crops that are sown in winter and harvested in the following spring, of the northern regions of India. A survey on the impact of cold wave on the Rabi crops showed that the economic losses were to the tune of 6230 million Indian rupees in the state of Rajasthan during 2005–2006 Rabi season alone.

Raghavan (1967) used 51 years of data (1911-1961) to prepare a detailed climatology of cold waves and severe cold waves over India and Pakistan. The study revealed that Jammu and Kashmir experiences maximum cold waves in a season. Subramayya and Surya Rao (1976) used 150 IMD stations for the period 1954-56 to examine heat and cold wave occurrence over India. They have found that for the country as whole, maximum heat wave and severe heat wave occur in the month of May. Maximum severe cold waves occur in the month of January.

In this monograph, the definitions of heat and cold waves are discussed in Chapter-2. In the chapter-3, long term climatology of cold waves and observed long term trends are discussed. For this purpose, a long- term, quality-controlled daily gridded temperature data set has been used. In the chapter-4, long term climatology of heat waves and observed long term trends are discussed. In the chapter-5, the physical mechanisms of heat waves and in the Chapter-6, physical mechanisms of cold waves are discussed in terms of large-scale dynamics and local factors. In the Chapter-7, the forecasting aspects (in all time scales, short range to seasonal) are discussed in terms of synoptic setting for such heat and cold waves. Skill of short to medium range forecasts, extended range forecasts and seasonal forecasts are also discussed using weather prediction models of Ministry of Earth Sciences (MoES)/ IMD as well as other TIGGE weather prediction models. In the last chapter-8, the main aspects of heat and cold waves are summarized and impacts and adaptation to heat waves are briefly discussed.

Chapter -2

Cold and Heat Wave Indices and Methodology

There are no universal definition of heat and cold waves. Heat and Cold wave events are anomalous situations with above (below) normal temperatures respectively. The criteria used to define how much above/below normal could differ. India Meteorological Department (IMD) uses criteria for heat and cold waves using station temperature data. Definitions of heat and cold waves based on area average or gridded temperature data are however different but very similar.

Heat waves have wide range of impacts on different sectors. Because of this, the definition of heat waves will be different for different applications. Some studies (Alexander et al. 2006, 2007; Fischer and Schar 2010; Fischer et al. 2011; Avila et al. 2012; Jiang et al. 2012; Perkin and Alexander 2013) used ETCCDI indices for heat wave analysis and these indices are not good enough to heat stress related studies. The indices like Predicted Mean Vote (PMV) and the Physiological Equivalent Temperature (PET) are used for the health related studies (Matzarakis et al. 1999; McGregor et al. 2002; Pantavou et al. 2008). Another index named Heat Index (HI) also known as apparent temperature (Steadman 1979, Steadman 1984) used for heat stress related studies in many regions (Zahid and Rasul 2009; Rajib et al. 2011; Rakib 2013; Opitz-Stapleton et al. 2016; Jaswal et al. 2017) as it combines air temperature and relative humidity.

There are some similarities across these heat wave matrices, all definitions include at least one form of temperature (maximum, minimum or average temperature) (Perkin 2015). A recent study (Perkin et al. 2012) compared the various heat wave characteristics obtained from 3 different indices (90th percentile for maximum temperature, the 90th percentile for minimum temperature, and positive extreme heat factor (EHF)) and it indicates that qualitative measurements across the indices are

similar but the quantitative values are different. This implies the importance of selecting an appropriate index for the impacted region.

People residing in a place for sufficiently long time get more or less acclimatized to the normal weather conditions of that place. Human body is quite sensitive to any physiological change which takes place due to significant departure of weather conditions from normal. These definitions are designed to take the physiological changes also into account.

2.1 **Heat wave Indices.**

India Meteorological Department (IMD) considers only maximum temperatures (Tmax) for defining heat waves. They define heat wave as " if the maximum temperature of a station reaches at least 40°C or more for Plains, 37°C or more for coastal station and at least 30°C or more for Hilly region ". The detailed IMD criteria of heat waves are given below (Table 2.1).

Table 2.1

Criteria used for declaring Heat Wave by India Meteorological Department (IMD)

Nomenclature	Departure from Normal Temperature
Criteria for Heat Wave/Severe Heat Wave	
a) When normal maximum temperature of station is 40^{o}C or less	
Normal	-1^{0} C to 1^{o} C
Above normal	2^{0}C
Appreciably Above Normal	3^{o} C to 4^{o} C
Markedly above normal/Moderate Heat Wave	5^{0} C to 6^{o} C
Severe Heat Wave	7^{o} C or above
b) When normal maximum temperature of station is more than 40^{o}C (The term moderate heat wave will not be used)	

Normal	-1^0 C to 1^o C
Above normal	2^0C
Heat Wave	3^o C to 4^o C
Severe Heat Wave	More than 5^0 C
c) When normal maximum temperature of station is 45^0C or more for two days or more	
The condition may be declared as Heat Wave	

To declare a heat wave, the above criteria should be met at least in 2 stations in the meteorological sub-division for at least two consecutive days.

For defining heat waves, there are more indices used in scientific literature, especially with area averaged or gridded data. The first one is the **90th percentile threshold of maximum temperature (Tmax90)** based on a 5-day window (Rohini et al. 2016).

The second index considered is the **Excessive Heat Factor (EHF)** (Nairn and Fawcett 2013; Perkins and Alexander 2013, Rohini et al. 2016). This index is based on two excessive heat indices, namely Excess Heat (EHI_{sig}) and Heat Stress (EHIaccl). The unit of EHF is $^oC^2$.

The Excess heat represents unusually high heat arising from a daytime temperature that is not sufficiently discharged overnight due to unusually high overnight temperatures. The Daily Mean Temperature (DMT) averaged over a three-day period is compared against a climate reference value to characterize this index. The unit of EHI_{sig} is ^{o}C.

The Excess Heat Index is calculated as

$$EHI_{\text{sig}} = \frac{(\text{T}_\text{i} + \text{T}_{\text{i}-1} + \text{T}_{\text{i}-2})}{3} - \text{T}_{95}$$

where T_{95} is the 95^{th} percentile of DMT (T_i) for the climate reference period of 1961-

1990. The daily mean temperature is the average of maximum and minimum temperatures as defined by

$$T = \frac{(T_{max} + T_{min})}{2}$$

The heat stress which arises from a period where the temperature is warmer, on average than the recent past. Maximum and subsequent minimum temperatures averaged over a three-day period and the previous 30 days are compared to characterize the heat stress. This is expressed as a short term (acclimatization) temperature anomaly. The unit of EHIaccl is ^{o}C. The heat stress is defined as

$$EHI_{accl} = \frac{(T_i + T_{i-1} + T_{i-2})}{3} - \frac{(T_{i-3} + \ldots + T_{i-32})}{30}$$

where Ti is the DMT on ith day.

The Excess Heat Factor (EHF) is defined as follows:

$$EHF = EHF_{sig} \times \max(1, EHI_{accl})$$

A heat wave is considered when the value of EHF is positive, and the daily climatological Tmax is greater than 35°C for consecutive three days or more. These criteria were selected carefully to choose the heat wave events occurring over the Indian sub-continent. The 35 °C criterion was used to restrict such events occurring over the hilly regions.

The significant associations between high temperature and mortality and morbidity have been studied in many parts of the world (Heo et al. 2019). Therefore, understanding associations between heat waves and various health outcomes is essential to prevent the current and future burden of heat impacts on human health. In many countries, the Heat-Health Warning Systems (HHWS) adopted thermal comfort indices, which quantify a combined effect of a series of meteorological factors (air temperature, humidity and wind) on perceived temperature, to represent the actual human thermal situation during heat waves. The effectiveness of a HHWS using a

thermal index (including ambient temperature) depends on how properly the heat wave definition can relate heat wave periods and related health problems, and choice of which thermal index to use is a critical public health issue for policy (Heo et al. 2019).

There are such indices to define and monitor heat waves in the context of its health impacts. Some of such indices are Heat Index (HI) and Wet Bulb Global Temperature (WBGT) (Heo et al. 2019). HI attempts to represent the human perceived temperatures by the impact of humidity. HI is an index that combines air temperature and relative humidity to determine a human-perceived apparent temperature to determine how hot it actually feels. It is a measure of the stress placed on humans by elevated levels of atmospheric temperature and moisture. It implies that an extended period of unusually high heat stress may have adverse health consequences for the affected population. The computation of HI is based upon the formula given by Steadman (1979) where the author has quantified the physiological effects of high heat and humidity on human being. The variables used in the formula include heat generation and loss, fabric resistance, vapour pressure, wind speed, solar radiation, terrestrial radiation, proportion of body clothed and other factors (Steadman, 1984). The Steadman's equation was further modified by Rothfusz (1990) by performing multiple regression analysis on the data from Steadman's table. Jaswal et al. (2017) used this index to study long term trends using IMD station data. More details of the index are available in Jaswal et al. (2017).

The equation used by the National Weather Service of the National Oceanographic and Atmospheric Administration (NOAA) is given below.

$$\mathbf{HI = -42.379 + 2.04901523*T + 10.14333127*R - 0.22475541*T*R - 6.83783x10^{-3}*T^2 - 5.481717x10^{-2}*R^2 + 1.22874 x 10^{-3}*T^2*R + 8.5282x10^{-4}*T*R^2 - 1.99x10^{-6}*T^2*R^2}$$

where, T= Ambient dry bulb temperature (^{0}F) and

R= Relative Humidity (Integer percentage).

Wet-bulb globe temperature (WBGT) is one of the most commonly used indices by many organizations since the 1960s. This index was originally invented in the 1950s in efforts to lower the risk of heat disorders during the training of the US Army and Marine troops. Since that time, WBGT has been applied in other settings, and is widely used for the evaluation of occupational heat stress exposure (Budd 2008; Alfano et al., 2014). WBGT is a weighted average of dry bulb (air) temperature, natural wet-bulb temperature and black globe temperature. Black globe temperature is a function of radiant heat, temperature, and wind while natural wet blub temperature measures the amount of cooling by humidity and wind (Budd, 2008). By incorporating black globe temperature, WBGT considers radiation effect whereas many other simplified thermal comfort indices do not. In sunny conditions, the weighting coefficients are 0.7, 0.2, and 0.1 for natural wet temperature, globe temperature, and dry-bulb temperature, respectively. At other times, the weighting coefficients are 0.7 and 0.3 for natural wet temperature and dry-bulb temperature, respectively, while the globe temperature is not considered in the calculation. Until recently, several approximation formulas of WBGT using readily available meteorological data (e.g., temperature, humidity, wind, and radiation) have been suggested for practical use as the original components for calculating WBGT are not standard meteorological monitoring data. Further details of WBGT are available in Heo et al. (2019).

The health risk assessment is subject to the designated heat wave periods, and more extreme heat wave definitions with the higher thresholds generally identify fewer heat waves of shorter duration and higher intensity. Thus, the definitions with higher thresholds, which reflect the most intense heat waves but also lead to the shortest heat wave periods and fewer designated heat waves, may not necessarily result in the strongest or the most significant health effect estimate.

Effectiveness of a HHWS to prevent health risks from heat exposure is subject to the precision of weather forecast. Temperature tends to be more accurately forecast

than other weather components, which may hinder the use of thermal indices that use other weather components for heat wave warnings. Currently, historical forecast data are available through an open data source for everywhere for components including temperature, humidity and wind speed.

Russo et al. (2014) introduced another index for heat wave activity, namely the Heat Wave Magnitude Index (HWMI). The computation of HWMI involves multiple stages that begin with the computation of daily threshold (90^{th} percentile) with reference to the baseline period (Das and Umamahesh, 2022). Next, the selection of heat wave events is carried out according to the minimum three consecutive days Tmax above the threshold. The selected heat wave is then grouped into sub-heat waves, where each sub-heat wave is a heat wave of three consecutive days. More details of this index are available in Russo et al. (2014).

2.2 **Cold Wave Indices**

Based on station temperature data, India Meteorological Department (IMD) uses the following definition of cold waves over India, as shown in Table-2.2

Table 2.2

Criteria for Cold Wave/Severe Cold Wave

Nomenclature	Departure from Normal Temperature
Criteria for Cold Wave/Severe Cold Wave	
a) When normal minimum temperature of station is 10^oC or more	
Normal	-1^0 C to 1^o C
Below normal	-2^0C
Appreciably Below Normal	-3^o C to -4^o C
Markedly Below normal/Moderate Cold Wave	-5^0 C to -6^o C
Severe Cold Wave	-7^o C or above
b) When normal maximum temperature of station is less than 10^0C (The term	

moderate cold wave will not be used)	
Normal	-1^0 C to 1^o C
Below normal	-2^0C
Cold Wave	-3^o C to -4^o C
Severe Cold Wave	-5^o C or less

Ratnam et al. (2016 b) considered cold wave events over India when the normalized area average Tmin anomalies are less than one standard deviation for four or more days. Some researchers used the 10^{th} percentile criteria for defining cold waves.

2.3 Temperature data

For studying heat and cold waves over India, researchers generally make use of IMD station data or IMD Gridded daily temperature data set. The IMD gridded temperature data set was prepared indigenously by IMD researchers in 2009 (Srivastava et al. 2009). The details of the IMD gridded temperature data set are given below.

IMD maintains around 550 surface observatories in the country, where daily surface air temperature observations (maximum and minimum) are taken. These data are compiled, digitized, quality controlled and archived at the National Data Centre (NDC) of IMD. However, daily data from 1969 onwards only are digitized and archived at NDC. Later this data set was updated with the daily temperature data from 1961. From the list of stations for which daily data are available, only those stations which have minimum 10 years of data, at least for 300 days in a year during the period 1971–2000, were selected for further analysis. The data were subjected to basic quality checks like rejecting values, greater than exceeding known extreme values, minimum temperature greater than maximum temperature, same temperature values for many consecutive days etc. Unusual high values were flagged

by putting a filter which allowed values only in the range mean±(1.76+0.8 N) standard deviation for further data analysis.

The interpolation was used a modified version of the Shepard's angular distance weighting algorithm for the present analysis. In order to avoid biases in the gridding, daily anomalies were used instead of the absolute values. For this purpose, climatological normal of maximum and minimum temperatures for the period 1971–2000 was calculated for each station. The daily anomalies were calculated as the difference of each daily temperature from its daily normal values. The present interpolation method requires an under-standing of the spatial correlation structure of the station data. Therefore, the interstation correlations were calculated to determine the distances over which observed temperature anomalies are related. For each month, for each pair of 395 stations lying within 2000 km, correlation was calculated and then binned according to their separation over intervals of 100 km. The mean correlation was estimated over each 100-km interval and a two-degree polynomial function was fitted to these values. For interpolating the station data, we have to define the radius of influence. This was estimated as the correlation length scale (CLS), which is defined as the distance at which the mean correlation, represented by the fitted function, fell below 1/e.

More details of this data set are available in Srivastava et al. (2009). This data set is being used very extensively by researchers worldwide.

Chapter 3

Climatology and long- term trends of Cold Waves

In this chapter, the long-term climatology and long-term trends of cold waves over India are discussed. For this purpose, the results based on the IMD criteria and criteria based on percentile have been used.

Cold waves are predominantly experienced during the period December-February, when minimum temperatures drop to very low levels, especially over the northern parts of India. Fig 3.1 a shows the long-term climatology of minimum temperatures (Tmin) and Fig 3.1 b shows spatial distribution of 10th percentile of Tmin. The long-term climatology was prepared using the daily minimum temperature data of 1971-2000. Daily temperature data developed by Srivastava et al. (2009) have been used for this analysis.

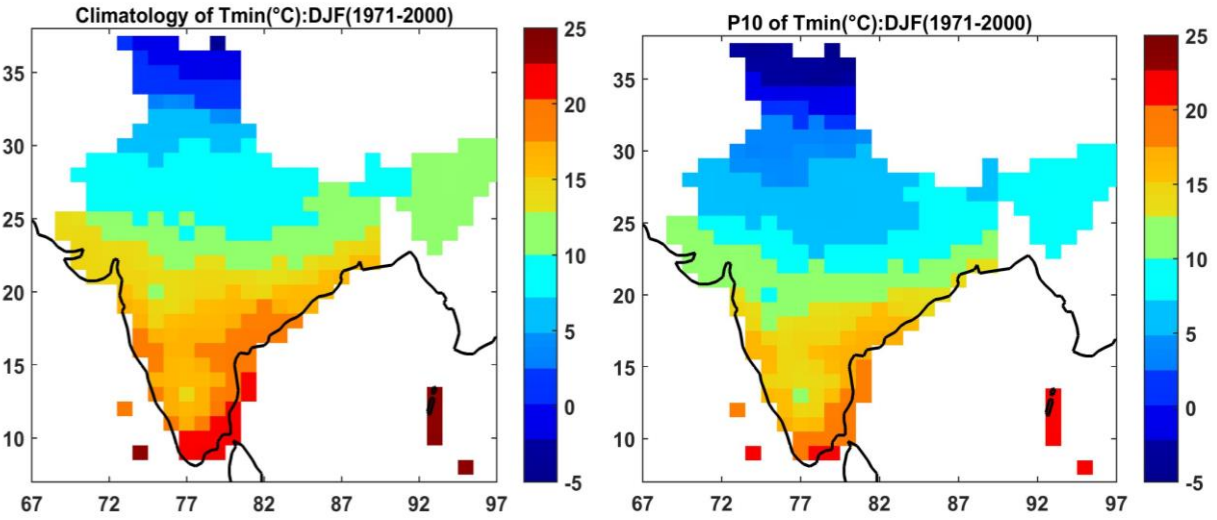

Fig 3.1 a) Climatology of seasonal (Dec-Feb) Tmin (^{o}C) (1971-2000) and b) 10th percentile of Tmin (^{0}C) during 1971-2000.

Seasonal Tmin values are below 15^{0} C over northern parts of the country, north of 20^{0}N. Over parts of Jammu and Kashmir, the Tmin values are even below zero. It is interesting to note that over the northern parts of the country, the isolines of

temperatures run parallel, with a large north-south gradient of over 10^0 C. North of 25^0 N, the 10^{th} percentile values of Tmin are generally below 7.5^0C. A large north-south gradient is also observed in this pattern over the northern parts of the country. There is hardly any north-south gradient over the southern peninsula. The coastal regions, especially the east coast, are relatively warmer compared to the inner parts of the southern peninsula, with Tmin values above 20^0 C.

3.1 Cold Wave Statistics Based on IMD Criteria

The criteria used by the IMD to define Cold Wave (CW) are listed in Table 2.2. From Table 2.2 it can be seen that CW/SCW conditions imply a certain drop in the daily minimum temperatures at a station compared to the respective normal climatological value. As shown in Table 2.2, a relatively intense CW is classified as severe CW or SCW.

In this section, we mainly discuss the results obtained by Smitha et al. (2016) on cold waves over India. They had considered 86 IMD stations for the analysis of cold waves over India. Fig. 3.2 a shows the spatial variation of mean number of Cold Wave (CW) days during the cold weather season (DJF) over the country expressed as days per season. Most of the areas except Kerala, coastal Karnataka, Tamil Nadu and coastal Andhra Pradesh experience 2 CW days or more per season. Many areas over northwest and some parts of central India experience 8 or more number of CW days.

Fig. 3.2 b shows the long-term trends in the number of cold wave days (CW) during the cold weather season (DJF) over the period 1971-2020. The blue (red) colour indicates decreasing (increasing) trends. Statistically significant trends (at a 95% significance level) are shown as filled triangles. It can be seen that many stations over the northern parts of India show a decreasing trend in CW days. Only a few stations over the central and eastern parts of the country show increasing trends. Fig. 3.2 c shows the spatial distribution of Severe Cold Wave (SCW) days for the period 1971-2020. It shows that most of the SCW days are observed over the central and north-western India and

they last for more than 2 days. There are hardly any SCW events over the southern peninsula and north-east India.

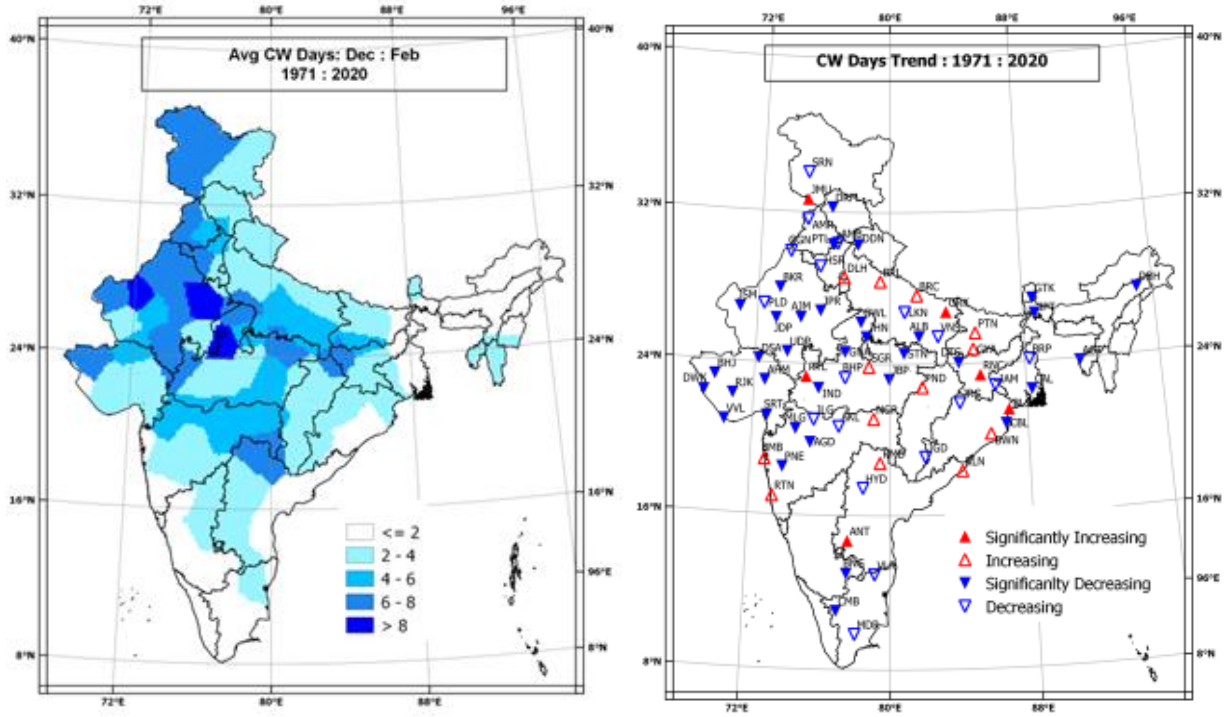

(a) (b)

Fig 3.2. a) Seasonal climatology map of number of CW days, b) Long term trends in number of cold wave (CW) days during the cold weather season (DJF) during the period 1971-2020. Blue (red) colour shows decreasing (increasing) trends. The trends which are statistically significant at 95% significance level are shown as filled triangles. The climatology was computed by averaging the number of CW days for the period (1971-2010). (After Smitha et al. 2016).

Fig. 3.3 a shows the spatial variation in the mean number of cold wave frequencies during the cold weather period (DJF) over the country during 1971-2020, expressed in numbers. In many areas in the northwest, about 8 cold waves occur during the season. North of 20^0N, the frequency of CW is more than four. Fig. 3.3 b shows the long- term trends in the number and frequency of CW during the cold weather season (DJF) during the period 1971-2020. The trends which are statistically significant at 95%

significance level are shown as filled triangles. Most stations in northern India show decreasing trends in the frequency of CW during the December-Feb season. A few stations over Punjab, Haryana and Andhra Pradesh show increasing trend but it is not statistically significant. The decreasing trend in the frequency of cold waves could be related to increase in minimum temperatures observed over India during the recent years. The maximum duration of cold wave days (Fig. 3.4 b) shows a decreasing trend in most parts of northern India. Fig. 3.5 clearly shows the decreasing trend in the frequency, duration and maximum duration of cold waves over India during the winter season. The long-term trend in CW frequency, CW days and CW duration is -0.36/decade, -0.62 days/decade and -0.37 days/decade respectively. These trends are statistically significant at 95% significance level.

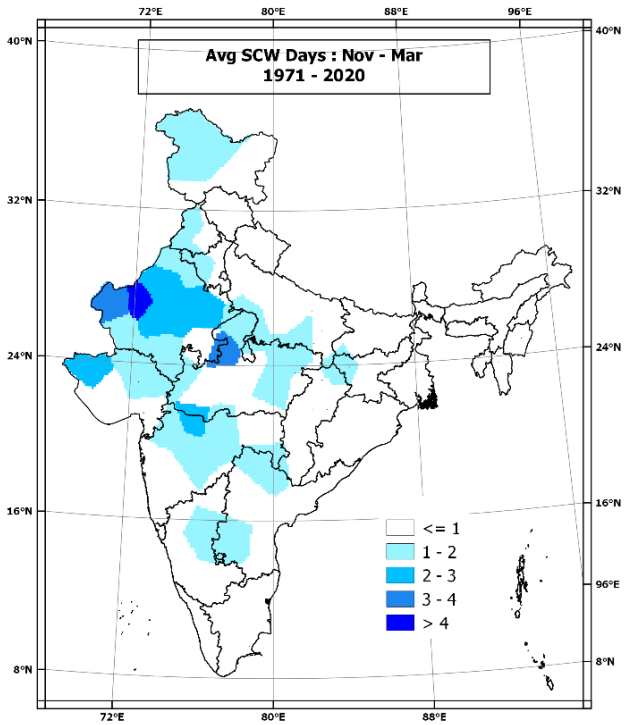

Fig. 3.2. c. Spatial distribution of Severe Cold Wave (SCW) days during November to March (After Smitha et al. 2016)

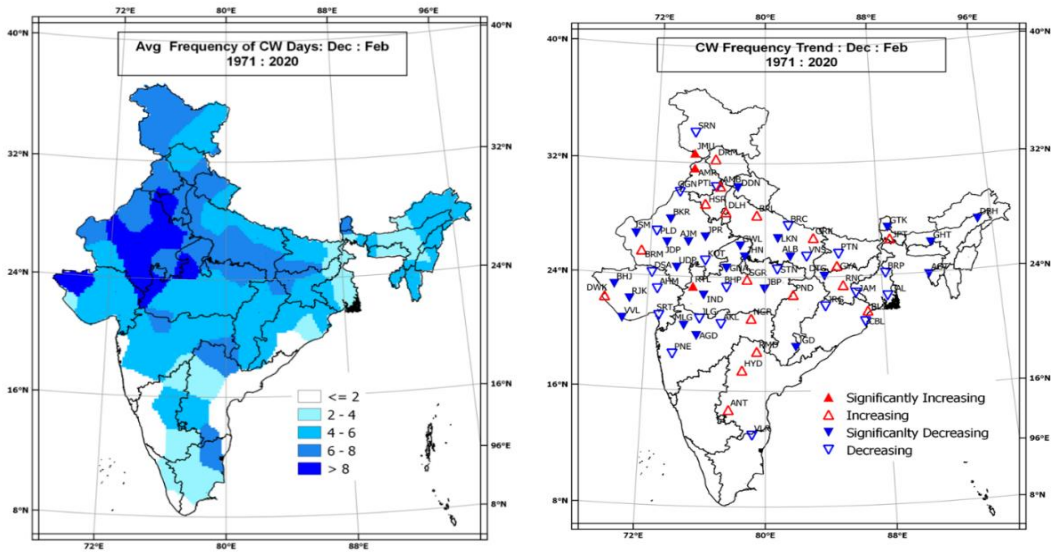

Fig 3.3. a) Seasonal climatology map of frequency of CW events, b) Long term trends in number of cold wave (CW) frequency during the cold weather season (DJF) during the period 1971-2020. Blue (red) colour shows decreasing (increasing) trends. The trends which are statistically significant at 95% significance level are shown as filled triangles (After Smitha et al., 2016)

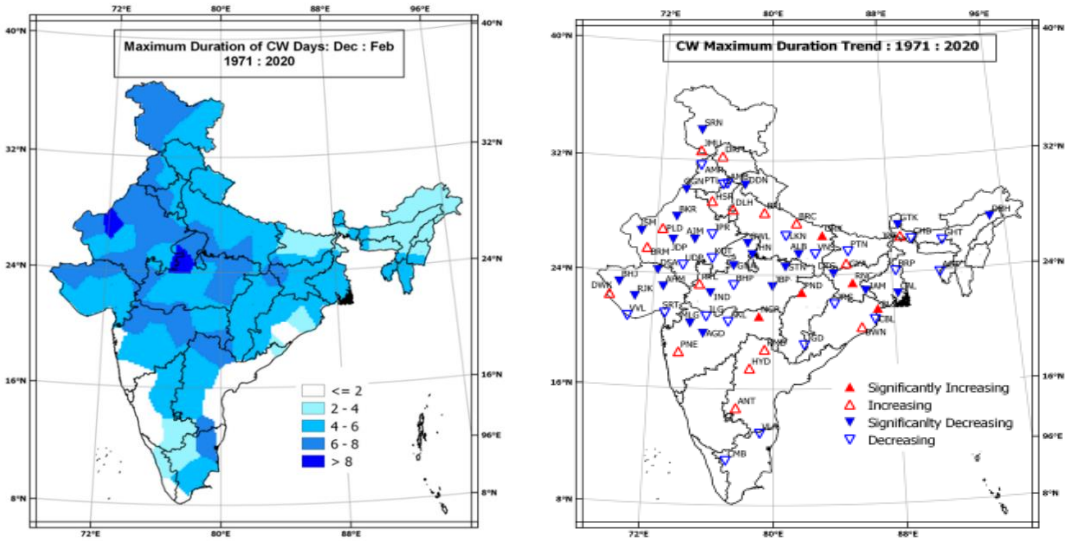

Fig 3.4 a. Seasonal climatology map of maximum duration of CW days during the cold weather season (December-February) b) Long term trends in maximum duration of CW days during the cold weather season (DJF) during the period 1971-2020. Blue (red) colour shows decreasing (increasing) trends. The trends which are statistically significant at 95% significance level are shown as filled triangles (After Smitha et al., 2016).

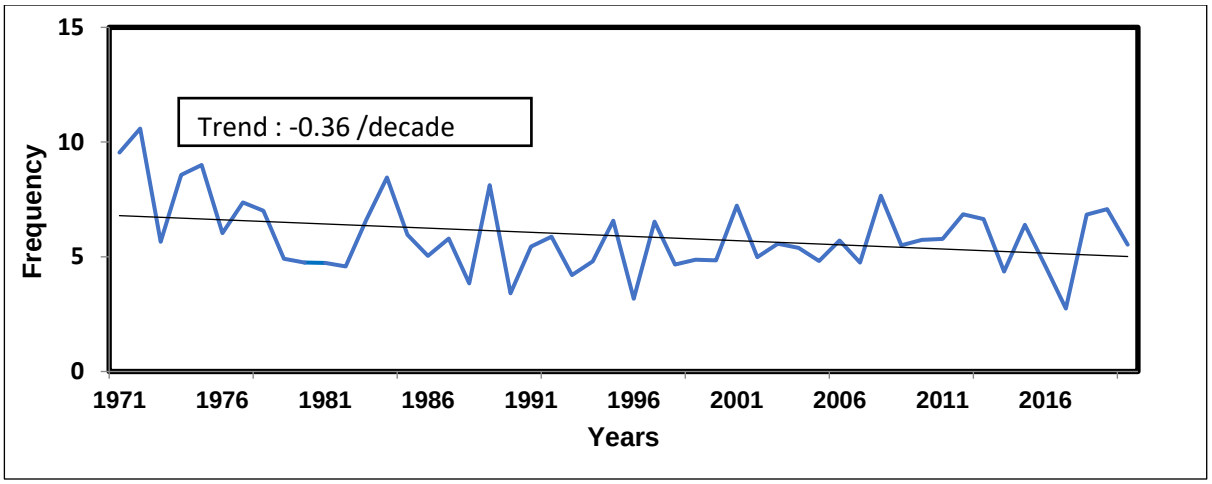

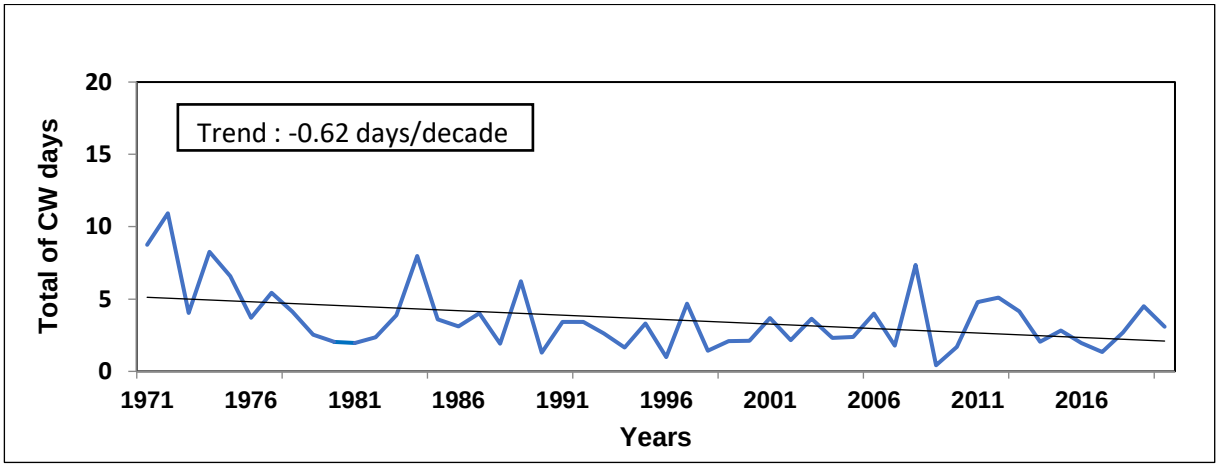

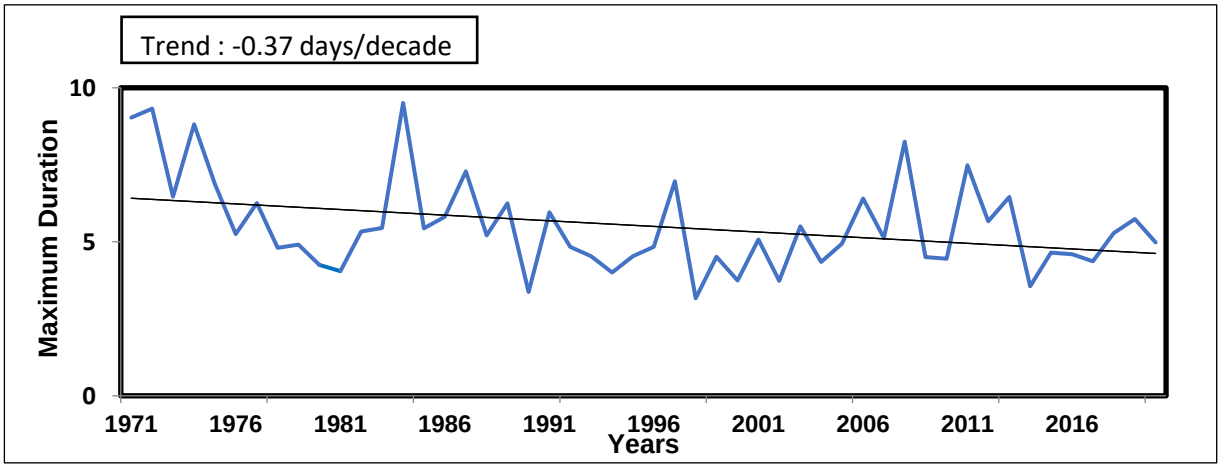

Fig. 3.5. Long term trends of a) frequency b) total of CW days and c) maximum duration averaged over the cold wave core for the period 1971-2020. (After Smitha et al., 2016).

Earlier studies (Pai et al. 2017 and Smitha et al. 2016) showed the relationship of occurrence of cold waves over India with the EL Nino and La Nina phases. To understand the impact of El Nino and La Nina on cold waves over India, composite spatial maps of mean CW days over India for El Nino/La Nina events are constructed. Fig. 3.6 a and b show the composite spatial maps of mean CW days over India for El Nino and La Nina events. These maps were prepared using data from 1971-2010. The composite map for El Nino shows a relatively lower frequency of CW days compared to the climatology map. However, the La Nina case shows that most areas experience significantly more CW days than the climatology, with large areas of the central and northwest India experiencing more than 8 CW days. An increase (decrease) in the frequency of SCW days [Fig. 3.7 a and b] was also observed over central parts of the country during the La Nina (El Nino) fall. Ratnam et al (2016 b) suggested that both ENSO phases (La Nina and El Nino) provide a favourable background for the occurrence of cold waves over India, however, more frequent in La Nina years. This aspect is further discussed later in the monograph.

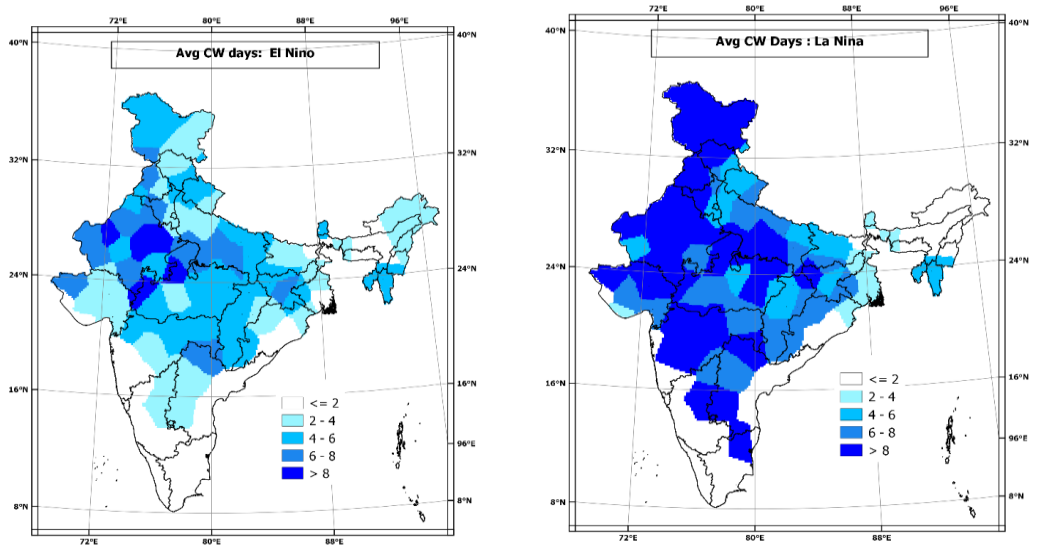

(a) (b)

Fig 3.6 a) Average CW days during the El Nino years and b) Average CW days during the La Nina years. (After Smitha et al., 2016)

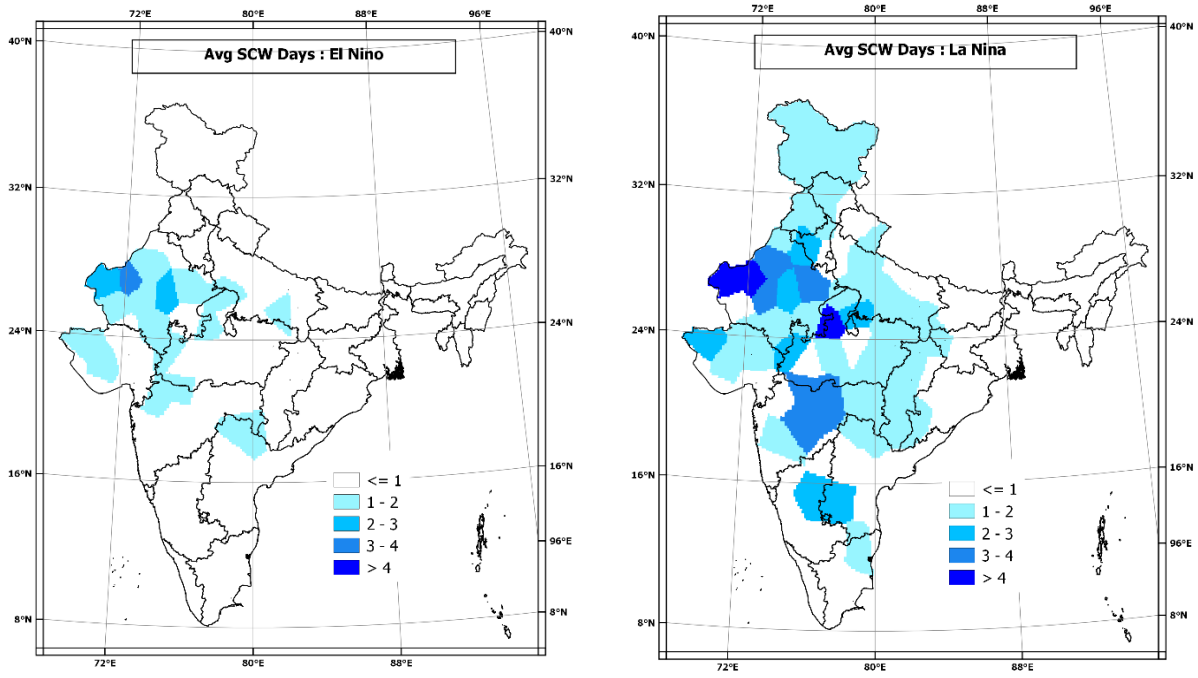

(a) (b)

Fig. 3.7 a) Average SCW days during the El Nino years and b) Average SCW days during the La Nina years (After Smitha et al., 2016)

Fig. 3.8 shows the duration of the longest CW period over each station across the country. The CW cycles with a duration of 10 days or more are shown in red. The stations with the longest CW periods of 10 days or more are in the north-west and central India. The station in Jammu and Kashmir experienced the longest duration of cold wave (18 days). Bikaner and Jodhpur in western Rajasthan experienced the longest CW period with a duration of 16 days. Gangtok in Sikkim experienced the longest CW period with 17 days (December 10 to 26, 1986). Even over Maharashtra, the maximum duration of CW days was more than 8 days. Most of the stations that experienced the longest CW period of 5 days or more are in North, Northwest and Central India. As mentioned earlier, there are no cold waves in the south of peninsular India.

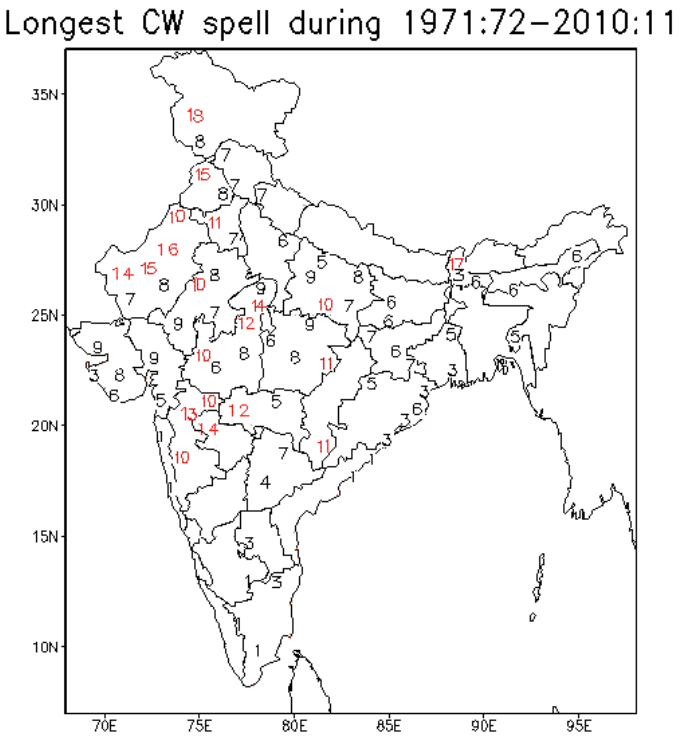

Fig. 3.8. Map showing the duration of the longest CW spell over each of the stations used in the study during the analysis period of 1971-2010. The duration of CW spells of 10 days or more are shown using red colour (After Smitha et al. 2016).

3.2 Cold Wave Statistics Based on Temperature Gridded data

In this section, the cold wave statistics based on gridded temperature data (area averaged over 1^0X 1^0 grids) is discussed. For this purpose, the IMD daily gridded temperature data (Srivastava et al., 2009) have been used. This analysis will provide us a different perspective about cold waves than the statistics based on IMD station data and IMD criteria.

For this analysis, December to February season is considered and the data from December 1970 to February 2021 have been used. The criteria considered for the analysis of cold wave and severe cold wave are given below:

A cold wave is considered if minimum temperature (Tmin) is less than 10^{th} percentile of daily climatological value and the climatological daily Tmin is less than

15°C. This condition should satisfy consecutively for three days to be considered as one cold wave event. Similarly, severe cold wave (SCW) is considered if daily Tmin is less than 5th percentile of daily climatological value and the climatological daily Tmin is less than 15^{0}C. It should be satisfied for three consecutive days to consider as one cold wave event. The period 1971-2000 was used as a reference period to calculate the climatology. The percentile has been calculated for a 5-day moving window.

Fig 3.9 shows the long term climatology of cold wave frequency, cold wave days (days) and cold wave intensity (°C) for the period 1971-2021, calculated using the above criteria. It is to be mentioned that the above criteria are based on departures from long term normal and not the actual minimum temperatures. To satisfy as a cold wave, the temperature departures should be more than this threshold (10th percentile).

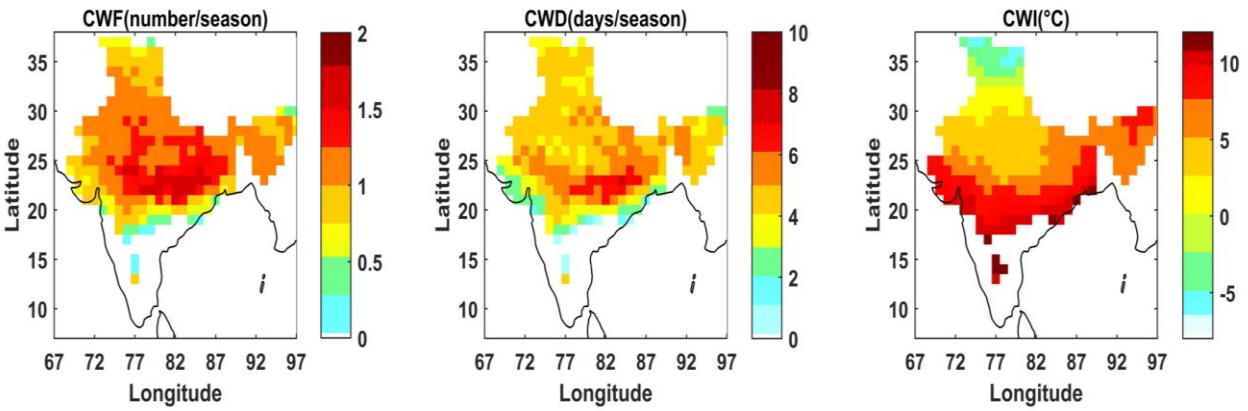

Fig 3.9 Climatology of a) CW frequency b) CW duration and c) CW Intensity based on the data of 1971-2021. The DJF season is considered for the analysis.

The greatest frequency of more than one event is observed over the northern parts of the country, north of 20^{0}N. In this region, more than 6 days of cold wave (CW) occur on an average. In some areas, the average number of CW days is also more than 8. The CW intensity is the lowest temperature measured during a CW event. In the extreme northern parts of the country, CW intensity is close to zero or below zero. With these criteria, no cold wave event is generally observed south of 20^0 N.

Fig. 3.10 shows the long-term climatology of severe cold wave frequency, severe cold wave days (days) and severe cold wave intensity (^{0}C) for the period 1971-2021. The maximum frequency of 0.5 SCW events is observed over the central parts of the country north of 20^0 N, which means that one event occurs every two years. In this region, an average of about 2 days of severe cold wave occurs. In some areas, the average number of CW days is also more than 8. The SCW intensity is the lowest temperature recorded during the SCW event. In the extreme northern parts of the country, the intensity of the cold wave is close to zero or below zero. With these criteria, no severe cold wave event is generally observed south of 15^{0}N.

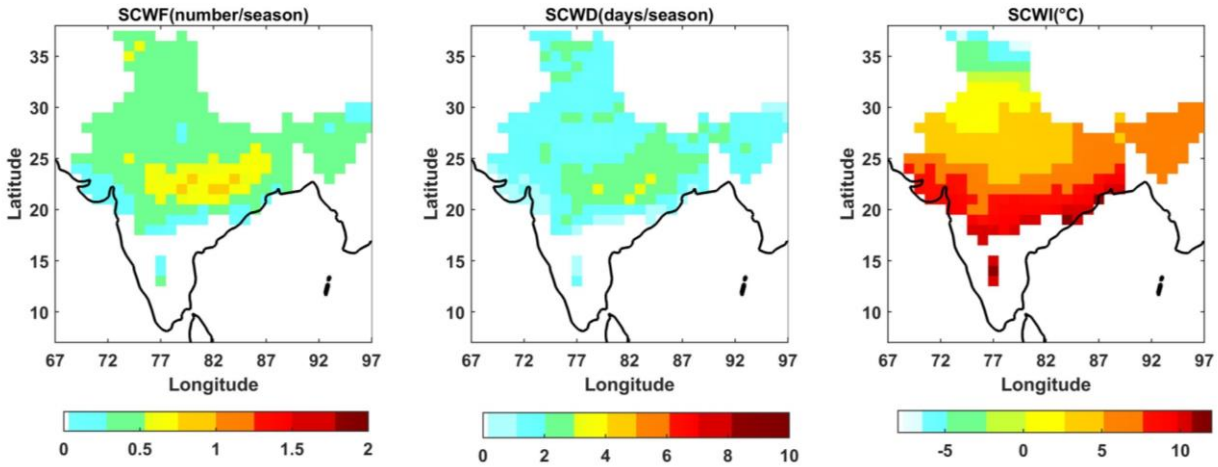

Fig 3.10 Climatology of a) SCW frequency b) SCW duration and c) SCW Intensity based on the data of 1971-2021. The DJF season is considered for the analysis.

Fig. 3.11 shows the long-term trends in CW frequency, duration and intensity for the period 1971-2021. These graphs show that the frequency and duration of CW is generally decreasing in most parts of northern India, except in Chhattisgarh, Jharkhand and Bihar, where a slight increase is observed. The declining trend is most pronounced in the north-western parts of the country where the duration of CW decreased by more than 1 day. However, this trend is also reflected in the spatial distribution of CW intensity. In most parts of north-western India, CW intensity is increasing, which means that the minimum temperatures observed during CW events are increasing. In the

north-eastern parts, especially over Bihar, the CW intensity decreases, which means that the lowest minimum temperatures decrease or, in other words, the CW events become harsher.

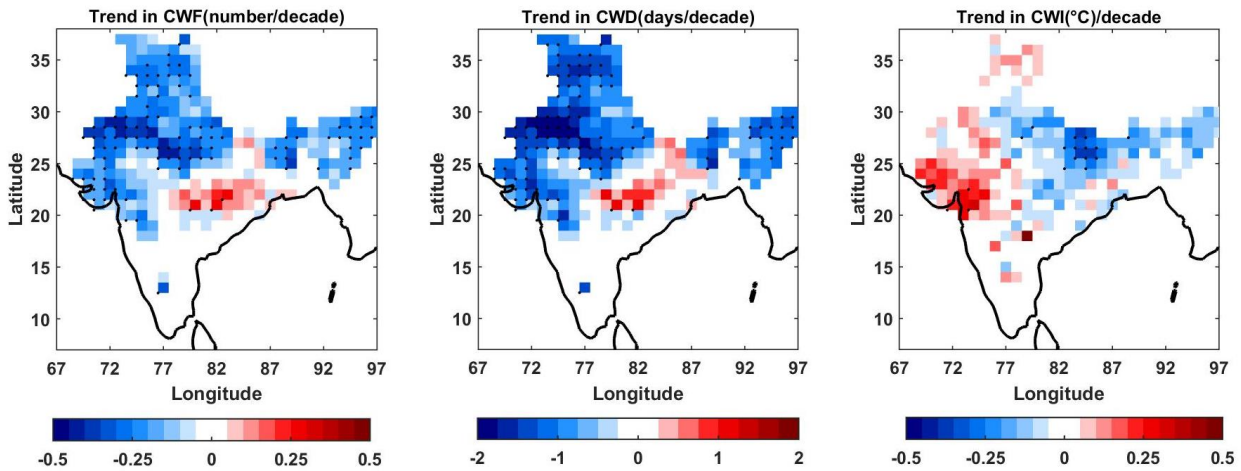

Fig 3.11 Trends of a) CW Frequency b) CW duration and c) CW Intensity. The trends are in decade. The data of 1971-2021 have been used to calculate these trends.

Fig. 3.12 shows the time series of a) frequency of cold waves and b) duration of cold waves over the period 1971-2020. The red line shows the linear trend and the dashed lines on either side of the trend line indicate the 95% confidence levels. The time series is averaged over a larger area: 72.5^0 E-87.0^0 E, 20.5^0 N-37.5^0 N. Both time series show a decreasing trend that is significant at the 95% significance level. The trend in frequency is 0.15 per decade and the trend in duration is 0.81 days per decade. The trend based on the IMD criteria (Fig. 3.5) for frequency is slightly higher than this trend value. However, the trend for duration is lower than the trend obtained from the gridded data. This could be due to the slight differences in the criteria used to define cold waves. While the IMD analysis used station data, the present analysis is based on area-averaged gridded data. However, both data sets show a very clear downward trend in CW frequency, days and duration, suggesting that the recent increase in minimum temperatures is leading to a decrease in the characteristics of cold waves over India.

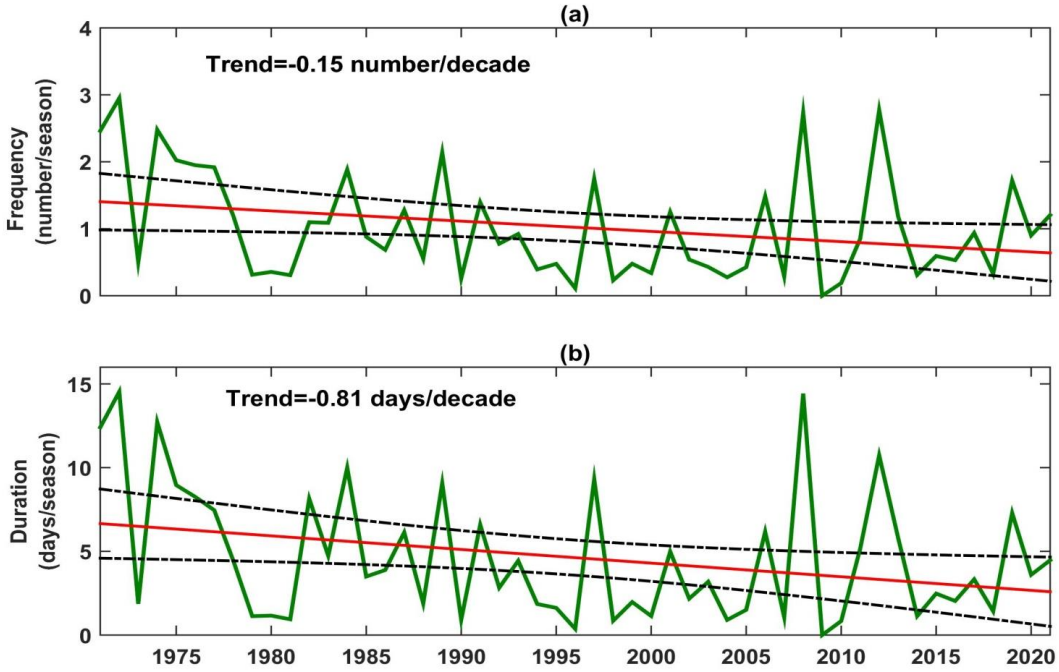

Fig 3.12. Time series of a) Cold Wave frequency and b) CW duration during 1971-2020. The red line shows the linear trend and dotted lines suggest 95% confidence level. The time series is averaged over a larger area 72.5^0 E-87.5^0 E, 20.5^0 N-37.5^0 N**.**

A further analysis is carried out to see the spatial pattern of ocean influence on cold waves. Fig. 3.13 shows the spatial pattern of correlation between cold wave duration and sea surface temperature (SST) using data from 1971-2020. SST data from HADI SST was used for this analysis. The spatial pattern shows very clearly that cold wave duration is negatively correlated with SST over the equatorial Pacific and Indian Oceans, suggesting that the La Nina phase of ENSO and the colder Indian Ocean cause more days of CW duration. The same type of conclusion was drawn by Smitha et al. (2016) using IMD data and IMD cold wave criteria. Ratnam et al. (2016 b) suggests that both La Nina and El Nino phases can cause cold waves. They referred to them as Type 1 and Type 2 events respectively. However, the Type 2 cold wave events that occur during the El Nino years are less frequent and only affect the northern parts of the country.

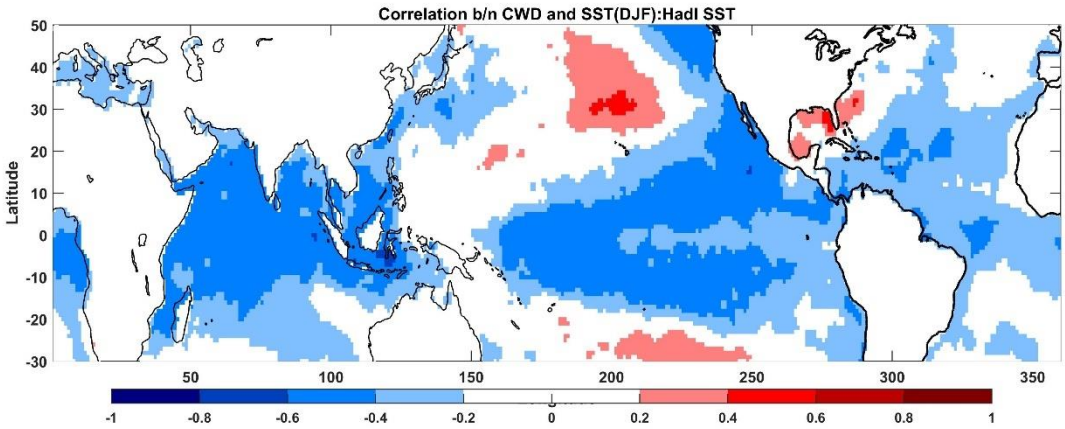

Fig 3.13. Correlation between Cold Wave Duration and Sea Surface Temperature (SST) during the DJF season. Period of data: 1971-2020.

Further, a list of CW events which persisted for more than 5 days is prepared using the 90th percentile criteria. For this purpose, data of 1971-2020 was used. Cold Wave events are calculated using area averaged minimum temperatures over the cold wave core zone (72.5^0 -82.5^0 E, 20.5^0 -35^0 N). The criteria for identifying the cold wave events are as follows:

1) Daily Tmin is less than the 10th percentile of daily climatological value and the climatological daily Tmin < 15^{0}C.
2) The cold wave event should persist with minimum duration of 5 days.

Table 3.1 shows such CW events that occurred during the period 1971-2020. The intensity suggests the lowest minimum temperature observed during the event. The longest cold wave event observed was 10 days during 01-10 December 1971. There are many cold wave events with 8 days of duration. The lowest Tmin recorded during the CW events was 0.93^{0}C during February 1974. On average duration of CW is 6 days. Table 3.1 also clearly suggests the cold wave frequency is decreasing during the recent years. During the decade 2011-2020, only six cold wave events were observed.

Table 3.1

List of cold wave events during the period 1971-2020

as per the 90th Percentile criteria based on IMD gridded data set

Year	Date	Intensity (ºC)	Total Duration (Days)
1971	1 Dec-10 Dec	4.74	10
	29 Jan-02 Feb	3.43	5
1972	6 Jan-12 Jan	2.97	7
	14 Feb-20 Feb	2.35	7
1974	5 Feb-10 Feb	0.93	6
1975	19 Dec-25 Dec	3.34	7
1976	8 Dec-13 Dec	3.74	6
1982	12 Dec-16 Dec	4.43	5
1983	01 Feb-06 Feb	3.49	6
1984	21 Feb-28 Feb	3.17	8
1985	18 Dec-25 Dec	3.46	8
1986	04 Jan-08 Jan	2.43	5
1989	10 Jan -15 Jan	2.22	5
	19 Feb-23 Feb	5.02	5

1991	01Jan-06 Jan	1.45	6
1993	20 Jan-24 Jan	2.87	5
1994	21 Dec-25 Dec	4.43	5
1997	8 Dec-14 Dec	3.09	7
2006	12 Dec-19 Dec	3.98	8
2008	21 Jan-28 Jan	2.43	8
	09 Feb-15 Feb	2.48	7
2011	18 Dec-22 Dec	4.48	5
	5 Jan-11 Jan	2.72	7
2012	10 Jan-14 Jan	2.95	5
2013	05 Jan-09 Jan	1.91	5
2019	26 Dec-31 Dec	2.96	6
2020	27 Dec-31 Dec	2.92	5

Chapter 4

Climatology and long- term trends of Heat Waves

In this chapter, the climatology and long-term trends of heat waves over India are discussed. For this purpose, the results based on the IMD criteria and the criteria based on the percentiles were used. As mentioned earlier, heat waves occur mainly during the period from March to June when maximum temperatures rise to very high levels, especially in the northern parts of India.

4.1 Heat wave climatology based on IMD Criteria.

In this section, long term climatology and long-term trends of Heat waves over India are discussed using the IMD station data and IMD criteria. For this purpose, the data of 1961-2020 have been used. The details of heat wave criteria followed by IMD are given in Chapter-2.

Fig 4.1a shows the average frequency of heat wave days using the data of 1961-2020. On an average more than 2 heat wave events occur over northern parts of the country and coastal Andhra Pradesh and Odisha. In some pockets, heat wave frequency even exceeds four in a season. Most of IMD stations are showing increasing trends of heat wave events during the 60-year period (1961-2020) (Fig 4.1.b) as shown by red triangles.

Fig. 4.2 shows the spatial distribution of the duration (days) of heat waves. The plot shows that heat waves last on an average 4-8 days. In some areas of central and north-western India and parts of Odisha and coastal Andhra Pradesh, the duration is more than 8 days. Over Gujarat and Chhattisgarh, heat waves last 2-4 days. Fig. 4.2 b shows the long-term trends in the duration of heat waves for the individual stations during the period 1961-2020. It clearly shows that most IMD stations show an increasing trend in the duration of heat waves during the March-June season.

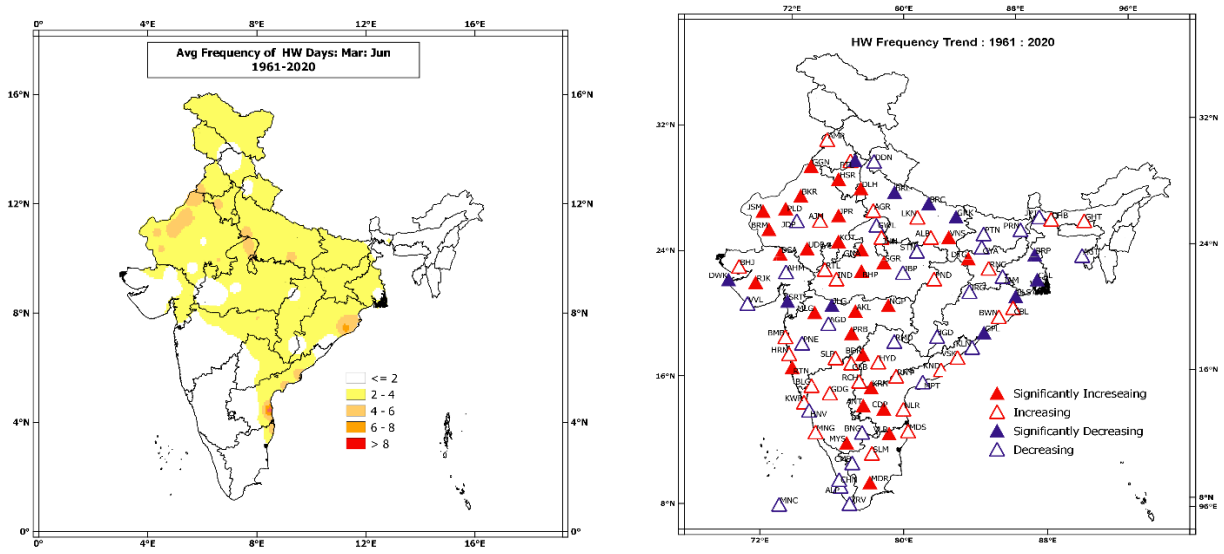

Fig 4.1 a) Heat wave average frequency during March-June for the period 1961-2020, b) HW frequency trends, station wise during the same period.

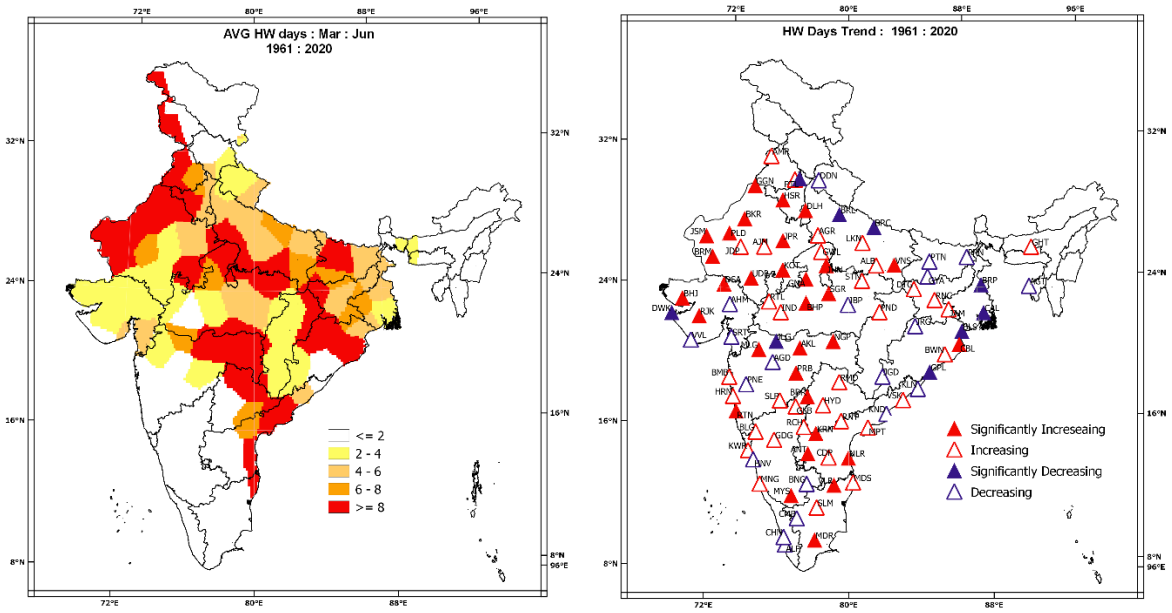

Fig 4.2 a) Heat wave average total duration (days) during March-June for the period 1961-2020, b) Station wise, HW duration trends during the same period.

Fig. 4.3 a shows the maximum duration of heat waves in March and June for the period 1961-2020. Fig. 4.3 b shows the long-term trends of maximum duration of heat

waves in the same period for the individual stations. On an average, the maximum duration of the heatwave is 2-4 days. In some areas in central and north-western India, it is more than 6 days. In coastal Andhra Pradesh, the maximum duration is more than 8 days. The maximum duration of heat waves during March to June also shows an increasing trend in the northern parts of the country. The trends at some stations in the northern parts of the country are statistically significant at 95% significance level.

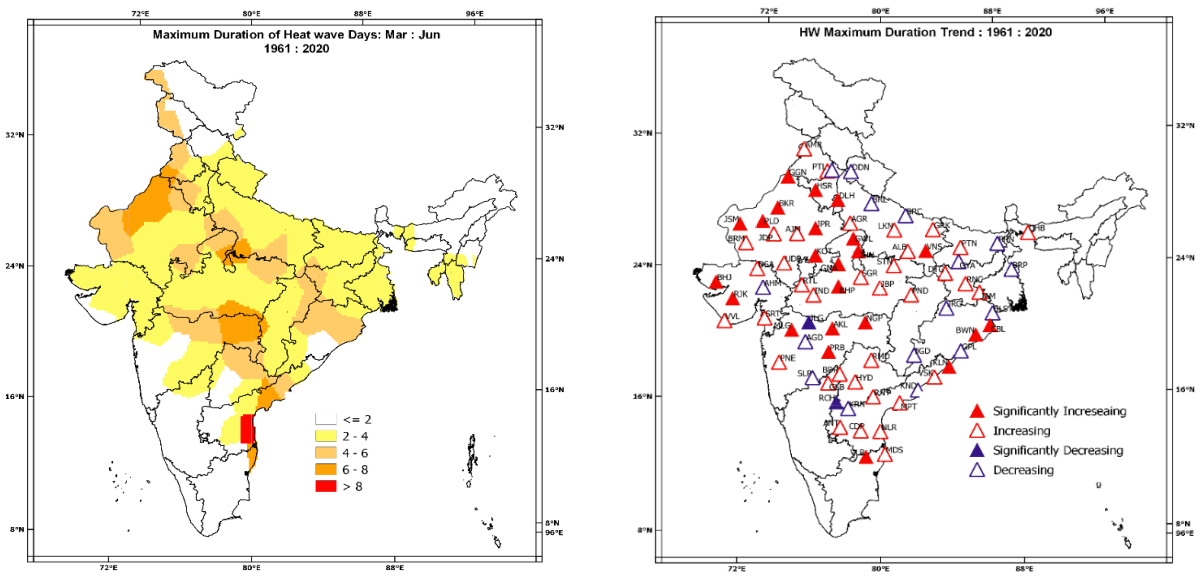

Fig 4.3 a) Maximum Duration of Heat Wave days during March-June for the period 1961-2020, b) Station wise, trends of maximum duration of heat waves during the same period.

Fig. 4.4 shows the spatial distribution of average severe heatwave (SHW) days from March to June for the period 1961-2020 based on the IMD criteria. This shows that SHW days tend to occur in the extreme northwest of India and in the eastern parts of India (Bihar, Jharkhand and surrounding areas), but 1-2 days during the hot weather season.

Earlier studies (Pai et al. 2017, Rohini et al. 2016, Ratnam et al. 2016 a) suggested a link between heat waves over India and the El Nino/Southern Oscillation (ENSO). El Nino (La Nina) is known to cause warming (cooling) around the globe, especially over

the tropics. Studies have shown that the frequency and duration of heat waves increases during El Nino years.

Fig. 4.5 shows the average heat wave days during a) El Nino years and b) La Nina years, which clearly shows that heat wave days are much more during the El Nino years than La Nina years. It is interesting to note that heat wave activity over the east coast of India however remains the same or slightly enhanced during the La Nina years. Ratnam et al. (2016 a) and Rohini et al. (2016) have done some detailed analysis to show how ENSO events can influence heat waves over India. This relationship between heat waves and ENSO events is further discussed in detail in Chapter 5.

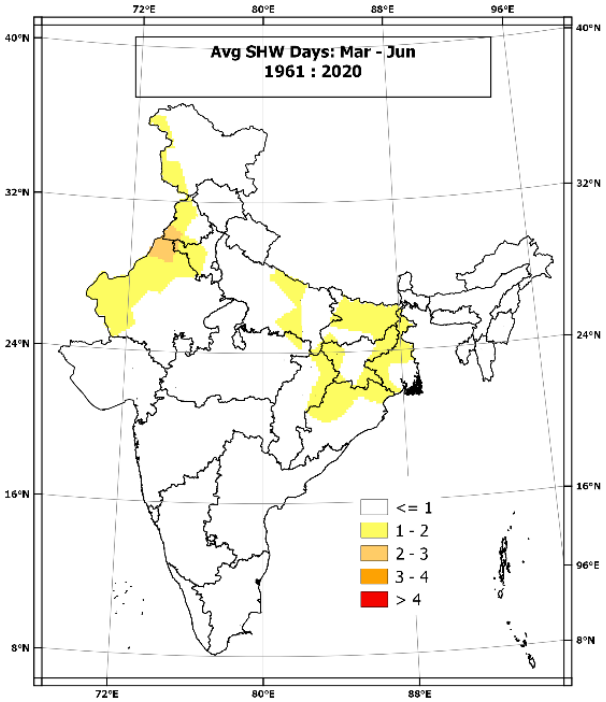

Fig 4.4. Spatial distribution of average Severe Heat Wave (SHW) days during March-June for the period 1961-2020.

Fig. 4.6 a shows the longest heat wave in days and Fig. 4.6 b shows the longest severe heat wave in days for the period 1961-2020. Over central and north-western India and coastal Andhra Pradesh, the longest heat wave days exceed 10 days at many stations. Over the far northwest of India, the longest heatwave even exceeded

15 days. The longest severe heat wave generally lasts more than 5 days in central and north-western India, while it is less than 5 days over the southern peninsula including the Andhra Pradesh coast.

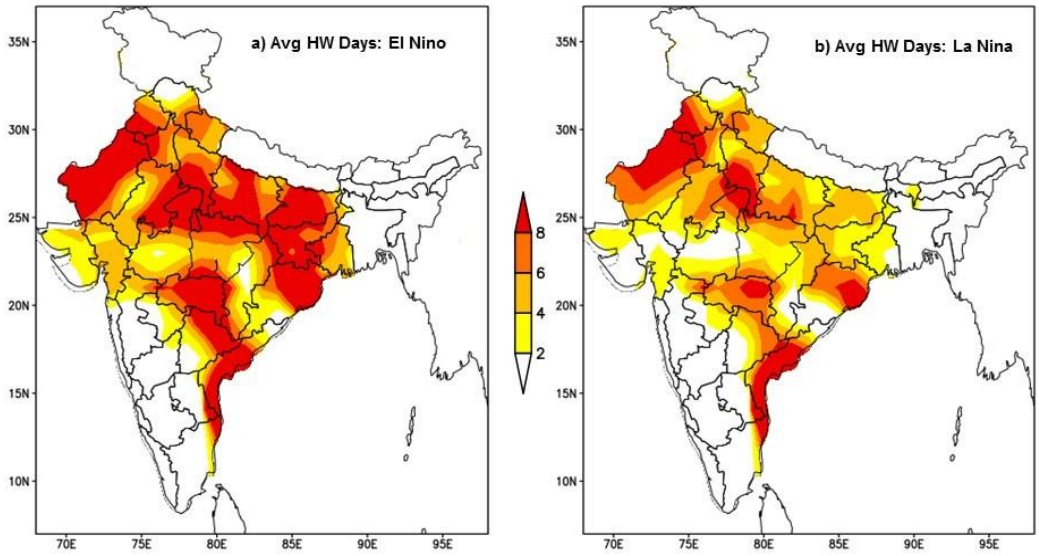

Fig 4.5. Average HW days during a) the El Nino years and b) La Nina years during the period 1961-2020.

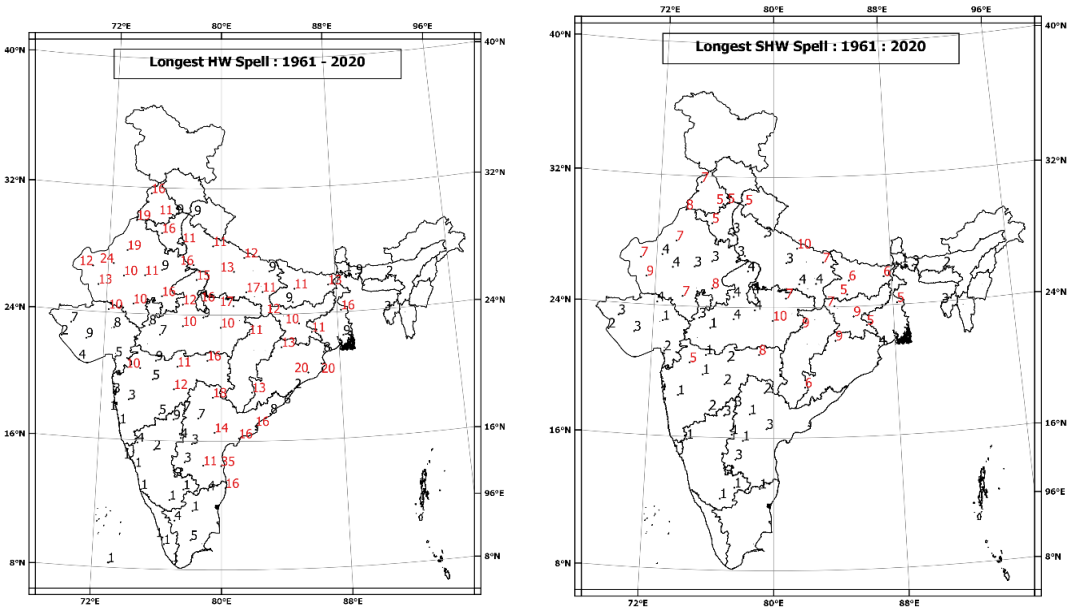

Fig. 4.6. a) Station wise longest heat wave spell during 1961-2020 b) Station wise longest Severe heat wave spell during 1961-2020.

4.2 Heat wave climatology based on area averaged temperature data

In this section, heat wave statistics based on the IMD grid data (Srivastava et al., 2009) are discussed. Based on the gridded data, two criteria can be used to define heat waves. The first is the 90th percentile and the second is the Excessive Heat Factor (EHF). These two criteria are discussed in detail in the Chapter 2. The statistics discussed below are based on the 1961-2021 data and the March-June (MAMJ) period is used to calculate the statistics. The period 1971-2000 has been considered for calculating climatology and temperature deviations.

Fig. 4.7 shows the spatial distribution of a) heat wave frequency, b) heat wave days and c) heat wave intensity in the period from March to June. Data from 1961-2021 were used for this analysis. Fig. 4.7 a shows two predominant areas for heat wave occurrence. One is over the central and north-western India. The other is the coastal area of Andhra Pradesh and Odisha. In the heat wave zone (central and north-western India), 1-2 heat waves occur on an average. Coastal Andhra Pradesh also experiences 1-2 heat waves per season. In most parts of central and north-western India, heat waves last for about 6-8 days. Heat waves also last for about a week in the coastal Andhra Pradesh. The spatial distribution of the intensity of the heat waves indicates that the maximum temperatures in the northern parts of the country exceed 44°C during the heat waves. In coastal Andhra Pradesh, the intensity of heat waves exceeds 40°C. However, due to the higher humidity in the region (because of its proximity to the sea), heat waves can have huge negative impacts on human health. For example, the 2015 heat wave on the Andhra Pradesh coast reportedly claimed 2500 lives.

Fig. 4.8 shows the spatial distribution of a) frequency of severe heat waves, b) duration (days) of severe heat waves and c) intensity of severe heat waves during the March to June.

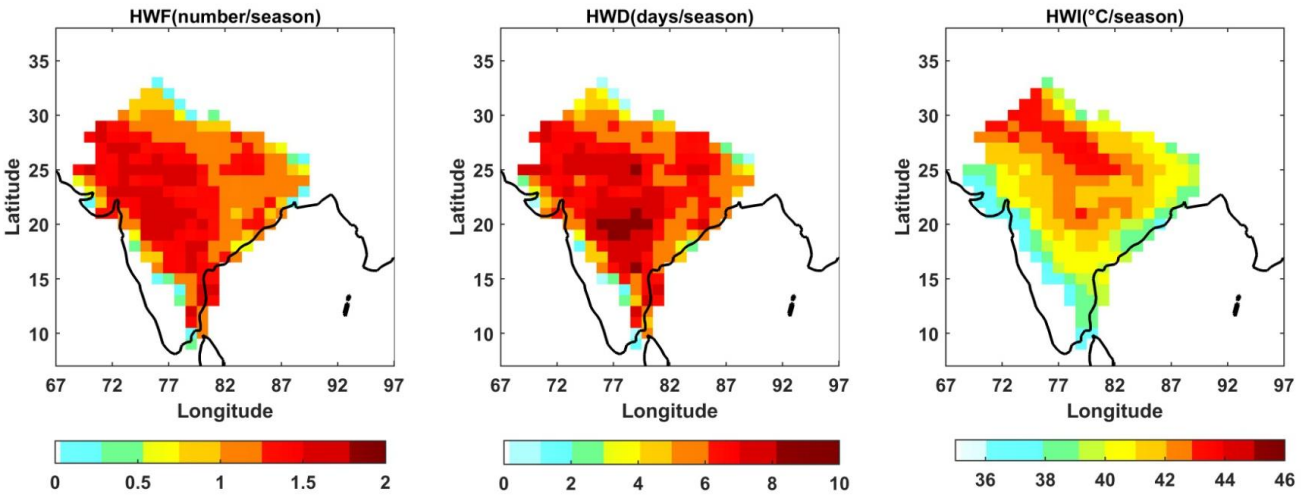

Fig 4.7. Spatial distribution of a) heat wave frequency, b) heat wave days and c) heat wave intensity during MAMJ. Period 1961-2021.

Fig. 4.8 a shows two predominant areas of severe heat waves, one over central and north-western India and another over the coastal Andhra Pradesh, where on average one severe heat wave occurs in 2 years. Severe heat waves last for about 3-4 days over central and north-western India. During severe heat waves, maximum temperatures exceed 45°C in the northern parts of the country.

Fig. 4.9 shows the long-term trends in a) HW frequency b) HW days and c) HW intensity, indicating that the frequency and duration of heat waves are increasing over central and north-western India. The frequency and duration of heat waves are also increasing in coastal Andhra Pradesh. The trend in duration is more than 1 day/decade. Most of the observed trends over central and north-western India and coastal Andhra Pradesh are statistically significant at 95% level of significance. Fig. 4.9 c shows that the intensity of heat waves (highest maximum temperatures) increased over the northern parts of the country, suggesting that higher maximum temperatures were observed during the recent heat waves. However, over the coastal Andhra Pradesh, the intensity of heat waves decreased. It is important to understand the physical causes for these observed trends.

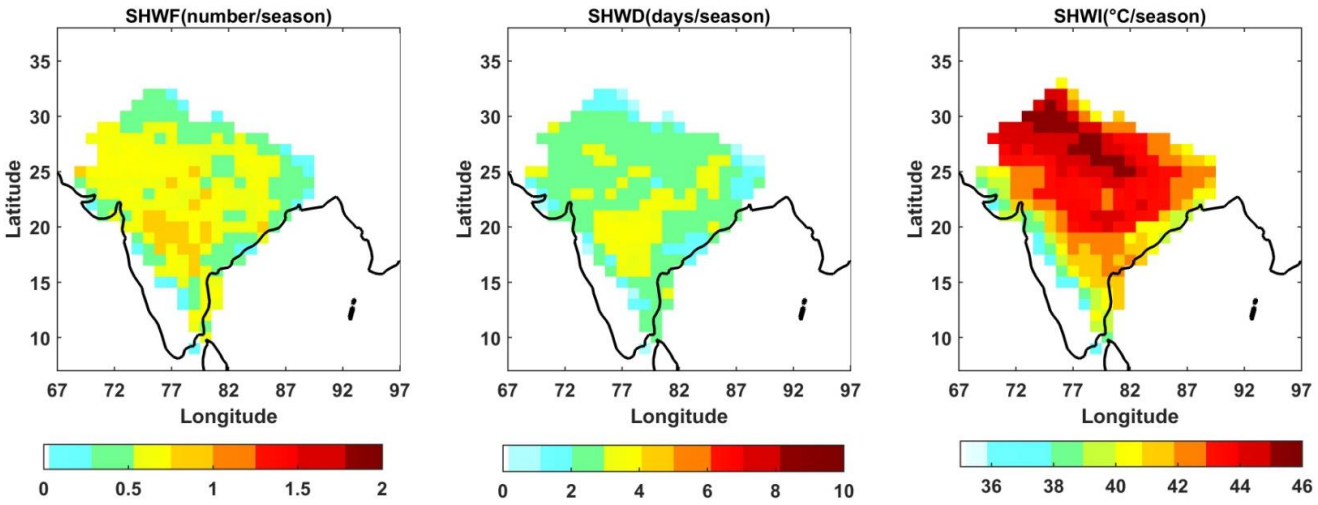

Fig 4.8. Spatial distribution of a) Severe heat wave frequency, b) severe heat wave days and c) severe heat wave intensity during MAMJ. Period 1961-2021.

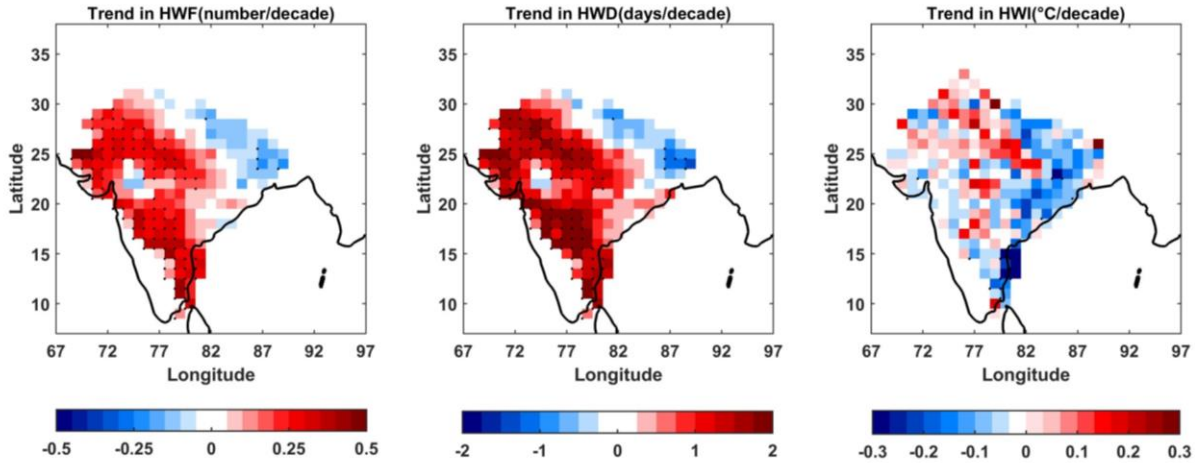

Fig 4.9. Spatial distribution of a) Trend in heat wave frequency (number/decade), severe heat wave days (days/decade) and severe heat wave intensity (^{o}C/decade) during MAMJ. Period 1961-2021. The trends which are statistically significant are shown as dots.

Fig. 4.10 a shows the average maximum heatwave days (days/season) and Fig. 4.10 b shows the trend (days/season) of maximum heatwave days. The maximum heat wave days are more than 6 days over central India (Maharashtra and Vidarbha) and eastern parts of central India (Jharkhand, Bihar). In northwestern India, it is generally more than 5 days. Over the coastal areas of Andhra Pradesh and Odisha, it is more than

5 days. In most parts of the country, the maximum duration of the heat wave shows a statistically significant upward trend (Fig 4.10 b).

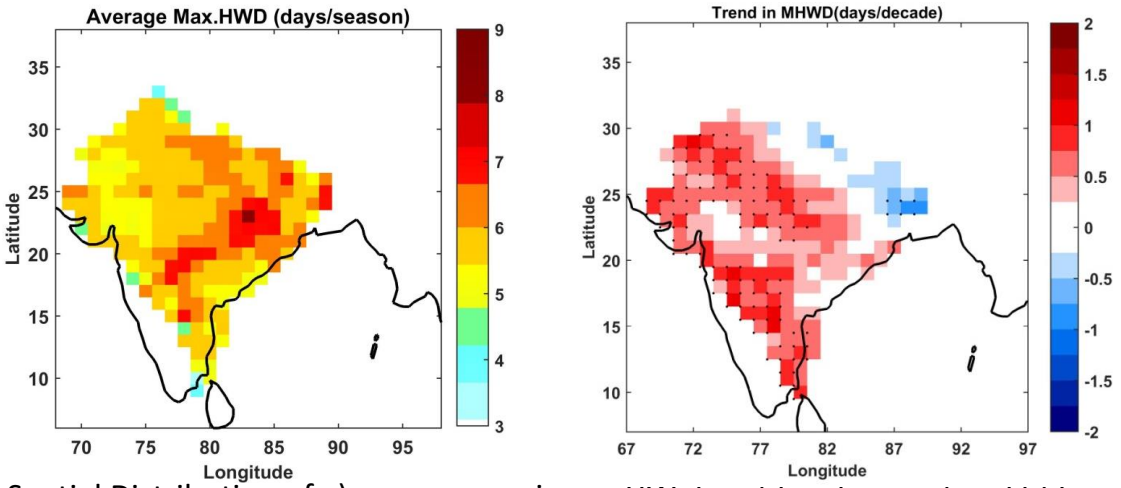

Fig 4.10. Spatial Distribution of a) average maximum HW days (days/season) and b) Long term trends. The trends which are statistically significant are shown as dots.

Fig. 4.11 shows the time series of heat wave frequency, heat wave duration and maximum heat wave duration averaged over northwest India (70^0 E-78^0 E, 22^0 N-31^0 N). The time series shows increasing trends in all three aspects of heat wave, frequency, duration and maximum duration. The observed trends are 0.16, 0.93 days and 0.31 days per decade, respectively, which are statistically significant at 95% significant level. Accordingly, the average duration of heat waves has increased by 6.5 days in seven decades (1961-20201), which is highly significant. The maximum duration has also increased by about 2 days in the same period.

Fig. 4.12 shows the time series of area-averaged heat wave frequency, heat wave duration and maximum heat wave duration averaged over the coastal region of Andhra Pradesh (12^0 – 16^0 N, 78^0 – 81^0 E) based on the 90th percentile criteria. The frequency, duration and maximum duration of heat waves are also showing increasing trends in coastal Andhra Pradesh. However, the trends (0.25/decade, 1.3 days/decade and 0.45 days/decade) are higher than the corresponding trends observed over northwest India. This is an interesting aspect to note and we need to find out the possible reasons for this.

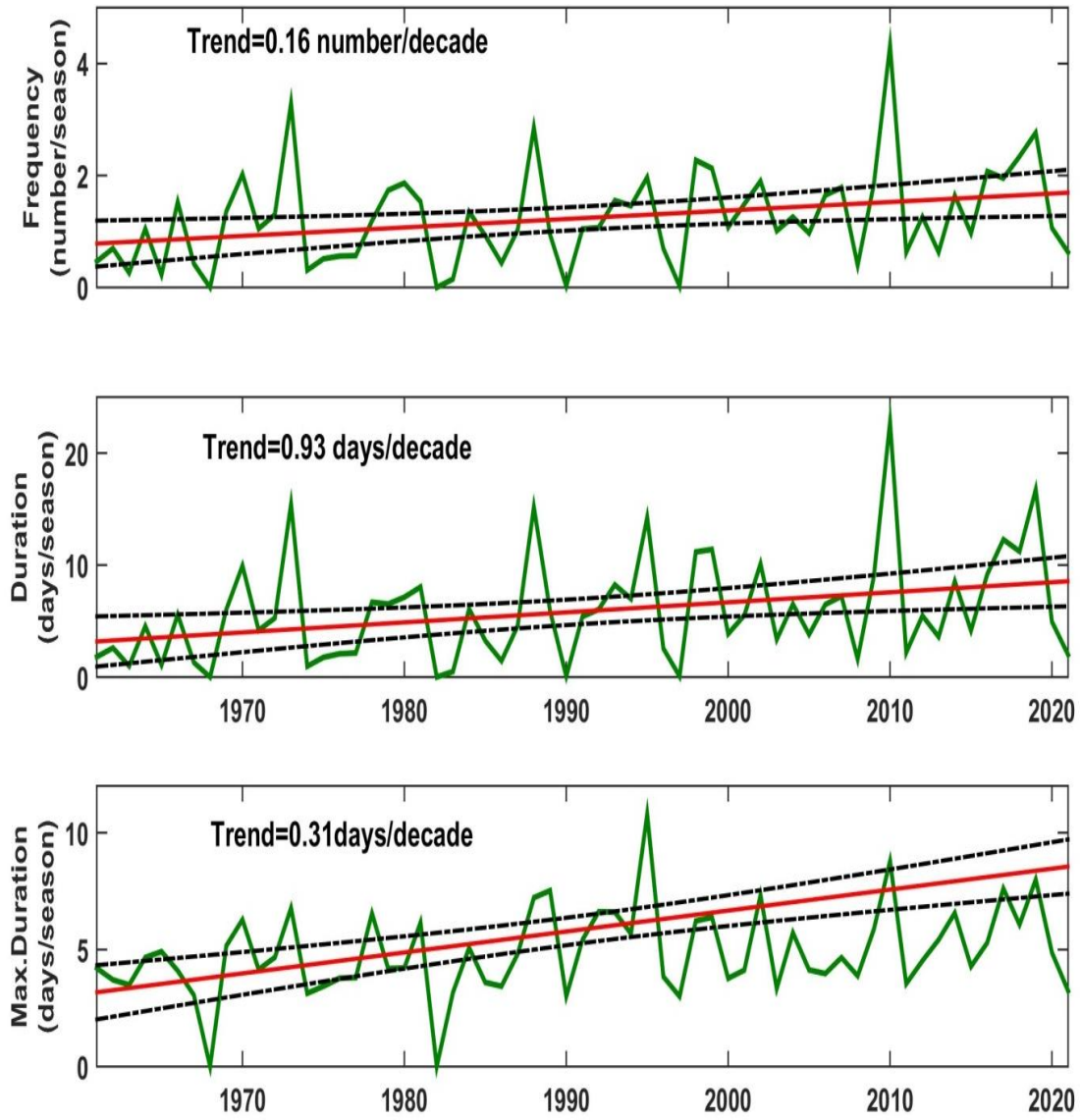

Fig 4.11. Time series of area averaged heat wave frequency, heat wave duration and heat wave maximum duration, averaged over northwest India (70E-78E, 22N-31N), based on 90th percentile criteria.

Fig 4.13 shows the time series of area averaged heat wave frequency, heat wave duration and heat wave maximum duration, averaged over northwest India (70^0 E-78^0 E, 22^0 N-31^0 N) based on the EHF criteria. Based on the EHF criteria also, there are increasing trends. There are long-term increasing trends of heat wave frequency,

duration and maximum duration over northwest India. However, the magnitude of the trends based on the EHF criteria is different from that based on the 90th percentile.

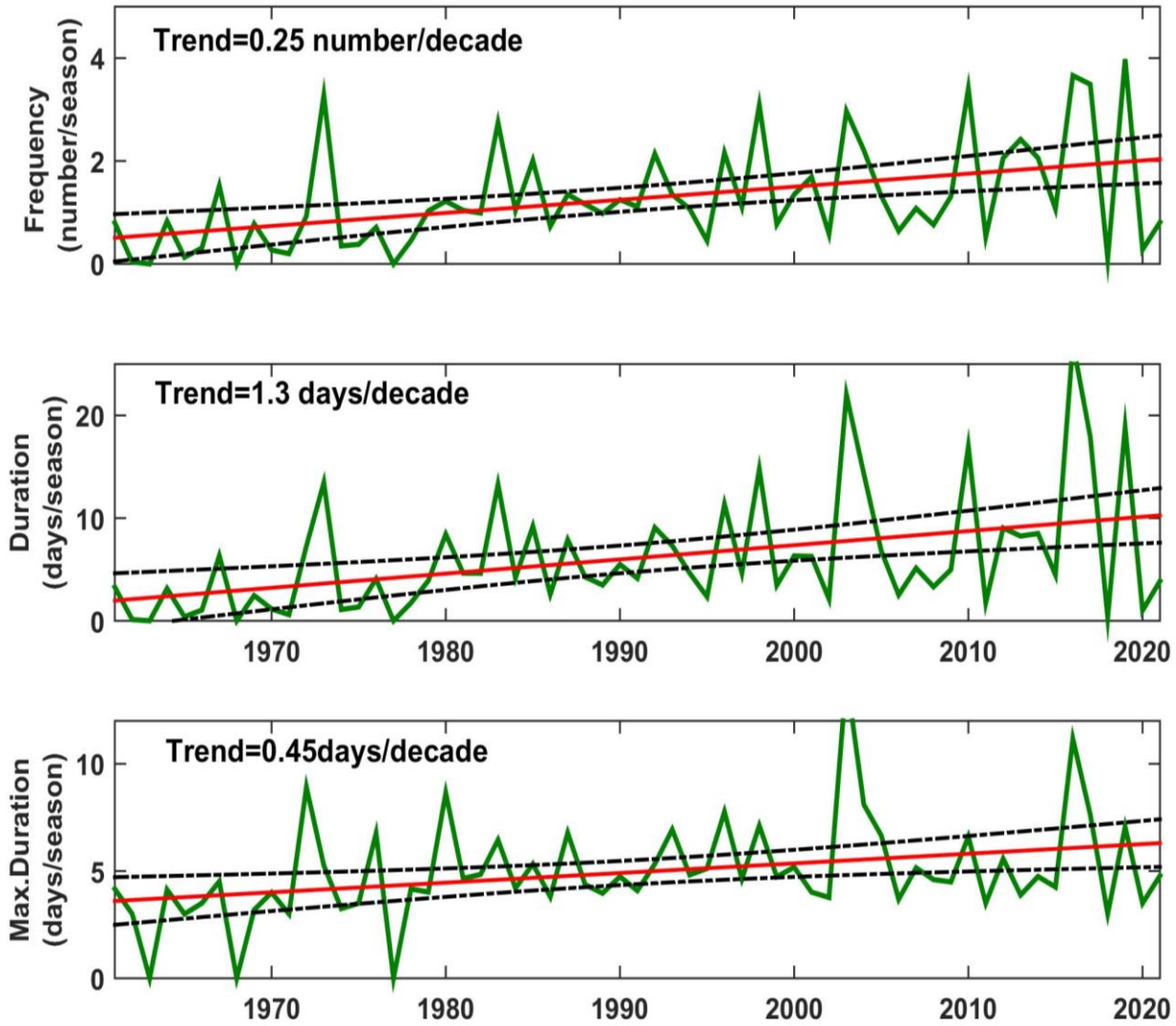

Fig 4.12. Time series of area averaged heat wave frequency, heat wave duration and heat wave maximum duration, averaged over Coastal Andhra Pradesh (12-16^{o} N, 78-81^{0} E), based on 90th percentile criteria.

Fig. 4.14 shows the time series of area-averaged heat wave frequency, heat wave duration and maximum heat wave duration averaged over the coastal region of Andhra Pradesh based on the EHF criteria. As in 90th percentile criteria, there are increasing

trends in the frequency, duration and maximum duration of heat waves in coastal Andhra Pradesh, though the magnitudes are different.

Sandeep and Prasad (2018) examined heat wave episodes over the east coast of India and their inter-annual variability. The heat wave episodes exhibit a significant intra-annual variability. Intensity of heat waves averaged over the east coast of India has shown an increase of 0.06^0 C per heat wave. The geopotential height anomaly, vertical velocity, and soil moisture exhibit significant intra-annual variability between the episodes and become decisive parameters for the maintenance and variability.

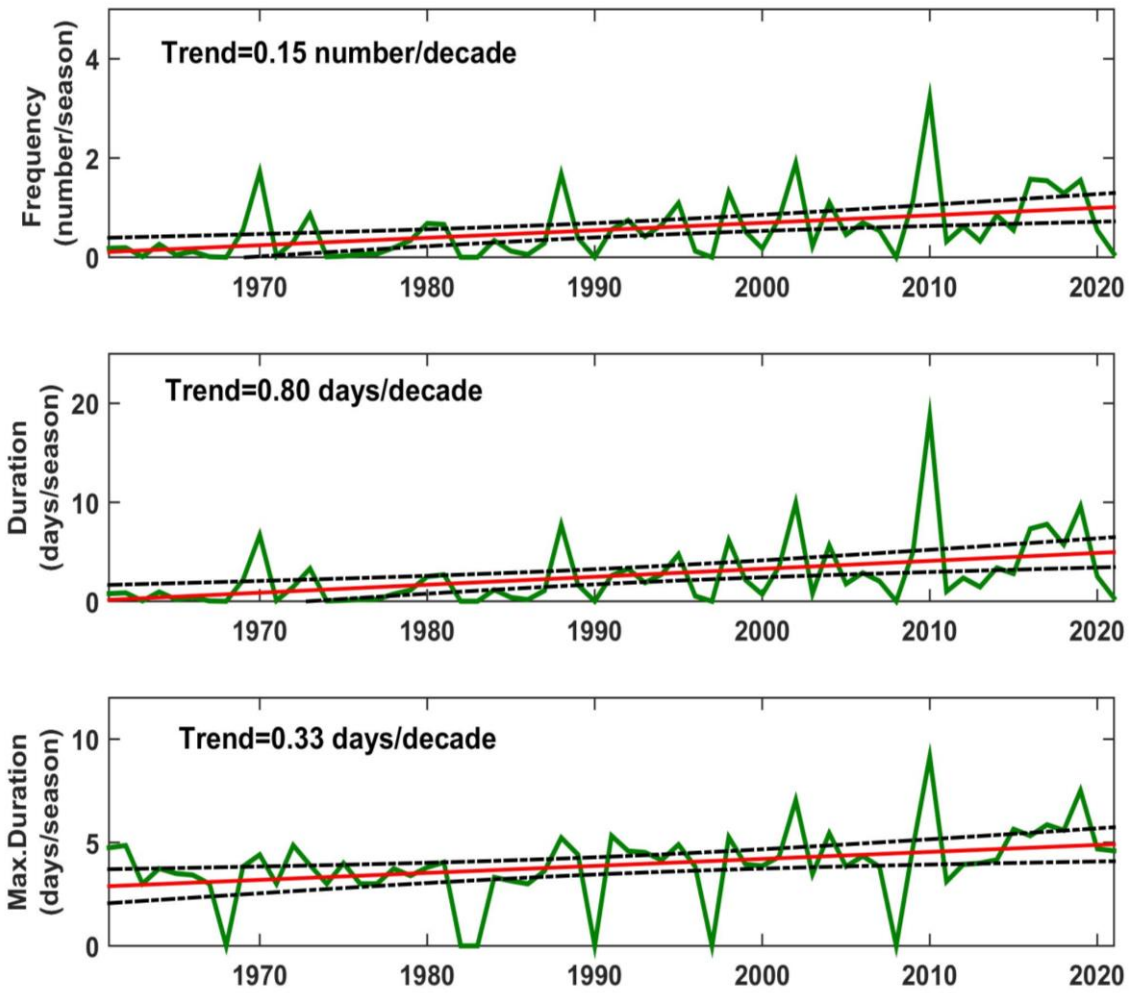

Fig 4.13. Time series of area averaged heat wave frequency, heat wave duration and heat wave maximum duration, averaged over northwest India (70^0 E-78^0 E, 22^o N-31^o N) based on the EHF criteria.

Table 4.1 shows a comparison of long-term trends of heat wave frequency, duration and maximum duration based on these two different criteria over northwest India and coastal Andhra Pradesh. In general, the trends based on EHF are lower than that based 90th percentile. The trends over east coast of India are relatively larger than the trends of heat waves over central and northwest India.

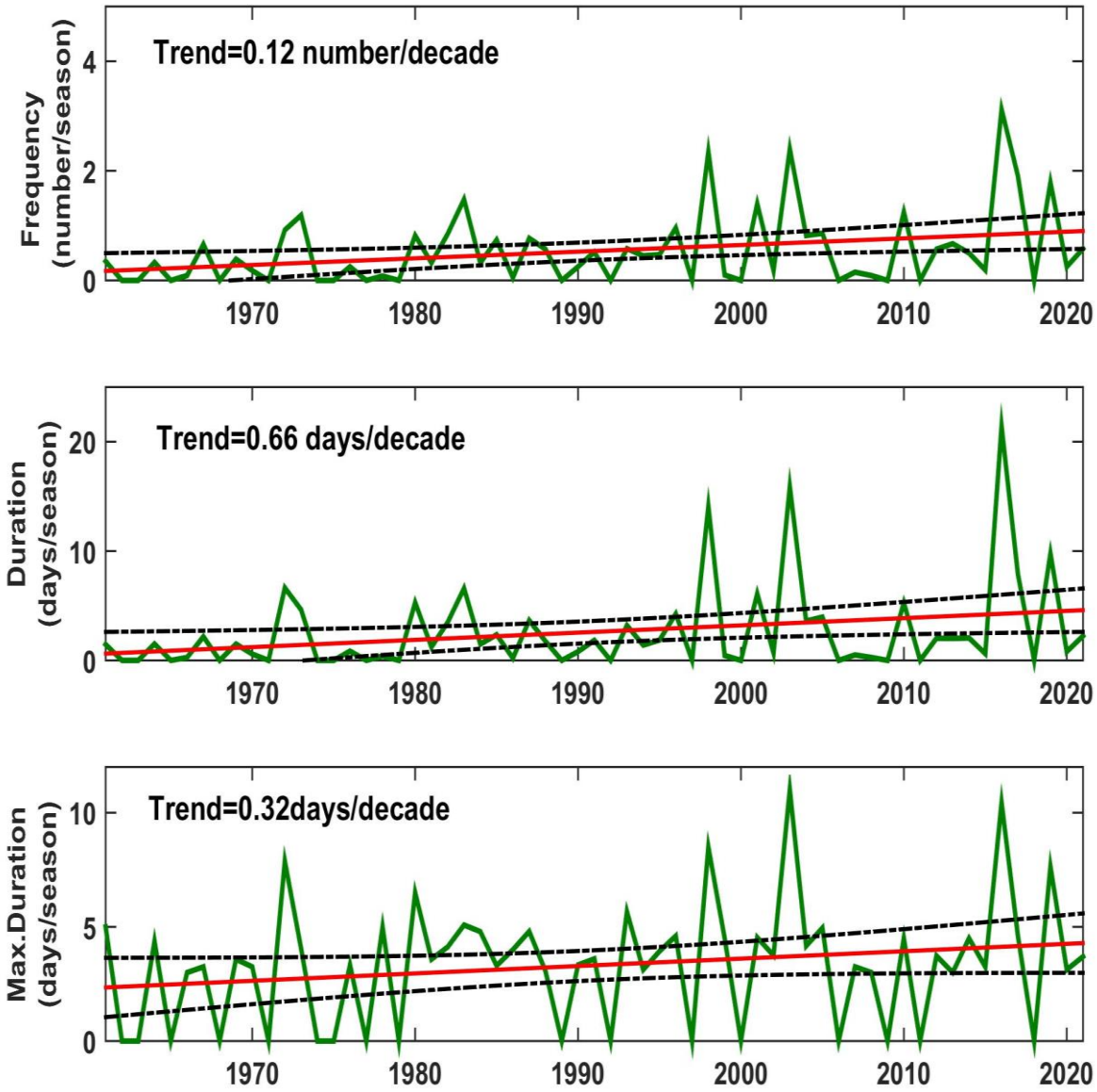

Fig 4.14. Time series of area averaged heat wave frequency, heat wave duration and heat wave maximum duration, averaged over Coastal Andhra Pradesh (12^0-16^0 N, 78^0-81^o E), based on EHF criteria.

Table 4.1

Long term trends of frequency, duration and maximum duration of heat waves over northwest India and coastal Andhra Pradesh

Area	Criteria	Frequency No/decade	Duration Days/decade	Maximum Duration Days/decade
Northwest India	90^{th} Percentile	0.16	0.93	0.31
	EHF	0.15	0.80	0.31
Coastal Andhra Pradesh	90^{th} Percentile	0.25	1.30	0.45
	EHF	0.12	0.66	0.32

Singh et al. (2021) analyzed long term trends of heat wave and severe heat wave events using IMD's gridded temperature data. The study found a spatio-temporal shift in the occurrence of heat wave events with a significantly increasing trend in three prominent heat wave prone regions that is northwestern, central, and south-central India, the highest being in West Madhya Pradesh (0.80 events/year), while a significantly decreasing trend was observed over Gangetic West Bengal (−0.13events/year). SHW events showed a southward expansion and a spatial surge during the decades of 2001–2010 and 2010–2016.

In order to obtain the relationships between the characteristics of the heat waves, the frequency (Fig.4.15 a) and intensity (Fig.4.15 b) of the heat waves are presented as a function of duration and mean areal extent. This analysis was carried out only for the heat wave prone area of northwest India, NWI (22°-31°N, 70°-77°E). Fig.4.15.a provides the probability of occurrence of heat waves per year based on the mean areal extent and duration. The most frequent heat waves (Fig.4.15.a. ~ 0.3 to 0.5 events per year, i.e. 16 to 27 events for 1961-2015) last 5 to 9 days with a mean intensity of about ~ 43°C. These heat waves have a mean areal extent of 15% to 30%. The moderately frequent heat waves (~0.2 events per year, i.e. 10 events for 1961-2015) have a duration of about 10 days with a mean intensity of 41°C and a spatial

extent of 25% to 40%. The rare heat waves (less than 0.1 events per year, i.e. 5 events for the period 1961-2015) have extremely high intensities (~45°C) and a longer duration (~ 9-20 days).

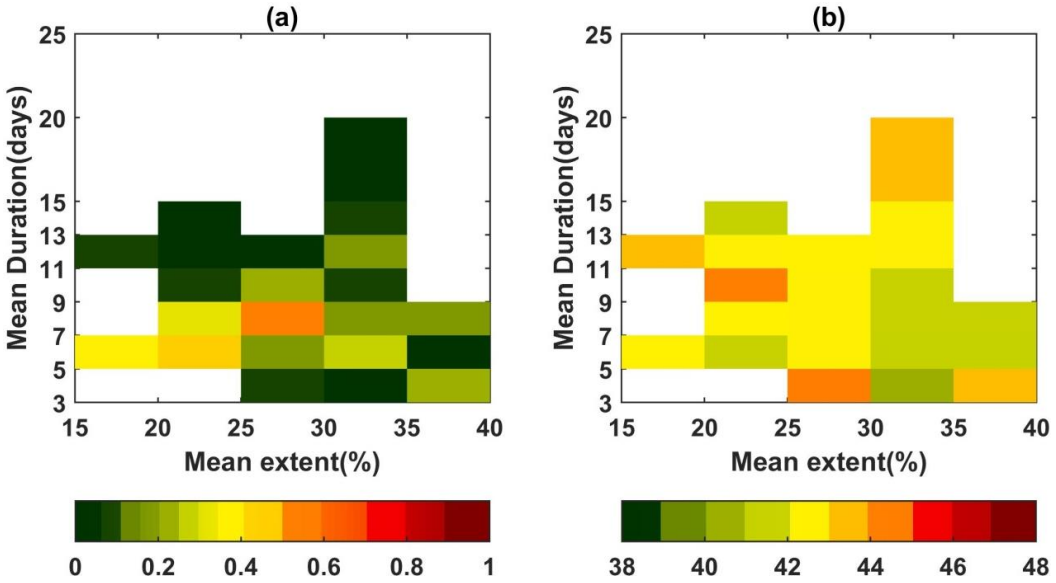

Fig. 4.15. (a) Heat wave frequency (events year^{-1}) as a function of mean areal extent and duration for AMJ season. For each bin, heat wave frequency is averaged over 1961-2015. (b) Heat wave mean intensity (°C) as a function of mean areal extent and duration. For each bin, mean intensity is computed as mean Tmax during heat wave events averaged over 1961-2015. (After Rohini 2020).

Table 4.2 shows the heat wave events over northwest India during the period 1961-2021, identified using the 90th percentile criteria and Table 4.3 shows the heat wave events over the coastal Andhra Pradesh during the period 1961-2021 based on 90th percentile criteria.

Table 4.2

Heat wave events over northwest India as per the 90th Percentile criteria during the period 1961-2021

Year	Date	Intensity(^{o}C)	Duration (days)
1970	23Apr-27Apr	42.8	6
	11May-18May	43.5	8
1973	20Apr-2May	42.4	13
	6May-10May	43.3	5
1978	9May-13May	42.8	5
1979	6Jun-10Jun	43.4	5
1980	18Apr-22Apr	41.4	5
1981	15Jun-23Jun	43.1	9
1984	23May-28May	43.4	6
1987	19Apr-23Apr	40.8	5
	26Jun-30Jun	41.6	6
1988	10-18APr	40.8	9
	8-15May	43	8
	26-31May	43.8	6
1989	12-23May	43.3	12

1992	16-21Jun	42.3	6
1993	3-8May	42.1	6
	8-12Jun	42.5	5
1994	29May-2Jun	44	5
1995	30May-9Jun	44.3	11
1998	21-28May	43.4	8
1999	8-12Apr	40.9	5
	29Apr-5May	42.5	7
2004	9-17Apr	40.6	9
2005	19-23Jun	41.8	5
2009	27Apr-1May	42.8	5
	20-27Jun	41.2	8
2010	8-20Apr	43.1	13
	19-26May	44.5	8
	19-23Jun	43.3	5
2013	18-24May	43.3	7
2014	4-11Jun	44.4	8

2016	15-21May	44.7	7
2017	12-21Apr	41.9	10
2019	29May-11Jun	44.5	14

Table 4.3

Heat wave events over the coastal Andhra Pradesh as per the 90th Percentile criteria during the period 1961-2021

Year	**Date**	**Intensity(^{o}C)**	**Duration (days)**
1967	1-9Jun	40.7	9
1972	5-14Jun	40.7	10
1973	26-30Apr	41.6	5
1976	2-7May	41.4	6
1980	19-28May	43.1	10
1982	2-6Apr	39.8	5
1983	1-21Mar	38.5	21
1984	22-27May	41.2	6
1985	23-28Apr	40.4	6
	1-5May	41.3	5
1987	7-15Apr	40.3	9

1990	20-26Apr	40.8	7
1992	5-10Apr	39.8	6
1996	8-18May	41.8	12
1997	29May-5Jun	41.3	8
1998	19-23Apr	40.5	5
	27May-5Jun	42.3	15
1999	12-16Apr	40	5
2000	26-30Apr	41	5
2001	10-14May	41.8	5
2003	18May-13Jun	43.1	26
2004	16Mar-26Mar	38.7	11
	14-20Apr	40.5	7
2007	15-21May	40.9	7
2010	1-7Apr	39.1	7
	9-14APr	39.7	6
2012	18-24Mar	38.1	7
2014	28Mar-1Apr	39.1	5
2016	18-22Mar	39.6	5

	1-7Apr	38.8	7
	11-17Apr	40.6	7
	19-26Apr	41.9	8
2017	30Mar-3Apr	38.7	5
	16-27Apr	40.5	12
2019	28Mar-3Apr	39.3	7
2021	30Mar-3Apr	39.9	5

4.3 Future projections of Heat Waves over India

In the earlier sections of the chapter, we discussed the observed long-term trends of heat waves over India. The frequency, duration and intensity of heat waves over India have shown an increasing trend over the last 50-60 years. Greenhouse gas emissions from fossil fuels are likely the cause of this observed trend in heat waves. In the future, greenhouse gas emissions from fossil fuels are likely to increase further. Logically, the next question is what might be the heat wave scenarios over India in the future climate.

Climate and Earth system models are the best tools available to understand future climate change under increased anthropogenic activities. Previous studies (Alexander and Arblaster 2009, Meehl and Tebaldi 2004) suggest that significant trends in temperature extremes in different parts of the world will continue into the twenty-first century. For heat waves over India, Rohini et al. (2019) examined nine CMIP5 models to understand how the frequency, intensity and duration of heat waves over India will increase due to increases in greenhouse gas emissions. They have considered the pre-monsoon season (April-June) for the analysis of heat waves as the frequency of heat waves that can affect human health is much higher during this season. The IPCC RCP4.5

scenario for the period 2024-2060 was used to assess future climate change scenarios. Long-term atmospheric circulation data are also used to understand future changes. Despite moderate variations in daily temperatures, the CMIP5 models showed a modest ability to realistically simulate the observed heat waves in terms of spatial pattern and frequency. The models suggest an increase of about two heat waves and an increase in the duration of heat waves by 12-18 days over the period 2020-2064.

In the future climate change scenario, the southern parts of India and the coastal areas of India, which are not currently affected by heat waves, are likely to be affected by heat waves. The spatial trend analysis of heat wave frequency (HWF) and heat wave duration (HWD) indicates that both HWF and HWD will increase significantly in central and north-western India, by 0.5 events per decade and 4-7 days per decade, respectively. Fig. 4.16 shows the observed and future changes in the frequency and duration of heat waves over northwest India as derived from 9 CMIP5 models and the multi-model ensemble model (MME). All CMIP5 models indicate a systematic increase in both the frequency and duration of heat waves over central and northwest India. According to the MME, northwest India could experience about 4 heat waves per season with a total duration of 30 days by 2060. This is a significant increase from the present climate.

As shown in Fig. 4.17, the future increase in heat waves is supported by the strengthening of the mid-tropospheric high and the associated subsidence over central and northwest India. Land surface processes such as soil moisture depletion and increased sensible heat fluxes are also responsible for the increase in heat waves. The CMIP5 models also suggest that El Nino Modoki events (with maximum warming over the central Pacific) may be responsible for the longer and more frequent heat waves over India in the future climate.

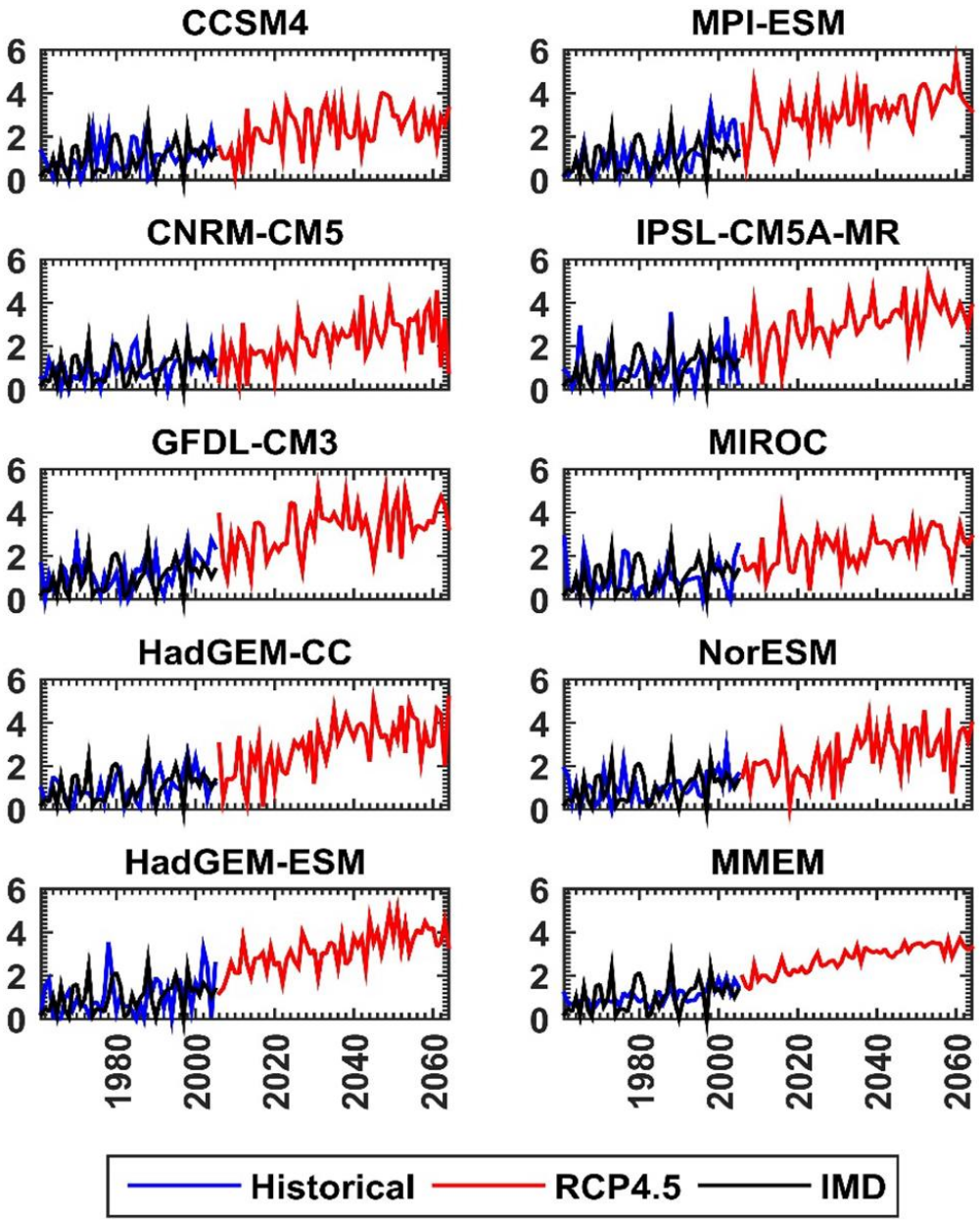

Fig 4.16 a. Time series of frequency (number/year) of heat waves averaged over the northwest Indian region 22^0-32^0 N, 70^0-78^0E as derived from observations and CMIP5 models. The IMD observations are shown in black colour. Model simulated frequency during the historical period (1961-2005) is in blue colour and future projection (2006-2064) is in red colour. (After Rohini et al. 2019).

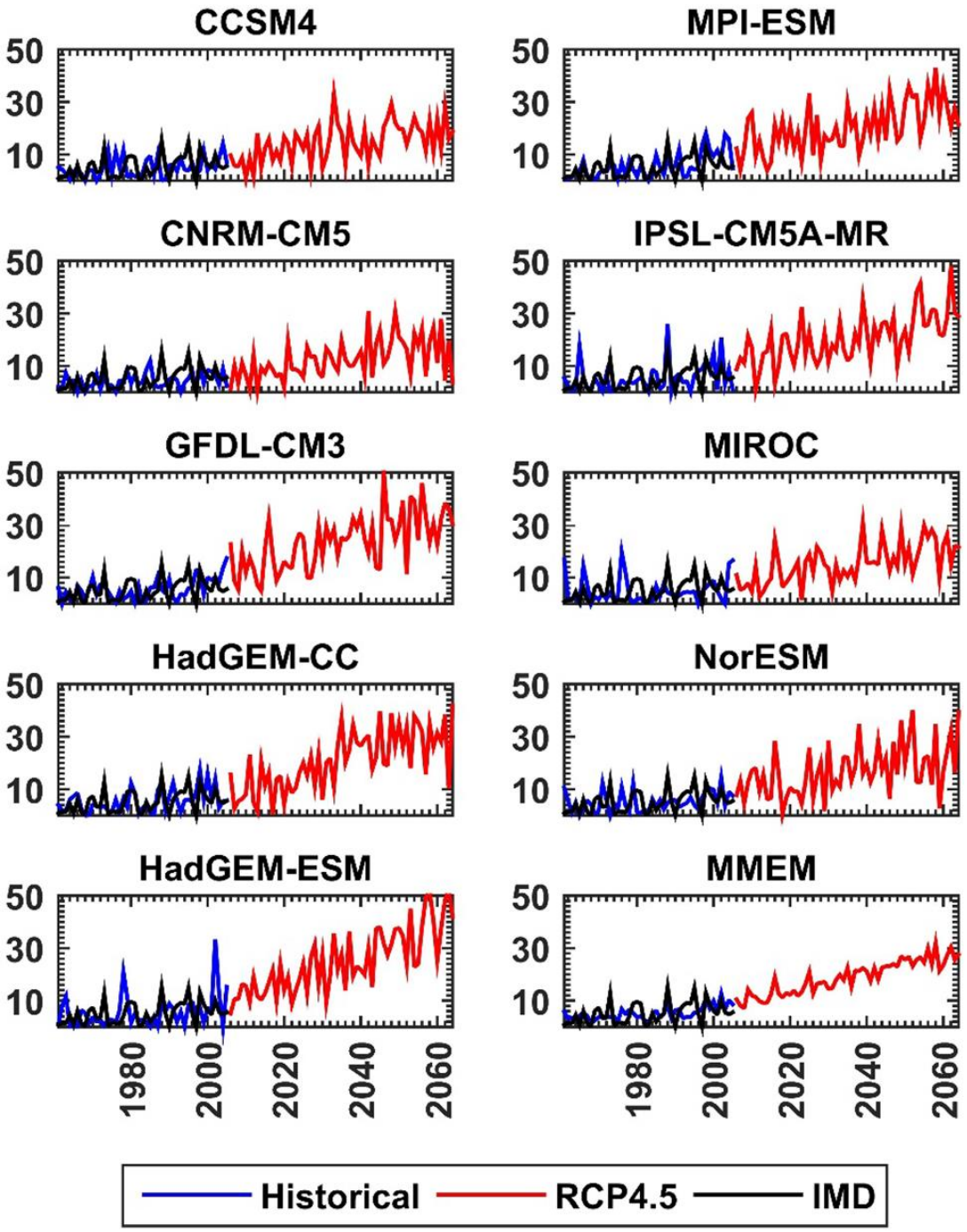

Fig 4.16 b. Time series of duration (days/year) of heat waves averaged over the region 22^0-32^0 N, 70^0-78^0E as derived from observations and CMIP5 models. The IMD observations are shown in black colour. Model simulated frequency during the historical period (1961-2005) is in blue colour and future projection (2006-2064) is in red colour. (After Rohini et al. 2019).

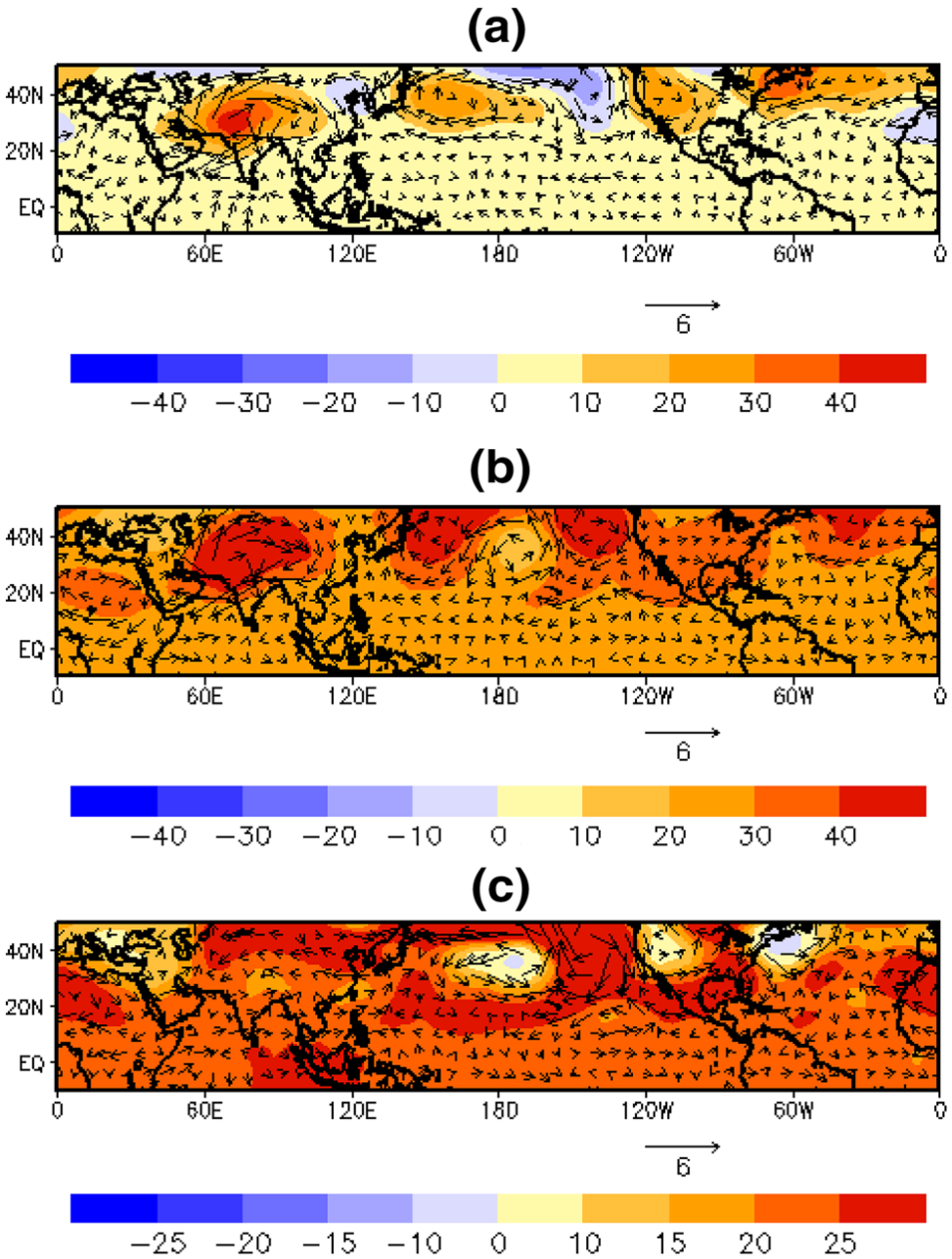

Fig 4.17. Composite anomaly of geopotential height (m) and wind vector at 500 hPa level from the CNRM-CM5 model during heat wave events a) historical period (1961-2005), b) future projection (2020-2064) and c) difference between future and present (Future-present). The period 1961-1990 was used as reference period for calculating the climatology.

Mishra et al. (2017) studied the exposure to heat waves in India in the current, 1.5^0C and 2.0^0C warming scenarios. They characterized the maximum potential exposure of people (without passive/active reduction measures) to severe heat waves in India. They showed that the frequency of severe heat waves will increase by 30 times the current climate by the end of the 21st century if the global average temperature is limited to 2.0^0 C above pre-industrial conditions. In contrast, the frequency under the RCP8.5 (business-as-usual" emissions) scenario will be about 2.5 times higher (than under the low warming scenario). Under the low warming target of 2.0^0 Celsius, population exposure to severe heat waves is projected to increase by 15 and 92 times current levels by the middle and end of the 21st century, respectively.

Mukherjee and Mishra (2018) used observations and model simulations from climate of 20th Century plus detection and attribution (D&A) and CMIP5 models to show that 1 and 3-day concurrent hot day and hot night (CHDHN) events have significantly increased. The frequency of 3-day CHDHN events is projected to increase 12-fold the current level by the end of 21st century and 4-fold by the mid-21st century under the high emission pathway of RCP 8.5. The increase in 3-day CHDHN be limited to only 2-fold by the end of 21st century under low emission scenario of RCP 2.6. Restricting global mean temperature below 1.5° from the pre-industrial level can substantially reduce the risk of 1 and 3-day CHDHN events and associated implications in India.

Ullah et al. (2022) examined projected heat stress and associated socio-economic stress in South Asia and its sub-regions using CMIP6 model data and GDP projections. They considered two common socio-economic pathways (SSP), namely SSP2-4.5 and SSP5-8.5, and three time periods: short-term, medium-term and long-term compared to the baseline period (1985-2005). The study found that the South Asian region has the potential for widespread changes in global wet bulb temperature (WBGT) of 6.50°C, which could exceed the theoretical limits of human tolerance by the mid-21st century. It

is noteworthy that the climate effect is more dominant than the population effect, while the changes in the GDP effect contribute to the overall change in GDP exposure.

Das and Umamahesh (2021) examined the future projection of heat waves over India using 13 CMIP5 and 12 CMIP6 model simulation data. The Heat Wave Magnitude Index (HWMI) was used to characterize heat waves over India. The study found that maximum temperatures are likely to increase in the future, leading to more intense, frequent and prolonged heat waves over India. Large regions in the south, northeast and west of the country, which are currently unaffected, are expected to be severely affected by heat waves.

Dubey et al. (2021) and Dubey and Kumar (2022) have undertaken an analysis of future projections of heat wave characteristics and dynamics over India using a high-resolution regional earth system model (ROM). The heat wave characteristics simulated by ROM are largely consistent with observations, although some discrepancies have also been noted. The typical synoptic features associated with heatwave days for the identified regions show the presence of an elevated geopotential height with an anomalous anticyclonic structure forming an atmospheric blockade over every region except the southeast coast. The projected frequency will double and the average duration will increase by 8-12 days per season by the end of the century. Severity will also increase by 2°-3 °C. Similarly, future dynamic features will be associated with an increase in geopotential height (thickness) and a gradual decrease in potential vorticity. According to the study, the frequency of heat waves will more than double by the end of the century in most regions except the Himalayas and the northeastern hills. The duration of heatwaves is also expected to increase by 8-12 days in most parts of the country. The severity of heat waves is also likely to increase by 2-30°C in the distant future.

Murari et al. (2015) examined intensification of future severe heat waves in India and their effect on heat stress and mortality. Their study revealed that heat waves are

projected to be more intense, have longer durations and occur at a higher frequency and earlier in the year. Southern India, currently not influenced by heat waves, is expected to be severely affected by the end of the twenty-first century.

There is therefore a general consensus that under future climate change, both the frequency and duration of heat waves are likely to increase significantly. Those regions where heat waves are not as frequent (such as the southern peninsula) are likely to be more affected in the future.

Chapter 5

Physical Mechanisms of Heat Waves

In the earlier chapters, we have discussed the observed climatology and long-term trends in heat and cold waves over India. There are systematic long-term increasing trends in heat waves (frequency, duration and intensity) over India. On the other hand, the frequency of cold waves is decreasing over the same period, suggesting that increase in temperatures is the main cause of these observed trends. Natural variability must also have played some role in modulating the frequency and intensity of heat waves. In this chapter, we discuss the physical mechanisms of heat waves in terms of large-scale dynamics and local or regional influences. The physical mechanisms of cold waves will be discussed in Chapter-6.

Heat waves are basically meteorological events, even when studied from a climatological perspective. Most heat waves last for about a week. The development of heat waves is caused by the synoptic environment and the interaction of large- and small-scale processes. Previous studies have shown that heat waves are usually associated with anticyclonic flows in the middle and upper troposphere that extend into the lower troposphere and dynamically lead to strong subsidence, clear skies, warm air advection and prolonged hot conditions at the surface (Black et al. 2004; Meehl and Tebaldi 2004; Perkin 2015). The blocking high (anticyclone) in the upper level, which blocks the passage of synoptic transients, has been responsible for many extreme heat waves, such as the 1995 Chicago heat wave (Meehl and Tebaldi 2004), the 2003 European heat wave (Black et al. 2004; Vautard et al. 2007; Vautard et al. 2013) and the 2010 Russian heat wave (Dole et al. 2011; Trenberth and Fasullo 2012). The persistent highs associated with the subtropical ridge are responsible for heat waves over Australia (Parker et al. 2014, Perkins 2015). In the Northern Hemisphere, the blocking/sustained highs responsible for heat waves are centred over the affected area (Black et al. 2004; Della-Marta et al.2007). Anticyclonic anomalies are often part of a large-scale stationary

Rossby wave pattern (Ratnam et al. 2016 a). Recent studies suggest that atmospheric Rossby waves have expanded meridionally in recent decades due to Arctic amplification (Francis and Vavrus 2012). These slower propagating Rossby waves in 500-hPa height fields favour heat waves (Francis and Vavrus 2012; Parker et al. 2014). All these studies suggest that the necessary ingredients of heat waves are persistent/blocking high-pressure systems (Perkins 2015 and reference therein).

Bedekar et al. (1974) while examining the heat waves over India found the following favourable factors for occurrence of heat waves.

a) Hot dry air should prevail over the concerned region
b) There should be a region of warmer dry air and an appropriate flow pattern for transporting the air over the region
c) There should be little or no moisture present in the upper air over the area
d) Sky should be practically cloudless to allow maximum insolation over the region.
e) The lapse rate should approach dry adiabatic in the airmass to allow warming to a considerable depth
f) There should be a large amplitude anticyclonic flow or thickness values should be considerably above normal in all layers.

Along with blocking/persistent high-pressure systems, the land surface processes also play a significant role in intensifying the heat waves (Alexander 2011; Hirschi et al. 2011; Mueller and Seneviratne 2012; Perkins 2015; Miralles et al. 2012, 2014). There are many observational as well as model simulated studies to understand the influence of land surface processes mainly on dry soil on heat wave across the globe (Diffenbaugh et al. 2005; Seneviratne et al. 2006; Seneviratne et al. 2010; Seneviratne et al. 2014; Fischer et al. 2007a, 2007b; Lorenz et al. 2010; Alexander 2011; Hirschi et al. 2011; Mueller and Seneviratne 2012; Nicholls 2012). Land surface processes affect extreme temperatures through changes in the lowest layer of atmospheric boundary layer.

The effects of soil moisture on temperature extremes are explained in Fig. 5.1 (taken from Alexander 2011). When the land surface is sufficiently moist, surface energy is balanced by the release of latent heat flux (Fig. 5.1a.) through evapotranspiration, which cools the surface and increases the concentration of water vapour in the atmosphere. This process leads to cloud formation near the surface. On the other hand, a dry soil increases the sensible heat flux (Fig. 5.1.b), resulting in a deeper, warmer and drier atmospheric boundary layer, which tends to inhibit cloud formation. Under dry conditions, an increase in sensible heat flux leads to warming of the near-surface atmosphere and creates a positive land-atmosphere feedback that tends to amplify heat waves (Alexander 2011).

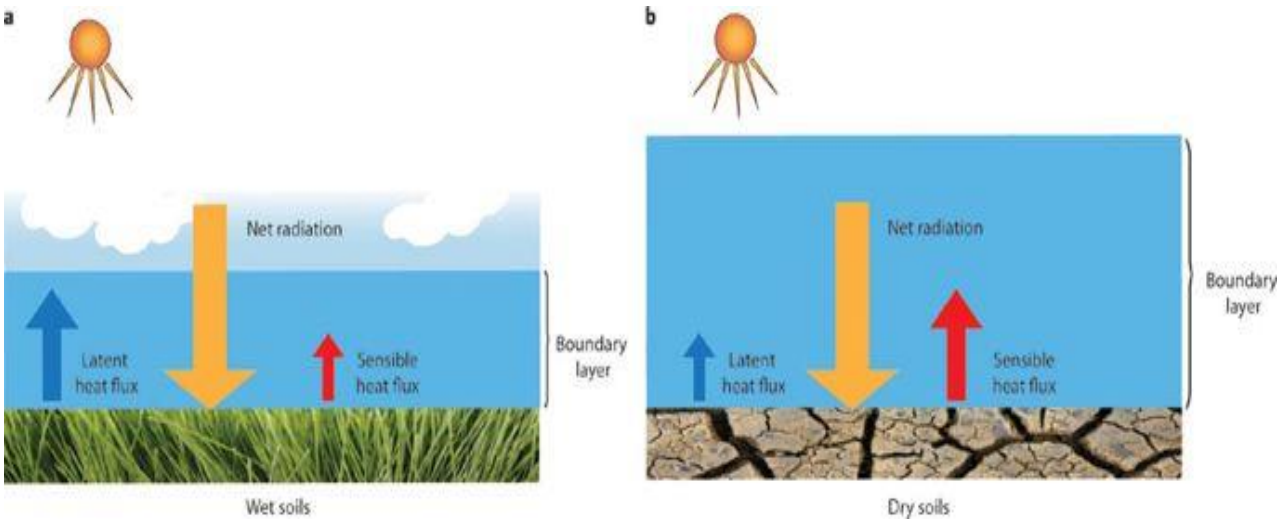

Fig. 5.1. Changes in the role of the land surface on temperature when soils are wet (a) and dry (b). A smaller boundary layer and sensible heat flux, and an enhanced latent heat flux occurs when soils are wet, however this is reversed under dry conditions. This explains in a simple context the coupling of drought and heat waves. Source (Taken from Fig. 1 of Alexander (2011)).

Variability in climate modes is another factor influencing heat waves (De and Mukhopadhyay 1998; Kripalani and Kulkarni 1999; Kenyon and Hegerl 2008; Alexander and Arblaster 2017; Arblaster and Alexander 2012; Hu et al. 2011, Hu et al. 2013; Wang et al. 2014; Rohini et al. 2016; Ratnam et al. 2016 a; Murari et al. 2016). Previous studies (Black and Sutton 2007; Alexander et al. 2007; Feudale and Shukla 2010) indicated the relationship between global sea surface temperature (SST) and heat waves. Variability in global SST anomaly patterns is important for modulating extreme temperatures (Alexander et al. 2007; Black and Sutton 2007).

A handful of studies investigated that climate mode variability, especially the El Nino/Southern Oscillation (ENSO), has a significant impact on extreme temperature events in many regions such as Europe, the Americas, Australia, India, China and South Korea, and Africa (De and Mukhopadhyay 1998; Kripalani and Kulkarni 1999; Kenyon and Hegerl 2008; Arblaster and Alexander 2012; White et al. 2014; Murari et al. 2016; Sun et al. 2016; Lee and Lee 2016; Luo and Lau 2019). However, the relationships between regional heat waves and ENSO depend on the mode phase, i.e. El Nino or La Nina (Arblaster and Alexander 2012; Luo and Lau 2019).

The Atlantic Multidecadal Oscillation (AMO) is a large-scale pattern of multidecadal variability in North Atlantic SST that has a significant impact on global and regional climate (Chylek et al. 2014). A study from the UK suggests that the AMO has an influence on variability in the frequency and duration of heatwaves (Sanderson et al. 2017). The AMO is also linked to the multi-decadal variability of summer heatwaves over Western Europe (Della-Marta et al. 2007). Over Australia, seasonal extreme temperatures are influenced by variability in climate modes such as ENSO, the Indian Ocean Dipole (IOD) and the Southern Annular Mode (SAM) (Nicholls et al. 1996; Min et al. 2013; Perkins 2015).

The impact of climate mode variability on heat waves in the Indian region is not well understood except for a few studies (De and Mukhopadhyay 1998; Pai et al. 2013;

Rohini et al. 2016, Murari et al. 2016). Murari et al. (2016) observed that warmer and prolonged heat waves occurred over India during the El Niño years. A better understanding of the physical drivers that lead to the occurrence of heat waves will be helpful for better predictability of these high-impact events.

5.1 Composite Analysis of Heat Waves over India

In this section, various aspects of the physical mechanisms of heat waves over India are discussed. To understand the physical mechanisms, a composite analysis has been carried out. For this purpose, a list of major heat waves that have occurred over NW India is provided. Then, a composite analysis of geopotential height and wind anomalies at 200 hPa and 500 hPa levels was carried out for the selected major heat wave events. The major heat waves were identified using the averaged daily maximum temperatures of an area (NWI, 22°-31°N, 70°-77°E, i.e. an area prone to heat waves) meeting the heat wave criteria (Tmax 90^{th} percentile criteria) for five consecutive days. The heat waves thus identified are listed in Table 5.1.

The wind anomalies averaged for these events at 200 and 500 hPa levels are shown in Fig.5.2 a and b, respectively. The composite anomalies indicate the presence of positive height anomalies and anomalous anticyclonic flow over the northern parts of India at the 200 hPa level, which also extends to the 500 hPa level. The composite also shows the presence of a quasi-stationary Rossby wave pattern with anomalous cyclonic and anticyclonic flow over the northern mid-latitudes. There is an anomalous blocking high over the North Atlantic and adjacent Europe and an anomalous low over central Asia. The anomalous high and associated anticyclonic flow is observed over the northern parts of India, the area where heat wave activity is predominant. The blocking highs prevent the mixing of cold polar air with warm tropical air, leading to surface warming.

Table 5.1

List of Severe Heat Wave Events over NW India

Year	Heat Wave Spell	Year	Heat Wave Spell
1967	23-29 Jun	1994	28 May-4 Jun
1970	23-27 Apr	1995	7-11 May,29 May-6 Jun
1971	8-12 Apr	1998	15-28May
1973	27Apr-2May	1999	6-12 Apr, 29Apr-4 May
1980	1-6 Jun	2002	1-8May
1981	15-23 Jun	2003	31May-5Jun
1987	18-23 Apr, 26-30 Jun	2005	18-22Jun
1988	13-18Apr, 6-14May	2006	4-8May
1989	15-23 May	2009	27 Apr-2 May
1991	31-7 Jun	2010	5-11 Apr,13-19 Apr,12-17May, 19-26May
1992	11-21 Jun	2012	2-10 Apr
1993	8-12 Jun	2013	17-23May

However, the anomalous high pressure over the northern parts of India is not associated with the classical blocking (as observed in the European heat waves), but with a subtropical high commonly referred to as a persistent high (Perkin 2015 and reference therein). The persistent high and associated anticyclonic flow in the middle and upper troposphere causes a sinking motion that leads to surface heating due to adiabatic compression. Fig.5.3 a shows the vertical velocity at 500 hPa, indicating a sinking motion (with positive values of omega) over the northern parts of the country.

These atmospheric conditions are also associated with depleted soil moisture (as shown in Fig.5. 3.b) and reduced precipitable water content over the northern parts of the country (Fig.5.3.c). These conditions are also combined with clear skies with large

positive anomalies of outgoing longwave radiation (OLR) (Fig.5. 3.d). Previous studies (Seneviratne et al. 2006; Fischer et al. 2007a, 2007b; Lorenz et al. 2010) showed that soil moisture-temperature interactions increase summer temperature variability, resulting in extreme temperatures when soil moisture is low. Reduced soil moisture leads to reduced latent heat transfer into the atmosphere, but enhanced sensible heat transfer induces positive feedback between atmospheric heating and further drying of the soil. A dry soil moisture condition along with persistent high (anticyclone) amplifies the positive feedback and enhances surface warming.

To further understand the occurrence of heat waves, an analysis was made from 5 days prior to the onset of heat wave up to the last day of heat wave and each event has been analyzed individually. Since duration of each heat wave events are different, for making a composite, 5 days from the onset date were considered. However, the entire duration was considered for the analysis of individual events. Composite analysis using ERA-Interim data set is presented here.

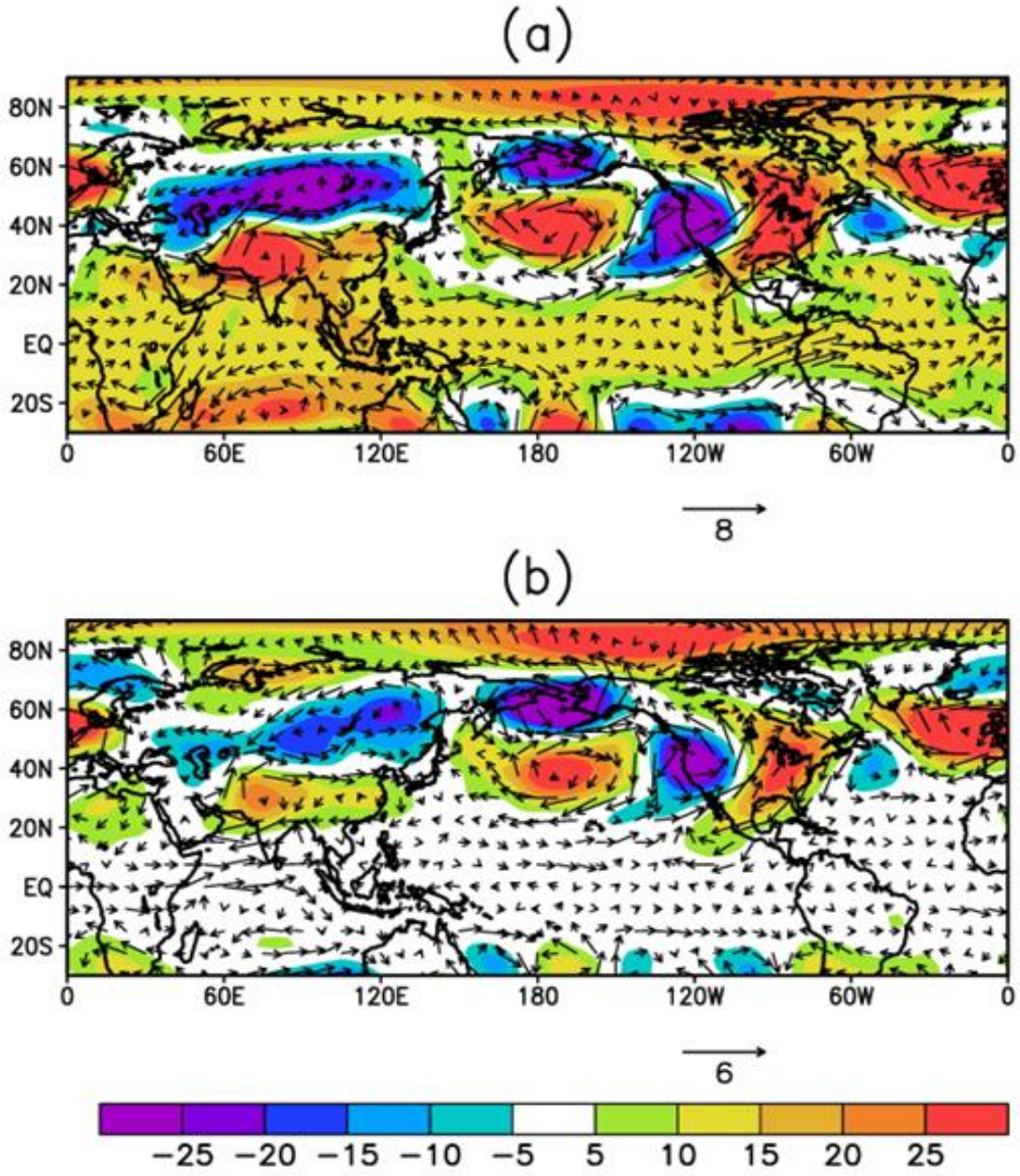

Fig 5.2. Composite anomalies of geopotential height (gpm) and vector winds at (a) 200 hPa level and (b) 500 hPa level during the major heat wave events. The major heat wave events are given in Table 5.1. The geopotential height in gpm is shown as shaded and the winds are shown as vectors (Taken from Rohini 2020).

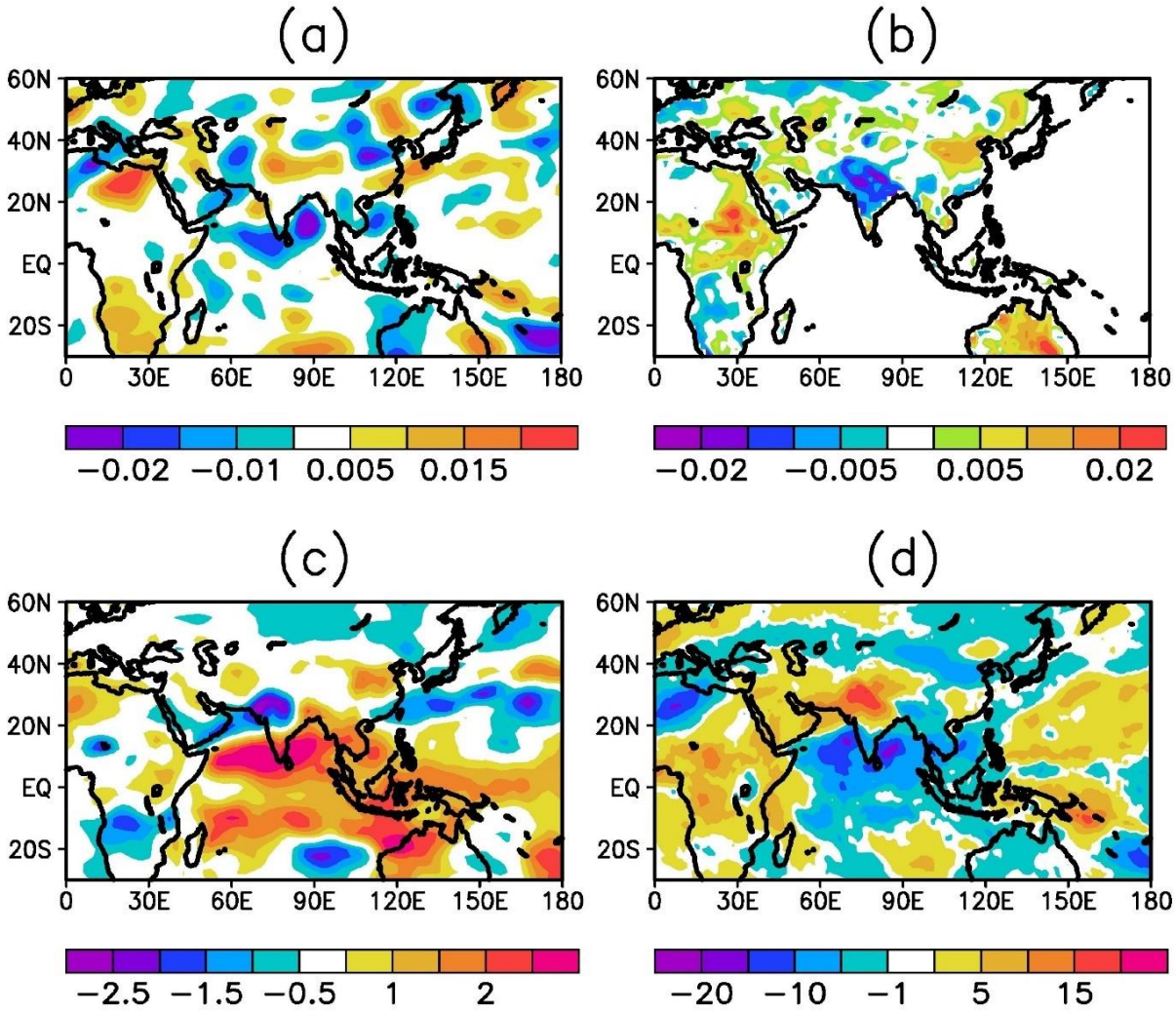

Figure 5.3. Composite anomalies of (a) 500 hPa Omega (Pa sec^{-1}) (b) Soil Moisture (fraction) (c) columnar precipitable water (Kg m^{-2}) and (d) Outgoing Long wave Radiation (W m^{-2}) during the major heat wave events (Table 5.1). (Taken from Rohini 2020).

The analysis suggests that the slowly developing mid-tropospheric anticyclone is the main synoptic component of the heat wave over India. It starts developing over North Africa and Saudi Arabia, 5 days before the onset of the heat wave, and is established over India by the 2nd day of the heat wave (Fig.5.4). The composite anomaly of Tmax and Tmin during each day of the heat wave is shown in Fig.5.5. Both Tmax and

Tmin show an increase in temperature (Fig.5.5) during the development of the anticyclone (Fig.5.4). The adiabatic compression of the air by the anticyclone contributes to the high surface temperatures during the heat waves over NWI. A large positive anomaly (> 1.5°C) of Tmin is observed from the first day of the heat wave over NWI (Fig.5.5). Elevated Tmin does not allow the necessary nighttime cooling to compensate for the high Tmax during heat waves (De et al. 2005). The analysis of all heat wave events shows that the occurrence of these events depends mainly on the anticyclones of the middle and upper troposphere. A similar analysis as in Fig. 5.5, as well as a time series analysis over NWI (heat wave prone area) was performed for each dynamic and physical parameter (such as wind, geopotential height, omega (vertical velocity), sensible heat flux, latent heat flux, soil moisture, OLR, net shortwave and net longwave radiation). This analysis shows that each event is influenced by large-scale dynamics. However, the influences of regional factors such as land surface processes vary from event to event. Therefore, the composite analyses (as in Fig.5.5) of these parameters are not shown here. However, the analyses of the individual events show that the amplified events are largely influenced by land surface processes.

A detailed analysis of the surface energy budget and the dynamics of the large-scale currents associated with these heatwave events showed that land surface processes do not necessarily play a dominant role in all events, except for the more intense events. Therefore, only the most intense events are considered for the analysis of the surface energy budget, discussed in the next section, 5.2.

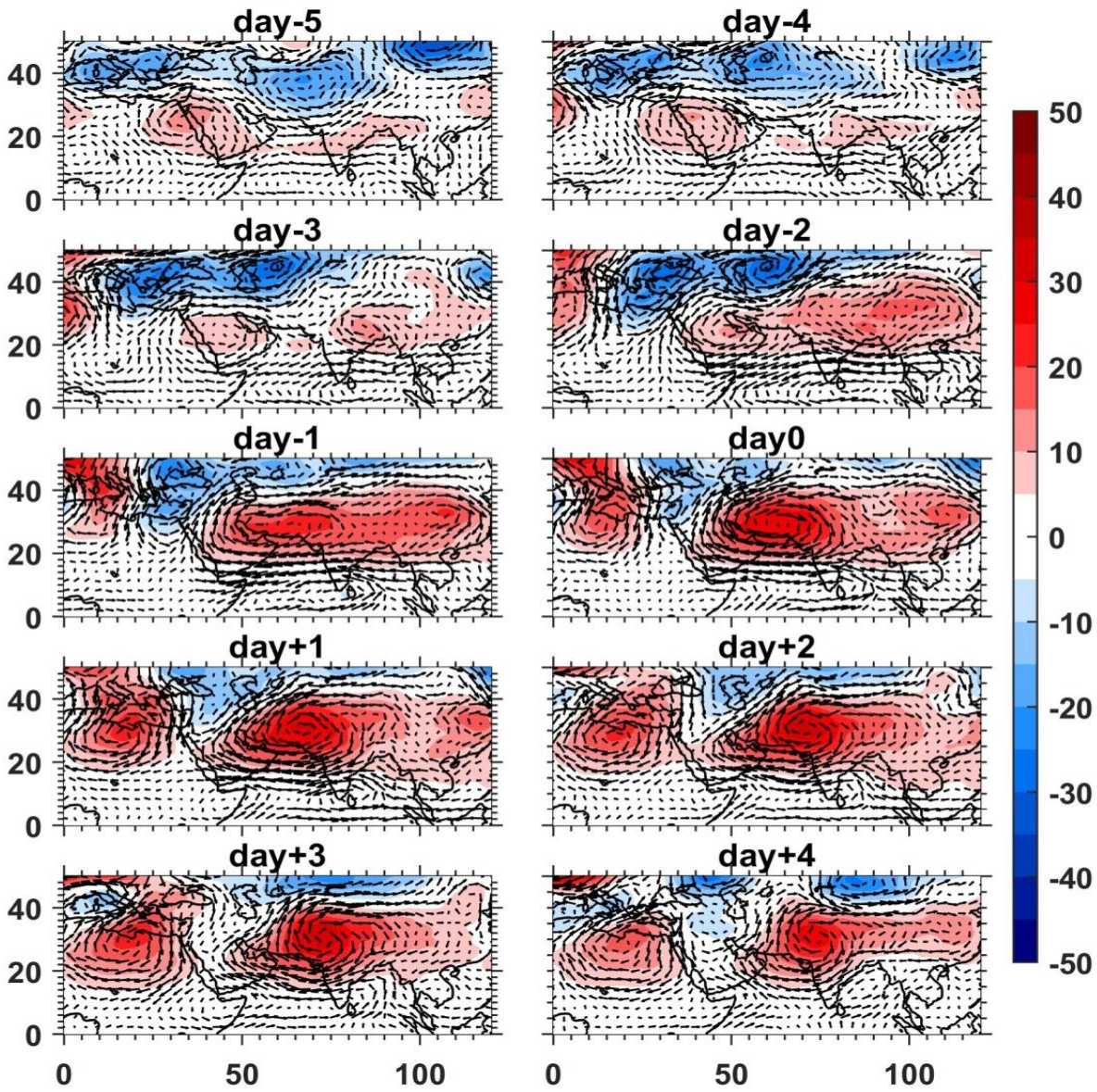

Fig. 5.4 Composite anomalies of geopotential height (m) and vector winds at 500 hPa level from 5 days prior to, to day 5 of heat wave event.

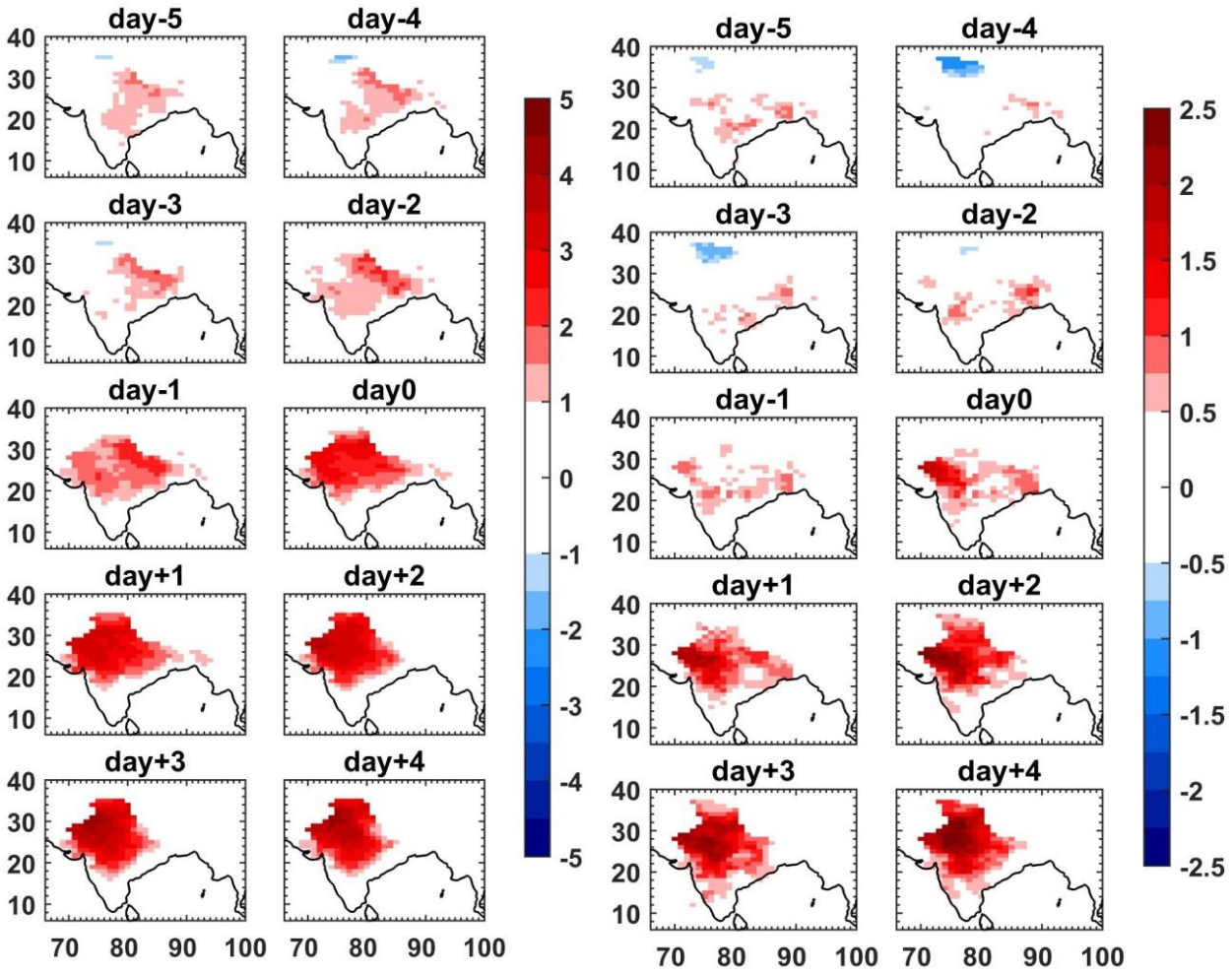

Fig. 5.5 Composite anomalies of Maximum temperature (Tmax °C; Left panel) and Minimum temperature (Tmin °C; Right panel) from 5 days prior to, to day 5 of heat wave event.

5.2 Analysis of Surface Energy Budget during heat waves

The physical processes which affect the surface radiation budget are also responsible for the temperature variations (Zhang et al. 2011). Surface temperature (T) variation with respect to time is expressed as follows (Oueslati et al. 2017)

$$c_s \frac{\partial T}{\partial t} = \Delta SWR + \Delta LWR + \Delta SH + \Delta LH$$

where C_s is the surface layer heat capacity, SWR is net shortwave radiation at surface, LWR is net long wave radiation at surface, SH is the surface sensible heat flux, and LH is the surface latent heat flux.

Based on 13 severe heat waves (Table 5.2), a composite analysis was performed based on ERA reanalysis data. Heatwave events were identified based on daily maximum temperatures averaged over the area (22°-31°N, 70°-77°E) that met the heatwave criteria (Tmax90 criteria). The role of surface radiation fluxes (shortwave and longwave radiation) and turbulent fluxes (sensible and latent heat fluxes) in modulating temperature during heatwave events was investigated. The results are shown in Fig.5.6.

Table 5.2

List of 13 severe heat wave events over NWI, used for composite analysis of surface energy budget analysis

Year	**Heat wave Spell**	**Year**	**Heat wave Spell**
1981	15-23 Jun	2003	31May-5 Jun
1988	6-14 May	2005	18-22 Jun
1989	15-23 May	2006	4-8 May
1993	8-12 Jun	2010	12-17 May, 19-26 May
1998	15-28 May	2013	17-23 May
1999	29 Apr-4 May	2014	2-11 Jun

Positive net shortwave radiation anomalies (SWR; Fig. 5.6.a) are observed in the northern and central parts of India during heat waves. This shows that the incoming solar radiation reaching the earth's surface is higher during these periods due to absence of clouds (Fig. 5.6.b). Earlier it was discussed that heat waves over India are

associated with an anomalous persistent high with anticyclonic flow complemented by clear sky and depleted soil moisture. The cloudless sky during the heat wave increases SWR at the surface, which in turn increases the anomalies in warm surface temperature. Strong negative net longwave radiation (LWR) anomalies, considered positive downward; Fig. 5.6.b) are observed in heatwave-prone areas, indicating that more infrared radiation is emitted from the Earth's surface into the atmosphere as the surface temperature increases due to stronger solar radiation. Positive SWR and negative LWR values indicate the absence of clouds over this region, which is due to anticyclonic conditions in the upper air.

Turbulent flow anomalies at the surface play an important role in intensifying the heat waves. During heat waves over northwest India, less precipitable water and lower soil moisture (Fig. 5.6.b and c) are observed. This condition leads to a decrease in evapotranspiration at the surface, which could further reduce the latent heat flux at the surface (Fig. 5.6.d) and increase the air temperature at the surface over this region. The LHF anomalies at the surface result from the anomalies in wind speed at the surface and the difference in specific humidity between the surface and the air at 10 m height. Negative latent heat flux anomalies (Fig. 5.6.d) are observed over northwest India during the heat wave.

To achieve the surface energy balance (Bowen Ratio) in dry soil, the hot land surface releases a large amount of sensible heat flux (SHF) during these events. Positive SHF anomalies at the surface (Fig. 5.6.c) occur as a result of the higher surface temperature due to the increased SWR at the surface in the absence of clouds together with the lower soil moisture. Increased SHF at the surface results in a deeper, warmer and drier atmospheric boundary layer (Fig.5.7 a), which together with the upper anticyclonic condition tends to inhibit cloud formation. An increase in SHF at the surface contributes to the warming of the near-surface atmosphere and creates a positive land-atmosphere feedback that tends to amplify and prolong heat waves.

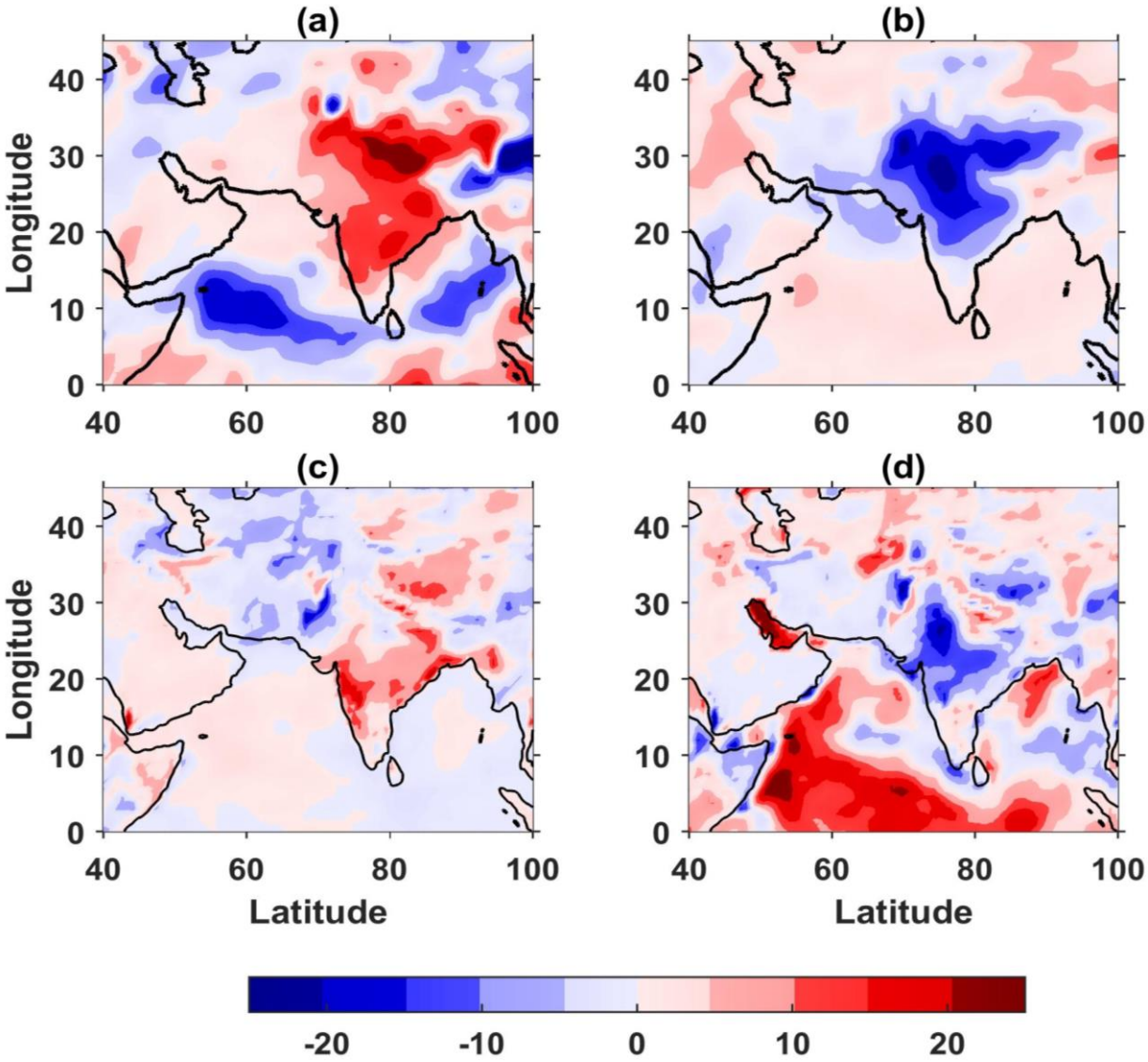

Fig. 5.6. Composite anomalies of (a) surface net short wave radiation (SWR; W m^{-2}) and (b) surface net long wave radiation (LWR; W m^{-2}) (c) surface sensible heat flux (SHF; W m^{-2}) (d) surface latent heat flux (LHF; W m^{-2}) during heat wave events mentioned in Table 5.2. Radiative fluxes (SWR and LWR) are counted positive downward. Turbulent fluxes (SHF and LHF) are positive upward.

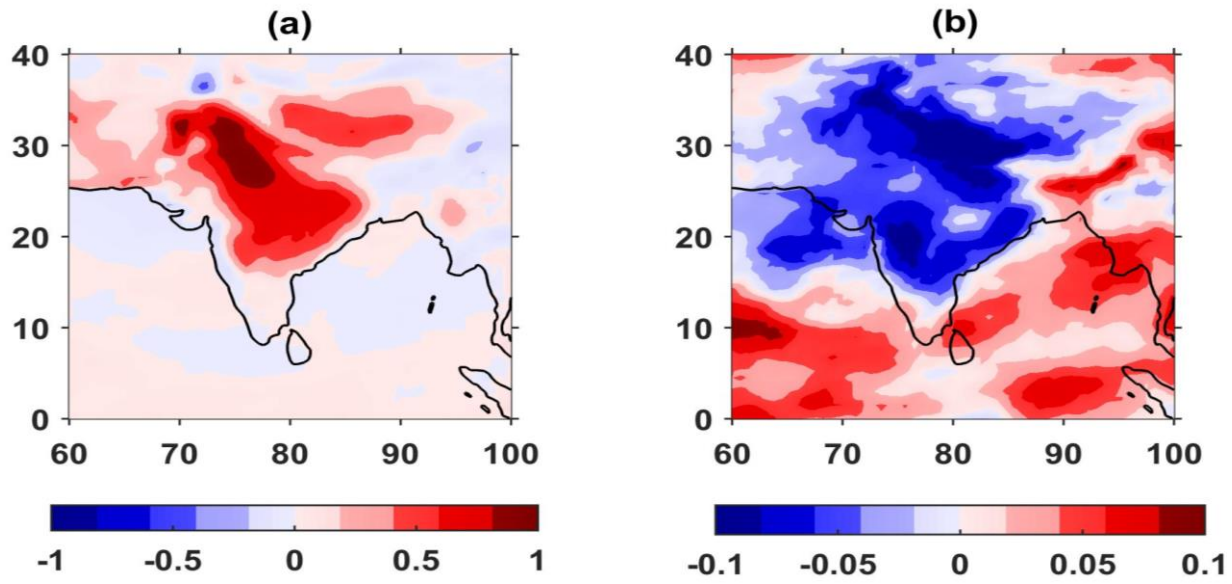

Fig. 5.7. Composite anomalies of (a) Maximum PBL height (Km) (b) Total cloud cover during heat wave events mentioned in Table 5.2.

5.3 Dynamical factors influencing heat waves over northwest India

To understand the dynamics of large scale flow associated with the occurrence of heat waves over India, a composite analysis of various dynamical parameters from Era Interim reanalysis was made with all heat wave events having minimum 5-day duration during the period 1981-2015. The results of the composite analysis are shown in Fig 5.8.

An area of large positive temperature anomaly at 850 hPa (Fig.5.8 b) extends over northern and central India, indicating prevailing heat wave conditions. During heat waves, the positive temperature anomalies extend even into the lower troposphere. The sea level mean pressure anomalies (Fig.5.8 a) show an anomalous low pressure area over the Indian landmass over NWI, indicating that northerly and northwesterly winds

bring more dry air to this region (Fig.5.8 c). The negative pressure anomalies also indicate higher surface air temperatures over the region. The dryness of the atmosphere over this region is also evident from the specific humidity anomalies at 850 hPa and 925 hPa (Fig.5.9). The composite analysis of the synoptic features suggests that a slow-moving transient anticyclone extending to 850 hPa in the lower troposphere with a heat low (Fig.5.8c) at the surface accompanied by a northerly to northwesterly flow and a deep layer of warm air are the general dynamic features of the heat waves over northwest India.

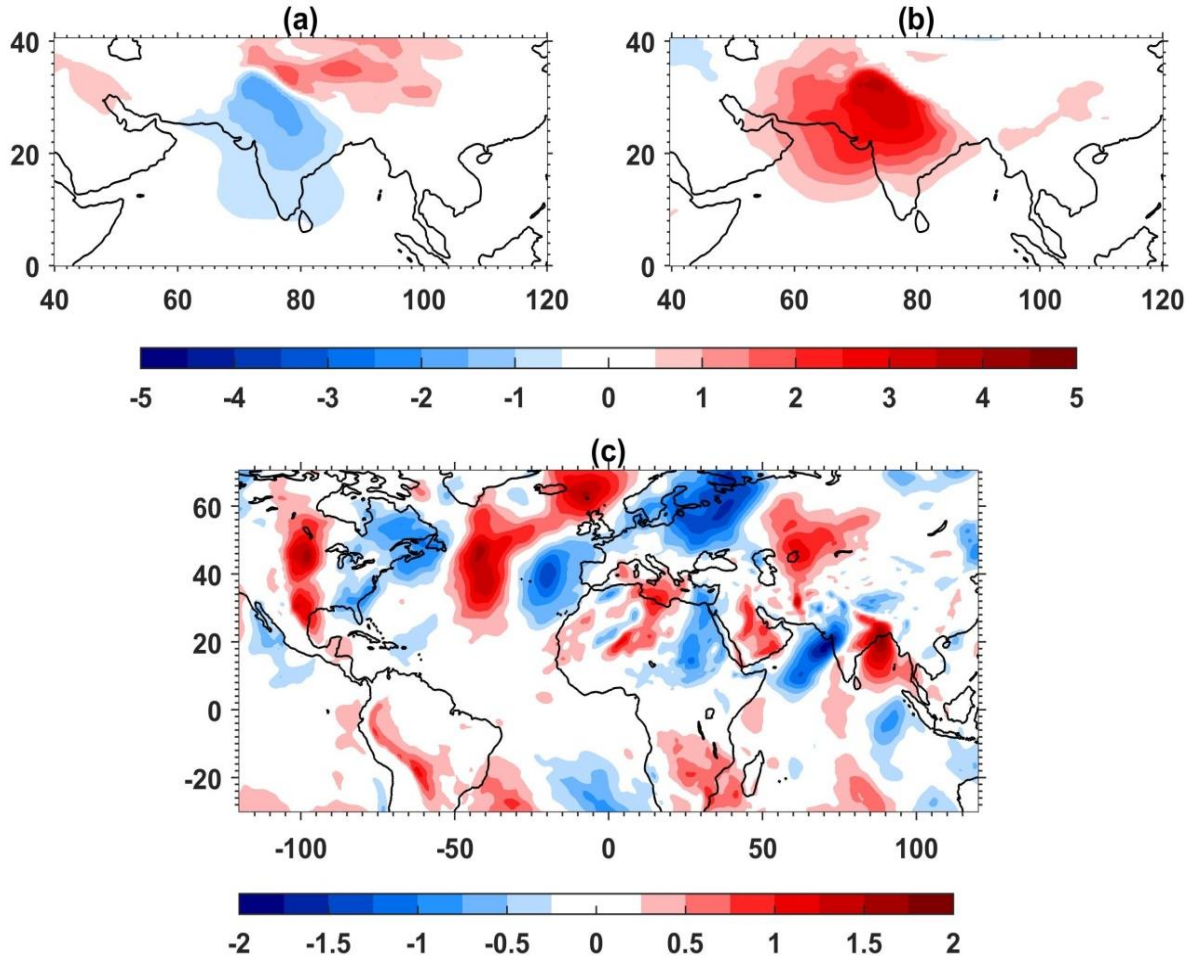

Fig. 5.8. Composite anomalies of (a) Mean Sea Level Pressure (MSLP; hPa), (b) 850 hPa temperature (K) (c) 850 hPa meridional wind (m s^{-1}) during heat wave events.

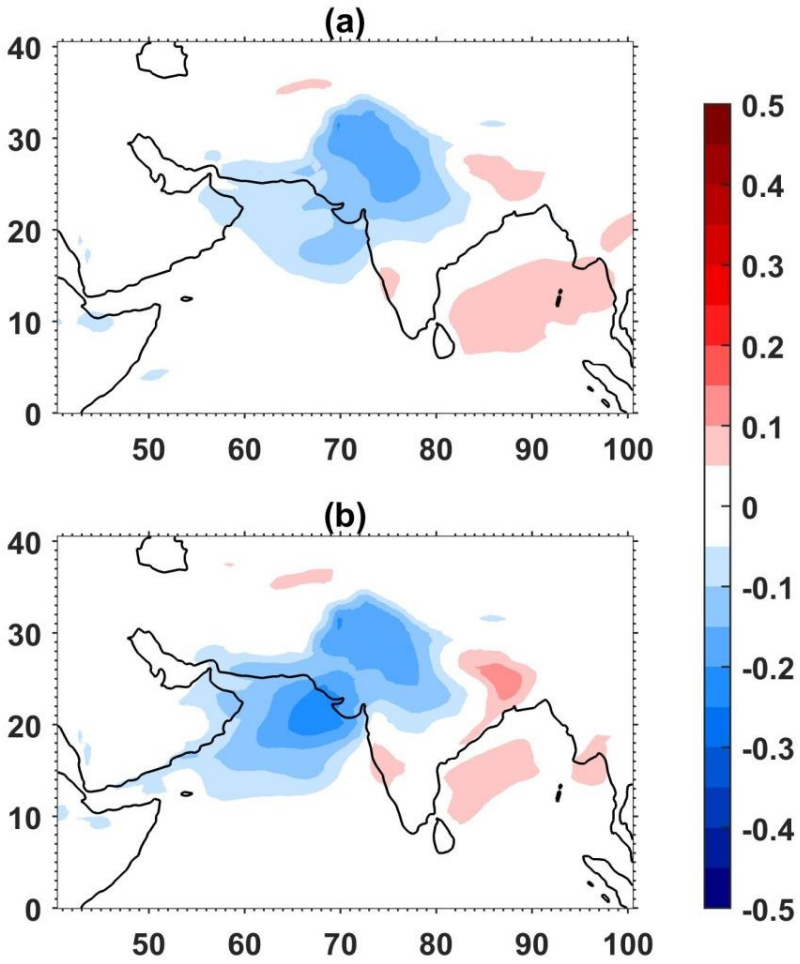

Fig. 5.9. Composite anomalies of Specific Humidity (kg kg^{-1}) at (a) 850 hPa (b) 925 hPa during the heat wave events.

Ratnam et al. (2016 a) found that the anomalous anticyclone observed over India during the heat wave is part of a quasi-stationary wave propagating from northwest Africa and related to blocking over the North Atlantic. The evolution of the 350-K potential vorticity (PV) anomaly from 4 days before the onset of the heatwave to the third day of the heatwave is shown in Fig.5.10. It gives an idea of the propagation of the atmospheric waves that led to the development of the heat wave over India. The anticyclonic PV develops slowly over Iran from the 2nd day before the heat wave and has developed over India on the 2nd day of the heat wave. Rathnam et al. (2016 a) suggested

that the expansion of cyclonic vorticity over western North Africa creates a source of anomalous Rossby waves near the entrance of the African Jet at 200 hPa, which in turn leads to the formation of an anomalous anticyclone over NW India. During heat waves, these Rossby waves increase in amplitude, move eastward and become established over NW and central India by the 3rd day of the heat wave (Fig. 5.10). The anomalies of 250-hPa meridional winds (Fig.5.11) also show the presence of a Rossby wave. Strong westerly winds during the AMJ season (Fig.5.11) can lead to the eastward propagation of these Rossby waves. The formation of an upper-level anticyclonic PV anomaly over northwest India indicates local dynamic conditions consistent with those responsible for the formation of heat waves over India.

The Hovmöller diagram (time-length diagram) of the 350-K PV anomalies and the 250-hPa meridional wind anomalies from 12 days before the onset to 7 days after the end of all heat waves (see Fig. 5.12) shows the mean propagation of the wave packets. 350-K PV anomalies and 250 hPa meridional wind anomalies are averaged over latitude 28°-32°N to produce Hovmöller diagrams. About 3-4 days before the onset of a heatwave, the mean high pressure area in this latitude band is most pronounced over 50°-65°E and moves eastwards. From 3 days before the onset of the heat wave, the dry regions (Pakistan, Afghanistan, Kuwait, etc.) are dominated by an area of high pressure. Up to 5 days after the end of the heatwaves, the entire latitudinal belt (28°-32°N) is dominated by an anticyclonic 350-K PV anomaly over longitude 60°E-100°E. Hovmöller diagrams of these two parameters (250 hPa meridional wind anomalies and PV anomalies) show a similar evolution of the wave packets, with wavelengths of about ~ 6000 km and a phase velocity of about ~ 8 m s-1 (values calculated from the graph).

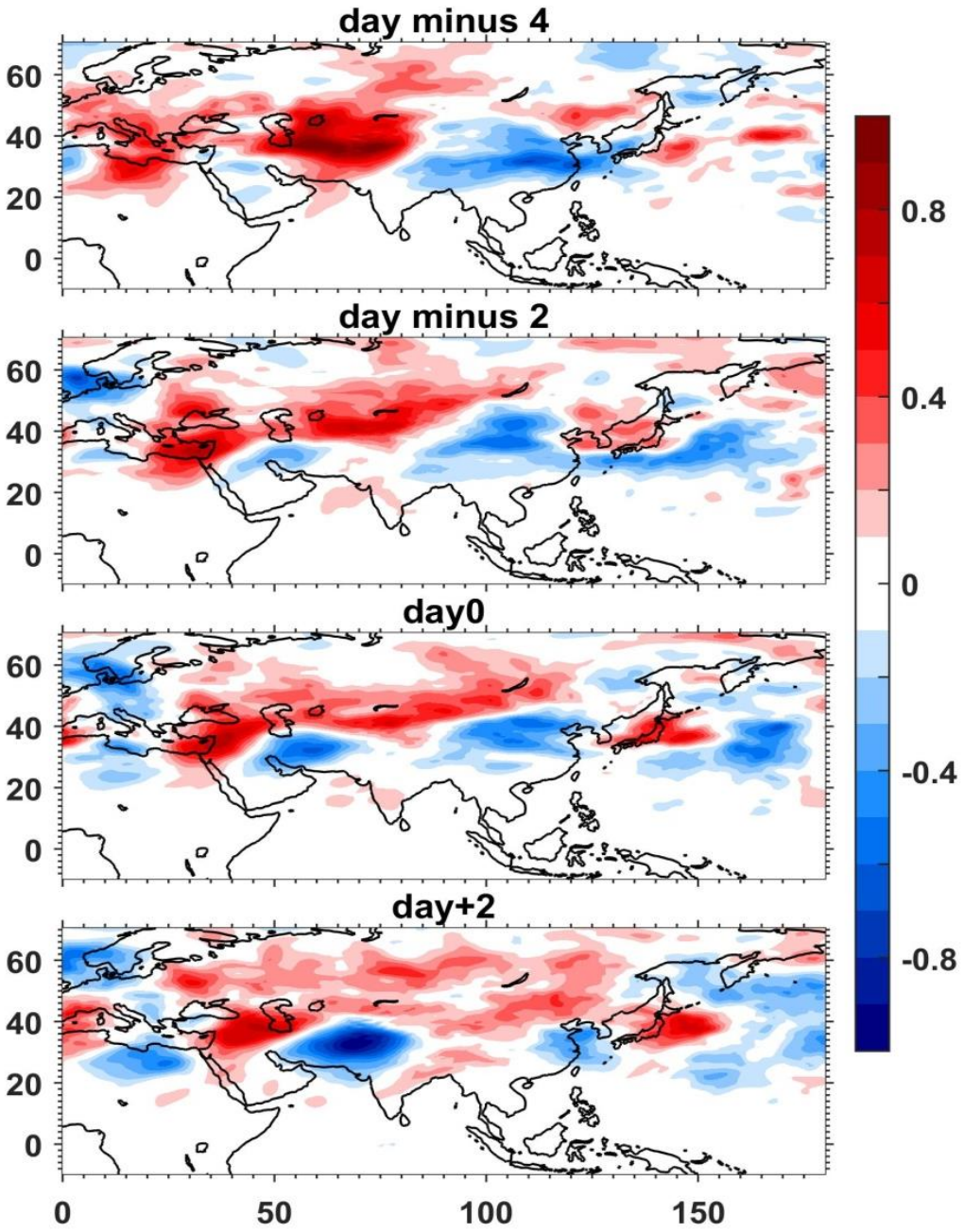

Fig. 5.10. Composite anomalies of (a) 350-K Potential vorticity (PV; PVU) from 4 and 2 days prior to, to day 3 of heat wave event. (Taken from Rohini 2020).

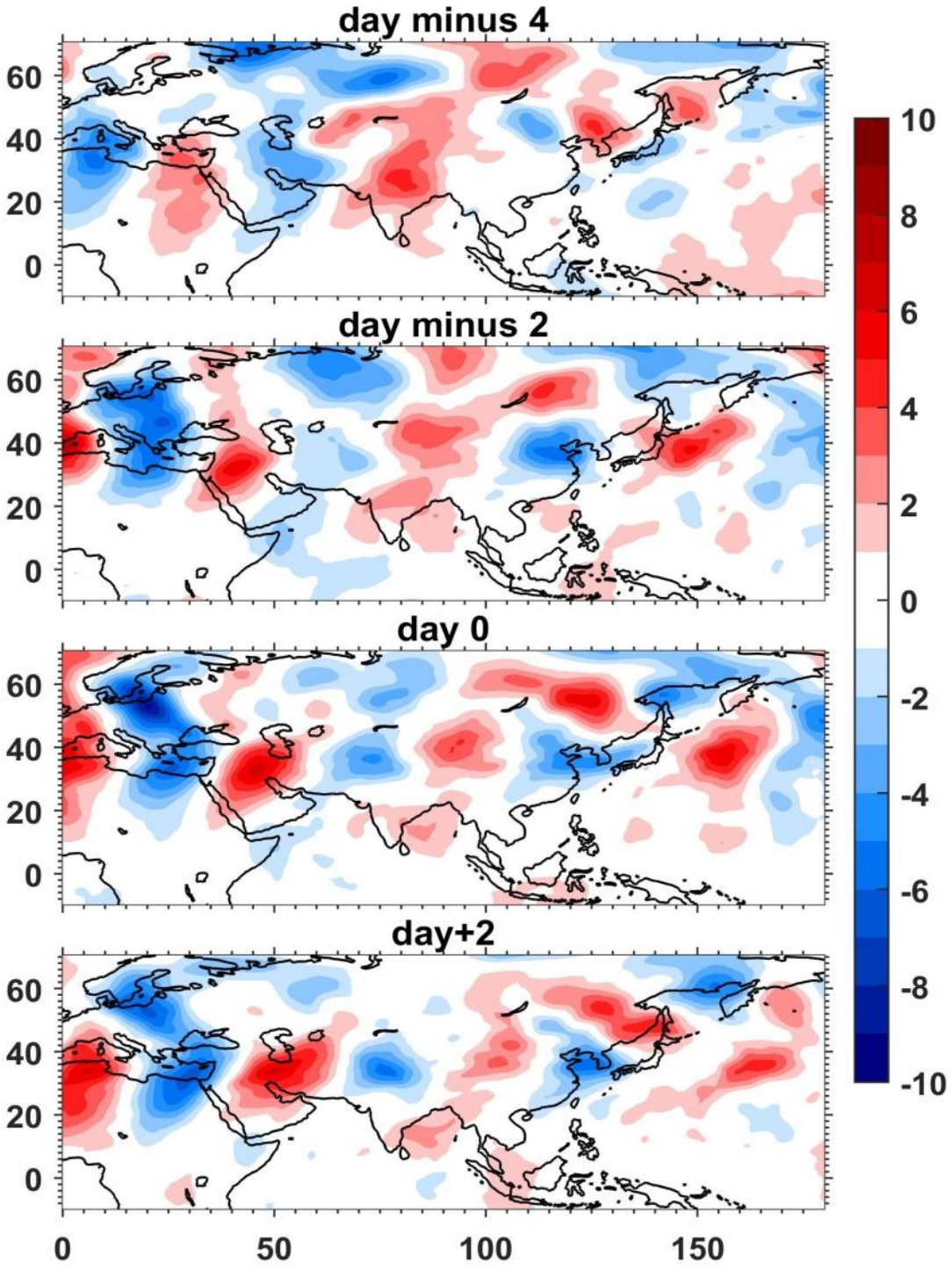

Fig. 5.11 Composite anomalies of 250 hPa meridional wind (m s^{-1}) from 4 and 2 days prior to, to day 2 of heat wave event. (Taken from Rohini, 2020).

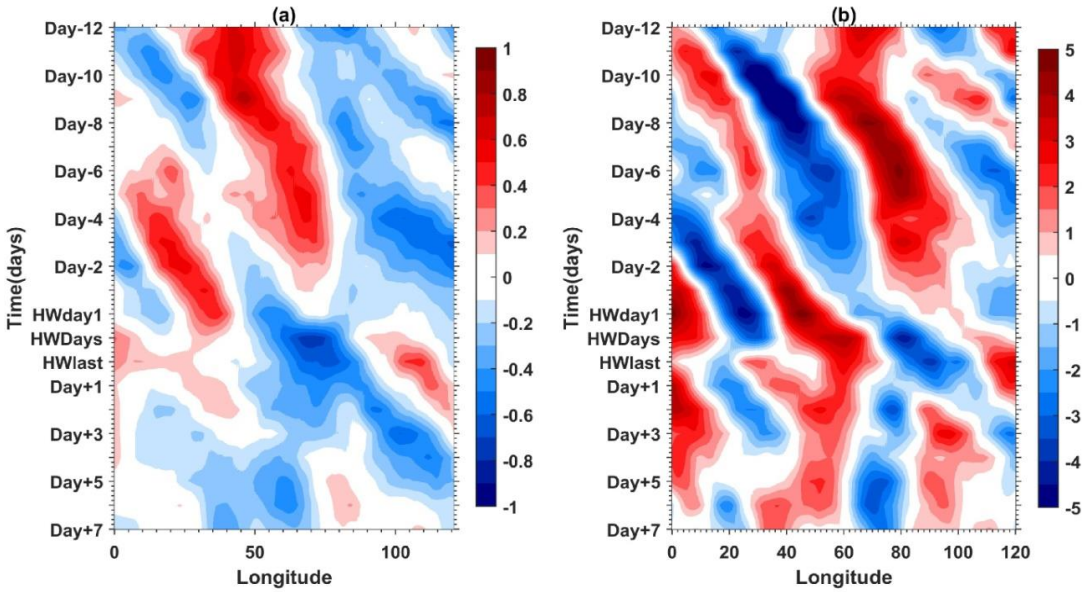

Fig 5.12 Hovmöller diagram from 12 days prior to onset up to 7 days subsequent to termination of all heat waves during 1981-2015. The latitude band averaged is 28°N-32°N: (left) 350-K PV anomalies (PVU) (right) 250-hPa meridional wind anomaly (m s^{-1}). (Taken from Rohini 2020)

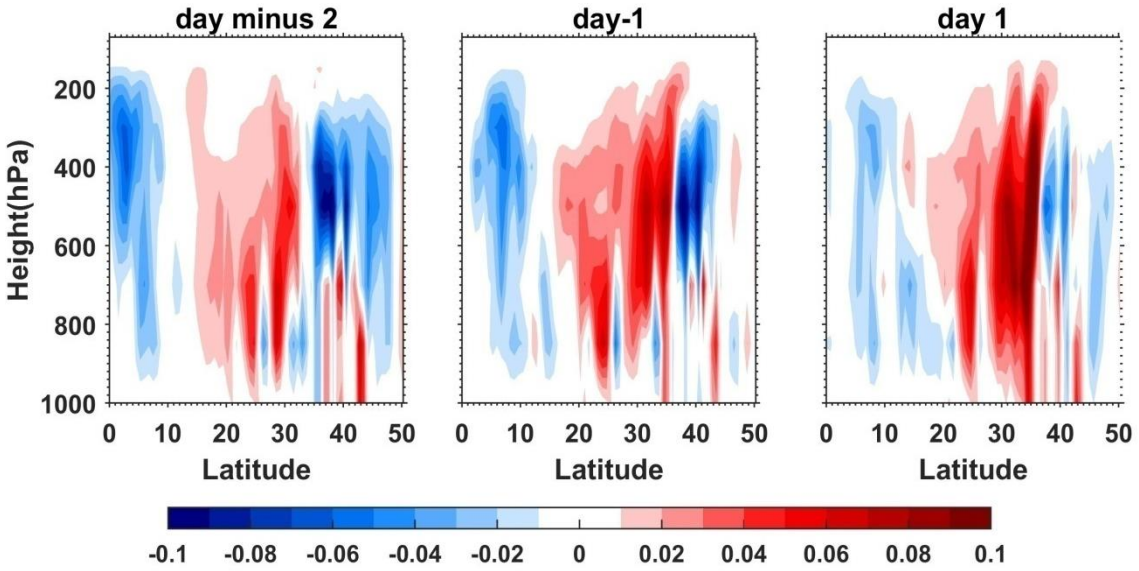

Fig. 5.13 Mean vertical cross section of omega (Pa s^{-1}) anomalies from 2 days prior to day 1 of all heat waves at 71.25°E longitude (Centre of anticyclone over India). (Taken from Rohini 2020)

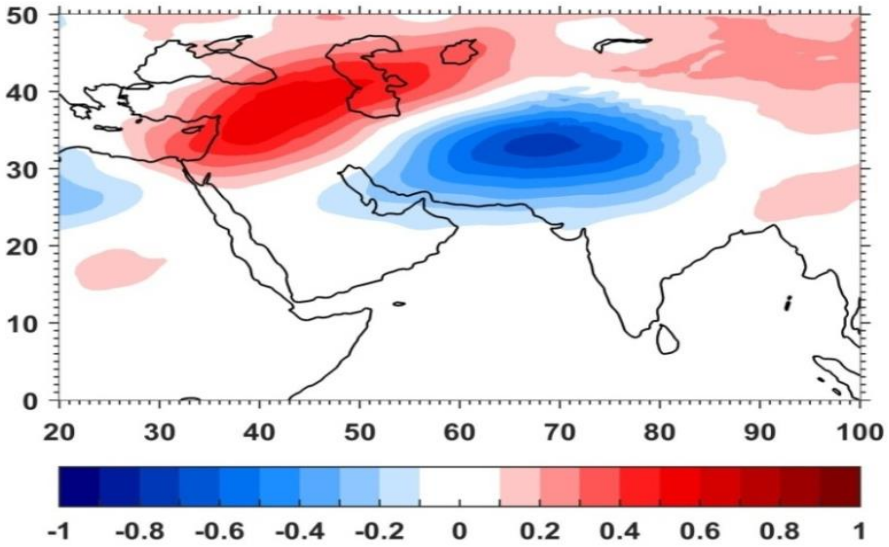

Fig 5.14. The composite anomaly of 350-K Potential Vorticity (PVU) during heat wave events. (Taken from Rohini 2020).

The latitude-height cross-section of vertical velocity (Omega) for all heat waves at 71.25° E longitude is shown in Fig.5.13. The centre of the anticyclonic anomaly is located approximately at 71.2° east longitude (Fig.5.14). During the two days preceding the onset of the heatwave, a region of ascent develops around 0°-10°N with a strong descent over 18°N-32°N. The air becomes warmer due to adiabatic compression (by the high-pressure area), which in turn contributes to high surface temperatures over NWI. The suppressed cloud formation due to the mean descent in this region contributes to the warming of the surface due to the increased solar radiation. This suggests that both advection of warm air from the northwestern part of India and adiabatic descent of air over this region contribute to the extreme warming.

5.4. **Dynamical factors influencing heat waves over East Coast of India.**

In this section, dynamical factors causing heat waves over the east coast of India are discussed. These discussions are based on the results of Ratnam et al. (2016 a).

Fig. 5.15 shows the anomalies of outgoing longwave radiation (OLR), stream function, SST, mean sea level pressure and moisture flux averaged for all heat waves that occurred over the east coast of India (Table 5.1).

Table- 5.1

Heat wave events over the east coast of India considered for composite analysis (Taken from Ratnam et al. 2016 a)

29 May- 4 June 1983	10 May-17 May 1996	14 May- 20 May 2008
01 May-07 May 1985	29 May-07 June 1997	26 May-03 June 2010
07 June-13 June 1986	09 May-15 May 2002	30 May-06 June 2012
17 May-23 May 1986	25 May-13 June 2003	
7 May-13 May 1994	15 May-21 May 2007	

Positive OLR anomalies over southern India and along the east coast of India indicate that the region is cloud-free. The 200 hPa composite eddy current function anomalies show a pair of anticyclonic anomalies over the western Pacific, similar to the Matsuno-Gill response to tropical Pacific cooling. Since the eddy current function anomalies over the Indian region do not show significant values, it can be assumed that the heat waves over the east coast of India are not caused by the quasi-stationary Rossby waves. There is also a significant anticyclone over the southern tip of India, which is indicative of the westerly winds emanating from the Indian landmass. Negative SST anomalies are observed over the equatorial central-east Pacific. Fig. 5.15 also shows an anomalous low pressure area along the east coast of India, indicating winds blowing out of India along the east coast. Moisture transport indicates that moisture from the Indian landmass is transported westwards, which significantly reduces the specific humidity over the region. The land-sea breeze, which is the main source of moisture over the coastal regions, is reduced by the anomalous circulation pattern over the region associated with tropical Pacific conditions. The reduction in moisture and

convective activity over the regions leads to an increase in temperatures and thus heat waves.

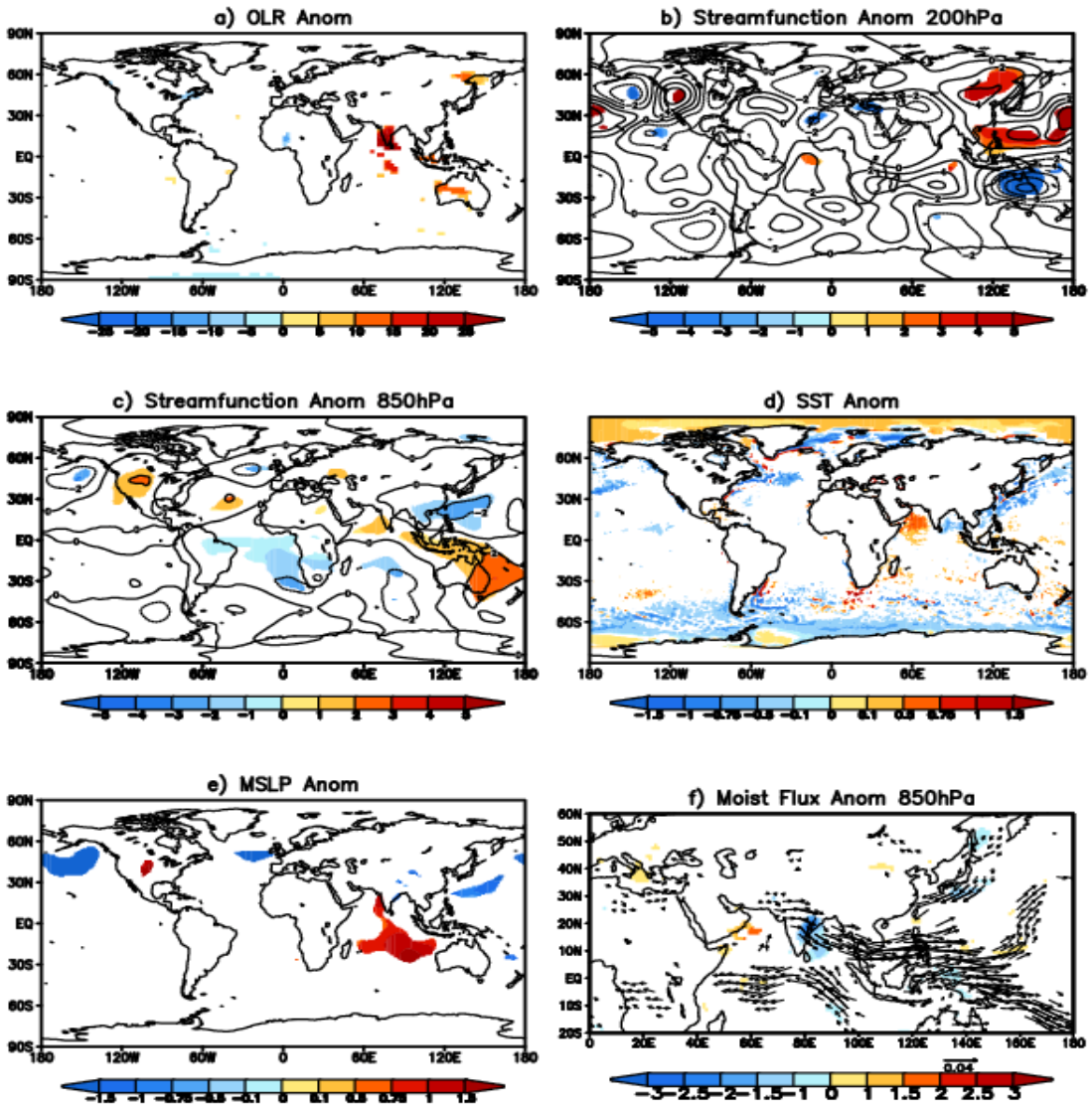

Fig 5.15. (a) Significant OLR anomalies of the composite of heat wave events over the east coast of India. (b, c) same as (a) but for streamfunction (X $10^6 m^2 s^{-1}$) anomalies at 200 hPa and 850 hPa respectively. (d,c) same as (a) but for significant SST (°C) and Mean Sea Level pressure anomalies. (f) same as (a) but for the significant moisture flux (kg $m^{-1} s^{-1}$) anomalies (vector) and the specific humidity (kg/kg) anomalies shaded at 850 hPa. (Taken from Ratnam et al. 2016 a).

Ratnam et al (2016 a) made a case study of heat wave which occurred during May 2015 to examine the dynamical factors causing the heat wave. The 2015 Indian heat waves claimed more than 2500 lives. Fig 5.16 shows eddy streamfunction anomalies at 200, 500 and 850 hPa, meridional wind anomalies at 200, 500 and 850 hPa, specific humidity, moisture flux, OLR and temperature anomalies.

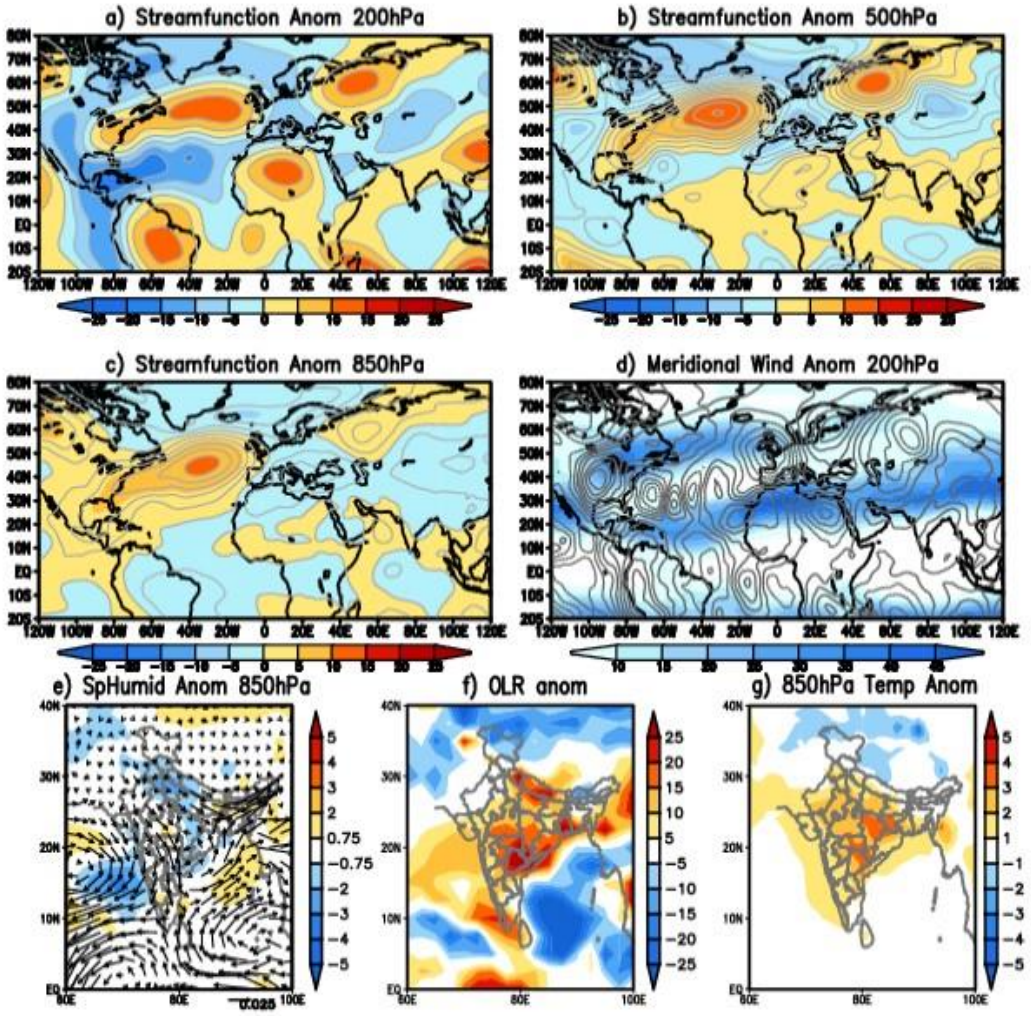

Fig 5.16. a) Eddy Streamfunction (X $10^6 m^2 s^{-1}$) anomalies at 200 hPa averaged over 21-31 May, 2015. (b, c) same as (a) but at 500 hPa and 850 hPa respectively. (d) 200 hPa meridional wind anomalies (contour) and zonal wind (shaded). (e) same as (d) but for 850 hPa specific humidity (Kg/Kg) anomalies (shaded) and moisture flux ($kgm^{-1}s^{-1}$) anomalies (vector). (f,g) same as ad but OLR and 850 hPa temperature anomalies respectively. (Taken from Ratnam et al. 2016 a).

An anomalous atmospheric blockage and associated cyclonic anomaly south of it is clearly evident in the North Atlantic. A wave train from West Africa is clearly visible in the meridional wind anomalies at 200 hPa along the westerly jet contributing to the anticyclonic anomaly over India. The cyclonic anomaly over India extends over parts of northwest India, central India and parts of the east coast of India. The anomalous cyclone over India transports anomalously dry air from northwest India inland. The transport of anomalously dry air from the northwest leads to anomalous reduction in humidity over the northern parts of India and along the southeast coast of India. The reduction in humidity is also evident from the positive OLR anomalies observed during the May 2015 heat wave. The clear sky increases the solar radiation over the surface and hence the temperatures.

5.5. Role of climate modes on the variability of heat waves

Studies on the role of climate variability in the occurrence of heat waves are needed to understand the influence of large-scale dynamics and its possible role in heat wave predictability. The role of the El Nino/Southern Oscillation (ENSO), the North Atlantic Oscillation (NAO) and the Pacific Decadal Oscillation in temperature extremes has been investigated in previous studies (Della-Marta et al. 2007; Kenyon and Hegerl 2008; Alexander and Arblaster 2009; Arblaster and Alexander 2012; Sanderson et al. 2017).

To investigate the possible relationships between heat wave events and tropical sea surface temperature (SST) anomalies, Rohini et al. (2016) conducted a canonical correlation analysis (CCA) using April-May-June (AMJ) SST and heat wave duration for the period 1961-2013. The spatial patterns and CCA time series of the first mode (CCA1) are shown in Fig. 5.17. The first mode for heatwave duration explains about 31% of the variability and that for SST 26.9%. The first SST spatial mode shows a large loading over the tropical Indian Ocean (Fig. 5.17.a), indicating a large influence of the tropical Indian

Ocean on the occurrence of heat waves over India. The first spatial mode of the heatwave shows a heavy load over the northwest of India with an opposite phase over the northeastern parts of the country (Fig.5.17.b).

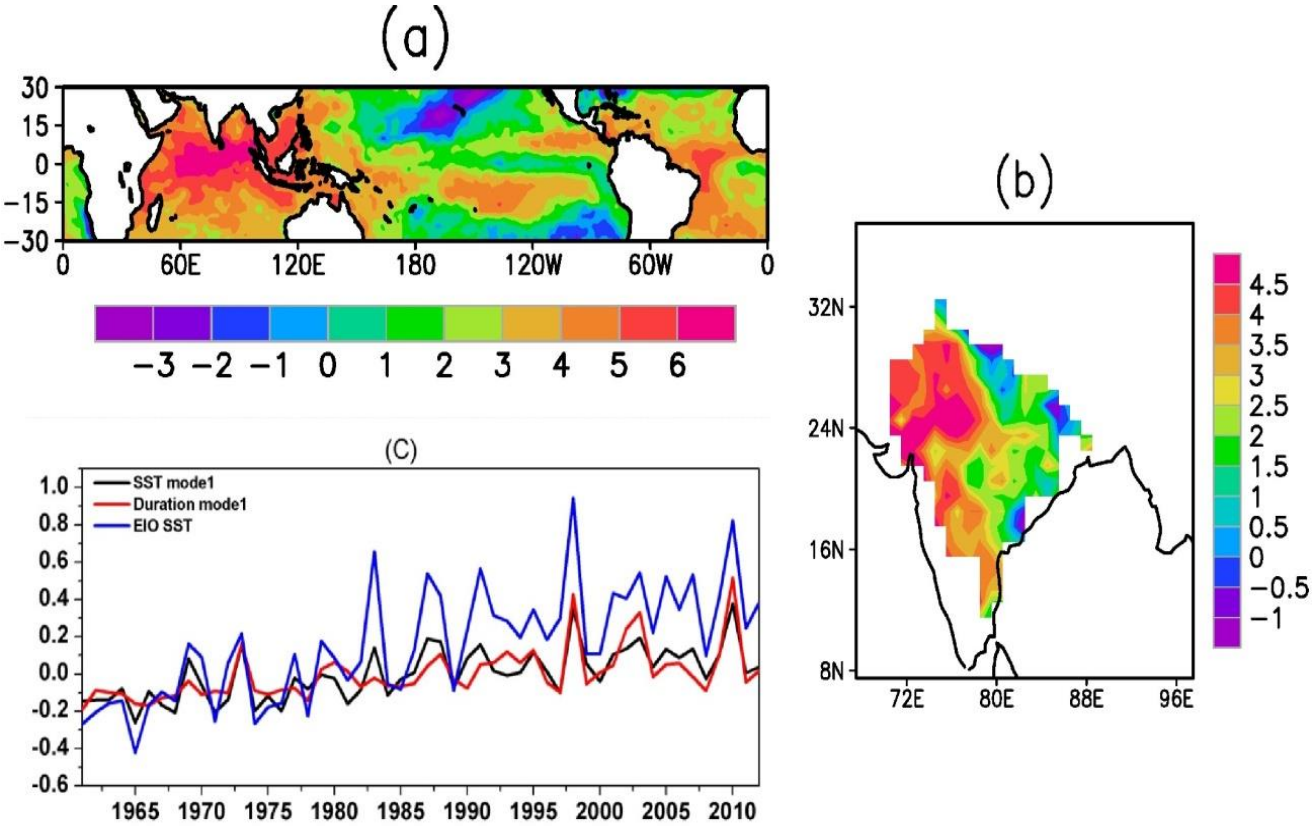

Fig. 5.17 The first canonical mode of the canonical correlation analysis of April-June SST and heat wave duration days for the period 1961-2013. (a) Spatial mode of SST (b) spatial mode of heat wave duration and (c) time series of first mode of SST(Black) and heat wave duration (Red). In (c), the time series of SST averaged over the equatorial Indian Ocean (10°S-10°N, 50°E-100°E) is shown in blue color line. (After Rohini et al. 2016)

The canonical time series of the first mode can also be seen in Fig. 5.17.c, which shows increasing trends in both SST and heatwave duration. Thus, the first canonical mode represents the increasing trends in the duration of heat waves over India and indicates the possible role of SST anomalies in the tropical Indian Ocean. The time series

of SST anomalies averaged over the tropical Indian Ocean (10°S-10°N, 50°E-100°E) is also shown in the same figure. The time series of the tropical Indian Ocean SST shows an increasing trend, as reported in previous studies (Roxy et al. 2014; Roxy et al. 2015). Therefore, the increasing trend in the duration of heat waves over the Indian subcontinent is partly influenced by the increasing sea surface temperatures over the tropical Indian Ocean. Positive SST anomalies over the equatorial Indian Ocean can cause local convection during the April to June season. The rising branch caused by convection in the equatorial Indian Ocean drops over the northern parts of India. The latitude-height cross-section of Omega (vertical pressure velocity; Fig.5.13) during the heat waves clearly shows the large-scale upward motion over the equatorial Indian Ocean and the downward motion over the northern parts of the country.

The spatial patterns and time series of the second mode are shown in Fig.5.18. The spatial pattern of the second mode of heat wave duration shows a dipole pattern (between northwest India and southeast India; Fig. 5.18 b), which explains 12% of the variance. The spatial pattern of the second SST mode shows a stronger loading from the tropical Pacific region (Fig. 5.18 a), suggesting that warming/cooling over the central Pacific, i.e. the ENSO phenomenon, is also an important factor influencing heatwave events over the Indian subcontinent.

The time series of frequency, duration and maximum duration clearly indicate a correlation between El Nino events and heat waves over India. It is clear that most of the years with above average heat wave activity over India are the years following El Nino events. For example, 1988, 1995, 1998 and 2010 are the years with above average heat wave activity, which represents the influence of El Nino activity during the 1987, 1994, 1997 and 2009 events. The earlier studies (De and Mukhopadhyay 1998; De et al. 2005; Pai et al. 2013) have also shown that the heat wave activity over India increases after an El Nino year. The third CCA mode is shown in Fig.5.19. This mode also indicates strong loading from the eastern equatorial Pacific and a horseshoe-shaped loading

pattern similar to the SST anomalies associated with a major El Nino event.

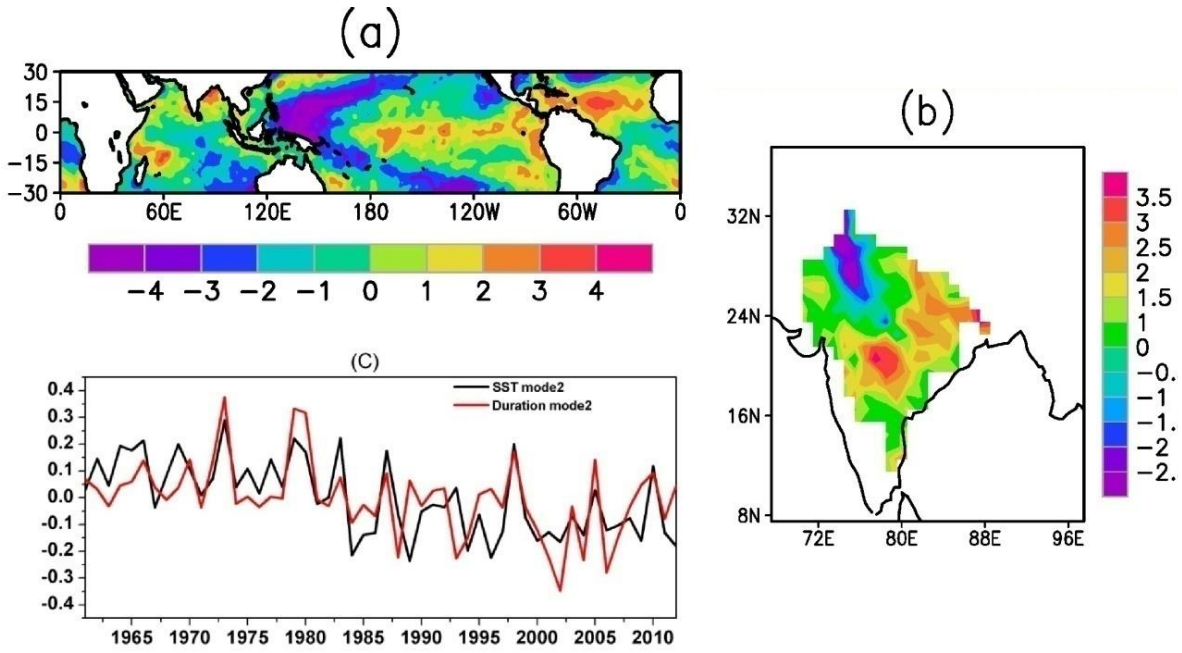

Fig. 5.18. The second canonical mode of the canonical correlation analysis of April-June SST and heat wave duration days for the period 1961-2013. (a) spatial mode of SST (b) spatial mode of heat wave duration and (c) time series of second mode of SST (Black line) and heat wave duration (Red line). (After Rohini et al. 2016)

The heat waves are thus associated with large-scale atmospheric anomalies combining a subtropical persistent high, a quasi-stationary Rossby wave over mid-latitudes, low soil moisture and clear skies. A composite analysis of 5 days prior to the onset of the heat wave revealed that an anticyclone in the upper troposphere was the main factor contributing to the heat waves over the Indian region. During the heat waves, it was observed that a slow-moving transient anticyclone formed over northwest India, which is part of a quasi-stationary wave extending from northwest Africa. The atmospheric column below the anticyclone becomes hotter due to adiabatic compression. These conditions result in clear skies with increased solar radiation at the surface, which in turn contributes to an increase in surface temperatures. Surface

conditions indicated dry soils with low soil moisture, leading to increased sensible heat fluxes at the surface during these events.

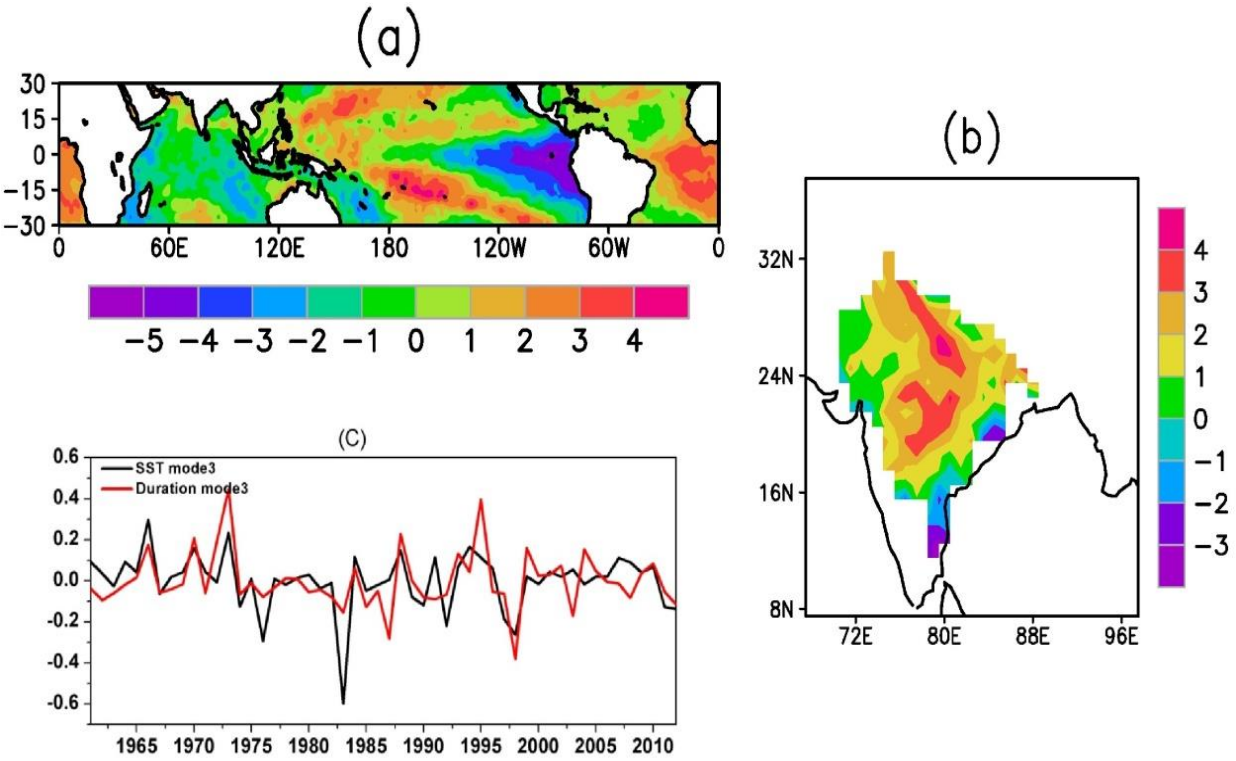

Fig. 5.19. The third canonical mode of the canonical correlation analysis of April-June SST and heat wave duration days for the period 1961-2013. a) spatial mode of SST b) spatial mode of heat wave duration and c) time series of third mode of SST (Black line) and heat wave duration (Red line). (After Rohini et al. 2016)

The study also highlighted the possible role of SST anomalies in the Indian Ocean and El Niño events over the equatorial Pacific in the occurrence of heat waves over India. Previous studies (Roxy et al. 2014; Roxy et al. 2015) indicated an increasing trend of SST anomalies over the tropical Indian Ocean in recent years, which is likely to continue in the future in the face of increasing greenhouse gases. Similarly, the study by

Cai et al. (2015) suggests that the mean climate of the tropical Pacific will change in the future due to greenhouse gas warming. The consequences of these changes in mean state include an increased frequency of extreme El Nino events. With the increasing trend of SST in the tropical Indian Ocean and the increasing frequency of extreme El Nino events, more frequent, intense and prolonged heat waves over the Indian subcontinent are likely in the near future.

5.6 Case Studies of Heat Waves

This section deals with two case studies of heat waves that affected the north-west of India and the east coast of India. During the period from 29 May to 11 June 2019, northwest India was affected by a major heat wave. The maximum temperature anomalies during this period are shown in Fig. 5.20. Another heat wave occurred on the east coast of India during 16-27 April 2017 and the maximum temperature anomalies during this period are also shown in Fig. 5. 21. The composite Tmax anomaly during the heat wave event over NW India exceeded 5^0C. The heat wave event affected the central and northwestern parts of India. The heat wave event over the southeast coast of India lasted for 12 days (16-27 April 2017). During the heat wave event, Tmax was above normal over the extreme northern parts of India as well as over the southeast coast of India. The Tmax anomaly over the southeast coast of India exceeded 5^0 C.

Fig. 5.22 shows the results for the heatwave event from 29 May to 11 June 2019, showing the composite anomaly of geopotential height (GPH) and winds at 200 hPa, 1-3 days before the heatwave event (top left) and during the heatwave event (top right). The same anomalies at the 500 hPa level are shown in the lower panels. The analysis was performed with NCEP/NCAR reanalysis data and the climatology used to calculate the anomalies was based on 1971-2000 data. At 200 hPa, a blocking high was observed near the Caspian Sea and the neighborhood 3 days before the heatwave, which intensified during the duration of the event. The blocking high was also observed at the 500 hPa level and was part of the Rossby wave pattern observed in the mid-latitudes. In

conjunction with this blocking high, an area of high pressure with anticyclonic circulation was observed at both 200 hPa and 500 hPa over the northern parts of India. The area of high pressure is more pronounced at the 500 hPa level. The anomalous anticyclone causes a subsidence over the region, which is a major factor in the development of a heat wave.

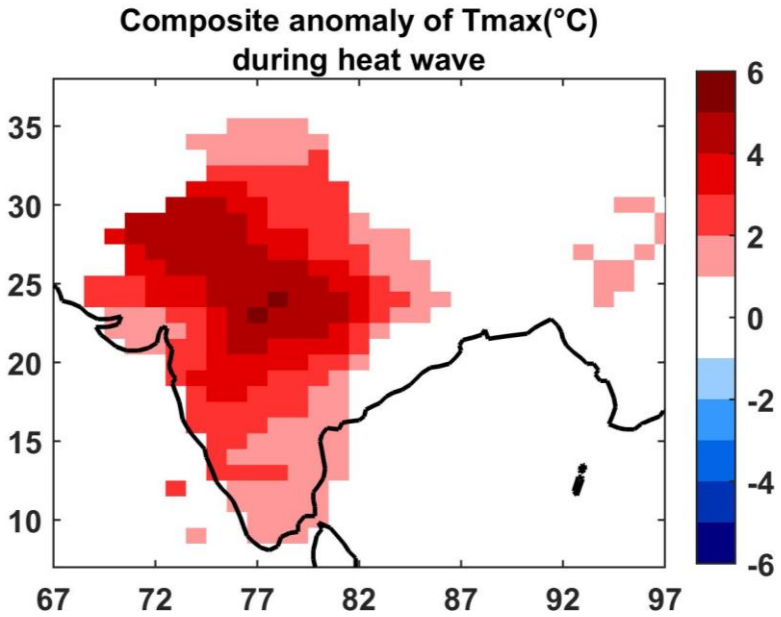

Fig 5.20. Maximum Temperature anomalies during the heat wave 29 May-11 June, 2019.

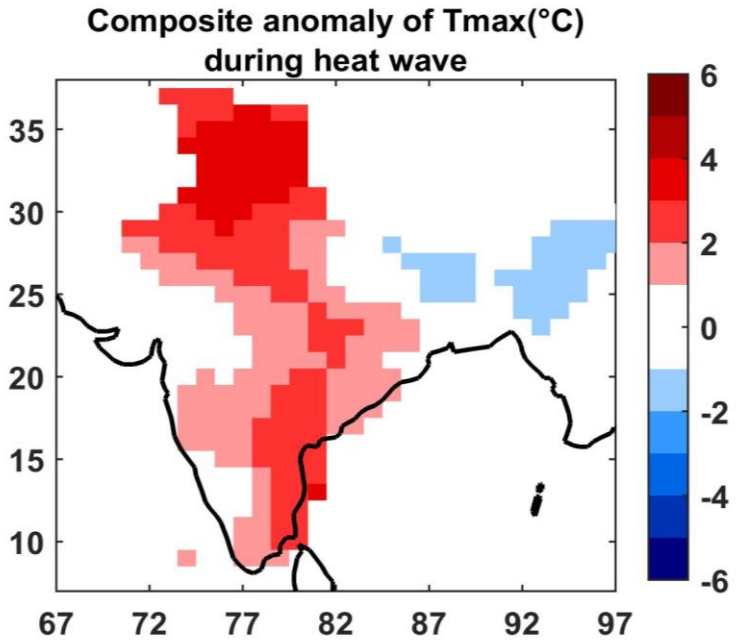

Fig 5.21. Maximum Temperature anomalies during the heat wave 16-27 April, 2017.

Heat Wave Event (29 May-11 June, 2019)

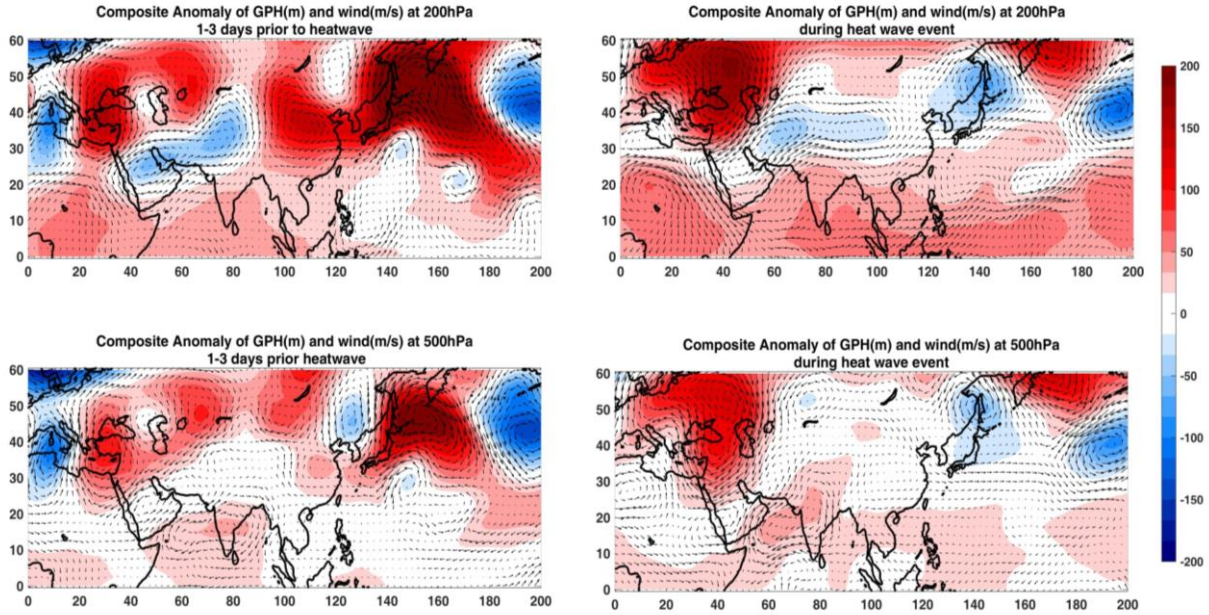

Fig 5.22. Composite anomaly of Geopotential Height (GPH) and winds at 200 hPa, 1-3 days before the heat wave event (top left) and during the heat wave event (top right). The same at 500 hPa are shown in bottom panels. The analysis was done with NCEP/NCAR reanalysis data. The climatology used to calculate anomalies was based on the data 1971-2000.

The lower atmosphere over northwest India was also drier (with negative specific humidity) even three days before the event and during the course of the heat wave (Fig. 5.23). Negative mean air pressure anomalies were observed over northwest India during the event (Fig. 5.24), which could be due to the higher surface temperatures during the event. This anomalous negative pressure area lead to northerly/northwesterly flow over northwest India brining dry and warm air to the region. A lack of soil moisture was observed over central and north-western India (Fig. 5.25) even before the onset of the heat wave. Low soil moisture enhances the intensity of the heat wave by increasing the sensible heat flux into the lower atmosphere as discussed earlier in this chapter. The

composite OLR anomalies before and during the heat wave (Fig. 5.26) also indicate clear skies over central and northwestern India without any convection.

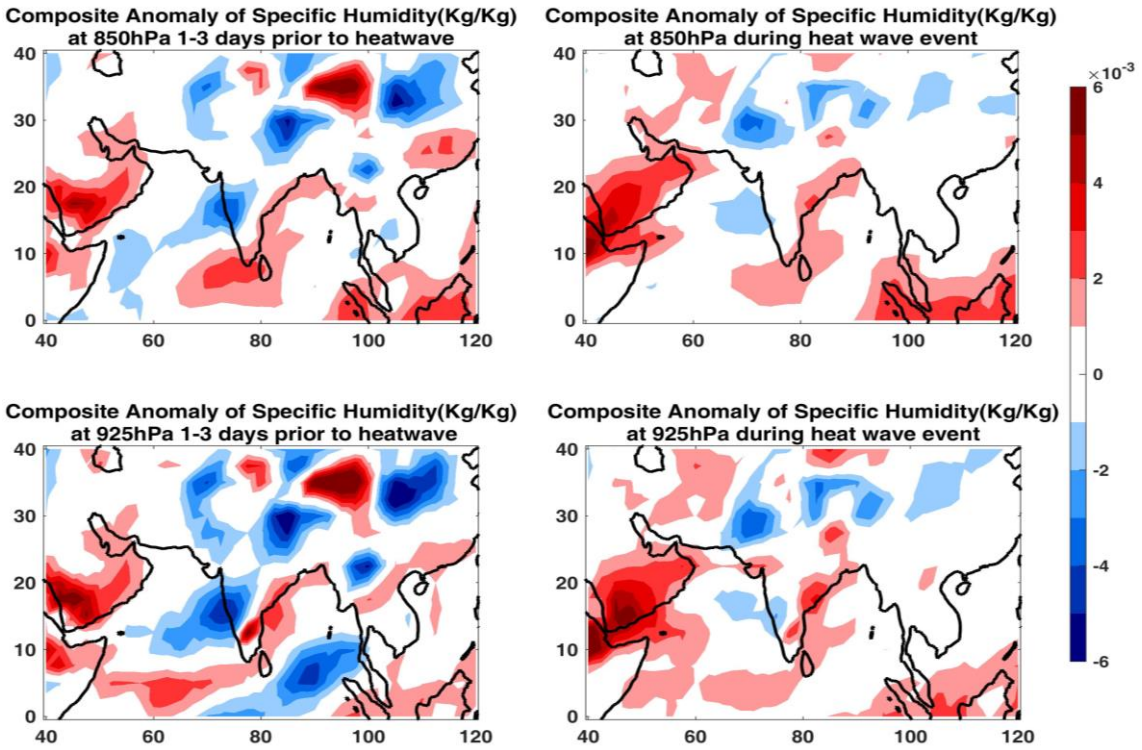

Fig 5.23. Average spatial distribution of specific humidity (kg/kg) at 850 hPa (above) and 925 hPa (below), 1-3 days before (left) and during the event (right).

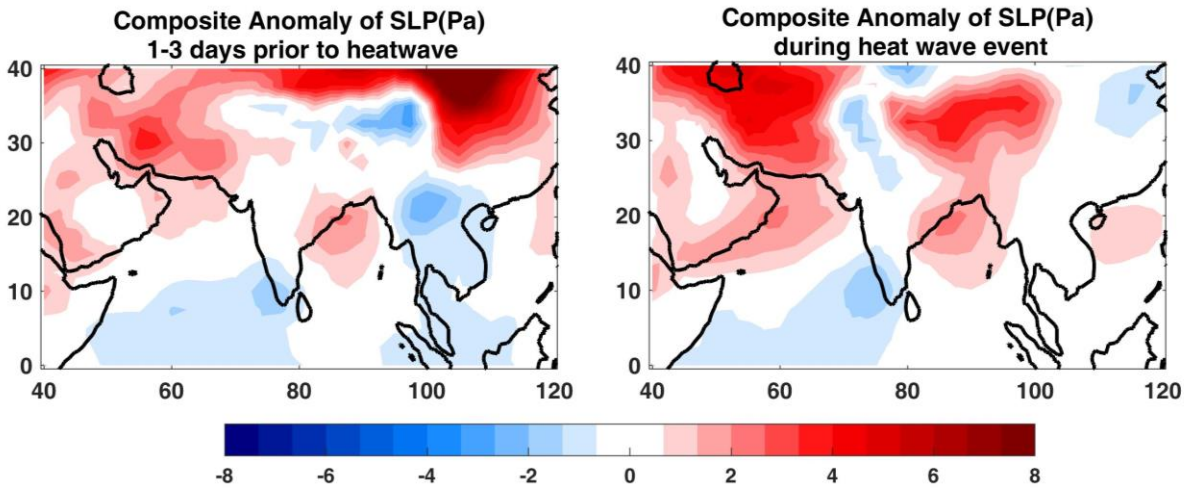

Fig 5.24. Composite anomaly of Sea Level Pressure (1-3 days prior to heat wave) (Left) and during the event (right).

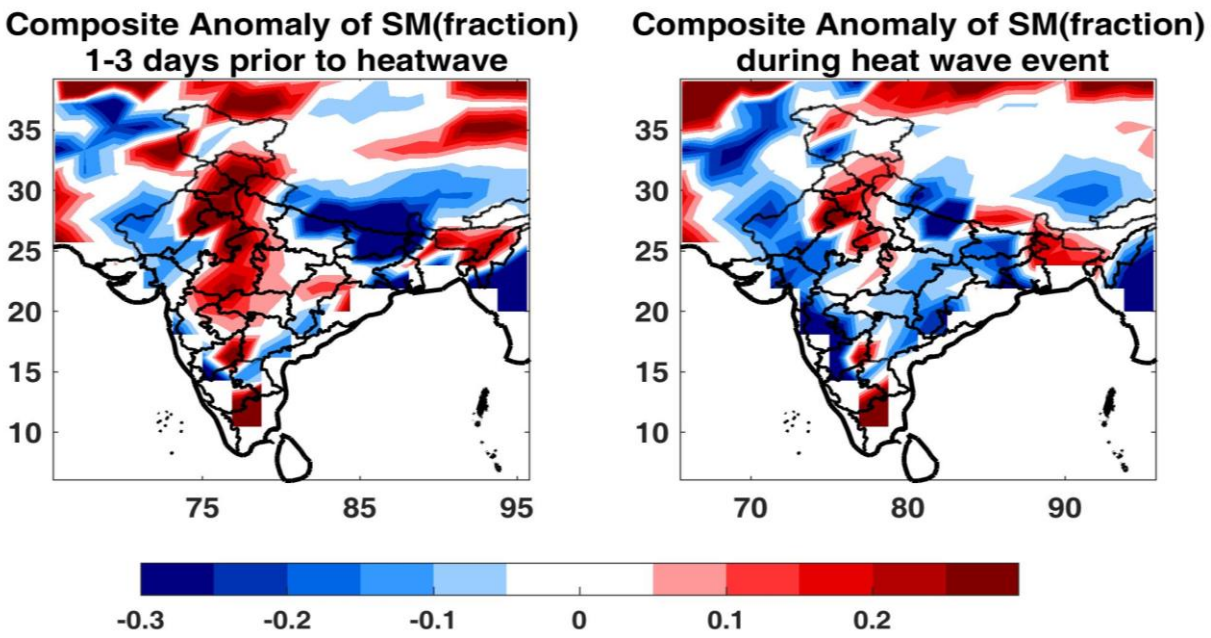

Fig 5.25. Composite Soil Moisture Fraction (1-3 days prior to heat wave) (Left) and during the event (right).

The heat wave region also exhibits a steep adiabatic lapse rate (9.80C/Km) (Fig. 5.27) in the lower troposphere, which facilitates the warm surface air to be lifted and spread to higher layers.

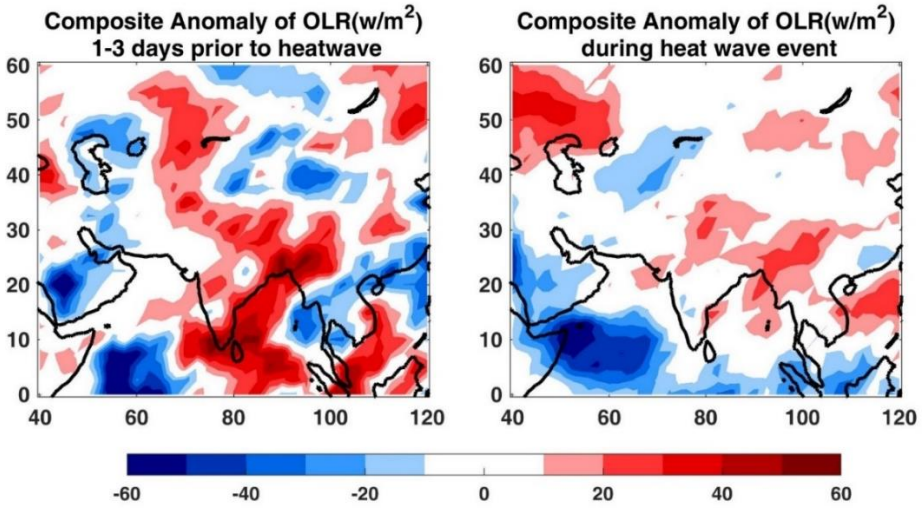

Fig 5.26. Composite Anomaly of Outgoing Longwave Radiation, OLR (1-3 days prior to heat wave) (Left) and during the event (right).

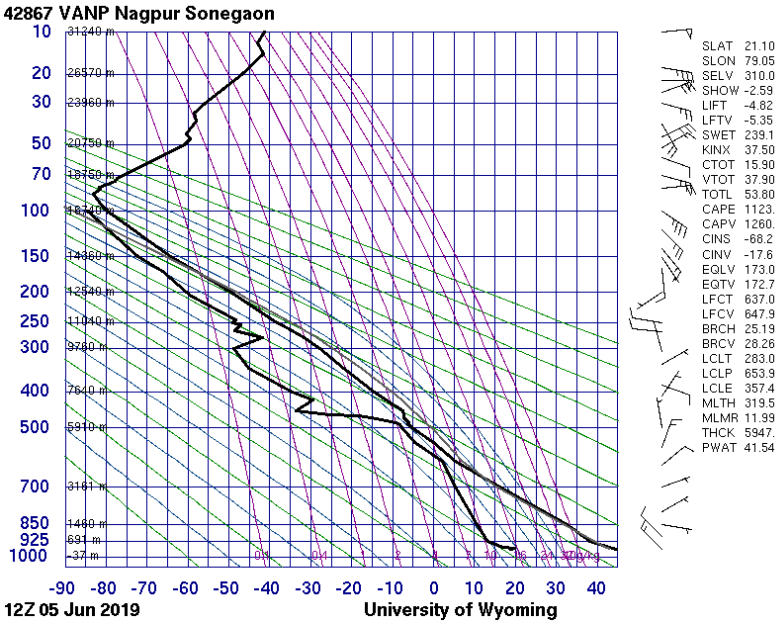

Fig 5.27. Vertical profile of temperature and moisture at Nagpur at 1200 UTC on 05 June, 2019 representing the region of heat wave.

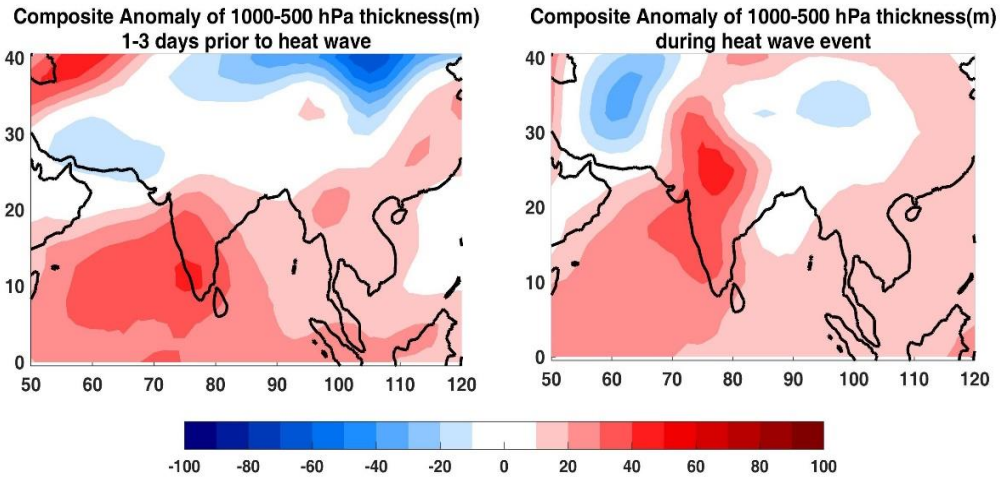

Fig 5.28. Composite anomaly of 1000-500 hPa thickness (m) 1-3 days prior to the heat wave (left) and during the heat wave (right).

Fig. 5.28 shows the composite anomaly of 1000-500 hPa thickness (m) 1-3 days before the heat wave (left) and during the heat wave (right). The most important feature of the 1000-500 hPa thickness is positive values over central and northwestern

India, indicating a warm lower atmosphere (up to 500 hPa) during the heat wave. It is important to note that this positive altitude anomaly occurs even three days before the onset of the heat wave (Fig. 5.28). Bedekar et al (1974) discussed the correlation between the thickness of the 1000-500 hPa layer and the severe heat waves in India. They presented many analyzed plots to show that in India the thickness of layer 1000-500 hPa has a clear correlation with the heat waves. It gives a taste of the evolution and decay of the heat waves. The decisive factor for the development of a heat wave is primarily the increasing thickness resulting from the warming of the layer. The winds that will indicate the transport of warm air in the lower and middle troposphere are northwesterly to westerly, north of 20^0N. The moderate westerly component persists throughout the period, supporting the transport of the warm air to the east. As the flow is fully continental, no moisture can penetrate over the affected region where the severe heat wave occurs.

Thus, the heat wave over northwest India was caused by atmospheric high (positive thickness anomalies) and anticyclonic flow (caused by the standing Rossby wave) and enhanced by low soil moisture (dry soil conditions) and clear skies. The anticyclonic flow causes subsidence to the surface from the middle troposphere. Longer clear skies allow more solar radiation to reach the earth's surface and contribute to a higher sensible heat flux. Drier soils also result in a lower latent heat flux and more sensible heat flux. It is therefore important to pay attention to these important physical conditions in the NWP model predictions to get insights of the possible development of a heatwave. These inferences are similar to the results obtained using the composite method of several heat waves. The details of the NWP model predictions for these heat waves are discussed in Chapter 7 to understand whether the current NWP models are good enough to predict heat waves in advance.

Next, we discuss the heat wave that affected the southeast coast of India from 16 to 27 April 2017. Fig. 5.29 shows the composite anomaly of geopotential height (GPH)

and winds at 200 hPa, 1-3 days before the heat wave event (top left) and during the event (top right). The same anomalies at the 500 hPa level are shown below. The 200 hPa circulation shows a pair of anomalous anticyclonic anomalies over the western Pacific, similar to the Matsuno-Gill response to tropical Pacific cooling (Ratnam et al. 2016 a). The anomalies have no significant values over the Indian region, suggesting that the heat waves over the east coast of India are not caused by the quasi-stationary Rossby waves like the heat waves over northwest India (as inferred by Ratnam et al. 2016 a also).

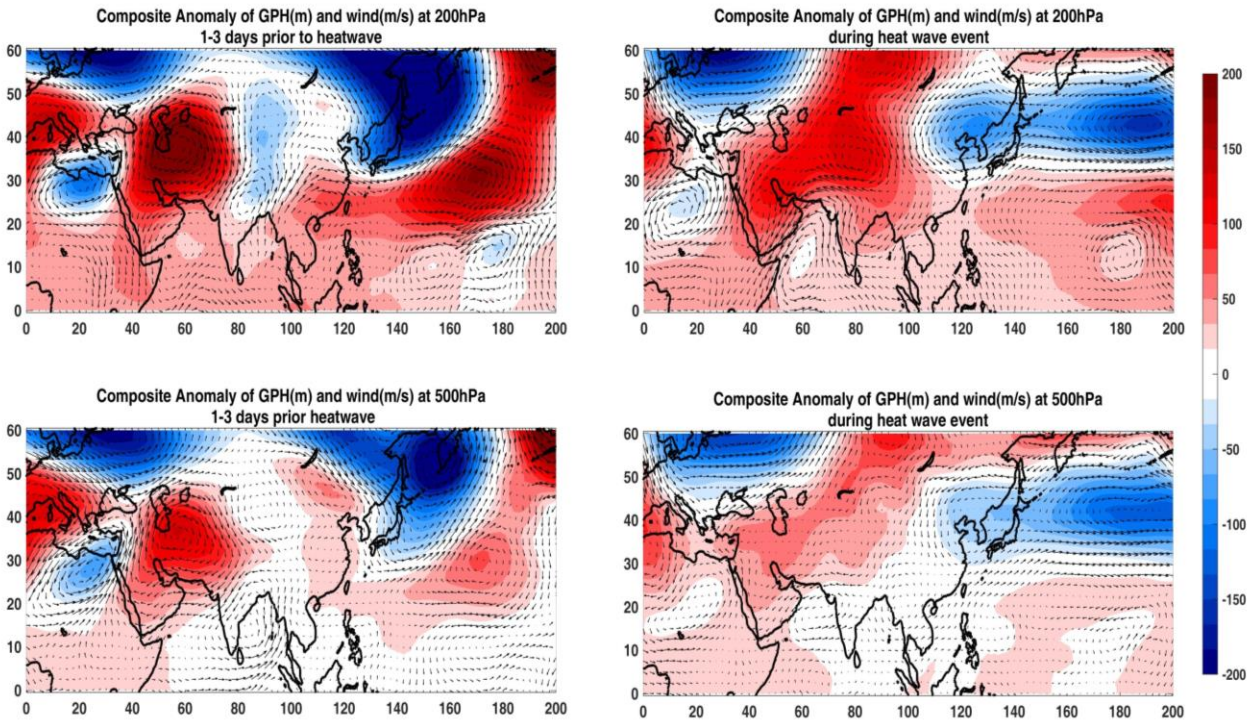

Fig 5.29. Composite anomaly of Geopotential Height (GPH) and winds at 200 hPa, 1-3 days (top left) before the heat wave event and during the event (top right). The same at 500 hP are shown below. Analysis was done with NCEP/NCAR reanalysis. The climatology used to calculate anomalies was based on the data 1971-2000.

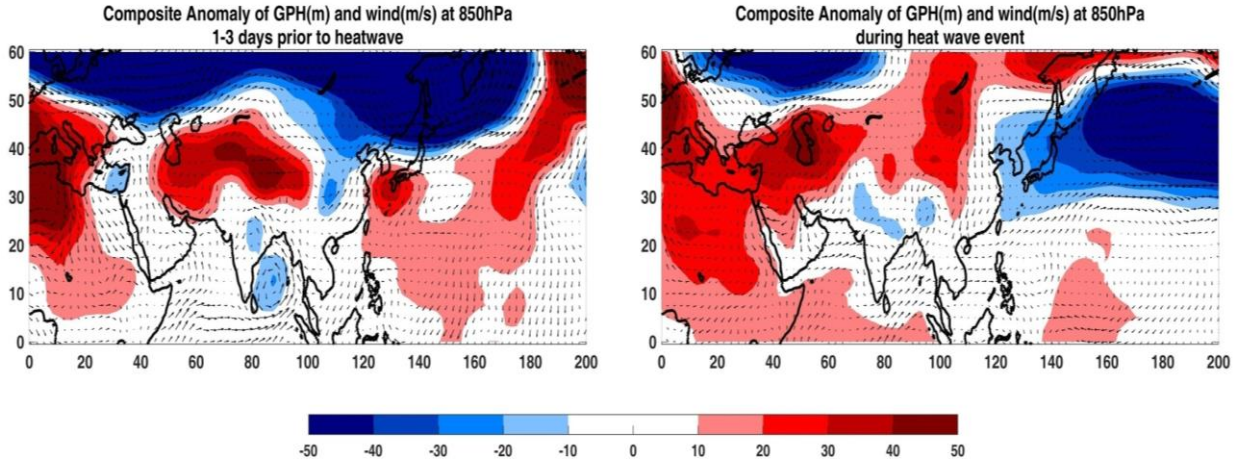

Fig 5.30. Composite anomaly of Geopotential Height (GPH) and winds at 850 hPa, 1-3 days (left) before the heat wave event and during the event (right). Analysis is done with NCEP/NCAR reanalysis. The climatology used to calculate anomalies was based on the data 1971-2000.

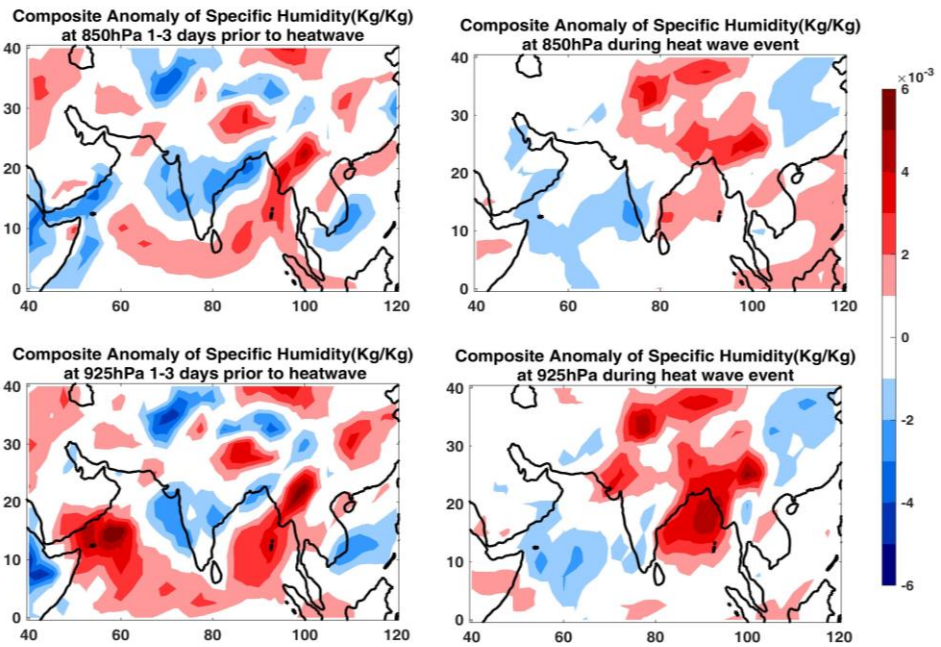

Fig 5.31. Composite anomaly of Specific humidity 850hPa, 1-3 days (top left) before the heat wave event and during the event (top right). Same at 925 hPa below. Analysis is done with NCEP/NCAR reanalysis. The climatology used to calculate anomalies was based on the data 1971-2000.

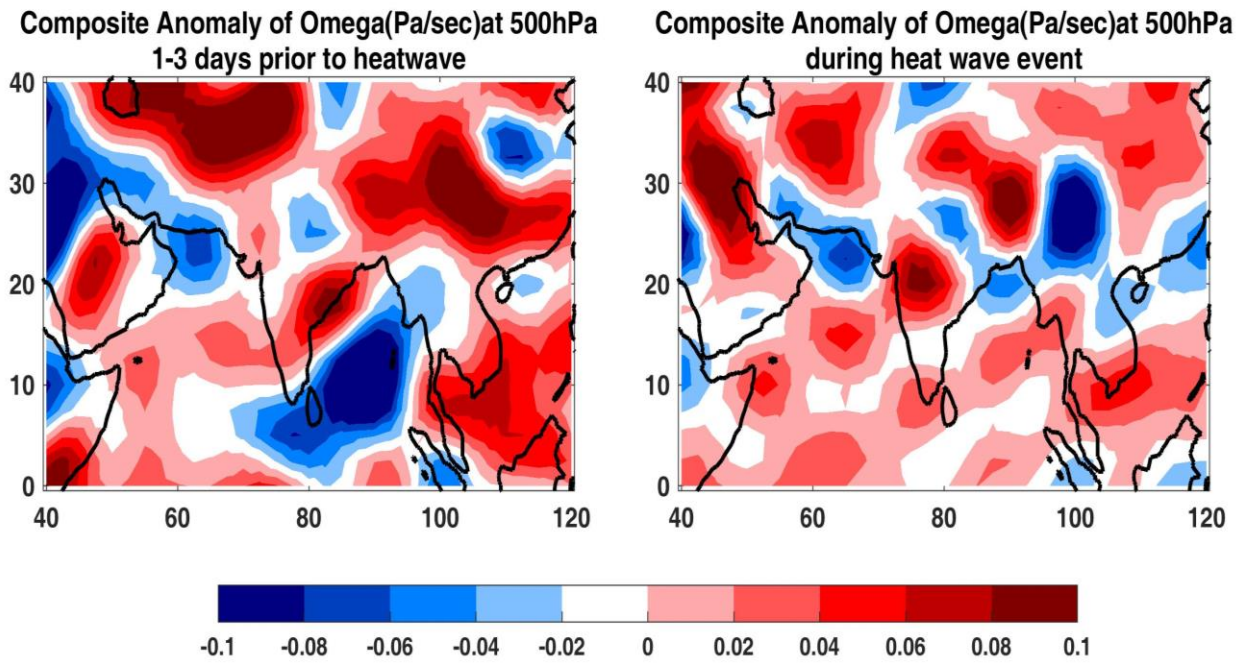

Fig 5.32. Composite anomaly of vertical velocity (Omega) at 500 hPa, 1-3 days (left) before the heat wave event and during the event (right). Analysis is done with NCEP/NCAR reanalysis. The climatology used to calculate anomalies was based on the data 1971-2000.

Before and during the heat wave, an area of high pressure with anticyclonic circulation at 200 and 500 hPa prevailed over the northwestern parts of India (Pakistan and Afghanistan). This anticyclone and the associated subsidence could be the main cause of the above-average temperatures observed over the extreme northern parts of India. Fig. 5.30 shows the anomalies of geopotential height and wind at 850 hPa before and during the heat wave. The most striking feature is the anomalous westerly winds over the southern peninsula, which leave the land region during the heat wave and join the low pressure area over the western Pacific. These anomalous westerly winds prevent the development of a sea breeze with cooler easterly winds. Ratnam et al. (2016 a) suggested that these westerly winds transported moisture out of the Indian landmass, which reduces the specific humidity along the east coast of India. Ratnam et

al. (2016 a) also noticed the presence of an anomalous low over the Bay of Bengal, before the heat wave event occurs.

Fig. 5.31 shows composite specific humidity anomalies, indicating below average specific humidity (drier air) over the southern peninsula before and during the heat wave. Vertical velocity (omega) (Fig. 5.32) indicates subsidence over the southern peninsula and thus clear skies. Ratnam et al. (2016 a) suggests that most heat waves over the east coast of India are influenced by negative SST anomalies over the equatorial Pacific and associated circulation anomalies or during the La Nina phase. The land-sea breeze, which is the main source of moisture over the coastal regions, is reduced by the anomalous circulation pattern associated with the tropical Pacific Ocean.

Chapter 6

Physical Mechanisms of Cold Waves

This chapter discusses the physical mechanisms of cold waves over India. There are not enough studies dealing with the physical mechanisms of cold waves over India. Cold waves usually occur due to the transport of cold air from higher latitudes in conjunction with the eastward moving westerly disturbances (Bedekar et al. 1974). As the subtropical westerly jet stream moves south towards India, these weather systems affect the northern parts of India during the winter season. Cold waves are often observed after the passage of westerly disturbances. The occurrence of cold waves due to the prevailing low pressure systems over the northern Arabian Sea is also observed (Bedekar et al., 1974). The easterly winds north of these systems bring cold air from higher latitudes.

The study by Bedekar et al. (1974) found that cold waves are caused by the inflow of very cold air from northern latitudes, i.e. from the extreme northwestern parts of the Indian subcontinent or even beyond. When this unusually cold air spreads over other parts of the country, it manifests itself as a cold wave in those parts. Therefore, any pressure system or synoptic situation that can cause an influx of cold air from these northern latitudes into India creates favourable conditions for the occurrence of a cold wave. A pronounced trough in the upper westerly wind zone is more or less a common feature of the western disturbance systems. Near the axis of these troughs, a pool of cold air can often be discerned in the upper layers. This pool of cold air always moves along with the troughs, and sometimes it can also be seen to spread to deeper layers to reach the ground and manifest itself as cold surface waves.

The cold air that accompanies these troughs has a fairly pronounced tilt to the east in the vertical with respect to the axis of the trough. Due to this characteristic of cold air troughs, it can be observed that cold waves generally develop much earlier (about 12-36 hours) in the upper layers of stations located far east of the trough axis than in the

surface layers of these stations. This characteristic feature is observed in most (about 80 %) of the severe cold-core depressions.

The recent study by Ratnam et al (2016 b) made a comprehensive analysis of the cold waves occurring over the Indian region and the associated physical mechanisms. They found that there are two types of cold waves over India, called type-1 and type-2 cold waves. This section discusses the detailed findings of Ratnam et al. (2016 b) in the context of cold waves over India.

Ratnam et al. (2016 b) identified cold waves using an index by taking an area average of minimum temperature (Tmin) anomalies over the region 71°E-80°E; 21°N-30°N (shown as a box in Fig. 6.1 a). A cold wave event is identified if the defined index on a selected day is less than one standard deviation and the anomalies persist for at least 4 days. Twenty-nine events were identified based on the criteria they adopted (which are similar to the IMD criteria). The cold waves occurring during the La Nina years are called TYPE1 events and the cold waves occurring during the El Nino years are called TYPE2 events. The TYPE1 and TYPE2 events thus identified are listed in Table 6.1 and Table 6.2 below. In general, TYPE1 events are more frequent compared to TYPE2 events.

Table 6.1

TYPE1 Cold Wave Events

(Taken from Ratnam et al. 2016 b)

1) 8–17 Nov 1983	8) 9–14 Jan 1989	15) 21–25 Jan 2008
2) 27–30 Jan 1984	9) 19–23 Feb 1989	16) 30 Jan-2 Feb 2008
3) 5–9 Feb 1984	10) 9–12 Feb 1989	17) 7–15 Feb 2008
4) 20–28 Feb 1984	11) 8–13 Dec 1996	18) 4–12 Jan 2011
5) 19–23 Dec 1984	12) 9–12 Jan 1999	19) 10–14 Jan 2012
6) 11–18 Feb 1985	13) 11–15 Dec 2005	20) 8–11 Feb 2012
7) 4–8 Jan 1986	14) 6–10 Jan 2006	21) 4–9 Jan 2013

Table 6.2

TYPE2 Cold Wave Events

(Taken from Ratnam et al. 2016 b)

1) 11–15 Jan 1983	4) 19–25 Dec 1986	7) 14–19 Jan 2003
2) 3–8 Feb 1983	5) 6–9 Dec 1987	8) 19–23 Feb 2005
3) 14–17 Dec 1986	6) 31 Dec 1990	

From these tables, it can be seen that most cold spells occur in the months of January (12) and February (10). Ratnam et al (2016 b) found that out of 29 events, 21 (8) occurred in La Nina (El Nino) years, suggesting that both phases of ENSO (El Nino and La Nina) favour the occurrence of cold waves over India. However, there is a tendency for more cold waves during the La Nina years.

The composite anomalies of various parameters of TYPE1 and TYPE2 cold wave events are shown in Fig. 6.1. The composite SST anomalies averaged over these 21 events in La Niña years show colder than normal SST anomalies along the equatorial central Pacific, extending from the central to the eastern Pacific, with concurrent warmer than normal SST anomalies in the equatorial western Pacific (Fig. 6.1 b). Similarly, the SST anomalies for the eight events corresponding to El Niño years show significantly positive SST anomalies in the equatorial Pacific, extending from the central to the eastern Pacific, with cooler than normal SST anomalies in the western Pacific (Fig. 6.1 c). Moreover, composite Tmin anomalies for TYP1 events show a marked decrease in Tmin over most parts of India (Fig. 6.1 d). On the other hand, for TYP2 events, a significant decrease in Tmin is mainly confined to north-western India, with positive anomalies along the east coast of India (Fig. 6.1.e).

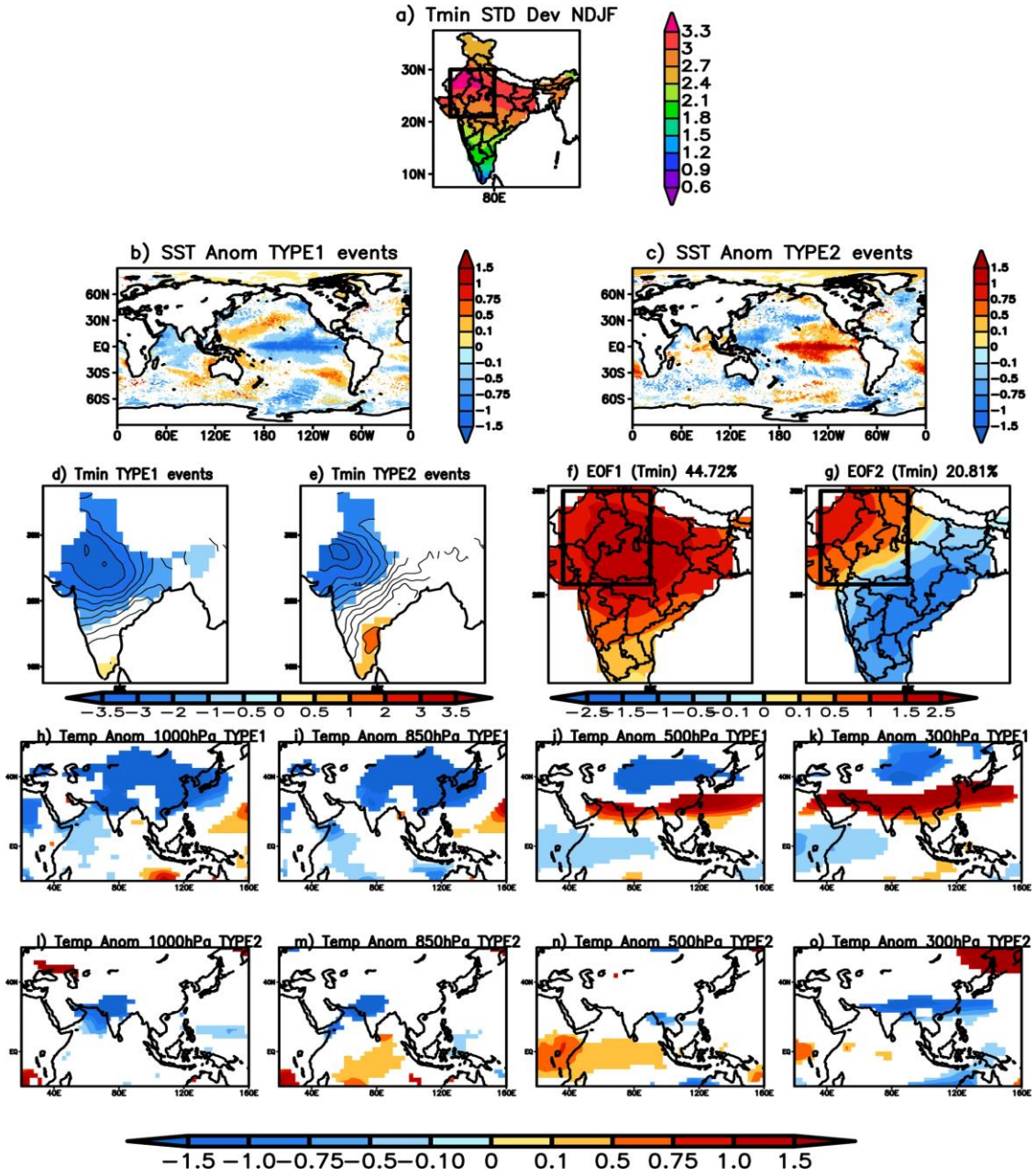

Fig 6.1 (a) Standard deviation of the Tmin (°C) from 1st Nov to 28th Feb over the period 1982 to 2013. (b) Spatial distribution of significant SST (°C) anomalies during TYPE1 events. (c) same as (b) but for TYPE2 events. (d) Significant Tmin (°C) anomalies associated with TYPE1 events (e) same as (d) but associated with TYPE2 events. (f) The first mode of EOF of Tmin anomalies. (g) The second mode of EOF of Tmin anomalies. (h–k) Significant air temperature anomalies (°C) at 1000 hPa, 850 hPa, 500 hPa and 300 hPa respectively during TYPE1 events. (l–o) Significant air temperature anomalies (°C) at 1000 hPa, 850 hPa, 500 hPa and 300 hPa during TYPE2 cold wave events. (Taken from Ratnam et al. 2016 b)

To objectively separate the modes of variation, an empirical orthogonal functional analysis (EOF) was performed over the region 70°E-90°E; 12°N-30°N. Figure 6.1f shows the first EOF mode, which explains 44.72% of the total variance. This mode has large loadings over the region with high standard deviation of Tmin temperatures (Fig. 6.1 a) and has a similar pattern to the spatial distribution of Tmin anomalies during TYPE1 cold wave events (Fig. 6.1 d). Moreover, the correlation between the Tmin anomalies averaged over the region 71°E-80°E; 21°N-30°N and the principal component of this mode is 0.91, which is very high. The second mode (EOF2) (Fig. 6.1 g) explains about 20.81% of the total variance and shows a dipole structure similar to the TYPE2 cold wave events (Fig. 6.1.e), with opposite phases over northwest India and along the east coast of India. The correlation of their principal component with the Tmin anomalies, averaged over the region 71°E-80°E; 21°N-30°N, is only 0.385. Thus, the analysis of EOF justifies the division of the observed cold wave events into TYPE1 and TYPE2 events.

During the TYPE1 cold wave events, colder air than normal is confined to about 850 hPa in the northern parts of India, while warmer air prevails at 500 hPa and above. Over India, the low pressure areas are an effective means of bringing in cold air from the north. During TYPE2 events, colder than normal temperatures are confined to the northwestern parts of India in the lower troposphere (Fig. 6.1 l-m). Temperatures over India are not significant at 500 hPa (Fig. 6.1 n), although significant anomalously cold temperatures are observed at 300 hPa over Indian latitudes during the TYPE2 events (Fig. 6.1 o).

Further details on the TYPE1 and TYPE2 events are discussed below.

6.1. TYPE1 Cold waves (associated with La Nina events)

Fig. 6.2a shows the spatial distribution of the composite anomalies of the output longwave radiation (OLR). In response to colder than normal SST anomalies, positive OLR anomalies (indicating less cloud cover) are observed over the equatorial central

Pacific, while negative OLR anomalies (indicating excessive cloud cover and more precipitation) are observed from the west of the Philippines to the east coast of India. Over northwestern India and into Pakistan, the prevailing colder air temperature in the boundary layer (Fig. 6.1 h-k) increases stability and thus limits convection development, resulting in positive OLR anomalies there (Fig. 6.2a).

To investigate whether remote teleconnection was the cause of the TYPE1 cold waves, composite 200 hPa vortices (without zonal mean) streamfunction anomalies (Fig. 6.2 b) were recorded. The composite (Fig. 6.2 b) shows the following prominent features that may have contributed to the TYPE1 cold wave events over India. i) A region of anomalous positive anomalies over the Ural-Siberian region and a wave train originating from there and extending to southern China, with a trough over most parts of China and a ridge over southern China and the northeastern parts of India, and ii) a region of anomalous anticyclone over the Indian landmass.

The feature that helps transport cold temperatures from higher latitudes to Indian latitudes and sustains the cold waves is also clearly seen in Fig. 6.2 b as an anticyclonic anomaly at 200 hPa over the Indian latitudes. The anomalous trough over China and the anomalous ridge over southern China extend from 500 hPa to 200 hPa (Fig. 6.2 c). At 850 hPa (Fig. 6.2 d), the anomalous ridge over the Ural-Siberian region and the associated trough over the Indochina region can be seen, causing cooler than normal temperatures over the region (Fig. 6.1 i). The north-south orientation of the cyclonic anomaly over northern India favours the advection of cold air from higher latitudes to India. The horizontal 850 hPa advection of the mean observed temperature by the mean observed winds was calculated (Fig. 6.2 e) to investigate whether the cold waves over India are caused by horizontal advection of cold air from higher latitudes.

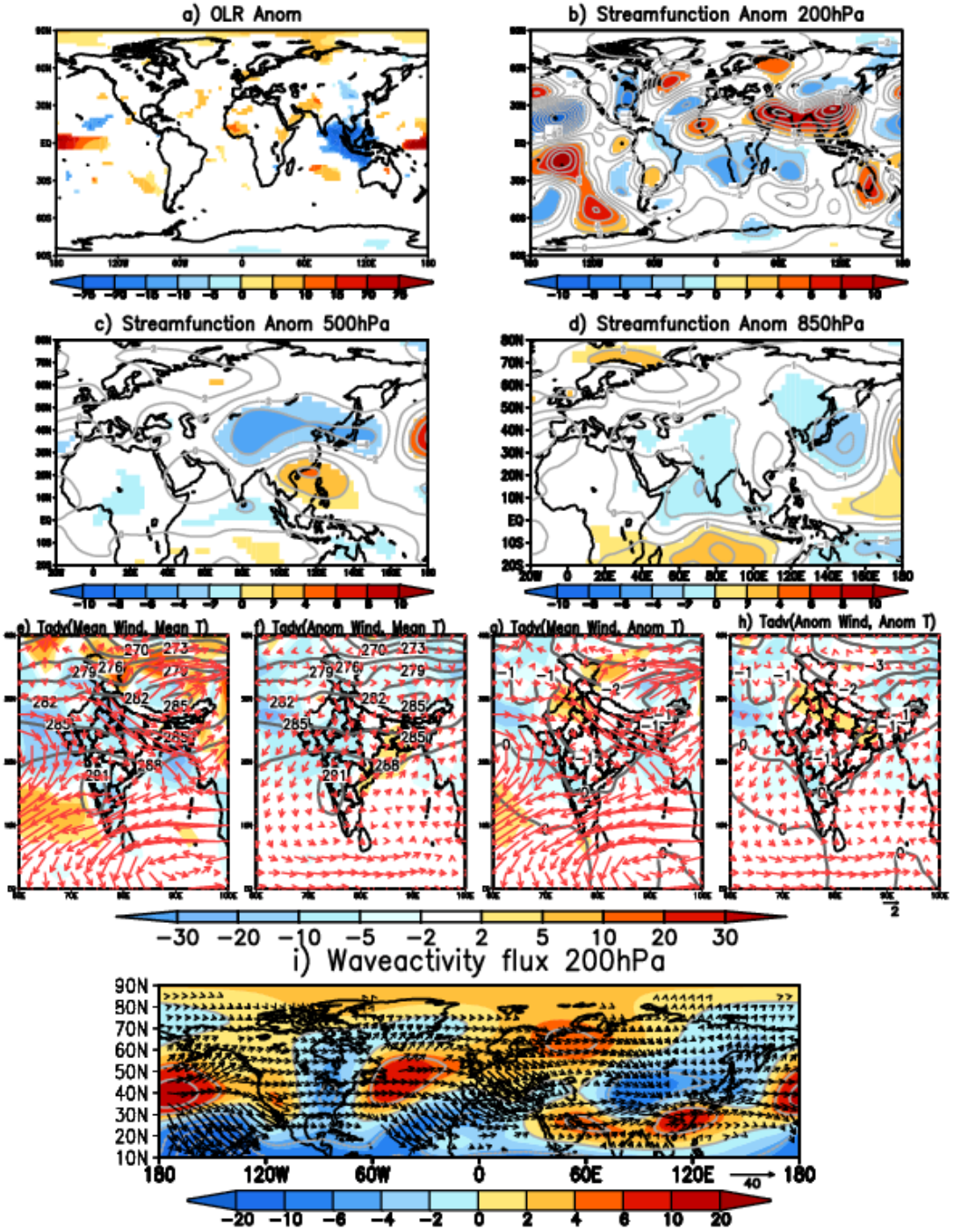

Fig 6.2. (a) Significant OLR (W/m^{-2}) anomalies of the composite of TYPE1 cold wave events. (b,c and d) same as (a) but for significant eddy streamfunction ($\times 10^6$ m^2 s^{-1} ; shaded) at 200 hPa, 500 hPa and 850 hPa levels respectively. (e) Horizontal temperature advection (shaded; $\times 10^{-6}$ °K s^{-1}) of mean temperature by mean winds at 850 hPa during

TYPE1 events. Contours represent mean temperatures and mean wind at 850 hPa is shown by vectors (f) same as (e) but advection of mean temperature by anomalous wind (shaded). Mean temperature (contour) and anomalous winds (vectors) are also shown (g) same as (e) but advection of anomalous temperature by mean winds (shaded). 850 hPa temperature anomalies are shown as contours and mean winds as vectors (h) same as (e) but advection of anomalous temperature by anomalous winds (shaded). Contours represent temperature anomalies and vectors represent anomalous winds at 850 hPa (i) Significant wave activity flux anomalies at 200 hPa (vector; either zonal or meridional component is significant) and the stream function anomalies (shaded) for TYPE1 cold wave events. (Taken from Ratnam et al. 2016 b).

During TYPE1 events, northwesterly winds are observed bringing cold temperatures from higher latitudes to the Indian subcontinent, resulting in a drop in temperatures over the Indian landmass (Fig. 6.2 e). From Fig. 6.2 f-h, it is evident that the advection of the observed mean temperature by the anomalous cyclonic response (Fig. 6.2f) largely explains the cold air advection over large parts of India. This term (Fig. 6.2f) makes a larger contribution than all the other terms (Fig. 6.2 g-h). The anomalous cyclonic winds bring warmer temperatures from the equatorial region, resulting in above-average temperatures on the east coast of India (Fig. 6.2f). The effect of cold advection by the anomalous winds is reduced over the northern parts of India by warm advection of anomalous temperature by the mean winds (Fig. 6.2 g) and also by advection of anomalous temperature by the anomalous winds (Fig. 6.2h). Both the advection of anomalous temperature by the mean observed winds (Fig. 6.2g) and by the anomalous winds (Fig. 6.2h) bring cooler temperatures to the upper Bay of Bengal and also to the western parts of India.

The low-level cyclonic anomaly observed over India during TYPE1 cold waves (Fig. 6.2 d) can be partly attributed to the seasonal mean equatorial cyclonic anomaly observed during the La Niña events. Fig. 6.3 shows composite OLR anomalies, 850 hPa eddy current function (shaded) and 850 hPa wind anomalies (vector) created by averaging monthly December-February anomalies during La Niña years from 1982 to 2013. In response to a spatially coherent negative OLR anomaly over the maritime

continent and western Pacific regions (Fig. 6.3a), a pair of cyclones can be seen spanning the equator over the Indian Ocean (Fig. 6.3b). The poleward flank of the northern hemispheric part of the cyclonic anomalies (Fig. 6.3 b) is favourable for bringing cold temperatures from higher latitudes to the Indian region in La Niña years.

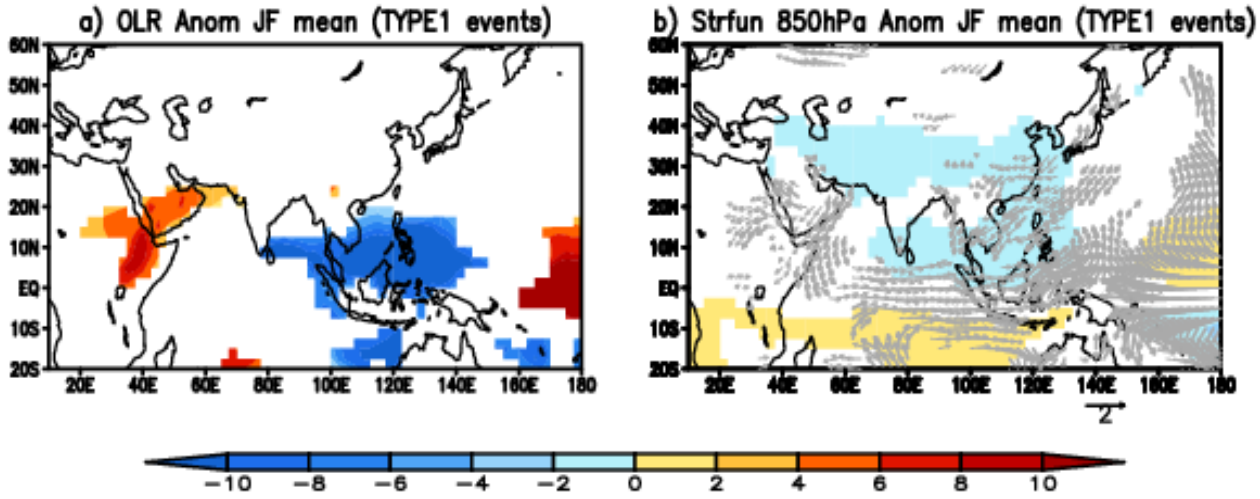

Fig. 6.3. (a) Significant OLR anomalies composited over Dec–Feb months during the La Niña years over the period 1982 to 2013. (b) same as (a) but is for significant eddy stream function ($\times 10^6$ m^2s^{-1}) anomalies at 850hPa and significant wind anomalies (vectors; either zonal or meridional component is significant).

To examine the progress of cyclonic circulation over northwest India and initiation of cold wave events, the 850 hPa eddy stream function anomalies of all the TYPE1 cold wave events from 5 days (DAY-5) before the event to the day the event started (DAY0).

The results are presented in Fig. 6.4. The Day-0 is considered the day when the events started. Five days before the TYPE1 cold wave events occurred over India (DAY-5) (Fig. 6.4a), anomalous high in the higher latitudes and the associated wave with the

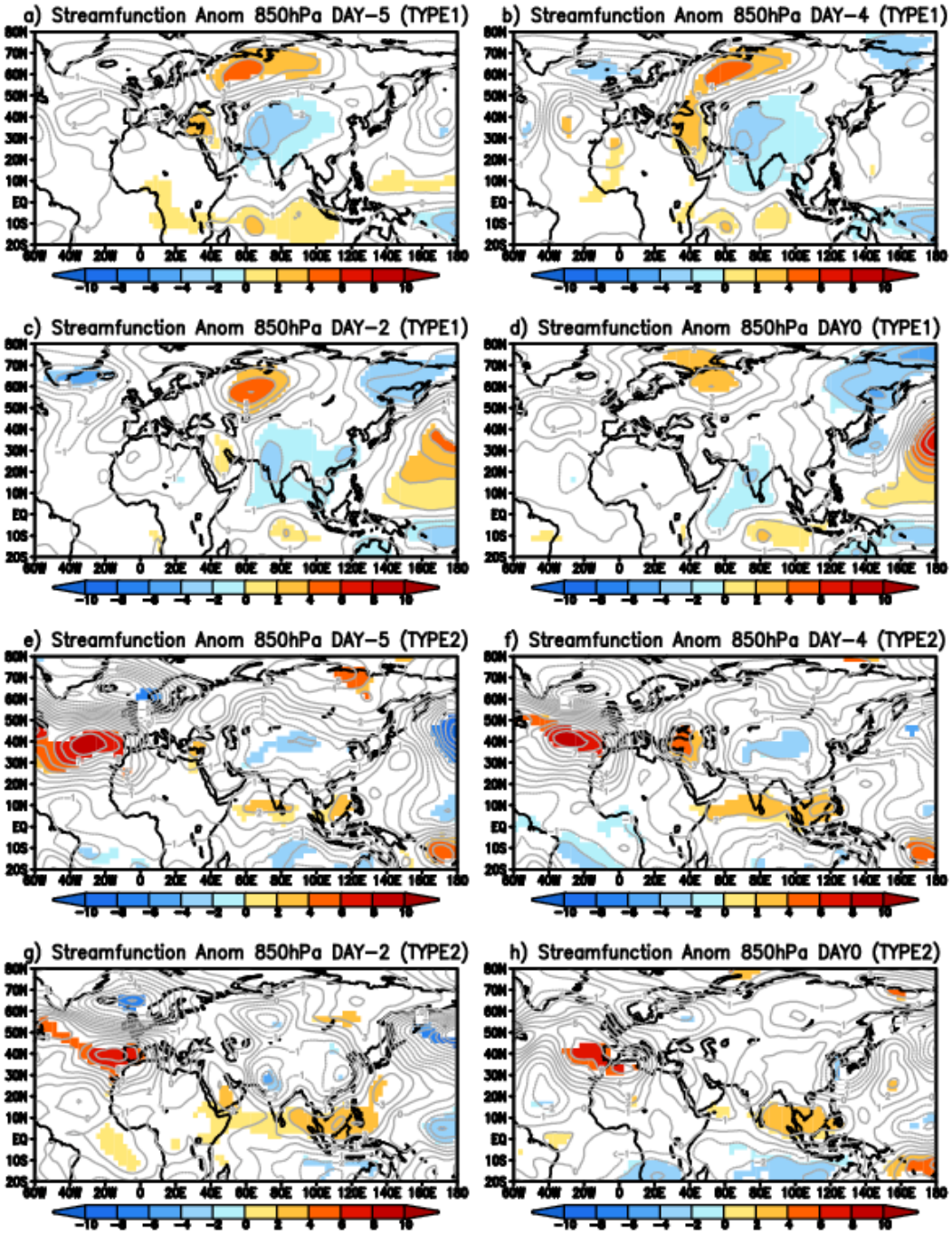

Fig. 6.4. (a) Composite of significant eddy streamfunction (×106m2 s−1) anomalies at 850 hPa five days before TYPE1 events (DAY-5). (b,c and d) same as (a) but four days (DAY-4) before, two days (DAY-2) before and on the day (DAY0) respectively of the TYPE1 event. (e–h) same as (a–d) but for TYPE2 cold wave events.

anomalous trough over China and over India are oriented north to south. The trough has a maximum to the northwest of India (Fig. 6.4a). The anomalous trough is seen moving eastward from DAY-4 (Fig. 5.4 b–d) and is seen covering the whole of the Indian landmass. Maxima in the cyclonic anomaly is seen over India from DAY-2, two days before the events started (Fig. 6.4 c). On DAY-0, the anomalous wave is oriented such that an anomalous cyclone is seen anchored to the Indo-China region. The anomalous cyclone to the south of equator in the Indian Ocean is seen from DAY-5 to DAY-0 (Fig. 6.4 a–d), however it intensifies from DAY-2 (Fig. 6.4c).

The anomalous high pressure over the Ural-Siberian region (Fig. 5.22b-d) that occurred during the TYPE1 cold wave over India is sometimes associated with an atmospheric blocking event. The question arises whether all atmospheric blocking events over the region can be associated with TYPE1 cold waves over India. When comparing the 76 blocking events during the La Niña years with the 21 TYPE1 cold wave events, Ratnam et al. (2016 b) found that 13 of the TYPE1 cold wave events were associated with atmospheric blocking events over the Ural-Siberian region. However, blocking over the Ural Siberia region is not a necessary condition to favour TYPE1 cold waves over India.

6.2 TYPE2 Cold waves (associated with El Nino events)

In this section, the details of TYPE2 Cold wave events are discussed. The composite of Tmin anomalies during TYPE2 cold wave events shows a significant negative anomaly confined to northwest India (Fig. 6.1e). The composite of OLR anomalies (Fig. 6.5a) shows negative anomalies in the equatorial central Pacific due to warmer SST anomalies in the region (Fig. 6.1c) and positive OLR anomalies over the west Pacific (Fig. 6.5a).

The associated eddy stream function anomaly at 200 hPa shows cyclonic anomalies covering whole of the Indian subcontinent and parts of China (Fig. 6.5b). The cyclonic anomaly over the Indo-China region is seen extending to lower levels and is also

seen at 500 hPa (Fig. 6.5c) and 850 hPa (Fig. 6.5d), similar to the often-observed extension of upper level troughs associated with western disturbances as closed lows in the lower troposphere. At 850 hPa (Fig. 6.5 d), the cyclonic anomaly is seen confined to the west coast of India. The other significant feature of the eddy streamfunction anomaly at 500 hPa and 850 hPa is a pair of anticyclones over the west Pacific, which is the well-known Matsuno-Gill response to the equatorial west Pacific SST anomalies.

The main difference between TYP1 and TYP2 events is the barotropic pattern of cyclonic anomalies over India in TYP2 (in TYP1 it is baroclinic). Therefore, the cyclonic anomalies over India in TYPE1 and TYPE2 low-level events appear to be driven by different processes. During the TYPE2 cold wave, northwesterly winds bring cold temperatures to the northwestern parts of India, causing cold temperatures, while southerly winds bring warm temperatures from the equatorial region to the central and northern parts of India, causing warm temperatures over the region (Fig. 6.5e) (Ratnam et al. 2016 b). The western flank of the anomalous depression over the west coast of India, a response to the Pacific convection anomalies, brings cooler temperatures from higher latitudes to northwestern India (Fig. 6.5f) and the eastern flank of the anomalous cyclonic circulation brings warmer equatorial temperatures to central and northern parts of India (Fig. 6.5f). The advection of cold temperatures to northwestern India and warm temperatures to other parts of India is also due to the advection of anomalous temperatures by the observed mean and anomalous winds (Fig. 6.5 g-h). The anticyclonic anomaly over the western Pacific and the Bay of Bengal also contributes to the advection of warm temperatures onto the Indian landmass (Fig. 6.5 e-h). The above analysis shows that the maintenance of TYPE2 cold waves over India and their limitation to the northwestern parts of India can be largely explained by the advection of temperatures from the higher latitudes and equatorial regions by the mean and anomalous winds observed during the TYPE2 cold waves.

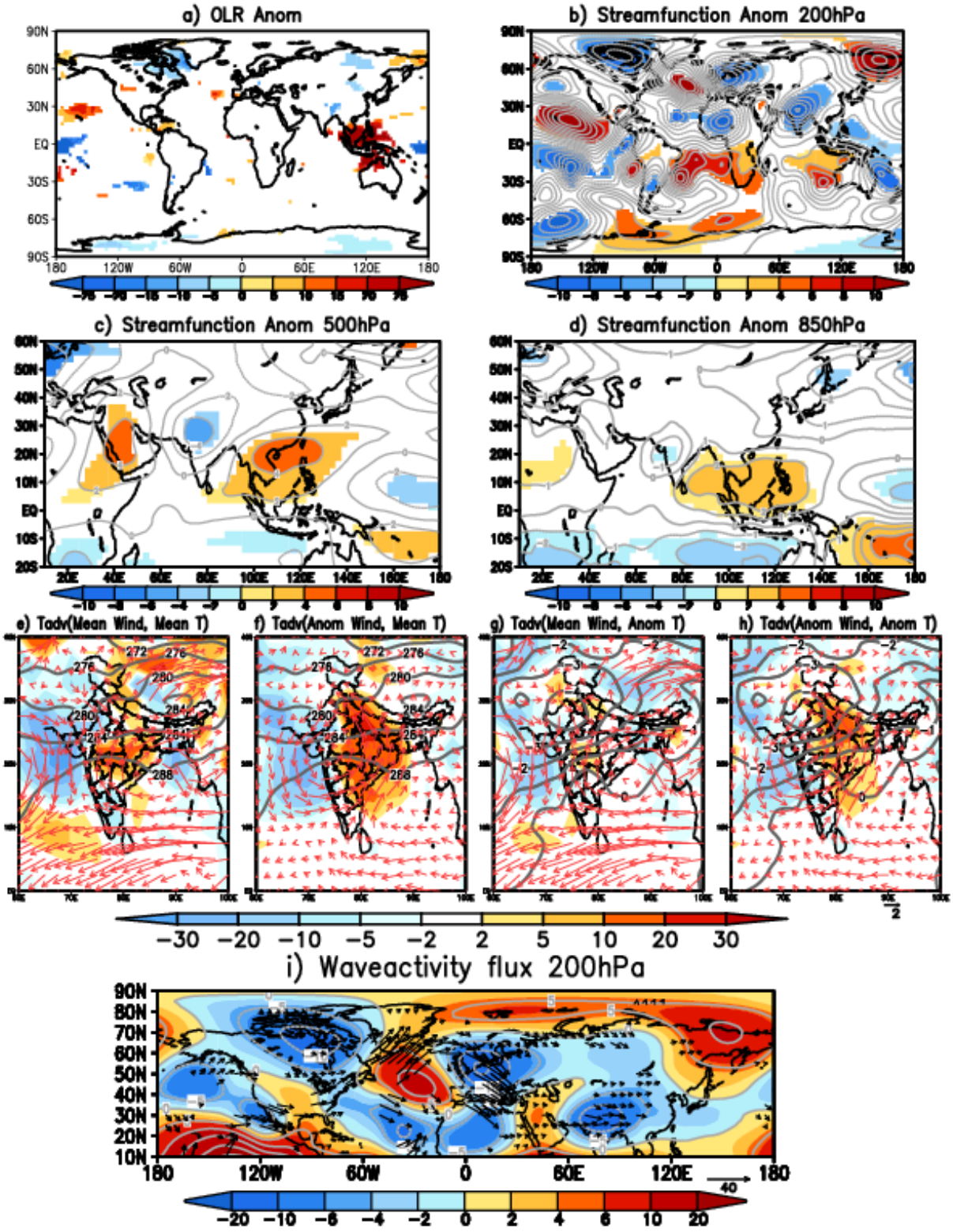

Fig 6.5. Same as Fig. 6.2 but for the TYPE2 events.

Mandal et al (2022) analyzed the skill to predict cold waves (CW) over India over a long period of time. They suggested that long CW events (> 7 days) are favoured by the La Nina condition and short CW events by the neutral condition in the Pacific. The blocking high northwest of the Indian longitude with a very slow movement of the westerly trough eastward is also associated with the long CW events. For short events, the blocking high is not so significant. Their study found that CW events are usually observed in association with the passage of the westerly trough on its back side (behind the trough) due to cold air advection from the higher latitudes. There is an anomalous westerly trough along the longitude of about 80^0 E, which attracts cold air from higher latitudes at 850 hPa due to the anomalous winds. La Nina conditions probably intensify the southwesterly jets and lead to cold winters over the northern and central parts of the country.

6.3 Case Study of a Cold Wave

In this section, a case study of cold wave which affected northern parts of the country is examined. During 26-31 December 2019, a cold wave gripped north India with negative temperature departures exceeding 5^0C (Fig 6.6). Negative temperatures anomalies were observed over most of north India (north of 20^0N). It may be important to note that 2019 was a La Nina year and as discussed earlier, the occurrence of cold waves during La Nina years is more frequent.

Fig. 6.7 shows the wind circulation anomaly at 200 hPa (top) and 500 hPa (bottom), a few days before the onset of the cold snap (24-26 December 2019). The circulation anomalies clearly indicate the presence of an anomalous cyclonic circulation just north of India and a deep trough extending from there across northwest India into the north Arabian Sea. This indicates the passage of a westerly disturbance over northern India, a few days before the cold wave started. During the cold wave, strong winds from northern India flow into central and northwestern India (Fig. 6.8 a) with strong meridional winds from the north (Fig. 6.8 b). These northerly winds bring cold air

to central and north-western India. The meridional northerly flow is not only observed at 700 hPa, but extends throughout the troposphere up to 150 hPa (Fig. 6.9), indicating that deep northerly winds from the north are flowing towards the Indian subcontinent, bringing cold and dry air towards north India.

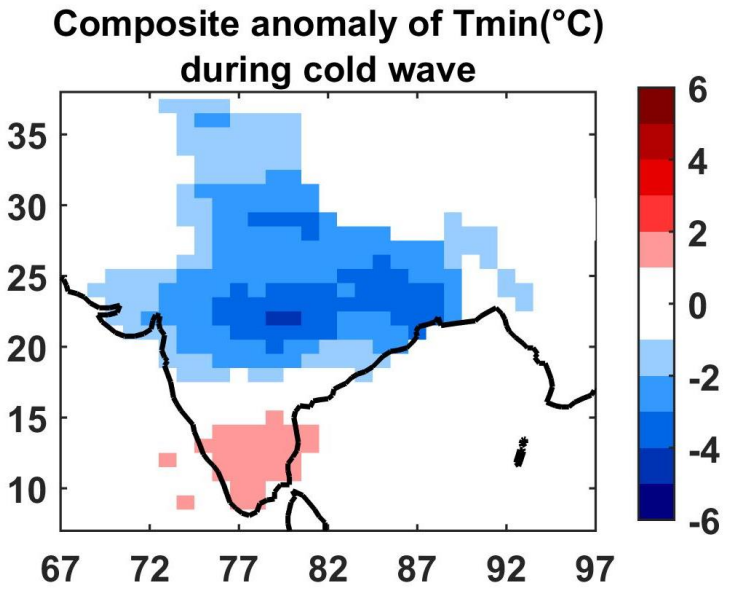

Fig 6.6. Minimum Temperature anomalies during the cold wave (26-31 Dec 2019) over north India.

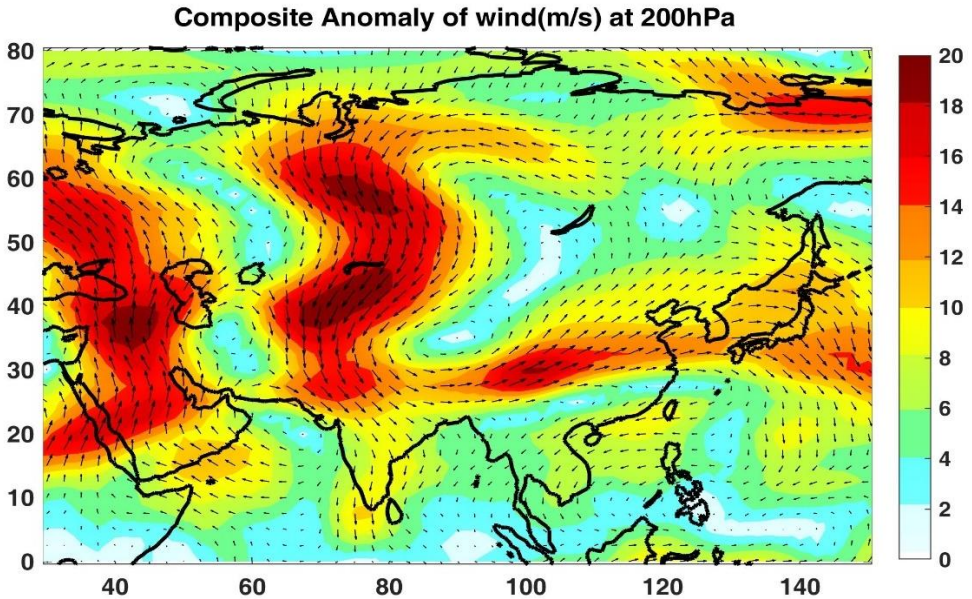

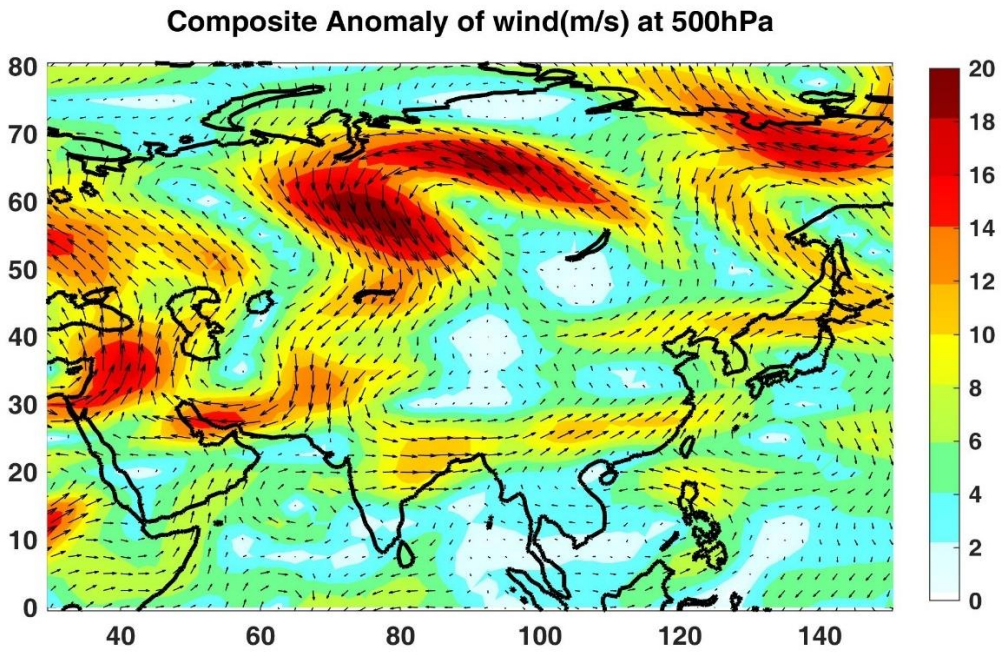

Fig 6.7 Composite wind anomalies at 200 hPa (above) and 500 hPa (below) during 24-26 Dec, 2019, just before the start of the cold wave. The anomalies have been computed using the climatology of 1972-2010.

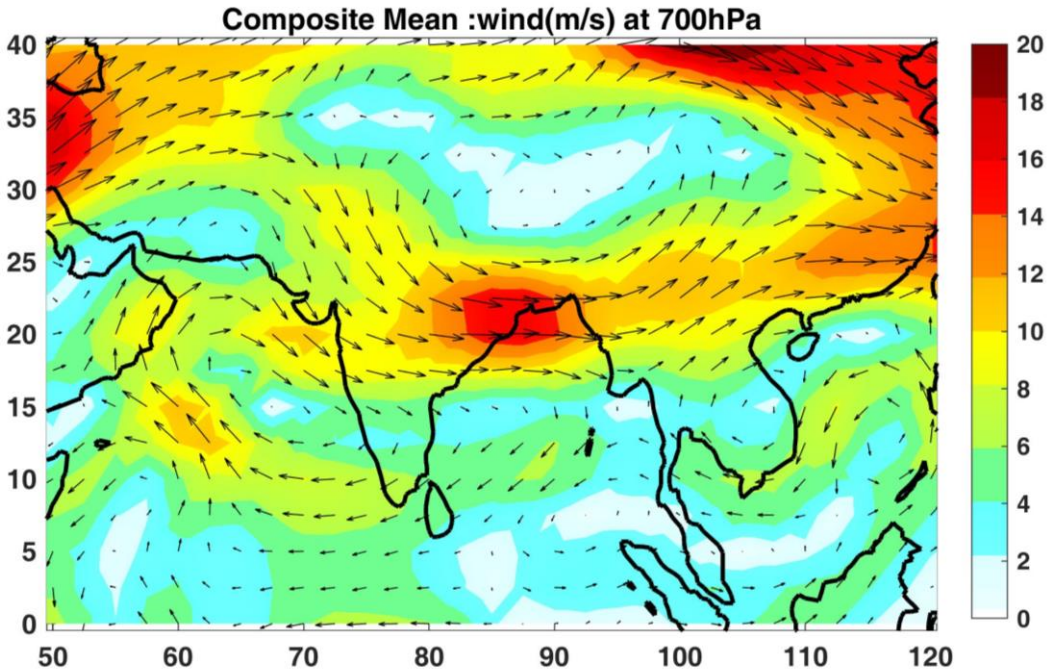

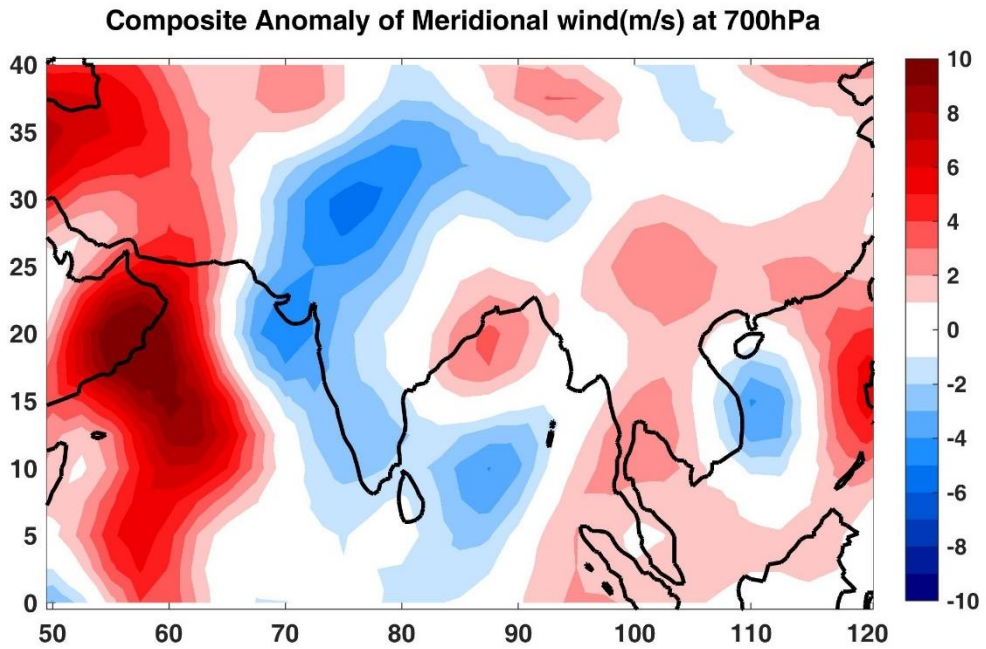

Fig 6.8. a) Composite 700 hPa mean vector winds during 26-27 Dec, 2019 (above) and b) meridional wind anomalies at 700 hPa (below) during the same period.

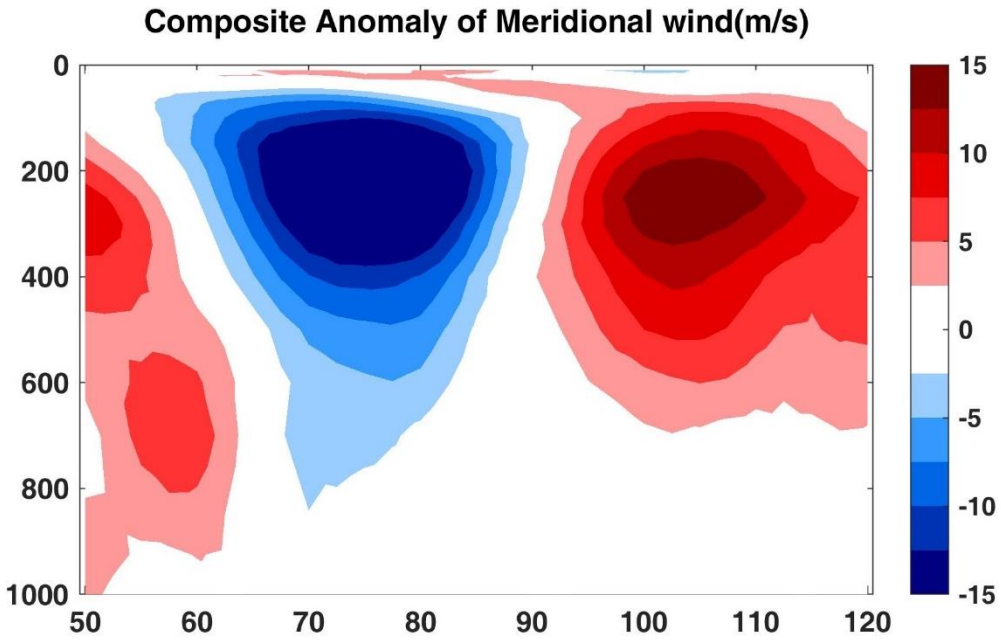

Fig 6.9. Longitude-Height profile of meridional wind anomalies (m/s) during the period 26-28 Dec, 2019, averaged over latitude 20^0-30^0N.

It is interesting to note that before the onset of the cold wave, cold air temperature anomalies are observed in the upper troposphere over the northern parts of India, but towards the eastern side of the core zone of the cold wave. This cold air anomaly is associated with the passage of a westerly disturbance prior to the cold wave event (Fig 6.10 a). Bedekar et al (1974) also discussed this aspect in the IMD forecast manual and suggested that meteorologists can get signals of a cold wave, even two days before, if we look at the temperature anomalies in the middle and upper troposphere. Negative temperature anomalies are first observed in the upper troposphere in the Indian subcontinent before they manifest in a cold wave over the surface. This aspect can be clearly seen in Fig. 6.10 b, the longitude-altitude profile of average temperature anomalies during the cold wave period (26-28 December 2019). A westward tilt of the temperature anomalies can be seen. The maximum temperature anomaly in the middle and upper troposphere is seen east of the cold wave region over the surface.

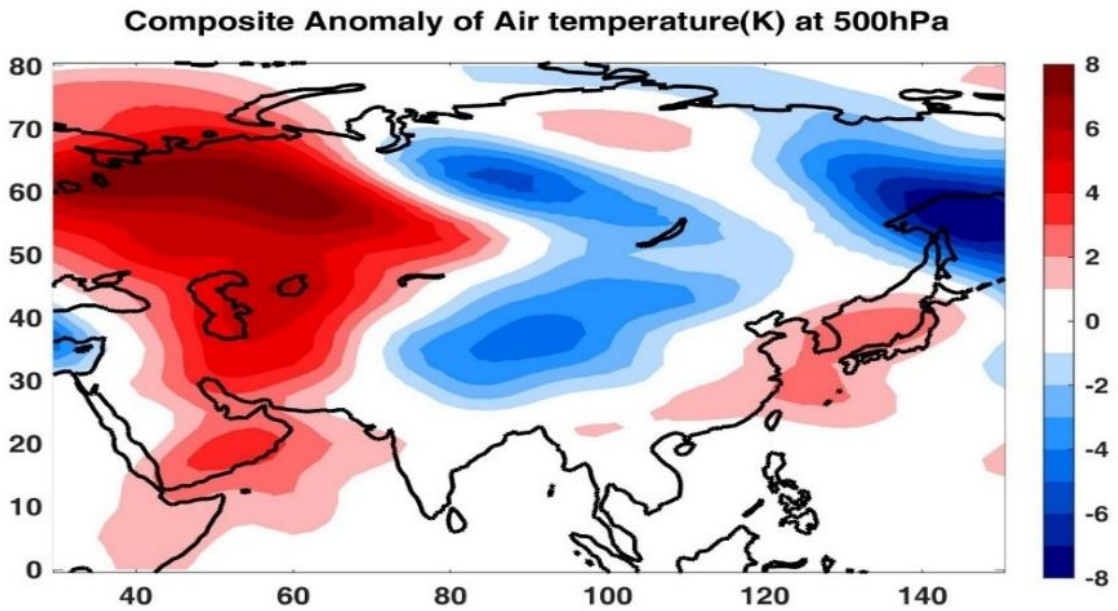

Fig 6.10 a. Composite air temperature anomalies (K) at 500 hPa during 24-26 Dec 2019.

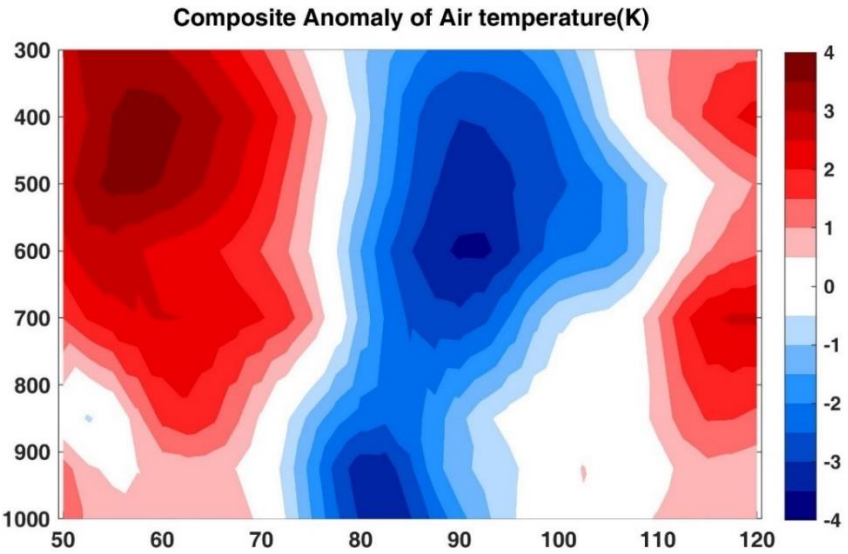

Fig 6.10 b. Longitude-Height profile of air temperature anomalies (K) from 1000-300 hPa, averaged over latitudes 20^0-30^0N, during 26-28 December 2019.

Fig. 6.11 shows the same vertical profile but for specific humidity. This indicates the presence of dry air from the surface up to 500 hPa during the cold wave over central India. Positive specific humidity anomalies are observed east of 100^0 E, which could be associated with the passage of the western disturbance and the associated moisture intrusion. Behind the western disturbance (west of the upper air trough), cold and dry air flows into northwest and central India, triggering a cold wave.

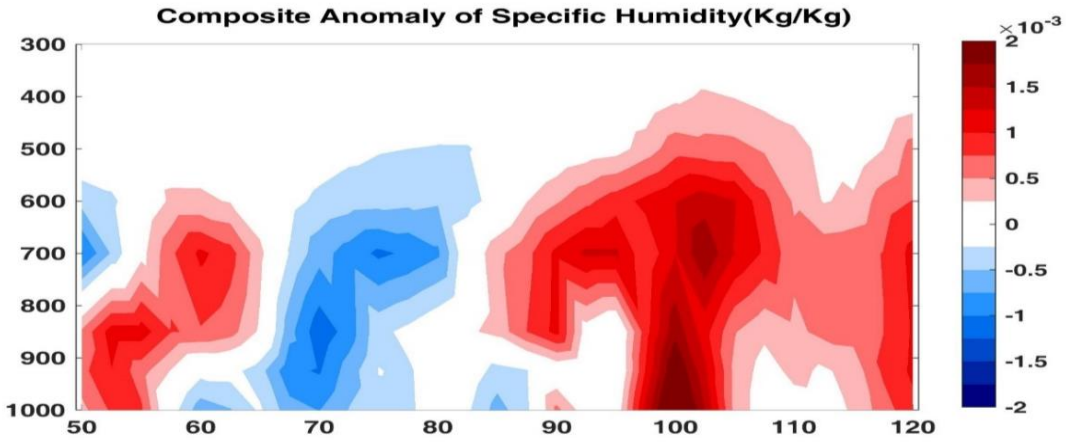

Fig 6.11. Longitude-Height profile of Specific Humidity anomalies (Kg/kg) from 1000-300 hPa, averaged over latitudes 20^0-30^0N, during 26-28 December 2019.

Chapter 7

Prediction of Heat and Cold Waves over India

This chapter discusses the predictability of heat and cold waves and the capabilities of numerical weather prediction (NWP) models in predicting them over India. Since heat and cold waves can have profound impacts on human health, agriculture and energy supply, it is important to understand the predictability of heat waves and how good the NWP models are in forecasting at different time scales.

In recent years, numerical weather prediction (NWP) models have improved in predicting weather events with large impacts such as heat waves, cold waves and heavy precipitation. There are many reasons for this, such as higher quality observations, better data assimilation methods and improved physical parameterization techniques etc. In India, few studies have been conducted on real-time prediction of heat waves. Recently, such studies have been conducted to explore the capability of extended range forecasting (Pattanaik et al. 2017; Mandal et al. 2019; Mandal et al. 2022). Real-time extended-range forecasting of heat waves over India in 2015 showed that both deterministic and probabilistic forecasts with a lead time of 2 weeks provided an indication of a subsequent extreme temperature over different parts of India (Pattanaik et al. 2017). Another study by Mandal et al. (2019) suggests that the real-time extended range forecasting system (IITM-IMD) is capable of predicting heat waves over the Indian region with a lead time of 2 weeks. A recent study (Singh et al. 2017) shows that ensemble forecasting has considerable ability to detect extreme temperature events compared to deterministic forecasts. In another study, Mandal et al. (2022) investigated the capability of extended-range forecasts for cold waves using the MoES/IITM extended-range forecasting system.

In section 7.1, we first discuss the skill of state of the art Numerical weather prediction models at the leading weather prediction centres like ECMWF, UK Met office and NCEP, USA. To accelerate the improvement of forecast accuracy for large impact

weather events (Swinbank et al. 2016), a global research programme called The Observing System Research and Predictability Experiment (THORPEX) Interactive Grand Global Ensemble (TIGGE) was launched in 2005 by the World Meteorological Organisation (WMO). The main objectives of TIGGE include improving international collaboration on ensemble predictions, understanding prediction errors, and developing new techniques for combining ensembles from different sources (Raoult and Fuentes 2008; Worley et al. 2008; Bougeault et al. 2010). The aim was to accelerate improvements in the forecasting of large impact weather events with lead times of 1 day to 2 weeks. Ensemble forecast data from ten global NWP centres from October 2006 are available in the TIGGE data archive (https://www.ecmwf.int/en/research/projects/tigge). Matsueda and Nakazawa (2014) have shown that probabilistic ensemble prediction products from TIGGE successfully predicted extreme weather events such as the Russian heatwave in 2010, the floods in Pakistan in 2010 and Hurricane Sandy in 2012.

Out of the ten models, we have considered only the best three models, which have long term data for validation. Table 7.1 shows the three TIGGE models considered for the verification analysis.

The verification methods like mean error (ME), root mean square error (RMSE) and Pearson's correlation coefficient (CC) are used in this study. The methods used for verifications are illustrated below.

A. Mean Error (ME)

$$ME = \frac{1}{N}\sum_{i=1}^{N}(F_i - O_i)$$

B. Root Mean Square Error (RMSE)

$$RMSE = \sqrt{\frac{1}{N}\sum_{i=1}^{N}(F_i - O_i)^2}$$

Where F_i = forecasted ensemble mean of Tmax, O_i = observed Tmax and N is the total number of events

C. Ensemble Spread (ES)

$$ES = \sqrt{\frac{1}{M}\sum_{n=1}^{M}(y_n - \overline{y})^2}$$

where, $\overline{y}$ is the ensemble mean, y_n is the n^{th} ensemble member and M indicates the total ensemble members.

Forecast verification scores using contingency table

Contingency table is a useful summary of observed and the forecasted weather events. The table does not comprise a verification method itself, but various forecast scores can obtain based on this table. In this study, various scores calculated from two-by-two contingency table to evaluate the performance of the heat-wave forecast are probability of detection (POD), false alarm ratio (FAR), threat score (TS), and equitable threat score (ETS).

A. Probability of Detection (POD)

It is the ratio of number of hits to the total number of events observed. POD is very sensitive to hits, but it is not including false alarms. Its values vary from 0 to 1. POD is 1 for perfectly forecasted events and it is computed by

$$POD = \frac{hits}{hits + misses}$$

B. False Alarm Ratio (FAR)

It is the ratio of the total false alarms to the total events forecasted. Its value varies from 0 to 1 and a perfect score is 0.

$$FAR = \frac{false\ alarms}{hits + false\ alarms}$$

C. Threat Score (TS)

The threat score is also known as the critical success index (CSI). It is a frequently used standard verification measure. It is the ratio of number of correct forecast events to the total number of occasions on which that event was forecast and/or observed. It has a range of 0 to 1 with a value of 1 indicating a perfect score.

$$TS = CSI = \frac{hits}{hits + missess + false\ alarms}$$

D. Equitable Threat Score (ETS)

It is also known as the Gilbert skill (GSS). It explains how accurately the predicted yes events agree with the observed yes events. It is referred to as the ratio of successes. The values vary between -1/3 and 1; 0 indicate no skill and 1 denotes the perfect skill.

$$ETS = GSS = \frac{hits - hits_{random}}{hits + missess + false\ alarms - hits_{random}}$$

where,

$$hits_{random} = \frac{(hits + false\ alarms)(hits + misses)}{total}$$

7.1 Short to Medium Range Prediction Skill of NWP models from TIGGE

This section discusses the results of reviewing the short to medium term prediction of heat waves over India using the TIGGE models.

For this purpose, heat wave events with the 90th percentile threshold of maximum temperature (Tmax90) were selected using the gridded Tmax data from IMD (Srivastava et al., 2009). Fourteen heat wave events with a duration of at least 3 days were identified over northwest India during the period 2008-2013. For all three TIGGE

models, continuous daily hindcasts are available only for the common period of 2008-2013. The present analysis is based on 14 events during this period and is shown in Table 7.2. For this analysis, the daily Tmax values predicted by the model were used after removing the climatological bias based on the reference period 2008-2013. Continuous daily Tmax hindcasts are not available for all three models beyond 7-day forecasts. Therefore, heatwave predictability was only analyzed for a lead time of 1-7 days.

Table 7.1

Details of the TIGGE models considered in this study

Model Name	Number of Ensemble Members	Forecast length(days)	Model Resolution
National Centres for Environmental Prediction (NCEP)	20	16	T126
UK Meteorological Office (UKMO)	23	15	N640
European Centre for Medium-Range Weather Forecasts (ECMWF)	50	15	TL639(0- 10day)/ TL339(10-15day)

The mean bias (Model minus observation) of all the three models during 14 heat wave events (composite) is shown in Fig. 7.1. Maximum Temperature (Tmax) over central and northwest India is overestimated in NCEP model and underestimated in the ECMWF model. UKMO has shown less bias as compared to other two models over the heat wave prone area. Therefore, further verifications were made using bias corrected temperatures data with IMD observations.

Table 7.2.

Heat wave events identified for heat wave prone area based on the IMD observations

2008	26 Apr-29 Apr
2009	27 Apr- 2 May, 20 Jun-22 Jun
2010	5 Apr – 19 Apr, 27 Apr-29 Apr, 12 May-17 May,19 May-26 May,11 Jun-14 Jun,19 Jun-22 Jun, 26 Jun-28 Jun
2011	6 Jun-8 Jun
2012	2 Apr-10 Apr,30 May-01 Jun
2013	17 May-23 May

Fig.7.2 shows the ensemble mean and spread of TIGGE model predictions over the heatwave prone area (NWI) during all 14 heatwave events. The ensemble spread measures the difference between ensemble members. The ensemble mean is the average value of the predicted variables across all ensemble members. Ensemble spread and ensemble mean are calculated for the averaged Tmax value (bias corrected) during each heat wave event with a lead time of 7 days. All three models showed a lower spread for most events for forecasts with a lead time of 1 to 4 days. The scatter increases with the forecast time. For the UKMO model, the scatter is larger for most events than for the other two models. The scatter between ensemble members is lower for NCEP, followed by ECMWF. The scatter of the ensemble in the NCEP model is much lower compared to the other two TIGGE models for all heat wave events with different lead times. The coarser resolution of the NCEP model could be the reason for this smaller ensemble spread. The area-averaged maximum temperatures of the ECMWF model is almost identical to the IMD observation for most events.

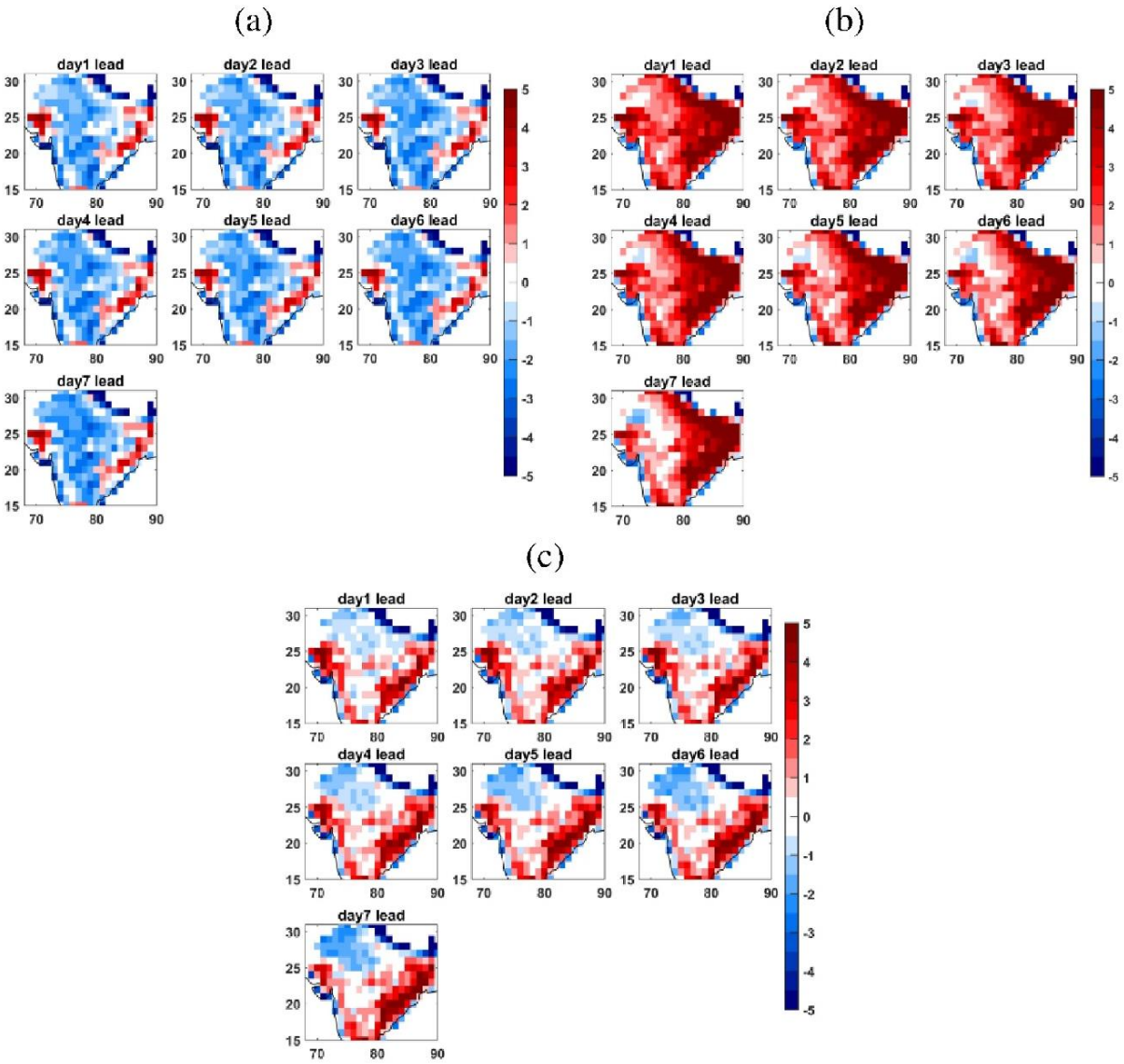

Fig 7.1. Model Bias (model-observations) in maximum temperatures (^{0}C; using Ensemble mean) of TIGGE models (a) ECMWF (b) NCEP and (c) UKMO during heat wave spells. (Taken from Rohini and Rajeevan 2023).

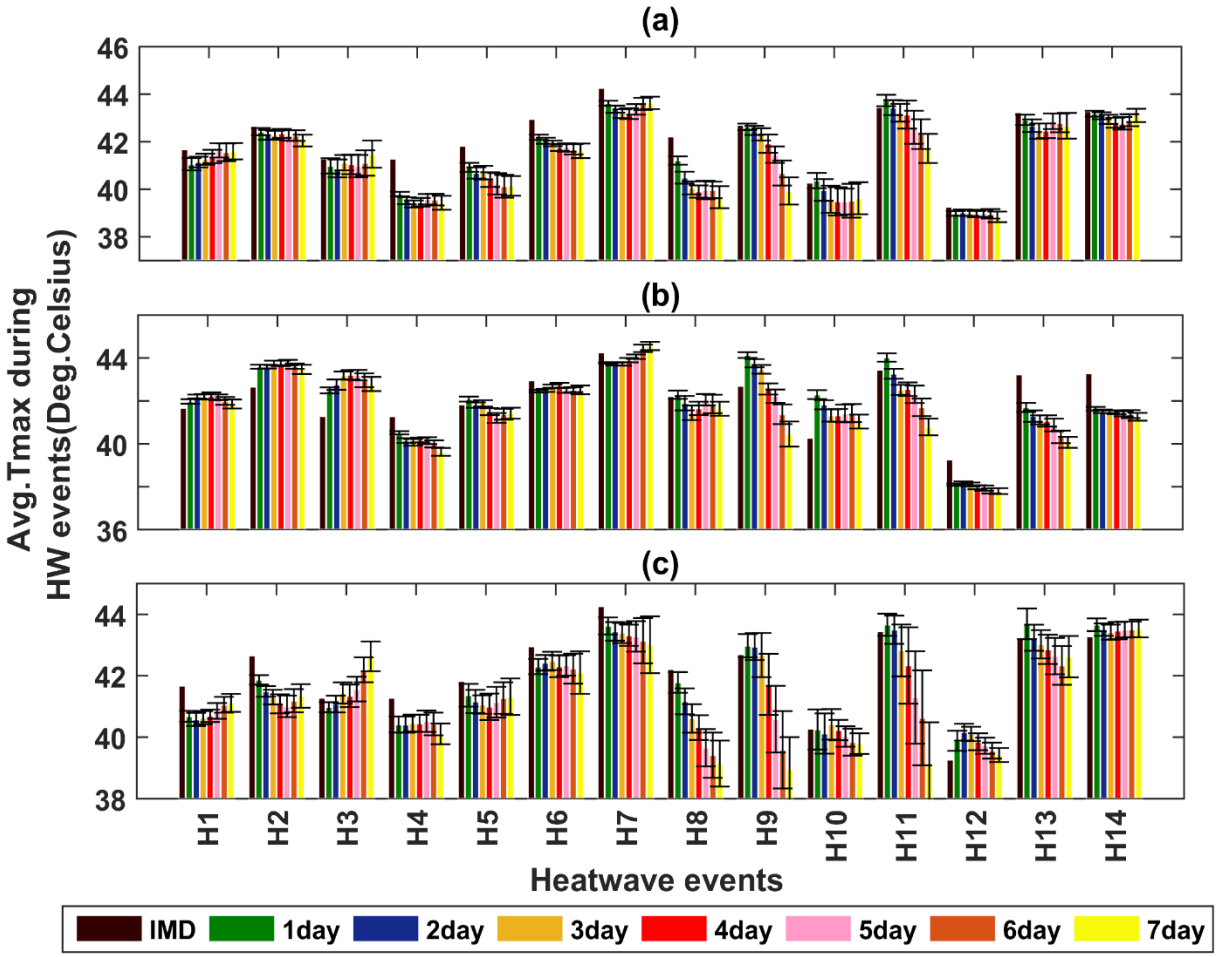

Fig 7.2. Ensemble mean (^{0}C) and ensemble spread (^{0}C) of (a) ECMWF (b) NCEP and (c) UKMO during the 14 heat wave events (H1-H14). Ensemble spread is shown as a bar (black color) and ensemble mean as color bar. Each color indicates the forecast lead time and observations. The Heat wave events considered are given in Table 6.2. (Taken from Rohini and Rajeevan 2023).

The spatial distribution of the bias-corrected Tmax (ensemble mean) of the TIGEE models is shown in Fig.7.3. The spatial pattern is well predicted in all three TIGGE models, but the magnitude is different from the observations. These models are able to capture the spatial distribution of Tmax reasonably well up to a prediction time of 7 days.

In addition, the verification values of all these models were calculated using 14 cases for northwest India. The verification values such as mean error (ME), root mean square

error (RMSE) and correlation coefficient (CC) were calculated and the results are given in Table 7.3. Verification statistics are calculated using area-averaged Tmax values (bias corrected) over heatwave vulnerable areas (NWI) during these events. The ME for all forecast periods is negative for the ECMWF and UKMO models, which means that the model forecasts underestimate Tmax compared to the observations. The magnitude of ME and RMSE increases with forecast time. The RMSE is lower for ECMWF than for UKMO, followed by the NCEP model. All model predictions show a significant correlation (statistically significant at 95% significance level) with observations in all prediction periods. The ECMWF model has a fairly high correlation with the observations (above 0.90), even with a lead time of 6 days. However, CC is relatively smaller in the NCEP model. The NCEP model shows relatively less ME compared to the UKMO model. The skill of the model predictions can be improved by increasing the ensemble size (Kharin et al. 2001). This could be the reason why the ECMWF model with 50 ensemble members shows higher skill and the NCEP model with 20 ensemble members shows lower skill.

In addition, the statistical verification values such as Threat Score (TS), Equitable Threat Score (ETS), False Alarm Ratio (FAR) and probability of detection (POD) were calculated to understand the predictability of the heat wave over northwest India. For this analysis, model predictions for the period 2008-2013 were evaluated. The criterion for detecting a heatwave is 'when the daily Tmax (bias-corrected) exceeds the value of the upper 90th percentile climatological Tmax' for three or more consecutive days. the 90th percentile is calculated in a 5-day moving window and the reference period used for calculating climatology is 2008-2013.

Table 7.3.

Verification statistics (Mean Error, Root Mean Square Error and Correlation Coefficient (CC)) of TIGGE models for14 heat wave events over India. ME, RMSE and CC are calculated for the heat wave prone area (HWPA).

Forecast lead time →		1-day	2 day	3 day	4 day	5 day	6 day	7 day
ECMWF	ME (°C)	-0.20	-0.41	-0.51	-0.55	-0.55	-0.57	-0.64
	RMSE (°C)	0.38	0.51	0.62	0.72	0.74	0.83	1.02
	CC	0.97	0.97	0.96	0.93	0.93	0.91	0.83
UKMO	ME (°C)	-0.08	-0.23	-0.35	-0.60	-0.74	-0.86	-0.98
	RMSE (°C)	0.56	0.65	0.71	1.10	1.15	1.42	1.78
	CC	0.91	0.88	0.88	0.74	0.74	0.61	0.45
NCEP	ME (°C)	0.13	-0.05	-0.16	-0.23	-0.29	-0.48	-0.73
	RMSE (°C)	1.07	1.06	1.12	1.12	1.18	1.33	1.54
	CC	0.71	0.69	0.67	0.68	0.65	0.61	0.57

Heat wave events are calculated from observations using the same criteria for the same time period. If at least two days of the predicted event match the observation, it is considered a hit. The verification values such as TS, ETS, POD and FAR of heat wave prediction of three TIGGE models (ECMWF, UKMO and NCEP) for a forecast of 1-7 days are shown in Fig.7.4.

The skill of the models reaches a high threshold value up to a forecast period of 5 days for all three models (Fig.7.4). TS the values of ETS and POD decrease and FAR

increases with the length of the forecast. A high value of POD indicates that the model can predict the majority of observed 'yes' events. POD Values are greater than 0.55 for all three models for a prediction length of 1-7 days. For ECMWF, observed events are predicted about 91% of the time on day 1, with a slight decrease to 81% on day 5. UKMO predicted about 91% of cases on Day 1, dropping slightly to 55% on Day 5, and NCEP predicted about 82% of cases on Day 1, dropping slightly to 64% on Day 5. It goes without saying that ECMWF has relatively higher POD values than the other two models. The false alarm rate is less than 0.4 for days 1-5, which means that the false alarms are less than the number of hits. From day 6 onwards, there are more false alarms, which are approximately equal to the number of hits, especially for the UKMO and NCEP models. However, the ECMWF model has shown a higher skill score (POD ~0.72 and FAR 0.33) for 6 days lead time, suggesting that this model can provide a better forecast for heat waves up to six days lead time.

The Threat Score (TS) indicates the proportion of correct predictions. TS evaluates only the hits without considering the correct negative predictions. TS is significantly lower than or equal to POD. All three models show a higher threshold of TS (ECMWF ~ 0.91, UKMO ~ 0.77 and NCEP ~ 0.75) at a forecast of 1 day and these values reduce to half at a forecast of 6 days. ETS corresponding to TS also showed a higher threshold (ECMWF ~ 0.64, UKMO ~ 0.39 and NCEP ~ 0.49) up to a lead time of 5 days.

From this forecast verification analysis, it can be concluded that all three TIGGE models are capable of providing early warnings for heat waves with a lead time of at least 5 days. However, the ECMWF can forecast heat waves with 6 days lead time with reasonable accuracy and competence.

Singh et al. (2017) analyzed the skill of prediction of heat waves over India using the NCMRWF ensemble and deterministic models. The results indicated that an appreciable competence of the ensemble forecast at detecting extreme events compared to the deterministic forecast. Locations of the events are also better captured

by the ensemble forecasts. Further, it is noted that ensemble system smooths down the unexpectedly increasing signals, thereby reducing the false alarms and thus proving to be more reliable than the deterministic forecasts.

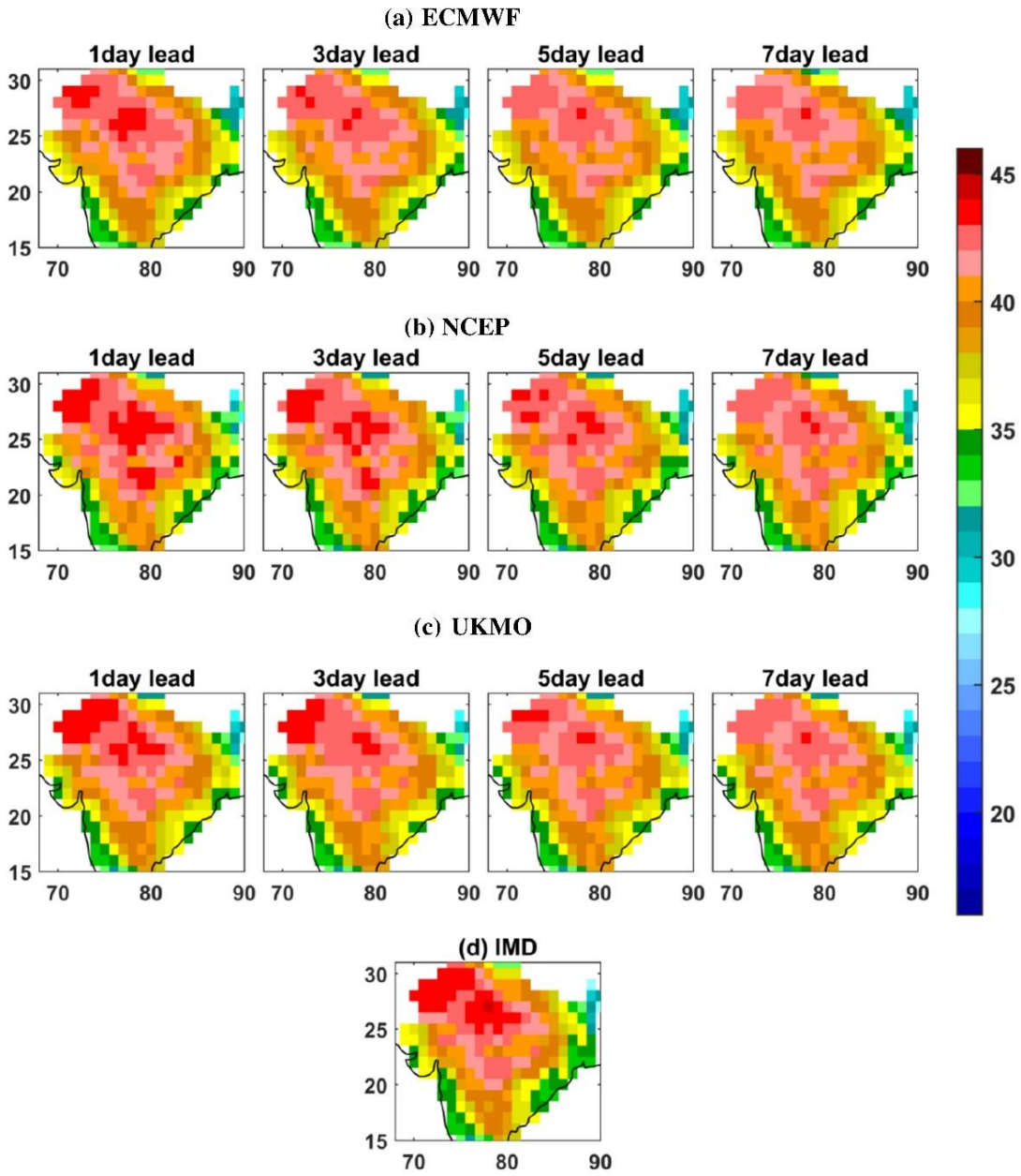

Fig 7.3. Composite **s**patial distribution of maximum temperature (^{0}C; using Ensemble mean) during heat wave events from TIGGE models (a) ECMWF (b) NCEP and (c) UKMO along with IMD observation. The heat wave events considered for the composite analysis are given in Table 7.2. (Taken from Rohini and Rajeevan 2023).

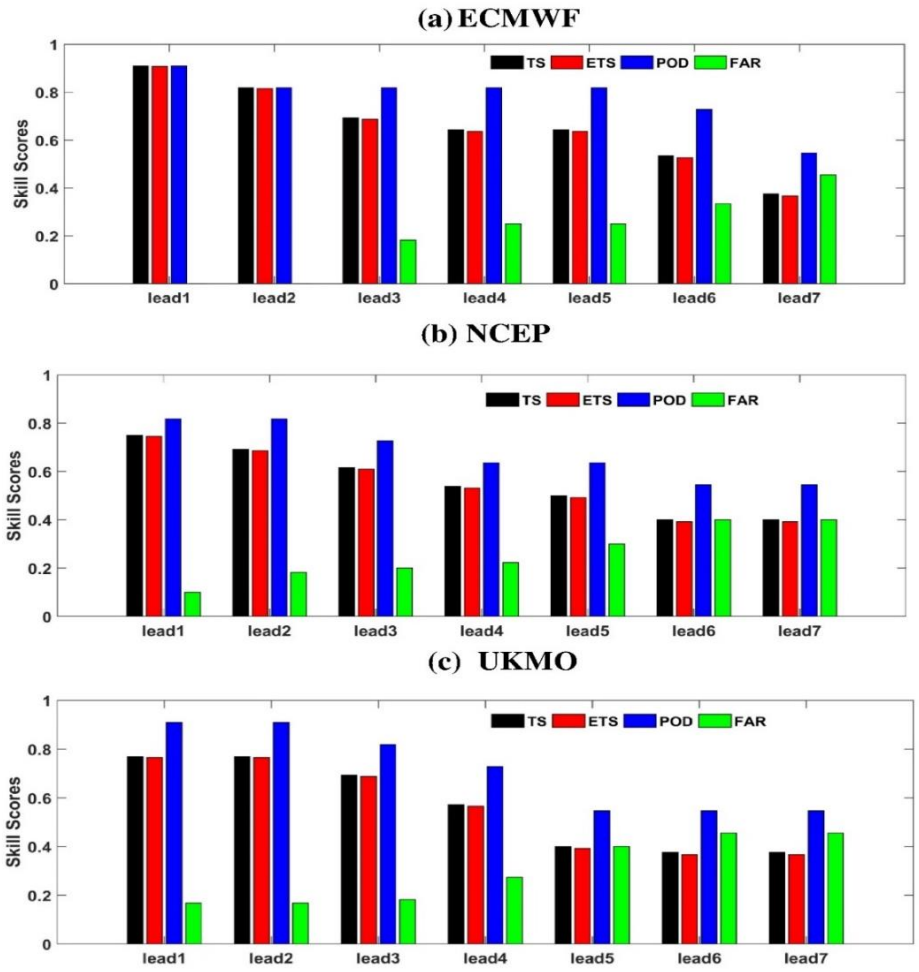

Fig 7.4. Threat Score (TS), Equitable Threat Score (ETS), Probability of detection (POD) and False Alarm Ratio (FAR) for heat wave forecast verification from (a) ECMWF (b) NCEP and (c) UKMO. (Taken from Rohini and Rajeevan 2023).

7.2 Short to Medium Range Forecasts using IMD/IITM models

In this section, a detailed analysis of the predictive ability of the IMD/IITM GFS and GEFS models is carried out for two heat waves and one cold wave case studies. The heat waves considered are (a) 29 May to 11 June 2019, which affected central and northwest India, and (b) 20 March to 03 April 2021, which affected the east coast of

India. The cold wave considered is the event of 26 to 31 December 2019, which affected central and north-western India.

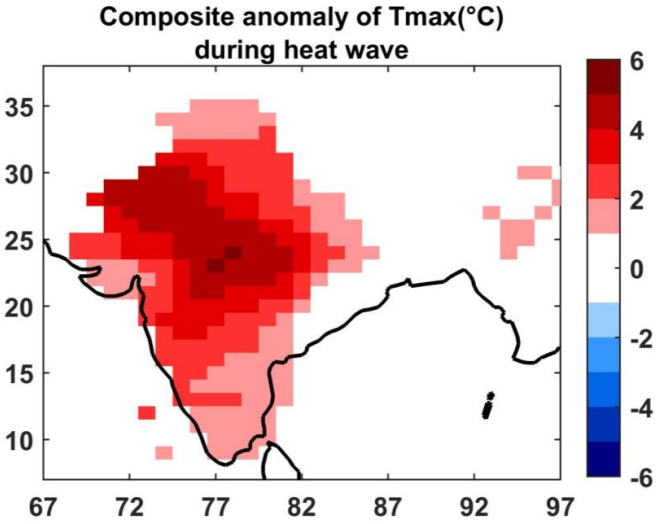

Fig 7.5. Max Temperature anomalies (^{0}C) during the heat wave of 29 May-11 June, 2019.

Fig. 7.5 shows the maximum temperature departures for the period from 29 May to 11 June, derived from IMD data (Srivastava et al. 2009). The deviations are in the order of 4^0-6^0 C over central and north-western India. Fig. 7.6 shows the probability of Tmax > 45.0^0 C in 24 hours (top), 72 hours (middle) and 120 hours (bottom) for three representative days, 29 May (left), 02 June (middle) and 11 June (right). These probabilities were derived from the IITM GEFS ensemble model. The probability predictions indicate that there is more than 50% probability of Tmax above 45^0C over central and north-western India. Fig. 7.7 and Fig. 7.8 show the predicted Tmax and its deviations for three representative dates (29 May, 02 June and 11 June) based on the IMD/IITMGFS model.

These plots also very clearly suggest the GFS prediction system was capable of predicting Tmax exceeding 44^0C over central and northwest India with large departures from long term normal, even at 120 hrs lead time (5 days ahead). The model also predicts very well the presence of dry air (with negative RH departures) over the heat wave region during this period (Fig 7.9).

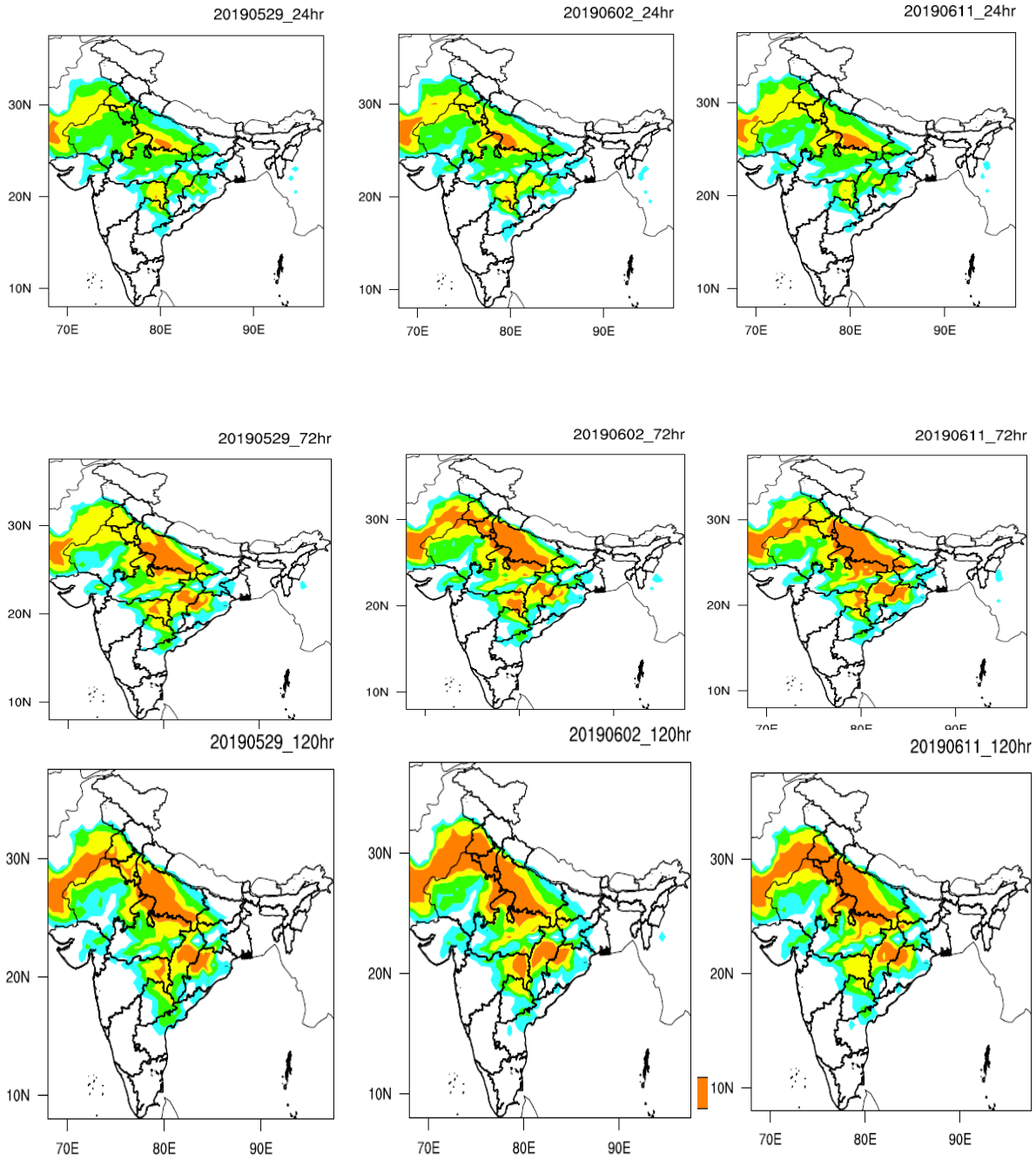

Fig 7.6 Probability of Tmax > 45.0^{0}C in 24 hr (top), 72 hr (middle) and 120 hr (bottom) for 29 May (left), 02 June (middle) and 11 June (right) columns. These probabilities are derived from the IMD/ IITM GEFS Ensemble model.

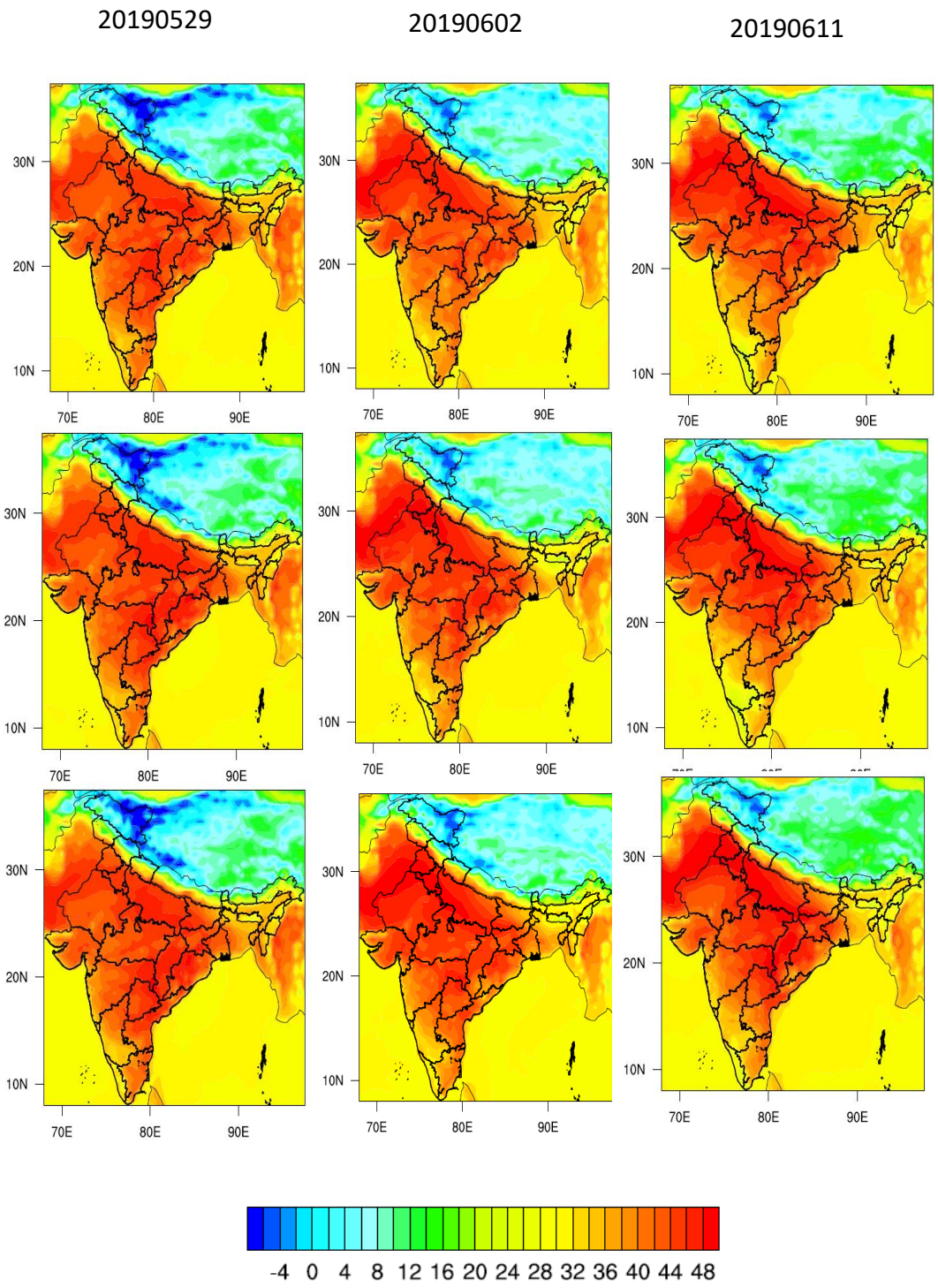

Fig 7.7. Predicted maximum temperatures (^{0}C) for 29 May (left column), 02 June (middle) and 11 June (right) at lead time of 24 hrs (top panel), 72 hrs (middle) and 120 hrs (bottom). These forecasts are from the IMD/IITM GFS model.

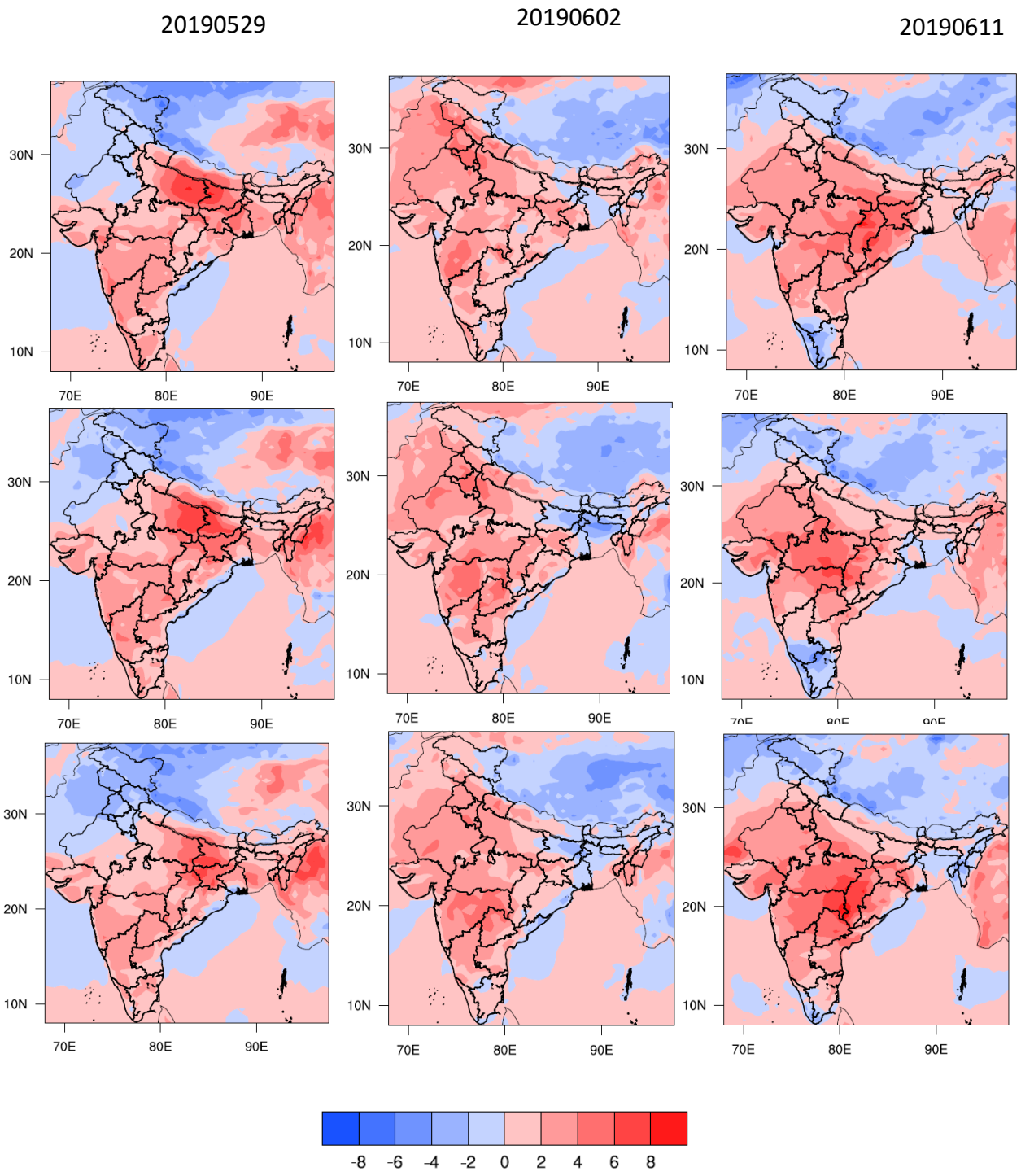

Fig 7.8. Predicted maximum temperature departures (^{0}C) for 29 May (left column), 02 June (middle) and 11 June (right) at lead time of 24 hrs (top panel), 72 hrs (middle) and 120 hrs (bottom). These forecasts are from the IMD/IITM GFS model.

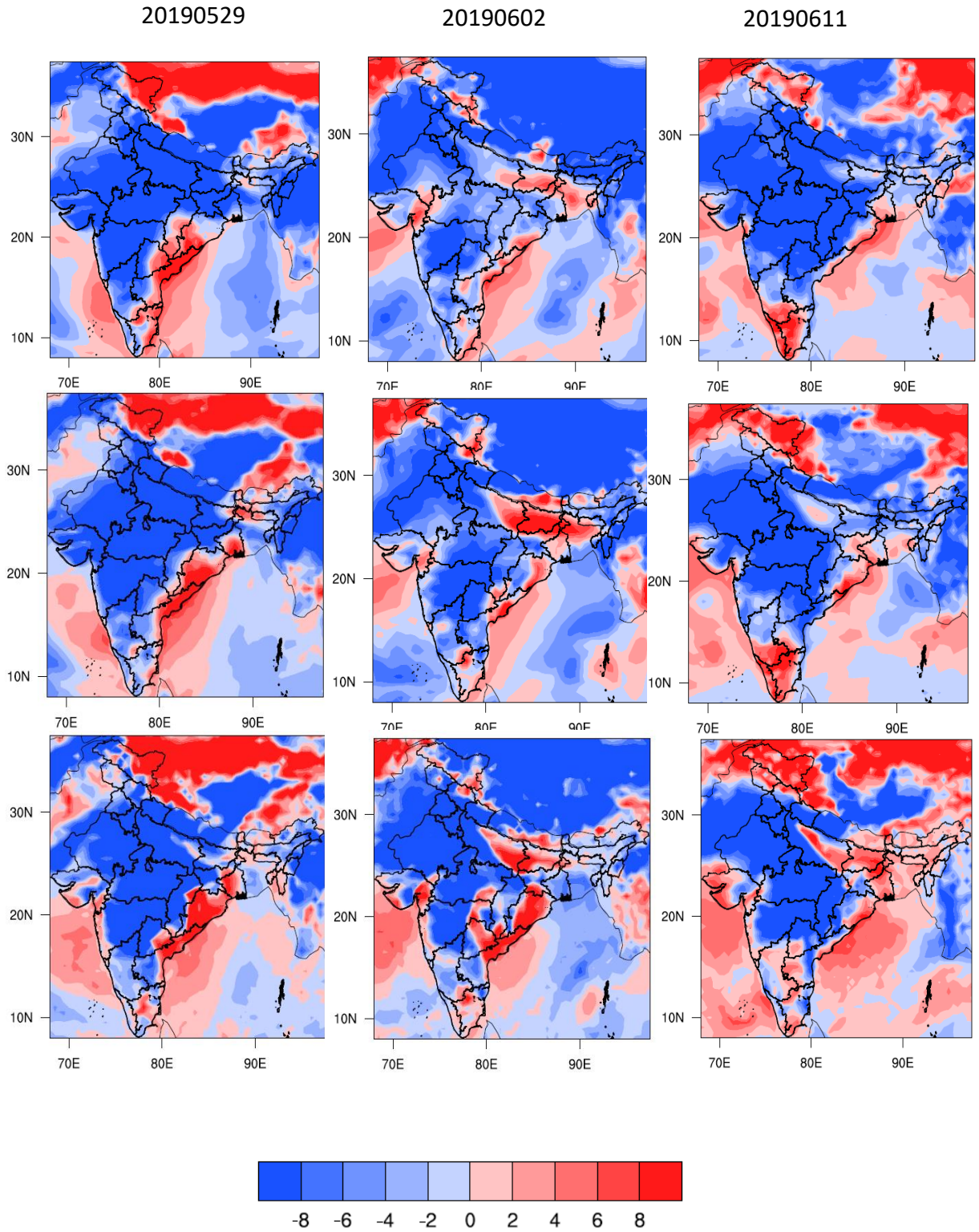

Fig 7.9. Predicted Relative Humidity Departures (%) for 29 May (left column), 02 June (middle) and 11 June (right column) at lead time of 24 hrs (top panel), 72 hrs (middle) and 120 hrs (bottom). These forecasts are from the IMD/IITM GFS model.

The predictions of the 200 hPa and 850 hPa circulation features (Fig. 7.10 a) indicate that the model predicts the basic dynamics associated with the heat waves over the Indian region reasonably well. At 200 hPa, in the mid-latitudes, deep troughs and ridges could be observed in association with the Rossby wave pattern. A blocking high is observed over the Caspian Sea and adjacent areas. The 850 hPa plots indicate a large-scale high pressure and a north-south ridge (anticyclonic flow) over central and northwestern India. Fig. 7.10 b shows similar plots but for 11 June 2019. This abnormal wind circulation and associated subsidence is the main cause for the occurrence of heat waves over India. Thus, the GEFS and GFS models could predict the heat wave between 29 May and 11 June 2019.

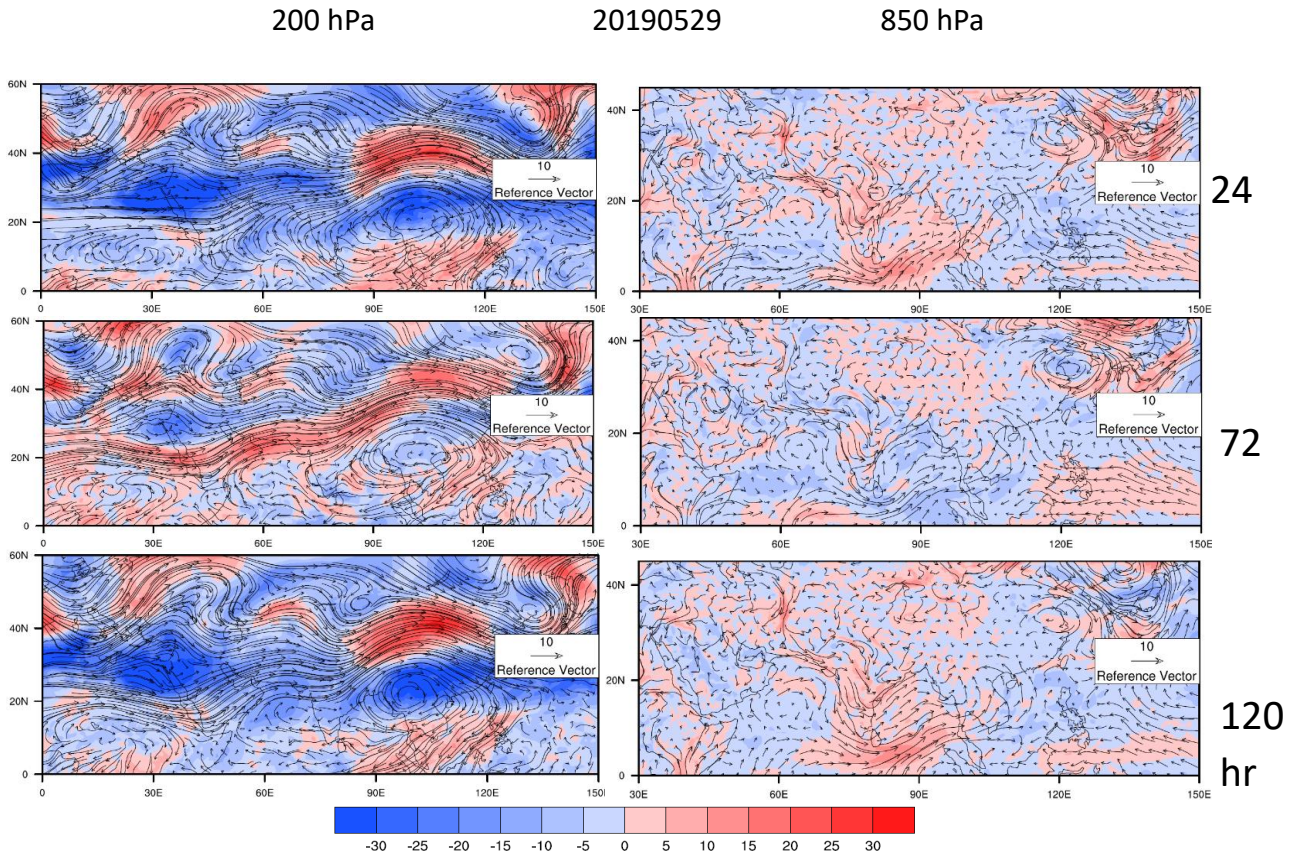

Fig 7.10 a Predicted Wind vectors with the anomalous wind magnitude in shaded (m/s) for 200 hPa (first column), 850 hPa (second column) on 29 May 2019. The forecasts are for 24 hr (top panel), 72 hr (middle panel) and 120 hrs (bottom panel).

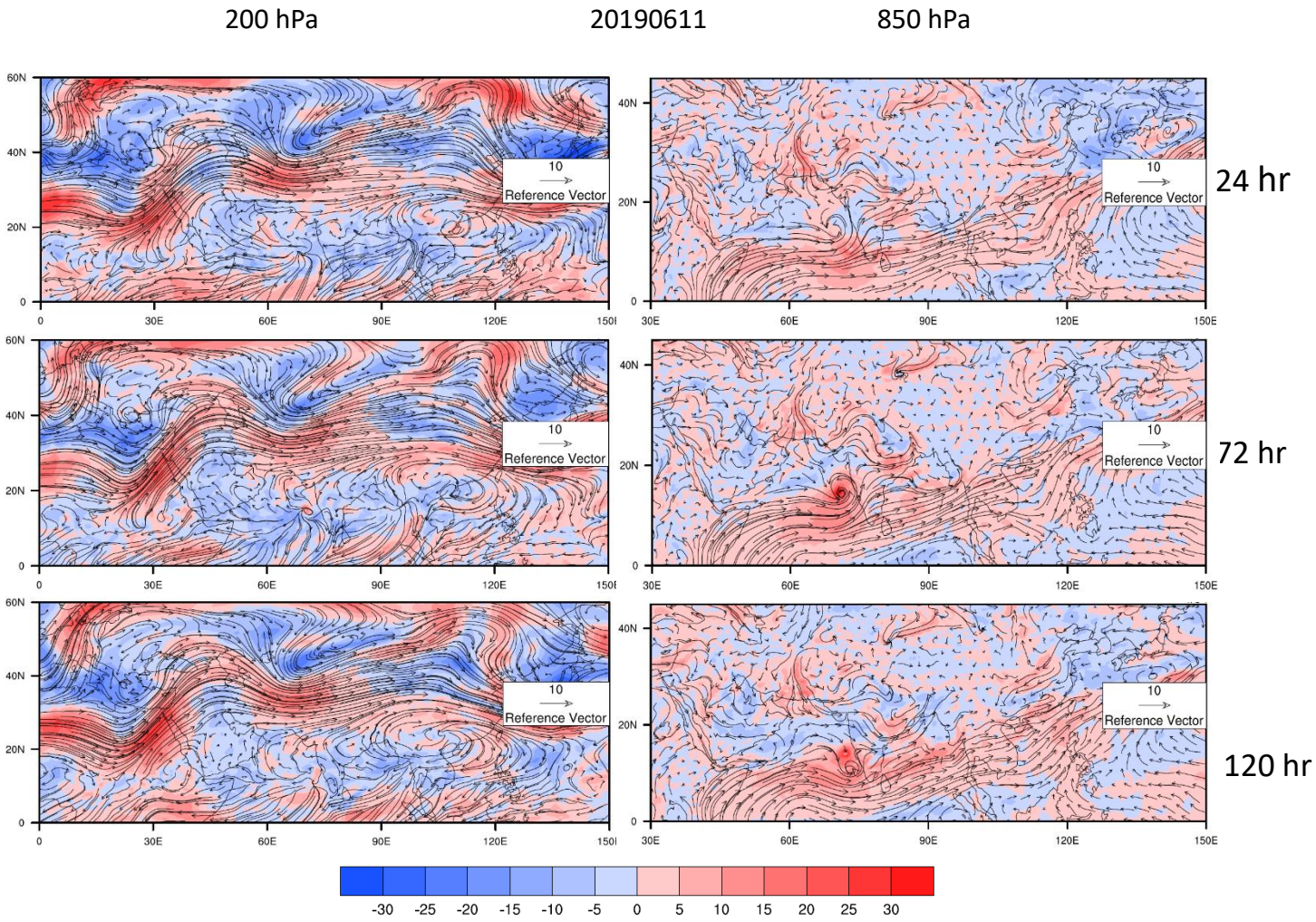

Fig 7.10 b Predicted Wind vectors with the anomalous wind magnitude in shaded (m/s) for 200 hPa (first column), 850 hPa (second column) on 11 June 2019. The forecasts are for 24 hr (top panel), 72 hr (middle panel) and 120 hrs (bottom panel).

We shall now discuss about the heat wave on the east coast of India. This event was observed in the region between 30 March and 03 April 2021. Fig. 7.11 shows the predicted maximum temperatures on three representative days, 30 March, 31 March and 02 April with a lead time of 24, 72 and 120 hours respectively. The plot clearly shows that the model was capable of predicting the occurrence of daily maximum temperatures of more than 40°C over the east coast of India, especially on 31 March and 02 April 2021. The model was also able to predict positive temperature deviations of more than 4.0^0C over the east coast of India (Fig. 7.12).

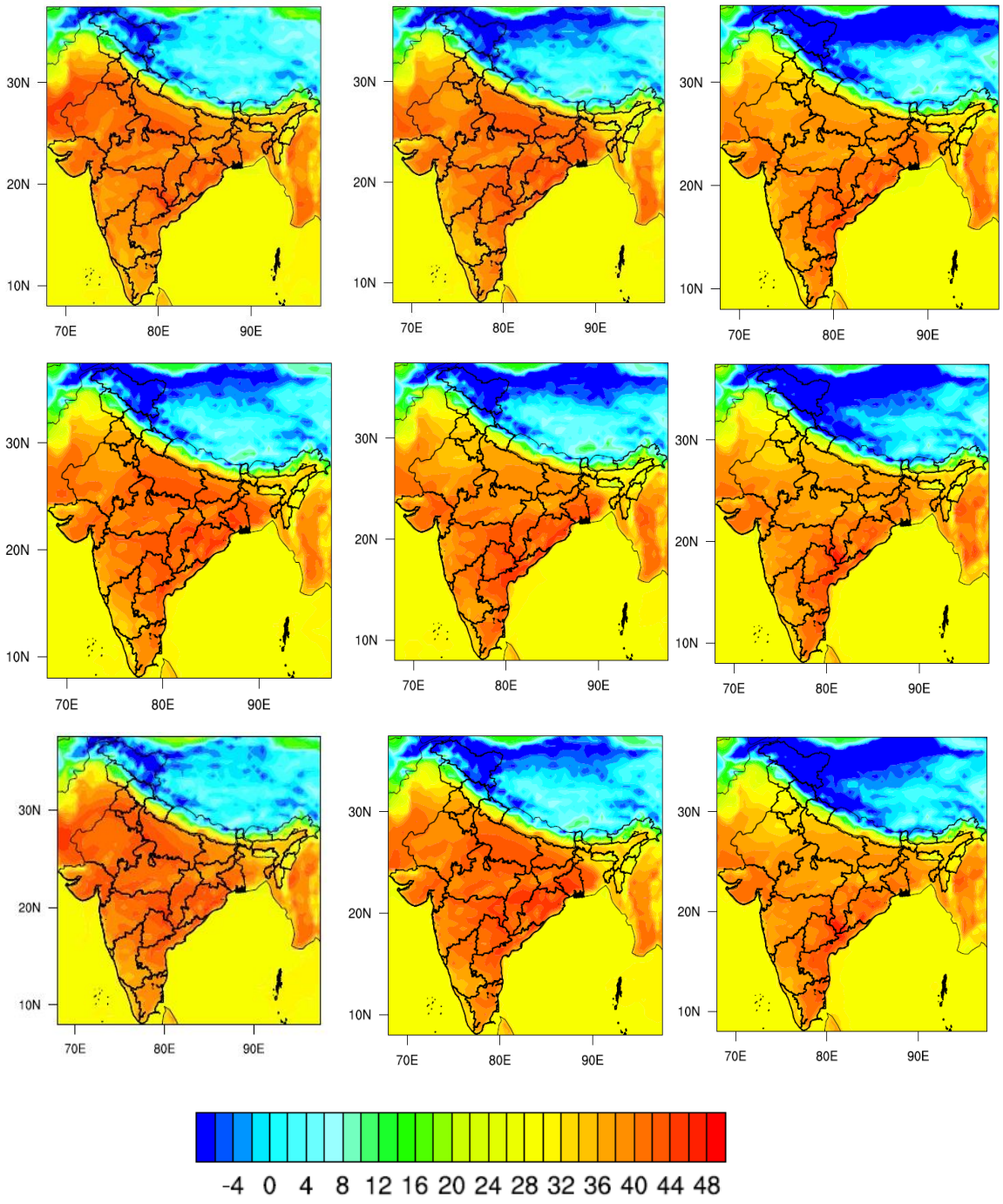

Fig 7.11. Predicted Maximum Temperatures for 30 March (left column), 31 March (middle) and 02 April (right column) at lead time of 24 hrs (top panel), 72 hrs (middle) and 120 hrs (bottom). These forecasts are derived from the IMD/IITM GFS model.

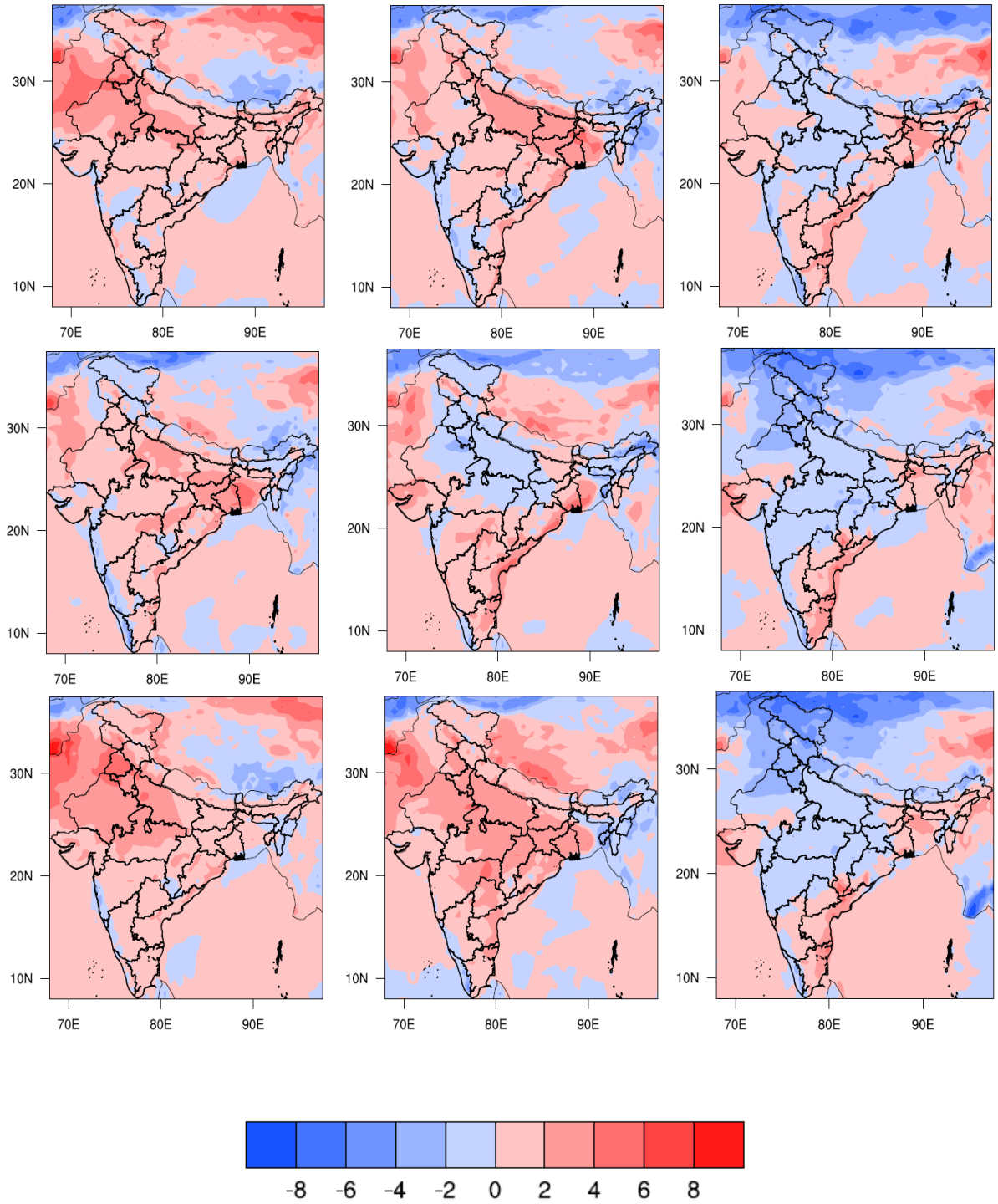

Fig 7.12. Predicted Maximum Temperature anomalies for 30 March (left column), 31 March (middle) and 02 April (right column) at lead time of 24 hrs (top panel), 72 hrs (middle) and 120 hrs (bottom). These forecasts are derived from the IMD/IITM GFS model.

Fig 7.13 shows predicted relative humidity departures, which suggest that the model predicted presence of dry air over the east coast of India during the heat wave event, very accurately.

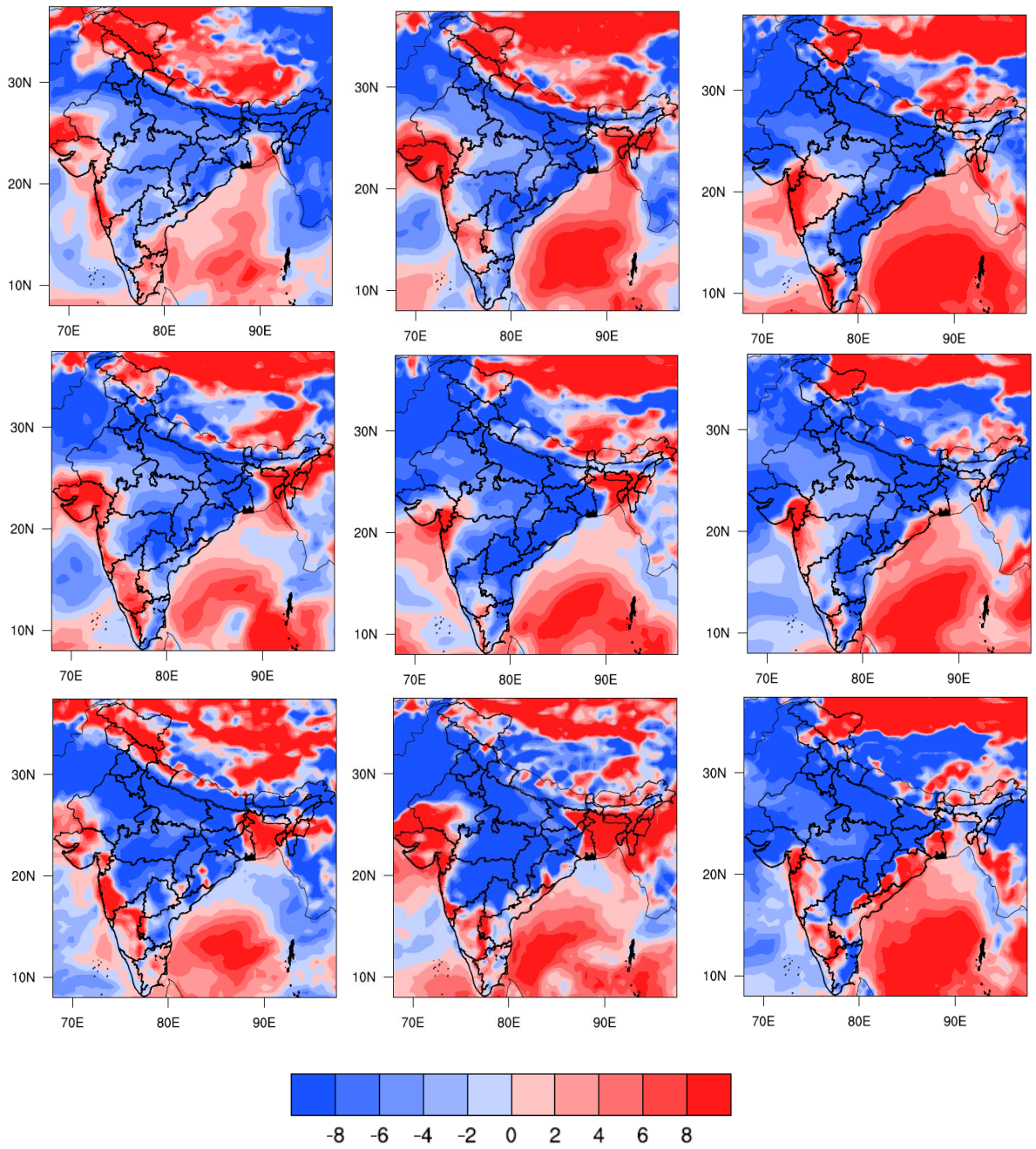

Fig 7.13. Predicted Relative Humidity departures (%) for 30 March (left column), 31 March (middle) and 02 April (right column) at lead time of 24 hrs (top panel), 72 hrs (middle) and 120 hrs (bottom). These forecasts are from the IMD/IITM GFS model.

One of the important dynamical factors for such heat waves over the region is the presence of westerly winds in the lower troposphere over the east coast of India, which suppress the onset of the ocean breeze that could otherwise bring more easterly and cold winds (Ratnam et al. 2016 a) The westerly wind anomalies are caused by the anomalous circulation features over the Pacific associated with La Nina conditions. Fig. 7.14 shows that the model accurately predicted the presence of westerly winds at 850 hPa over the east coast of India on 30 March and 02 April.

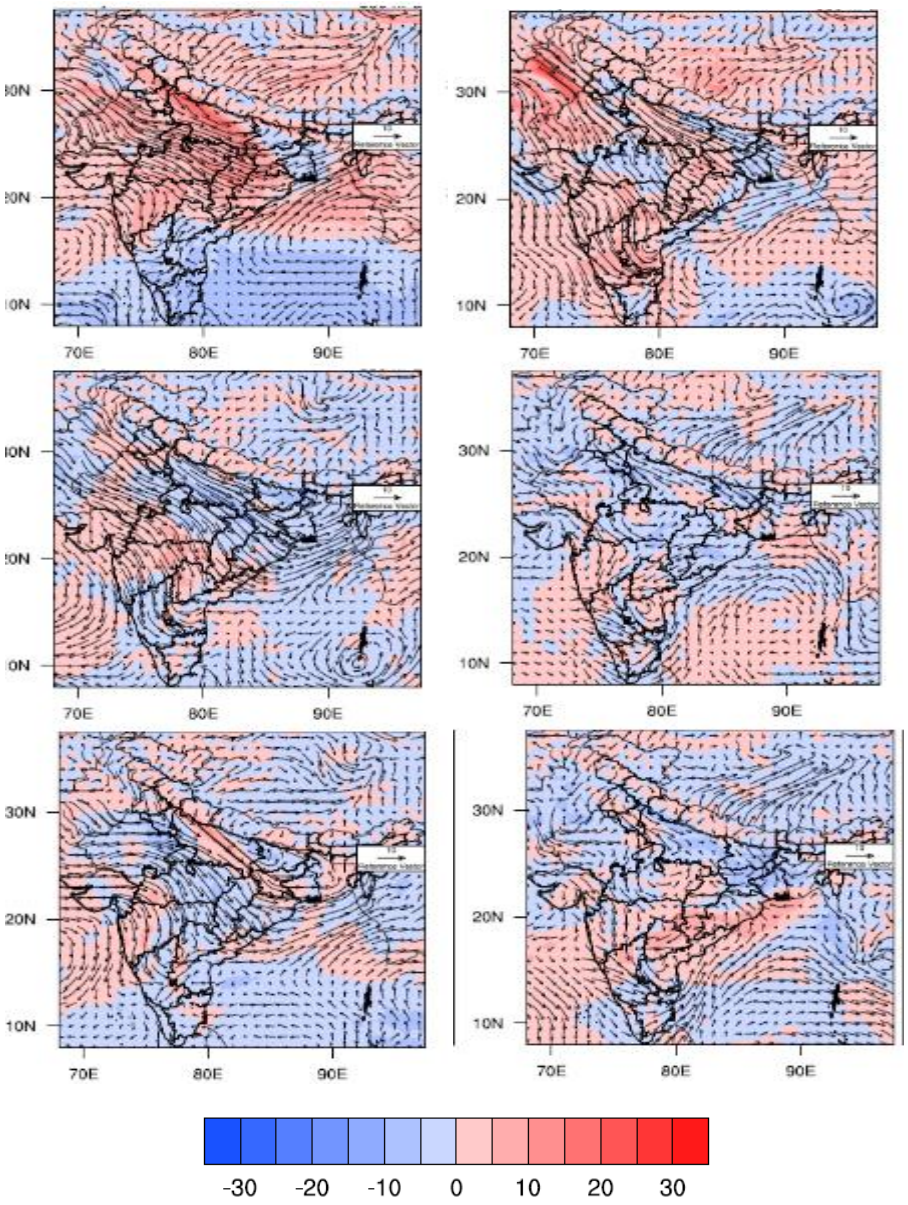

Fig 7.14. Predicted winds at 850 hPa with anomalous wind magnitude (shaded) for 30 March (left column), and 02 April (right column) at lead time of 24 hrs (top panel), 72 hrs (middle) and 120 hrs (bottom). These forecasts are from the IMD/IITM GFS model.

Another case study of the forecast of a cold wave over India is analyzed using the IMD/IITM GFS model forecasts. The cold wave occurred between 26 and 31 December 2019 and the detailed diagnosis of the cold wave was discussed in Chapter 6. Here we discuss the GFS model forecast for this cold wave event. Fig. 7.15 shows the predicted minimum temperatures for 27, 29 and 31 December 2019 with a lead time of 24, 72 and 120 hours. It is very interesting to note that the model is able to predict the intensity of low minimum temperatures and major negative deviations (Fig. 7.15) over central and north-western India. The model predicted minimum temperatures below 5°C over the northern parts of the country on 31 December 2019. The model predictions are comparatively more accurate for December 29 and 31. The model predicted negative temperature deviations of more than 5°C over the northern parts of the country (Fig. 7.16). The model also predicted very well (Fig. 7.17) the presence of dry air over central and northern India on all the three days. In the Chapter 6 it was noted that the cold waves, especially the severe cold waves, are associated with the passage of westerly disturbances over the northern parts of the country. Once the weather system passes, cold northerly winds with dry air from northern latitudes penetrate the Indian mainland, triggering a cold wave.

In this case of cold wave, the IMD/IITM GFS model is able to predict dry northerly winds over central and northwestern India on 27 December 2019, even with 120 hours of lead time as shown Fig. 7.18.

The above three case studies (two heat waves and one cold wave) suggest that the IMD's operational weather prediction model has capability of predicting the onset and intensity of heat and cold waves quite reasonably.

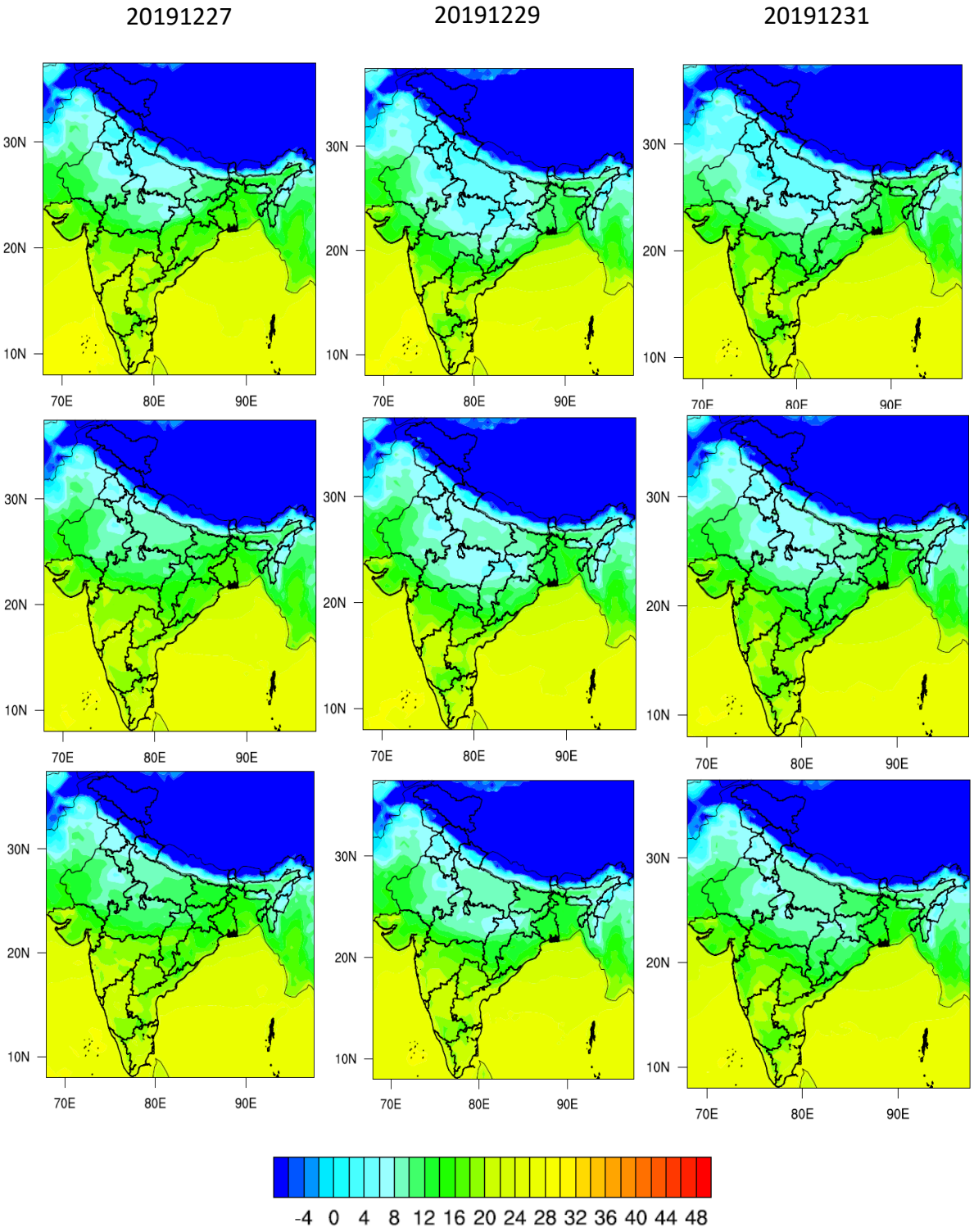

Fig 7.15. Predicted minimum temperatures for 27 Dec (left column), 29 Dec (middle) and 31 Dec, 2019 (right column) at lead time of 24 hrs (top panel), 72 hrs (middle) and 120 hrs (bottom). These forecasts are from the IMD/IITM GFS model.

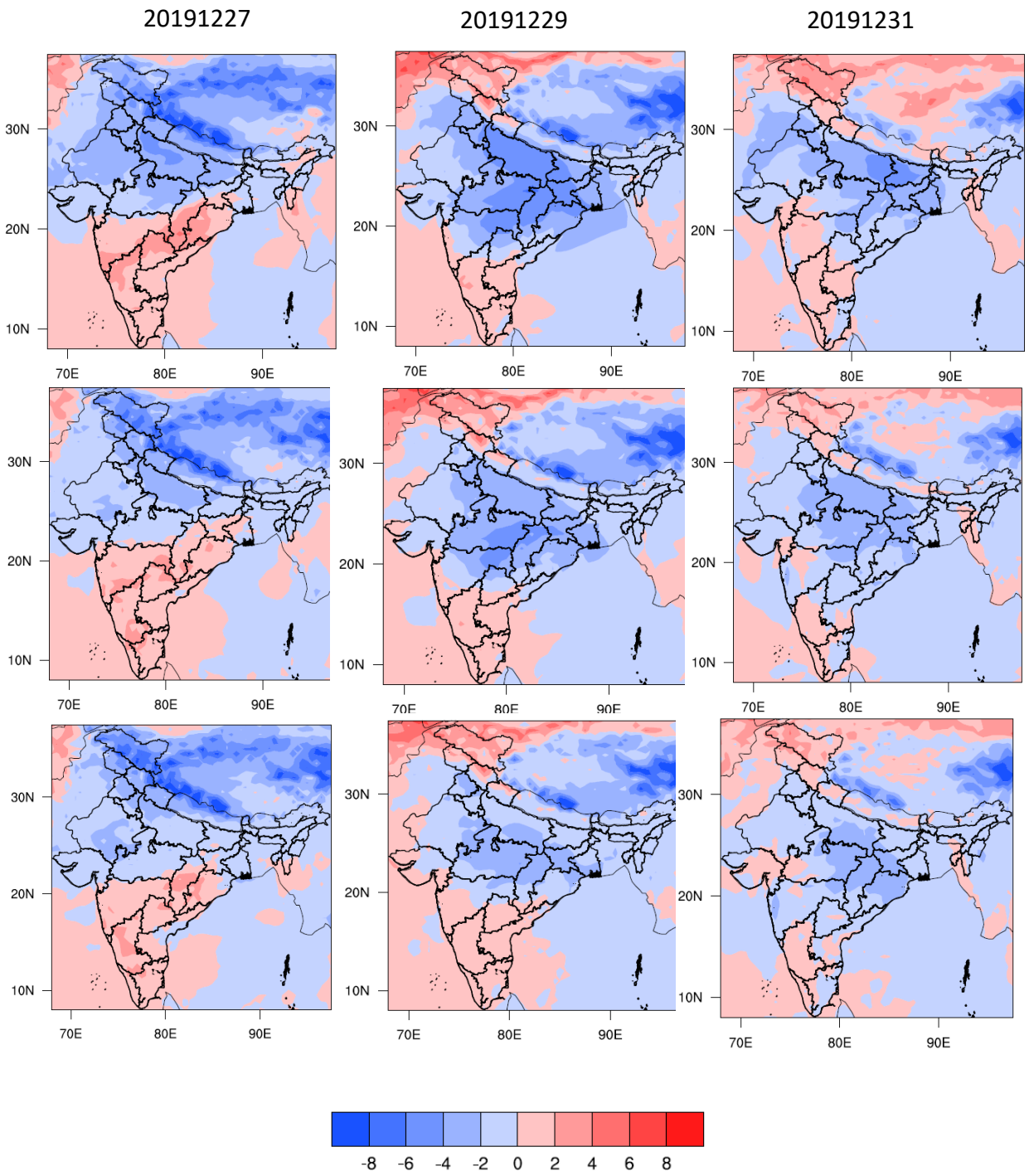

Fig 7.16. Predicted minimum temperature departures for 27 Dec (left column), 29 Dec (middle) and 31 Dec, 2019 (right column) at lead time of 24 hrs (top panel), 72 hrs (middle) and 120 hrs (bottom). These forecasts are from the IMD/IITM GFS model.

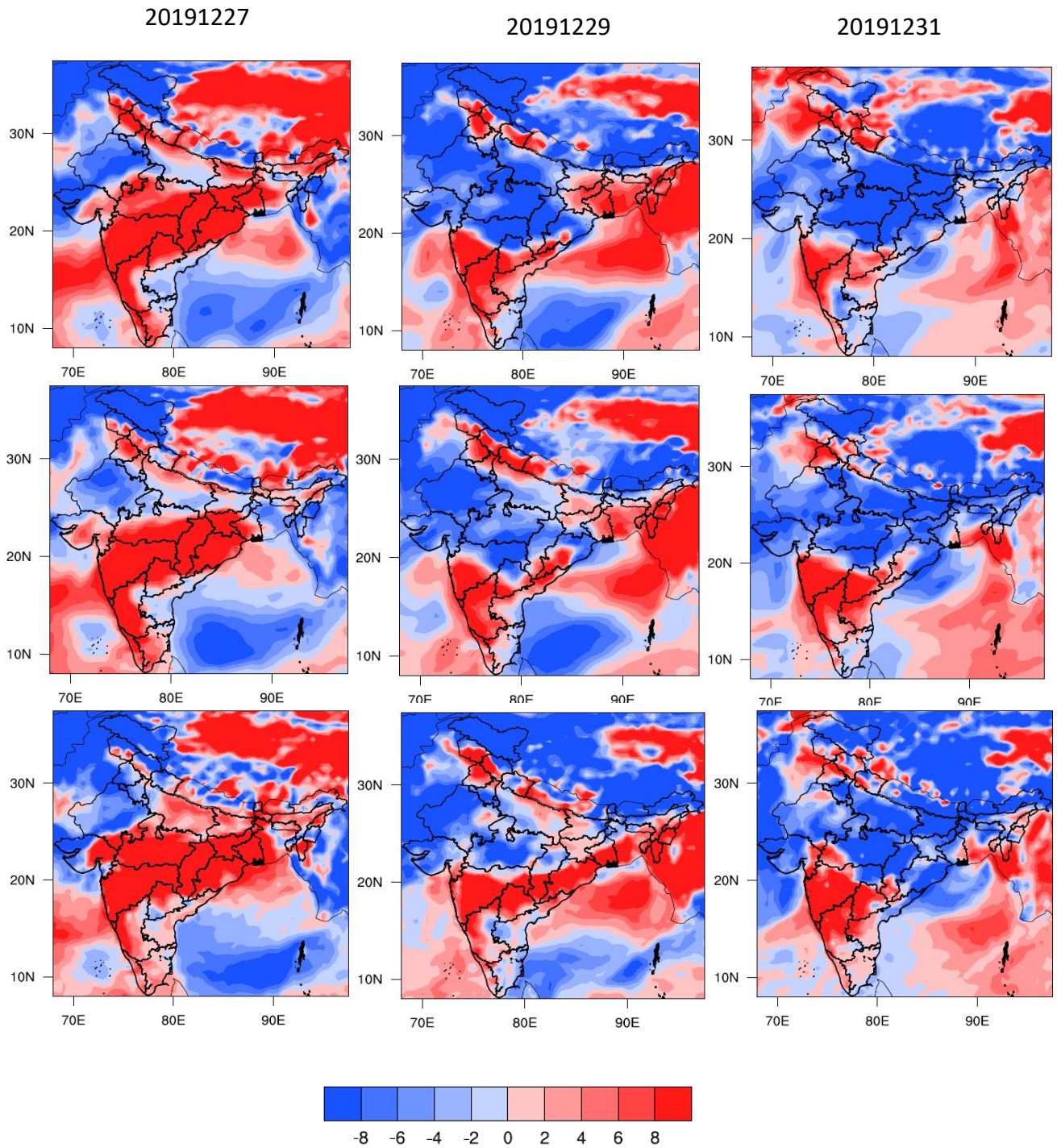

Fig 7.17. Predicted relative humidity departures (%) for 27 Dec (left column), 29 Dec (middle) and 31 Dec, 2019 (right column) at lead time of 24 hrs (top panel), 72 hrs (middle) and 120 hrs (bottom). These forecasts are from the IMD/IITM GFS model.

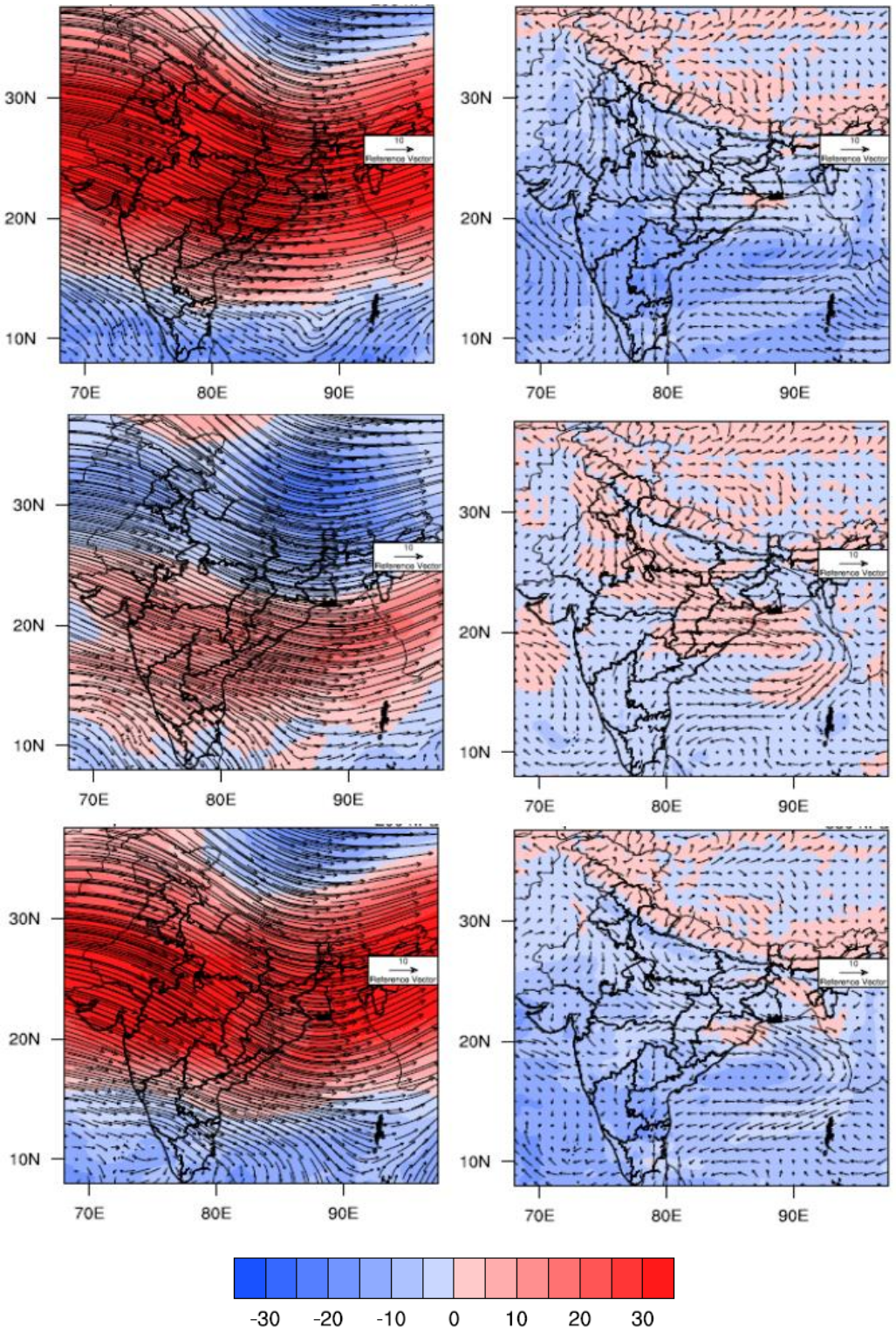

Fig 7.18. Predicted winds (m/s) along with anomalous wind speed (shaded) at 200 hPa (left) and 850 hPa (right) for 27 Dec, 2019 at lead time of 24 hrs (top panel), 72 hrs (middle) and 120 hrs (bottom). These forecasts are from the IMD/IITM GFS model.

7.3. Extended Range Prediction of Heat and Cold Waves.

This section discusses the model skill to predict heat and cold waves on longer range time scales (up to 1 month) using some specific case studies.

Pattanaik et al. (2017) studied the 2015 heat wave on the east coast of India and its prediction using the MoES extended-range forecasting system. Their study found that real-time deterministic and probabilistic forecasts for many parts of India in late May and early June 2015 indicated an impending heat wave associated with a strong northwesterly wind over the main Indian landmass, which delayed the sea breeze and led to heat waves. The study demonstrated the ability of the coupled model to provide early warning of such a deadly heat wave so that disaster managers can take appropriate action to minimize loss of life and property due to abnormal temperatures.

Mandal et al. (2019) studied the prediction of heatwaves over a longer period (March to June) using data from 1981-2010. They identified three regions prone to heatwaves, namely the northwest, southeast and northwest-southeast regions. They considered heat waves of at least six consecutive days. They found that the MOES/IITM extended-range forecasting system has reasonable capability to forecast heatwaves over India. The study shows that the prediction system has great potential to give a general indication of the onset, duration and end of the following heat wave with sufficient lead time, albeit with some spatio-temporal errors.

Fig. 7.19 shows the results of the verification of extended-range forecasts using the MOES/IITM extended-range forecasting system. The prediction system is the CFSv2-based multi-model ensemble (MME) prediction system. Since the model is known to have biases in temperature, the Tmax values predicted by the model were corrected before further analysis. Fig. 7.19 a-d shows the week-wise anomaly correlation coefficient (significant at 99.9% significance level) of Tmax in March-June for the hindcast period. Fig. 7.19 a,b show that the forecast system has high values of anomaly correlation coefficients for the week 1 and week 2 lead time over most parts of the heat

wave prone regions. Over the central and northwestern regions, significant anomaly correlation coefficient (ACC) values are found even for week-3 and week-4 lead time, showing the usefulness of the forecast system.

They used a different skill score, namely the Symmetric Extremal Dependence Index (SEDI), which is widely used for deterministic testing of predictions for rare binary events. To evaluate the SEDI values, they considered probabilistic heatwave predictions as deterministic predictions by setting some threshold values for the probability of heatwave occurrence (e.g. 30%, 50%, etc.). Fig.7.19 e-p show the week-wise SEDI values for 70% (Fig.7.19 e-h), 50% (Fig.7.19 i-l) and 30% (Fig.7.19 m-p) probability of heatwave occurrence from week 1 to week 4. The positive SEDI values indicate that the prediction system is better than chance and higher positive values mean better skill.

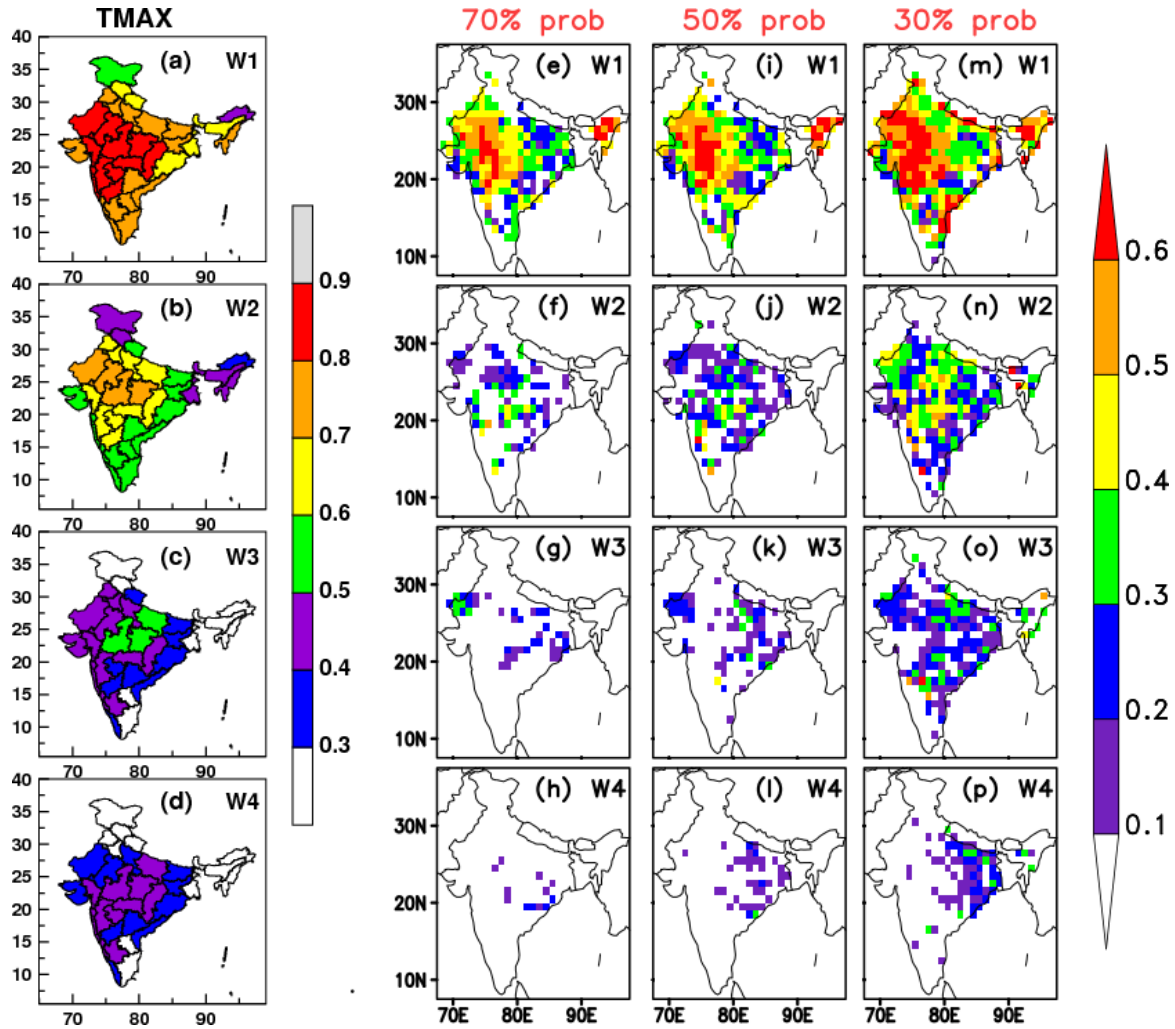

Fig. 7.19. (a–d) ACC, (e–h) SEDI values for 70% HW probability, (i–l) SEDI values for 50% HW probability and (m–p) SEDI values for 30% HW probability for different week lead during MAMJ for the hindcast period 2003–2017. The left colour bar (for a-d panels) indicates the ACC values with 0.1 intervals, whereas the right colour bar (for e-p panels) represents the SEDI values with 0.1 intervals. (Taken from Raju Mandal 2022).

The results show that in week 1, the extended-range forecasting system has a good ability to predict heat wave events even with a probability of 70% over most parts of the regions prone to heat waves. In week 2, it shows reasonable ability up to a probability of 70% with decreasing values for higher probabilities. With a probability of 50%, the forecast has a reasonable ability to predict over some parts of the NW and SE regions even in week 3.

Fig. 7.20 shows the verification of a set of forecasts (over a 15-year period, 2003-2017) for two regions, namely NW India (Fig. 7.19 a) and SE (Fig. 7.19 b) for different lead times, week 1 (red lines, week 2 (green lines), week 3 (blue lines) and week 4 (purple lines). The sample of predictions includes all model grid points over the selected region and for the verification period.

The reliability plot (or attribute plot) measures how closely the forecast probabilities of an event (here a heatwave) match the actual probability of observing the event. It groups the forecasts into bins according to the probability output along the horizontal axis. The frequency with which the event was observed for that subset of forecasts (i.e. the observed frequency) is then plotted on the vertical axis. For perfect reliability, the prediction probability and the observed frequency should be equal and the point should lie on the diagonal line (shown as a solid black line). The deviation from the diagonal line towards the lower side represents the overprediction property of the prediction system. The black dashed lines refer to the climatological forecast probability (vertical) and the observed frequency (horizontal). The horizontal dashed line is also called the "no-resolution" line. The "no skill" line is indicated by the red dashed line where the Brier Skill Score (BSS) becomes zero. The skilled region is represented by the

grey coloured area where the BSS scores are positive (Mandal et al. 2019).

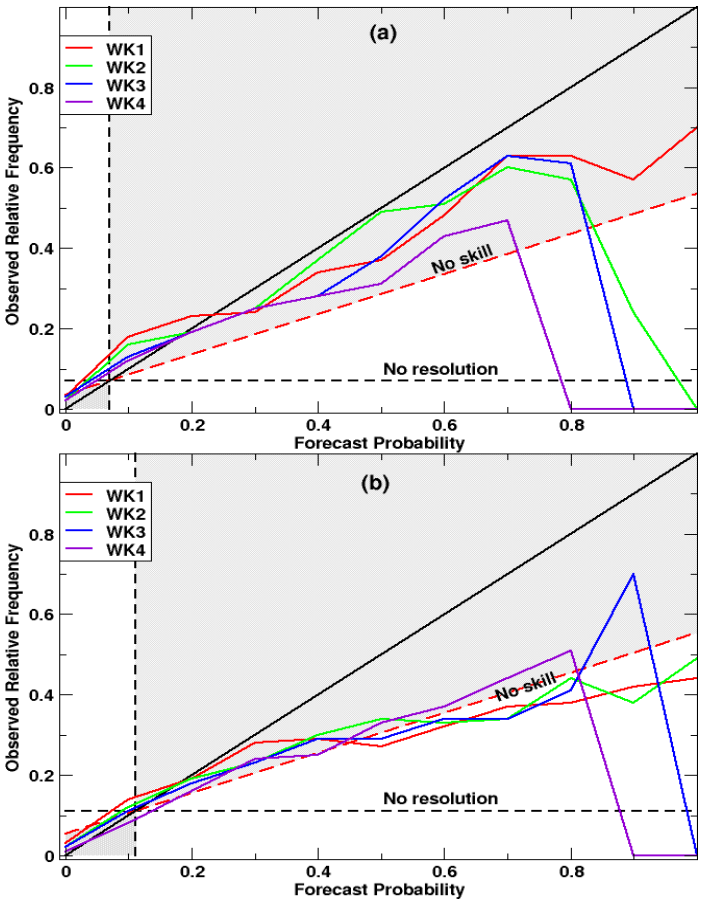

Fig. 7.20. Reliability diagrams for the HW event (satisfying the proposed HW criterion) during MAMJ (2003–17) for two heat wave prone regions namely NW (a) and SE (b) for four different leads: week1 (red lines), week-2 (green lines), week-3 (blue lines) and week-4 (violet lines). (Taken from Raju Mandal et al. 2019).

In Fig. 7.20, the reliability curves have a positive slope (up to 70% and 80% forecast probability for the NW and SE regions, respectively), which means that as the forecast probability of the event increases, the probability of the event occurring also increases. This means that the forecasts have a certain reliability. For the NW region, the reliability plots for all weeks are within the shaded area and have a positive slope up to the forecast probability. However, as the lead time increases, the tendency to over-predict also increases. The forecast system is very good at predicting heatwave events

up to week 4 in this region, but only up to a forecast probability of 70%. However, at extreme forecast probabilities, the extended-range forecasting system shows no competence except for a week 1 lead. For the southeast region, the reliability plots are competent for all four weeks at a forecast probability of 50% and then slightly exceed the "no skill" line up to a forecast probability of 80%, illustrating its usefulness in decision making. The prediction system tends to over-predict in this range.

Mandal et al (2022) investigated the ability to predict CW events using the MoES/IITM extended range prediction system. The CW events were identified if the standardized Tmin anomalies averaged over the area are less than -1.0 for four consecutive days during the winter season (Nov to Feb) during 1951-2022. The results are shown in Fig. 7.21. The correlation coefficients of anomalies (ACC) between the observed and predicted Tmin have been calculated for all meteorological sub-divisions of India. High values of ACC are observed in the northern, northwestern, central and eastern parts of the country till week 2. In week 3, parts of central and northern India show significant ACC values. In addition, SEDI values were calculated to further investigate the ability of the forecasting system. SEDI values above (below) zero mean that the prediction system is skillful (poor). Raju Mandal et al. (2022) also examined five case studies of CW events and their analysis showed that the prediction system was reasonably accurate in predicting the events up to a lead time of 2 weeks. The results are shown in Fig. 7.21, which shows the observed and predicted probabilities of these cold wave events with different initial conditions. The extended-range forecasting system is able to predict the probability of cold waves occurring almost 10-15 days in advance. This early prediction should help disaster managers to keep an eye on the approaching cold waves and take appropriate measures to deal with them.

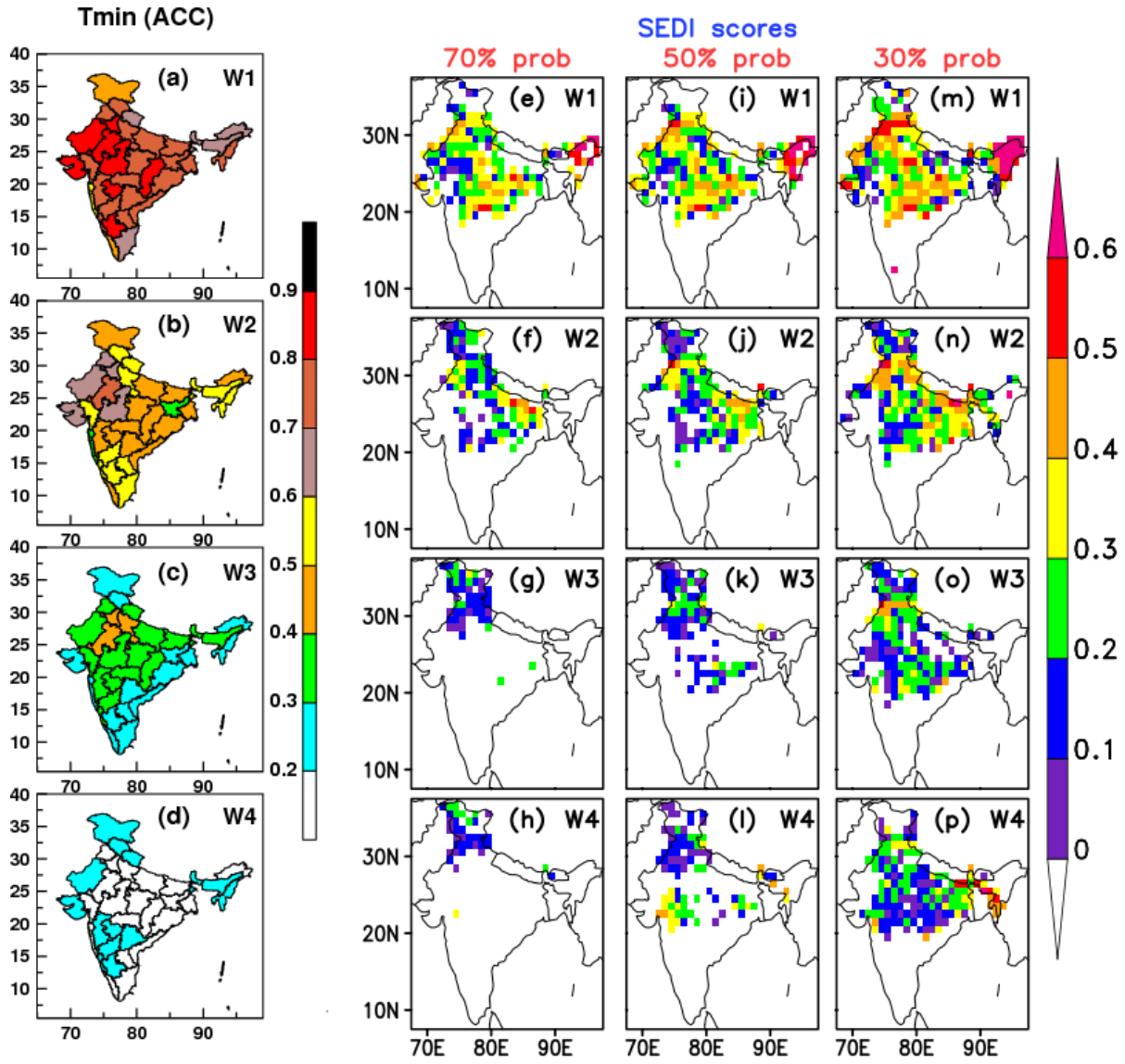

Fig 7.20 a–d Anomaly Correlation Coefficient (ACC) of minimum temperature (Tmin); e–h SEDI values for 70% CW probability; i–l SEDI values for 50% CW probability; and m–p SEDI values for 30% CW probability for different week leads (W1–W4) during NDJF for the hindcast period 2003–2017. ACC above 0.2 is significant at 5% level using a hypothesis test for the population correlation coefficient with about (or more than) 100 independent samples spatially for each sub-division and for each week lead during the season. (Taken from Raju Mandal 2022).

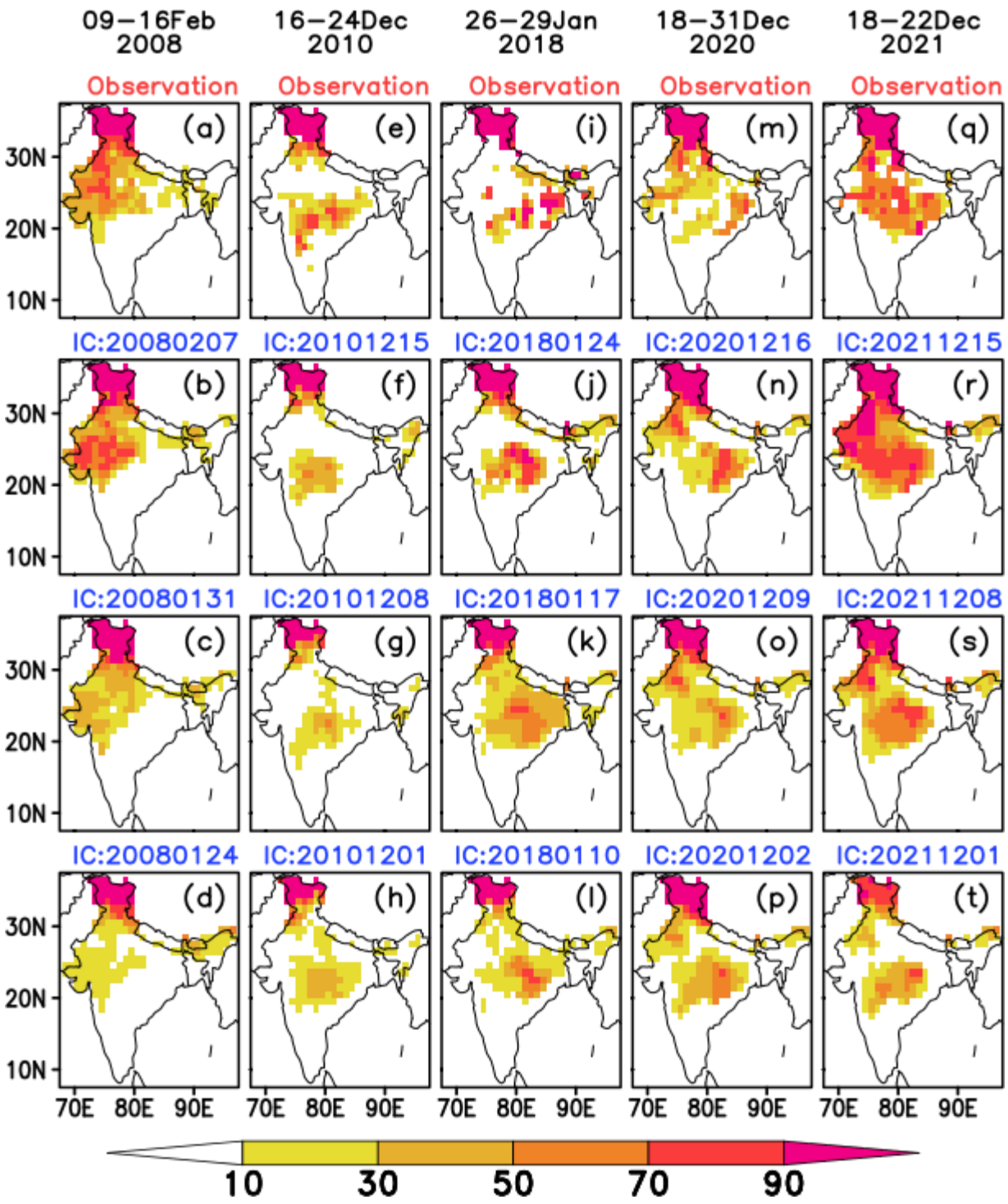

Fig 7.21. Probabilities (%) of occurrence of CW events (column-wise). Row 1 represents observed and row 2–4 represent the model predicted values from nearest three ICs for individual event. a–d Event-1: 09–16 Feb 2008, e–h event-2: 16–24 Dec 2010, i–l event-3: 26–29 Jan 2018, m–p event-4: 18–31 Dec 2020 and q–t event-5: 18–22 Dec 2021. (Taken from Raju Mandal 2022).

7.4. **Seasonal Forecasting of Heat Waves**

Since heat waves can have negative impacts on our lives, it is important that we are able to predict heat waves on all time scales, from the short-term to the seasonal. In this section, the capability of the IMD/IITM coupled seasonal forecast model (CFS V2.0) is assessed to investigate the model fidelity in predicting heat waves on seasonal time scale. The results discussed are from the recent publication by Rohini et al, (2022 b). For this purpose, the hindcasts (for the period 1981-2017) of the Monsoon Mission CFS Model (MMCFS) were used to assess the heat wave prediction skill. The IMD temperature dataset was used for the model verifications.

For the present analysis, daily hindcasts of February initial conditions (IC) were considered for the months of April to June during the period 1981-2008. These hindcast records are based on 10 ensemble members. Fig. 7.22 shows the annual cycle of Tmax, Tmin and Diurnal Temperature Range (DTR) from the observations and the MMCFS model, and the ensemble range from the model. It is interesting to note that the model captured the annual cycle of Tmax, Tmin and diurnal temperature range (DTR = Tmax - Tmin) quite well, but with a higher magnitude throughout the period. The DTR is higher during the AMJ season (> 13^0 C) in both the model and observations and is overestimated in the model. However, the standard deviation of Tmax and Tmin is slightly underestimated in the MMCFS. The magnitude of the annual cycle of Tmax and Tmin is overestimated, especially during the AMJ season. The extent of the annual cycle of Tmin is better captured by the model than that of Tmax. The overestimation of Tmax in the model could be due to the effects of atmospheric aerosols and the misrepresentation of surface fluxes and atmospheric radiative transfer in the model (Rohini et al. 2022 a). During April to June, there is an abundance of aerosols over the northern parts of India due to natural and anthropogenic processes. Since the model does not particularly consider the radiative effects of aerosols, the model may have overestimated the Tmax over India.

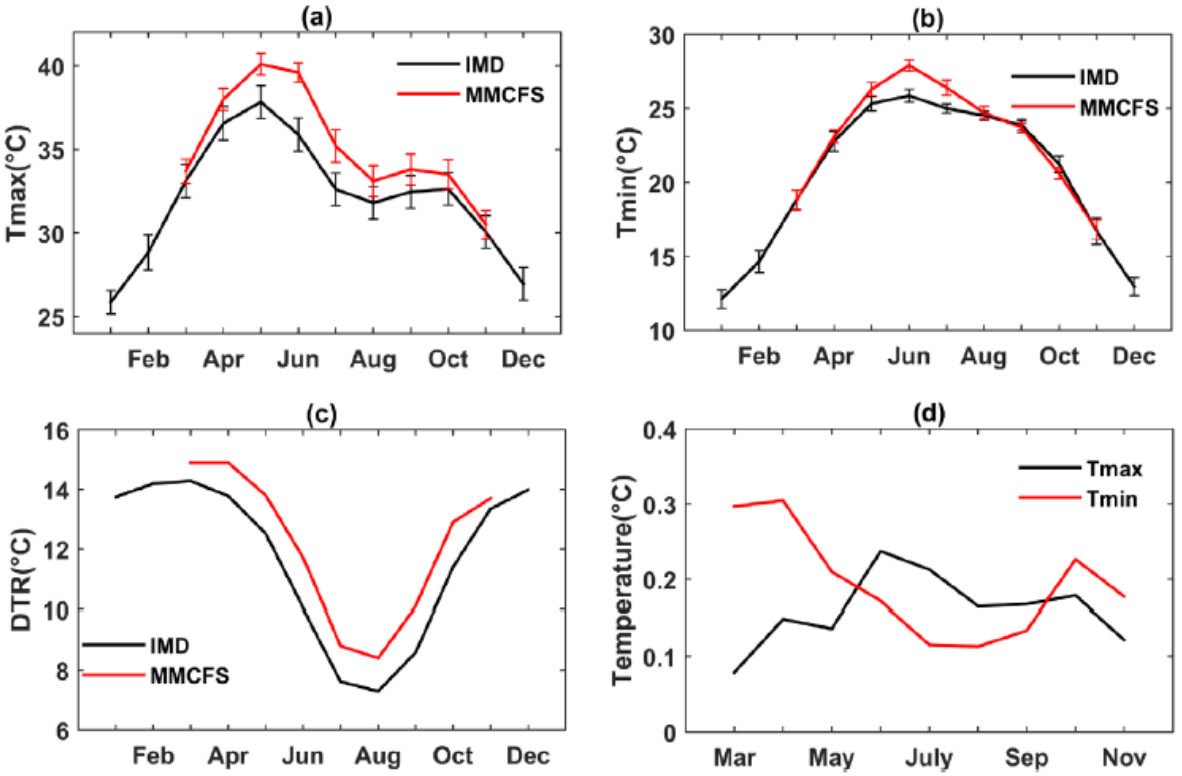

Fig 7.22. Annual cycle of (a) Tmax (C), (b) Tmin (C), (c) diurnal temperature range (DTR; C) averaged over India (excluding northeast India) for the period 1981–2017, simulated in MMCFS model (in red colour) along with IMD observation (given in black colour). Standard deviation of Tmax and Tmin has been plotted as error bar in (a, b). (d) Ensemble spread of Tmax and Tmin from the MMCFS model.

The spatial correlation plots of the seasonal model temperatures with the IMD observations are shown in Fig. 7.23. For this analysis we used bias-corrected temperatures. The results show positive correlations of Tmax, Tmin and Tmean of the model with the IMD observations over most of the country. The correlations are significant (at 95% level of significance) for most grid points over the heat wave prone area for all three temperatures.

The region of central and northwestern parts of India is identified as one of the global "hot spots" of land-atmosphere coupling (Koster et al. 2004; Halder et al. 2018). This suggests that land surface processes play an important role in temperature

variability in this region. The MMCFS model has shown significant skill over northwest India, where land-atmosphere coupling is the strongest. This could be due to the realistic initialization of the land surface data in the model runs.

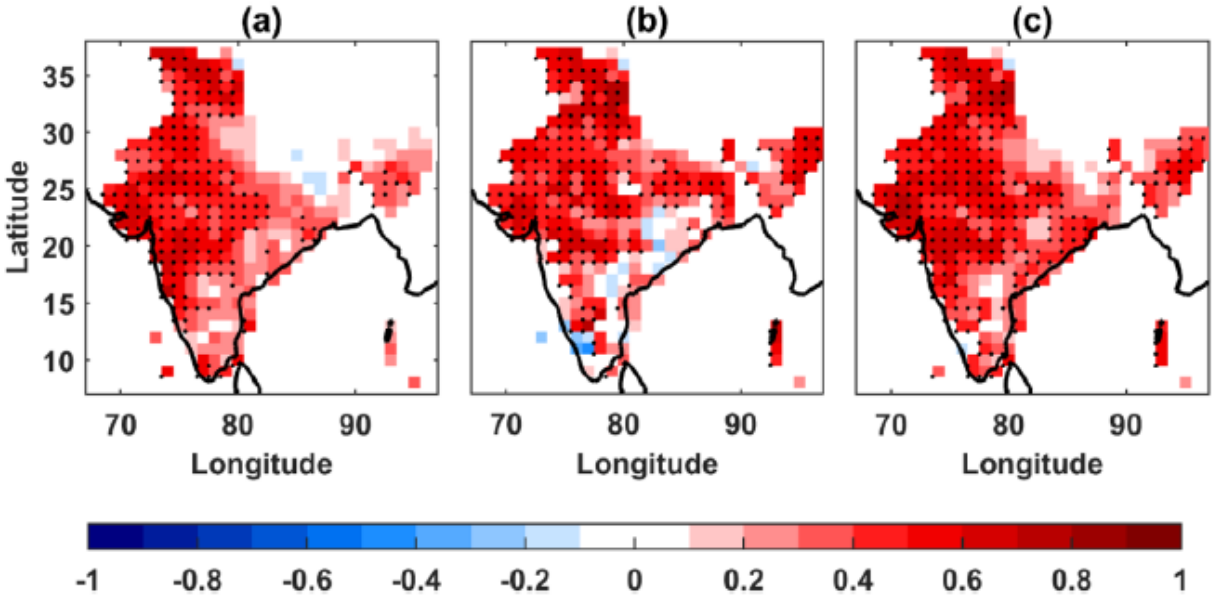

Fig.7.23. Correlation coefficient for seasonal mean temperatures. (a) Tmax (C), (b) Tmin (C), (c) Tmean (C) between model hindcasts and IMD observations during the period 1981–2017. Significant correlations at 5% significant level are highlighted with black dots.

The spatial distribution of heat wave characteristics during the study period is shown in Fig. 7.24. The spatial pattern of heat wave features was analyzed to determine how many heat waves occurred on average during the AMJ season in each year. It is important to note that the spatial distribution of HWF and HWD is well predicted in the model (Fig. 7.24). However, the model underestimated the extent of heat wave features, especially over east-central India and the east coast of the southern peninsular region. The magnitude of both HWF and HWD is predicted reasonably well over northwest India (NWI), where heat wave activity is predominant. The observed HWF is

1.1-1.4 events per year and HWD is 5-6 days per year over NWI. The model predicted HWF is 0.9-1.2 events per year and HWD is 4.5-5.5 days per year.

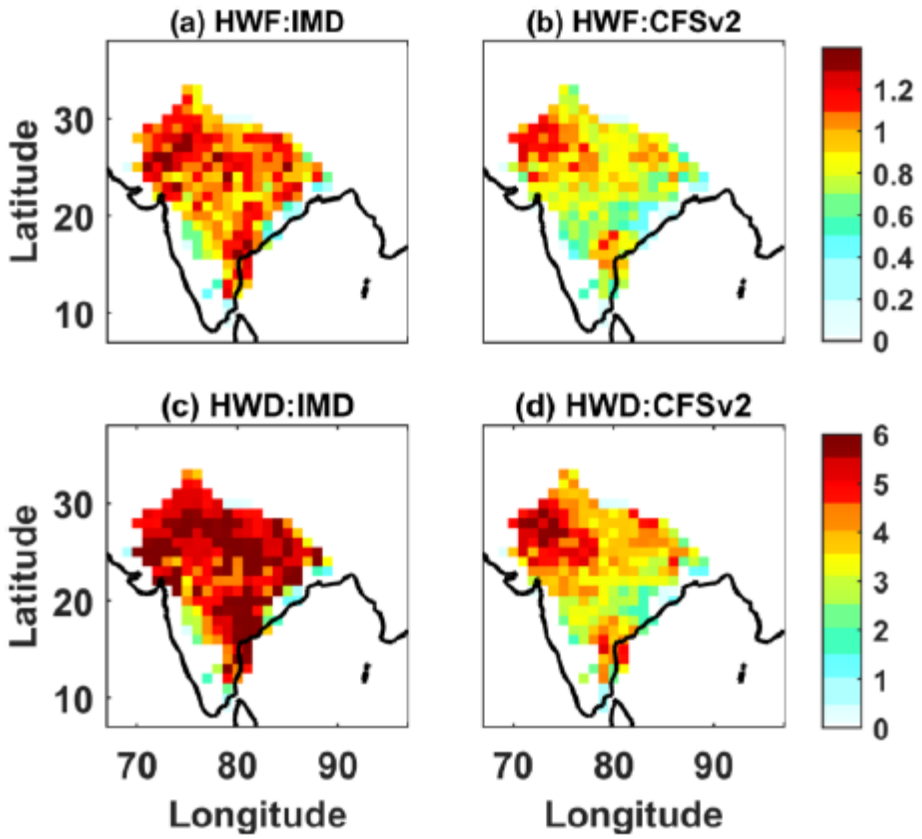

Fig 7.23. Spatial distribution of heat wave frequency (HWF; events /year) and heat wave duration (HWD; days/year) during AMJ season from IMD observation (a, c) and MMCFS hindcast runs (b, d), during 1981–2017.

The time series of HWF and HWD averaged over the heat wave prone area (NWI) are shown in Figure 7.25. The model shows a larger increase in HWF and HWD compared to the observations over the period 2003-2008. HWF and HWD show an increasing trend in both the model and the observations. However, the trends of HWF (0.3 events per decade in the model and 0.1 events per decade in the observation) and HWD (1.5 days per decade in the model and 0.6 days per decade in the observation) are slightly overestimated in the MMCFS model. The correlation coefficient between the model-predicted and observed time series of all heat wave characteristics averaged for

India is about 0.47 for HWF and 0.38 for HWD, and these values are statistically significant at the 95% significance level.

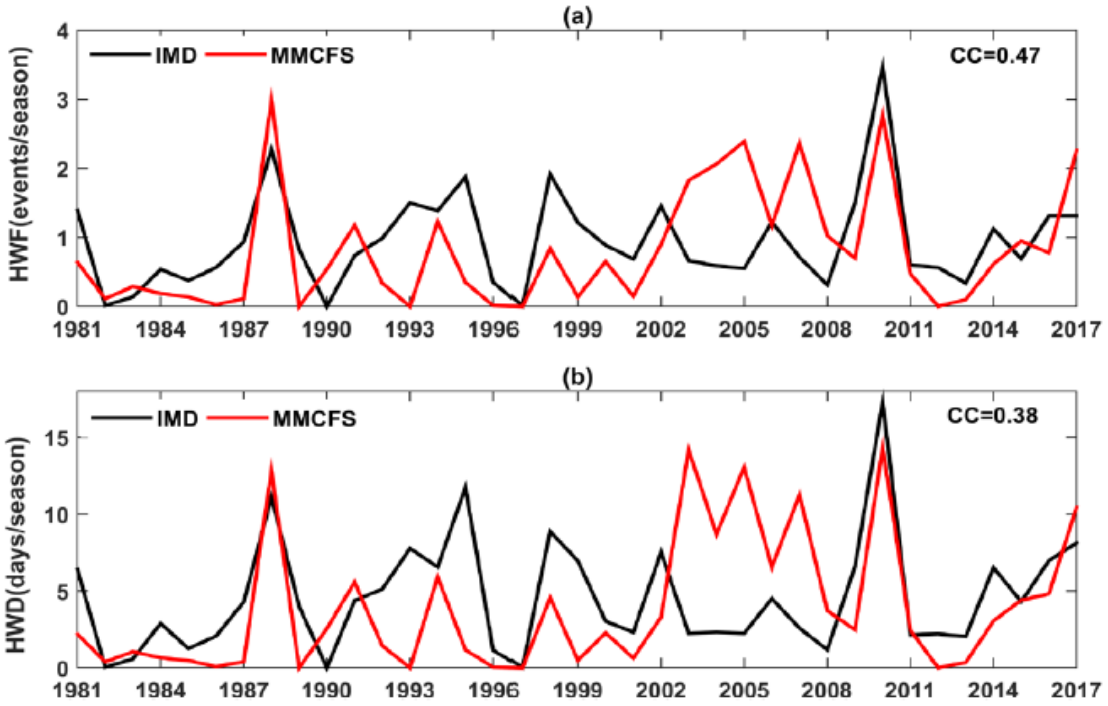

Fig.7.25. Time series of area averaged (over heat wave prone area; NW India) (a) heat wave frequency (HWF; events/season) and (b) heat wave duration (HWD; days/season) simulated by model along with observation for AMJ season during 1981–2017.

Fig 7.26 shows the correlation coefficients between the heat wave characteristics (HWF and HWD) predicted by the model and the IMD observations. The correlations of HWF are significant (95% significance level) in more grid points than HWD, mainly over northwest India. Both heat wave characteristics have negative correlations at some grid points, mainly over the north-eastern parts. The analysis suggests that the MMCFS model performs quite well in capturing the spatial coverage of heat wave characteristics at the seasonal scale, especially over northwest India. Thus, the analysis suggests that the MMCFS model is capable of skillfully predicting the temperatures (Tmax, Tmin and Tmean) and spatial distribution of heat wave characteristics seasonal time scales.

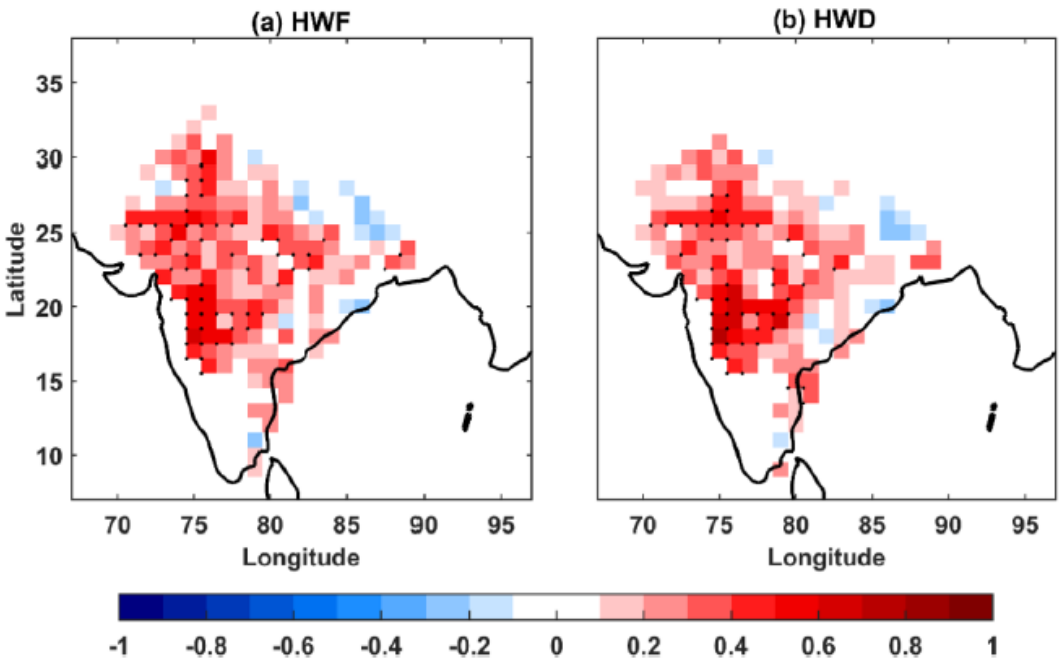

Fig 7.26. Correlation coefficients of MMCFS model with IMD observations (a) heat wave frequency (b) heat wave duration during AMJ season for the period 1981–2017. Significant correlations at 5% significant level are highlighted with black dots.

The MMCFS model reproduces the annual cycle of temperatures quite well, but with a higher mean and lower variability compared to the observations. The hindcasts of the model show significant ability to seasonally predict temperatures over most of northwest and central India.

The present analysis shows that while it is impossible to predict the exact characteristics of the heatwave (such as onset, duration and end) on a seasonal time scale, the correlation analysis between the heatwave characteristics predicted by the model and the IMD observations indicates a promising ability for most parts of northwest India. The overall analysis suggests that the MMCFS model hindcasts for February IC perform quite well in predicting maximum temperatures and heat waves over the country on a seasonal time scale.

Chapter 8

Impacts and adaptation

In this chapter, we discuss the impacts of heat and cold waves and adaptation strategies to cope up the adverse impacts of heat and cold waves.

8.1. Heat wave Impacts:

Heat waves affect human health and air quality, increase energy consumption, reduce crop yields, increase water loss and intensify droughts. In addition, exposure of crops to temperatures beyond a critical threshold can lead to crop failure. Heat waves also increase temperatures in buildings and cities (urban heat islands), cause disruptions in critical infrastructure networks, affect the economy through lower labour productivity, and exacerbate the impacts of other climate-related hazards such as droughts or forest fires.

Heat waves have claimed more lives in India than other natural hazards, with the exception of tropical cyclones. In March and June, they also lead to dry weather with lower humidity. However, heat stress due to increased humidity and temperatures can significantly endanger human life. Unfortunately, there is not much research on such heat stress episodes in India. Jaswal et al. (2017) made such an analysis of heat index over India. Heat Index (HI) known as apparent temperature, combines air temperature and relative humidity to determine how hot it actually feels. It has been shown that changes in the HI resulting from increases in atmospheric moisture can account for a considerable fraction of the total increases in the HI. The risk of heat-related illness becomes greater as the weather gets hotter and more humid. The human body normally cools itself by perspiration, or sweating, in which the water in the sweat evaporates and carries heat away from the body. However, when the relative humidity is high, the evaporation rate of sweat is reduced. This means heat is removed from the body at a lower rate, causing it to retain more heat than it would in dry air.

Im et al. (2017) examined the effects of heat waves and discussed the risks and vulnerability of people. Previous studies have shown that a wet bulb temperature of 35^0 C can be considered an upper limit for human survivability. Based on an ensemble of high-resolution climate change simulations, the study found that wet bulb temperature extremes in South Asia are likely to approach and exceed this critical threshold in a few places by the end of the 21^{st} century under the business-as-usual scenario of future greenhouse gas emissions. The greatest risk from extreme heat waves is in the densely populated agricultural regions of the Ganges and Indus river basins. Climate change, without mitigation, poses a serious and unique risk to South Asia, a region that is home to about one-fifth of the world's population, due to an unprecedented combination of severe natural hazards and acute vulnerability.

Heat waves have significant impacts on a number of aspects such as health, infrastructure performance, energy demand, building design, water quality and costs (Zuo et al. 2015). These impacts are significant and some of them even interact (e.g. costs and energy consumption). The study by Azhar et al. (2017) examined heat wave vulnerability over India. Their study revealed that of the total 640 districts considered, 10 districts are vulnerable in very high-risk category and 97 districts in high-risk category. The districts with higher heat vulnerability are located in the central parts of the country. These are less urbanized and have low rates of literacy, access to water and sanitation and presence of household amenities.

Zachariah et al. (2021) made a probabilistic assessment of extreme heat stress on India wheat yields under climate change. They showed an increase in magnitude, frequency and areal extent of heat stress episodes in the Indo-Gangetic Plains region during 1967-2018. Probabilistic estimates of below-average wheat production under scenario-averaged heat stress conditions are expected to rise by 8%–27% under the SSP5-8.5 climate change scenario, with Punjab showing the largest increase. Quantitative links between heat stress indicators and loss of crop yield highlight

increased agricultural vulnerability in India under climate change. The 2022 Indian heat wave impacted key geographies of wheat production in northwestern and central India (Sidhu, 2022). In 2022, due to strong heat wave activity, wheat production was expected to have fallen by 4.5 per cent, in some regions losses could be up to 15 per cent.

Anel et al. (2017) discussed the impact of cold and heat waves on the energy production sector. Cold and heat waves represent a significant problem for the electricity generation sector. The disruptions cold and heat waves can cause in power production are beyond their consumption impacts through, for instance, higher peak demand.

Nori-Sarma et al. (2019) addressed the impact of heat waves on mortality in northwest India. They found that even in areas with extreme high temperatures, heat waves present health risks for mortality. Their results indicate that relationships generated for temperature and mortality from developed country settings may not accurately characterize such relationship in the global south. The findings of differential impact depending on heat wave definition have critical implications for policymakers and merits additional study. Continued development of local data resources to assess the relationships between temperature and health in developing countries such as India, is important to accurately assess current health effects, as well as to inform future heat wave alerts globally under a changing climate.

Some of the main impacts of heat wave on human health are given below. Heat waves can impact health, agriculture and energy.

1. Heat exhaustion and heat stroke: Heat waves can cause heat exhaustion and heat stroke, which can be life-threatening if not treated promptly. Symptoms include nausea, dizziness, headache, rapid heartbeat, and confusion.
2. Dehydration: High temperatures can cause dehydration, particularly if people are not drinking enough fluids. This can lead to headaches, fatigue, and other health problems.

3. Respiratory problems: Heat waves can exacerbate respiratory problems such as asthma, as high temperatures can cause air pollution to accumulate and irritate the lungs.

4. Cardiovascular problems: High temperatures can also increase the risk of cardiovascular problems such as heart attacks and strokes, particularly for people with preexisting cardiovascular conditions.

5. Mental health: Heat waves can also impact mental health, leading to increased stress and anxiety, particularly for those who do not have access to air conditioning or other cooling measures.

Overall, heat waves can have significant impacts on human health, particularly for vulnerable populations. It is important to take precautions during heat waves, such as staying hydrated, staying indoors in air conditioning if possible, and avoiding strenuous activities during the hottest part of the day.

Overall, heat waves can have a significant impact on agriculture in India, with potentially serious consequences for food security and the livelihoods of farmers.

1. Crop failure: Heat waves can cause crops to wilt and die, leading to reduced yields or even total crop failure. The high temperatures can also cause damage to plant cells, reducing their ability to photosynthesize and produce food.

2. Reduced soil moisture: High temperatures can lead to increased evaporation of water from soil, reducing soil moisture levels and making it more difficult for crops to grow. This can lead to drought-like conditions, which can be devastating for farmers.

3. Pest infestations: Heat waves can create ideal conditions for pests and insects to thrive. This can lead to increased damage to crops and the need for more pesticides, which can be costly for farmers.

4. Livestock health: Heat stress can be a significant issue for livestock, causing reduced milk production, lower fertility rates, and even death in extreme cases. Farmers may need to take extra precautions to protect their animals during heat waves.

5. Water scarcity: Heat waves can exacerbate existing water scarcity issues, as water sources dry up more quickly and demand for irrigation increases. This can lead to conflicts between farmers and other water users, and can make it difficult for farmers to grow crops.

Heat waves also can have significant impacts on the energy sector, affecting the reliability of the energy grid, increasing costs, and potentially leading to power outages and other disruptions. The following impacts are very important.

1. Increased demand for electricity: During heat waves, demand for electricity tends to increase as people use more air conditioning and fans to stay cool. This can put a strain on the energy grid, leading to blackouts or brownouts if supply cannot keep up with demand.

2. Reduced power generation: High temperatures can reduce the efficiency of power plants, particularly those that rely on water for cooling. If water temperatures are too high, power plants may have to reduce their output or shut down altogether, leading to reduced electricity supply.

3. Transmission and distribution issues: Heat waves can also cause transmission and distribution equipment to fail, particularly if it has not been designed to handle high temperatures. This can lead to power outages and reduced reliability of the energy grid.

4. Increased risk of wildfires: Heat waves can increase the risk of wildfires, which can damage or destroy energy infrastructure, including transmission lines and power plants. This can lead to power outages and a need for costly repairs.

5. Increased energy costs: During heat waves, energy prices may increase as demand for electricity rises and supply becomes more constrained. This can lead to higher energy bills for consumers and businesses.

8.2 Adaptation to Heat Waves

The most effective way to reduce the negative impacts of a heatwave is to develop a comprehensive response plan that combines individual strategies into an integrated approach and includes cultural, institutional, technological and ecosystem-based adaptations. For example, the institutional plan could include weather forecasting, monitoring, and education and awareness. Appropriate education can ensure the health and safety of urban residents during heat waves, especially vulnerable groups such as older adults, children, people working outdoors and low-income communities. Zuo et al. (2015) found that structural/institutional and technological factors attract the most attention in the literature, while cultural/behavioral factors receive less attention. It is worth noting that these mechanisms are complementary and ultimately aim to improve the resilience of the urban and built environment to climate change. Indeed, an appropriate combination of these mechanisms can lead to more effective measures to cope with heat waves and their associated impacts. The effectiveness of these measures varies and depends on contextual factors such as cultural background, level of economic development, etc.

It is crucial to make adaptation choices to reduce the impact of these heat waves. Here are some of the adaptation choices that can be made for heat waves in India:

1. Increasing public awareness: One of the best ways to adapt to heat waves is by increasing public awareness. People need to know the signs of heat stroke and how to protect themselves from the sun's harmful rays. Government agencies can launch awareness campaigns through various media to educate people on the dangers of heat waves and the precautions to take during these times.

2. Improving the built environment: India needs to improve the built environment to make it more heat-resilient. This can be done by incorporating better insulation and ventilation systems in buildings, planting more trees, and increasing the green cover in cities. Such measures will help to reduce the urban heat island effect, which is a phenomenon where cities are much hotter than surrounding areas.
3. Providing cool shelters: Providing cool shelters is another adaptation choice for heat waves. The government can set up public cooling centers and shelters in public spaces where people can go to cool off during extreme heat. This can be especially useful for vulnerable populations such as the elderly, homeless, and those with chronic health conditions.
4. Changing work schedules: The government can implement policies to adjust work schedules during heat waves. For example, working hours can be shifted to the early morning or late evening when temperatures are cooler. This can help to reduce the risk of heat stroke and other heat-related illnesses in workers.
5. Developing early warning systems: Developing early warning systems can help people prepare for heat waves. The government can issue heat wave warnings through various media, including television, radio, and social media. This will help people take the necessary precautions to protect themselves from the heat.

It is important to note that these measures must be implemented on a large scale to make a significant impact and reduce the impact of heat waves in India.

Recurrent heat waves, already a problem in the rapidly growing and urbanising countries of South Asia will most likely worsen in a warming world. However, coordinated adaptation measures can reduce the negative health impacts of heat. Across India, state and district governments have responded by creating Heat Action Plans (HAPs) that prescribe a variety of preparedness activities and heat wave response measures across government departments to reduce the impact of heat waves (Aditya

Valiathan Pillai and Dalal 2023). To address this problem in Ahmedabad (Gujarat, India), a coalition was formed to develop an evidence-based heatwave preparedness plan and early warning system. Knowlton et al. (2014) discussed the details of developing and implementing South Asia's first Heat Health Action Plan in Ahmedabad (Gujarat).

Aditya Valiathan Pillai and Dalal (2023) published a report critically analyzing 37 heat action plans at city (9), district (13) and state (15) levels in 18 states. They identified several opportunities to strengthen India's HAPs. They also documented a wide range of solutions (covering 62 different types of interventions) prescribed in these HAPs, from promoting green roofs to federal school awareness programmes. The HAPs provide for a balanced mix of short- and long-term measures, although it is unclear to what extent these measures will be implemented. Long-term transformational measures such as climate-sensitive urban planning and changing cropping patterns are likely to have higher implementation costs than immediate measures, but could significantly reduce heat stress in the long term and facilitate the implementation of HAP. They found that most HAPs are not tailored to the local context and have an oversimplified view of the hazard. Almost all HAPs are inadequate in identifying and targeting vulnerable groups. HAPS are underfunded, lack transparency and have a weak legal basis.

In a recent study, Debnath et al. (2023) addressed the issues of heat wave impacts on public health, agriculture and other socio-economic and cultural systems. They argue that these impact can hinder or reverse the country’s progress in fulfilling the sustainable development goals (SDGs). The existing Climate Vulnerability Index (CVI) developed by the Department of Science and Technology, Government of India may underestimate the impact of heat waves on the country’s developmental effects. Linking Heat Index (HI) with CVI identifies more of India’s vulnerability and provides an opportunity to rethink India’s climate adaptation policies through international cooperation in designing holistic vulnerability assessment methodologies. They conclude that there is an urgent need to improve extreme weather impact assessment by

combining multiple layers of information within the existing climate vulnerability measurement frameworks that can account for the co-occurrence and collision of climate change events and non-climate structural SDG interventions.

Chapter 9

Summary

Heat waves and cold waves are extreme temperature events that occur due to anomalies in the atmospheric circulation on a planetary scale and are supported by local factors. It is well known that global warming triggers extreme temperature events like heat waves all over the world.

In India, a heat wave is declared by the India Meteorological Department (IMD) when the maximum temperature is above 40 degrees Celsius and 4.5 degrees above normal. A severe heat wave is declared when the temperature is above 40 degrees Celsius and 6.5 degrees above normal. Heatwaves usually occur in the period from March to June in central and north-western India (heatwave zone) and in the coastal areas of Andhra Pradesh and Odisha. In this region, the frequency of heat waves is slightly lower than in northern India.

On average, heat wave areas experience two heat waves during the season, lasting between five and seven days. However, the frequency of heatwaves, their duration and their maximum duration are increasing, which is due to global warming. In the heat wave areas of India, the total duration of heat waves has increased by about 2.5 days in the last 30 years. The Intergovernmental Panel on Climate Change (IPCC) projections indicate an increase of about two heat waves (12-18 days) by 2060. Heat waves could also spread to southern India, where no heat waves are currently reported.

A cold wave is said to occur when the normal minimum temperature at the stations is 100 C or more and is at least 50 C below normal. If the normal minimum temperature at stations is below 100 C, the deviation should be at least 30C to be called a cold wave. Cold waves are generally observed over central and north-western India during the winter season from December to February. Previous observations suggest that the frequency and duration of cold waves over India is decreasing, possibly due to the increase in minimum temperatures. There are two types of cold waves in India. One

is associated with La Nina, with central and northwest India affected by cold waves. The second type occurs during the El Nino phase, but such cold waves are generally confined to the extreme northern parts of India.

The physical mechanisms of heat and cold waves are well studied and understood. Heat and cold waves are caused by large-scale anomalies in atmospheric circulation and are exacerbated by local effects such as land surface processes that affect soil moisture. Studies suggest that heat and cold waves are also predictable. On a short- to medium-term time scale, they are predictable up to 5-7 days in advance. Predicting heat waves on longer time scales (at least up to two weeks) and on seasonal time scales is very possible.

With unchecked global warming, the probability of compound extremes such as the simultaneous occurrence of droughts and heat waves is also likely to increase. Until we have studied the causes in depth, it is difficult to attribute a heatwave to human influence. However, the 2003 heatwave in Europe and the 2010 Russian heatwave were clearly attributed to human influence. The recent heatwaves in March and April 2022 in northern India are also consistent with IPCC projections.

Thanks to the efforts of the Ministry of Earth Sciences, Government of India, there is now a reliable heat wave warning system in India that provides vital information at least a week in advance. There is also good synergy between the Meteorological Department of India and the central and state disaster management agencies, which has led to the development of heatwave action plans in some states. The report by NDMA (2020) illustrate how India successfully reduced mortality due to heat waves by adopting heat wave action plans and effective and coordinated implementation. However, there is a need for greater inter-agency collaboration on heatwave impacts and adaptation.

It is high time that the India Meteorological Department (IMD) starts systematic research into the health implications of the rise in temperatures and humidity for Indian

conditions. In the meantime, the IMD can use available indices such as HI, as used by Jaswal et al. (2017), for daily monitoring and forecasting of heat waves.

We need to establish evidence-based thresholds to develop and activate different responses to heat and cold waves. For example, we need to develop strategies to educate and sensitize the public, improve energy efficiency to reduce stress on electrical systems to avoid power outages and reduce the heat island effect, build cool shades and shelters (such as cyclone shelters), and develop evidence-based advance warning systems to reduce crop damage. A long road lies ahead!

References

Aditya Valiathan Pillai and Tamanna Dalal, 2023. How is India adapting to heatwaves? An assessment of heat action plans with insights for transformative climate action. Centre for Policy Research Report, March 2023, p21.

Alfano d'Ambrosio, F.R., Malchaire, J., Palella, B.I. and Riccio, G., 2014. WBGT index revisited after 60 years of use. *Annals of occupational Hygiene*, *58*(8), pp.955-970.

Alexander, L.V., 2011, Extreme heat rooted in dry soils. Nat Geosci 3:1–2. doi:10.1038/ngeo1045.

Alexander, L.V., Arblaster, J.M., 2009. Assessing trends in observed and modeled climate extremes over Australia in relation to future projections. Int. J. Climatol 29: 417–435.doi: 10.1002/joc.1730.

Alexander, L.V., Hope, P., Collins, Trewin, B., Lynch, A., Nicholls. N., 2007. Trends in Australia's climate means and extremes: A global context. Aust. Meteor. Mag. 56: 1–18.

Alexander, L.V., Zhang, X., Peterson, T.C., Caesar, J., Gleason, B., Klein Tank, A.M.G., Haylock, M., Collins, D., Trewin, B., Rahimzadeh, F., Tagipour, A., Kumar, K.R., Revadekar, J., Griffiths, G., Vincent. L., Stephenson, D.B., Burn. J., Aguilar. E., Brunet. M., Taylor. M., New. M., Zhau. P., Rusticcucci. M., Vazquez-Aguirre, J.L., 2006. Global observed changes in daily climate extremes of temperature and precipitation. J. Geophys. Res. 11: D05109. http://dx.doi.org/10.1029/2005JD006290.

Alexander, L.V., Arblaster. J.M., 2017. Historical and projected trends in temperature and precipitation extremes in Australia in observations and CMIP5. Weather and Climate Extremes 15: 34–56. https://doi.org/10.1016/j.wace.2017.02.001.

Añel, J.A., Fernández-González, M., Labandeira, X., López-Otero, X. and De la Torre, L., 2017. Impact of cold waves and heat waves on the energy production sector. *Atmosphere*, *8*(11), p.209.

Arblaster, J.M., Alexander. L.V., 2012. The impact of the El Niño-southern oscillation on maximum temperature extremes. Geophys Res Lett 39: L20702.

Attri, S.D., Rathore, L.S., 2003, Simulation of impact of projected climate change on wheat in India. Int. J. Climatol 23: 693–705. doi:10.1002/joc.896.

Avila, F.B., Pitman, A.J., Donat, M.G., Alexander, L.V., Abramowitz, G., 2012. Climate model simulated changes in temperature extremes due to land cover change. J. Geophys. Res. 117: D04108. doi:10.1029/2011JD016382.

Azhar, G., Saha, S., Ganguly, P., Mavalankar, D. and Madrigano, J., 2017. Heat wave vulnerability mapping for India. *International journal of environmental research and public health*, *14*(4), p.357.

Bedekar, D.C., Dekate, M.V., A.K.Banerjee, 1974. Forecasting Manual IV-6, Part IV, Heat and Cold Waves in India, India Meteorological Department.

Black, E., Blackburn. M., Harrison, G., Hoskins, B., Methven, J., 2004. Factors contributing to the summer 2003 European heatwave. Weather 59 (8):217–223.

Black, E., Sutton, R., 2007. The influence of oceanic conditions on the hot European summer of 2003. ClimDyn 28: 53–66.

Budd, G.M., 2008. Wet-bulb globe temperature (WBGT)—its history and its limitations. *Journal of science and medicine in sport*, *11*(1), pp.20-32.

Cai, W., Santoso, A., Wang, G., Yeh, S.W., An, S.I., Cobb, K.M., Collins, M., Guilyardi, E., Jin, F.F., Kug, J.S., Lengaigne, M., McPhaden, M.J., Takahash, K., Timmermann, A., Vecci. G., Watanabe, M., Wu. L., 2015. ENSO and greenhouse warming. Nature at. Clim. Chang. 5: 849-859. doi:10.1038/nclimate2743.

Chakraborty, D., Sehgal, V.K., Dhakar, R., Ray, M. and Das, D.K., 2019. Spatio-temporal trend in heat waves over India and its impact assessment on wheat crop. *Theoretical and Applied Climatology*, *138*, pp.1925-1937.

Chylek, P., Klett, J.D., Lesins, G., Dubey, M.K., Hengartner, N., 2014. The Atlantic multidecadal oscillation as a dominant factor of oceanic influence on climate. Geophys Res Lett 41:2689–2697.

Coumou, D., Rahmstorf, S., 2012. A decade of weather extremes. Nat. Climate Change 2: 491– 496. doi:10.1038/nclimate1452

Coumou, D., Robinso, A., Rahmstorf, S., 2013. Global increase in record breaking monthly-mean temperatures.Clim Change 118: 771-782.

Chaudhury, S.K., Gore, J.M., Sinha Ray, K.C., 2000. Impact of heat waves over India.Curr Sci 79:153–155.

Cowan, T., Purich, A., Perkins, S., Pezza, A., Boschat, G., Sadler, K., 2014. More frequent, longer, and hotter heat waves for Australia in the twenty-first century. J Clim 27(15): 5851–5871. doi:10.1175/JCLI-D-14-00092.1

Das, J. and Umamahesh, N.V., 2022. Heat wave magnitude over India under changing climate: Projections from CMIP5 and CMIP6 experiments. *International Journal of Climatology*, *42*(1), pp.331-351.

Dash, S.K., and Mamgain, A., 2011. Changes in the frequency of different categories of temperature extremes in India. J. Appl. Meteorol. Climatol 50: 1842–1858

De, U.S., Dube, R.K., Prakasa Rao, G.S., 2005. Extreme weather events over India in the last 100 years. J.Ind. Geophys.Union 9: 173-187.

De, U.S., Mukhopadhyay, R.K., 1998. Severe heat wave over Indian subcontinent in 1998 in a perspective of global Climate. Current Science 75(12): 1308-1311.

Debnath, R., Bardhan, R., and Bell, M.L., 2023. Lethal heatwaves are challenging India's sustainable development, PLOS Clim 2(4): e e0000156. https://doi.org/10.1371/journal.pclm.0000156

Della-Marta, P.M., Haylock, M.R., Luterbacher, J., Wanner, H., 2007. Doubled length of western European summer heat waves since 1880. J. Geophys. Res. Atmos. 112 (D15).

Diffenbaugh ,N.S., Pal, J.S., Trapp, R.J., Giorgi, F., 2005. Fine-scale processes regulate the response of extreme events to global climate change. Proc. Natl. Acad. Sci. U. S. A. 102 (44):15774–15778. http://dx.doi.org/10.1073/pnas.0506042102.

Dodla, V.B., Satyanarayana, G.C. and Desamsetti, S., 2017. Analysis and prediction of a catastrophic Indian coastal heat wave of 2015. *Natural Hazards*, *87*, pp.395-414.

Dole, R., Hoerling, M., Perlwitz, J., Eischeid, J., Pegion, P., Zhang, T., Quan, X.-W., Xu, T., Murray, D., 2011. Was there a basis for anticipating the 2010 Russian heat wave? Geophys. Res. Lett. 38:L06702. http://dx.doi.org/10.1029/2010GL046582

Dubey, A.K., Lal, P., Kumar, P., Kumar, A. and Dvornikov, A.Y., 2021. Present and future projections of heatwave hazard-risk over India: A regional earth system model assessment. *Environmental Research*, *201*, p.111573.

Dubey, A.K. and Kumar, P., 2022. Future projections of heatwave characteristics and dynamics over India using a high-resolution regional earth system model. *Climate Dynamics*, pp.1-19.

Dubey, A.K., Kumar, P., Saharwardi, M.S. and Javed, A., 2021. Understanding the hot season dynamics and variability across India. *Weather and Climate Extremes*, *32*, p.100317.

Feudale, L., Shukla, J., 2011. Influence of sea surface temperature on the European heat wave of 2003 summer. Part I: an observational study. Climate Dynamics 36(9–10):1691–1703.

Fischer, E.M., Seneviratne, S.I.,Vidale, P.L., Lüthi, D., Schär, C., 2007a. Soil moisture–atmosphere interactions during the 2003 European summer heat wave. J. Clim. 20 (20):5081–5099.

Fischer, E.M., Seneviratne, S.I., Lüthi, D., Schär, C., 2007 b. Contribution of land–atmosphere coupling to recent European summer heat waves. Geophys Res Lett 39: L19702. doi:10.1029/2012GL052730.

Fischer, E.M., Schar, S., 2010. Consistent geographical patterns of changes in high-impact European heatwaves. Nat. Geosci 3:398–403. doi:10.1038/ngeo866.

Fischer, E.M., Lawrence, D.M., Sanderson, B.M., 2011. Quantifying uncertainties in projections of extremes—A perturbed land surface parameter experiment. Climate Dyn 37:1381–1398. doi:10.1007/s00382-010-0915-y.

Francis, J.A., Vavrus, S. J., 2012. Evidence linking Arctic amplification to extreme weather in mid-latitudes. Geophys. Res. Lett. 39: L06801.

Hansen, A., Bi, P., Nitschke, M., Ryan, P., Pisaniello, D., Tucker, G., 2008. The effect of heat waves on mental health in a temperate Australian city. Environ Health Perspect 116:1369–1375. doi:10.1289/ehp.11339.

Heo, S., Bell, M.L. and Lee, J.T., 2019. Comparison of health risks by heat wave definition: Applicability of wet-bulb globe temperature for heat wave criteria. *Environmental research*, *168*, pp.158-170.

Hirschi, M., Seneviratne, S.I., Alexandrov, V., Boberg, F., Boroneant, C., Christensen, O.B., Stepanek, P., 2011. Observational evidence for soil-moisture impact on hot extremes in southeastern Europe. Nat. Geosci. 4 (1): 17–21.

Hondula, D.M., Vanos, J.K., Gosling, S.N., 2014. The SSC: a decade of climate–health research and future directions. Int. J. Biometeorol. 58: 109–20.

Hu, K., Huang, G., and Huang, R., 2011. The impact of tropical Indian Ocean variability on summer surface air temperature in China. J. Clim. 24: 5365–77.

Hu, K., Huang, G., and Wu, R., 2013. A strengthened influence of ENSO on August high temperature extremes over the Southern Yangtze River Valley since the late 1980s. J. Clim. 26: 2205–21.

IPCC, 2012. Climate Change 2012: Managing the Risks of Extreme Events and Disasters to Advance Climate Change Adaptation. A Special Report of Working Groups I and II of the Intergovernmental Panel on Climate Change, edited by C. B. Field et al 52 pp Cambridge Univ. Press, Cambridge, U. K and New York.

IPCC, 2014. Climate change 2014 synthesis report. In: Core Writing Team, Pachauri, R.K., Meyer, L,A, (eds) Contribution of working groups I, II and III to the fifth assessment

report of the Intergovernmental Panel on Climate Change. IPCC, Geneva, Switzerland, p 151.

Jaswal, A.K., Rao, P.C.S., Singh, V., 2015. Climatology and trends of summer high temperature days in India during 1969–2013. J Earth System Science. 124:1–15. doi:10.1007/s12040-014-0535-8, 2015.

Jaswal, A. K., Padmakumari, B., Kumar, N., Kore, P.A. 2017. Increasing trend in temperature and moisture induced heat index and its effect on human health in climate change scenario over the Indian sub-continent. J. Clim. Change Vol. 3: 11–25.

Jiang, Z., Song, J., Li, L., Chen, W., Wang, Z., and Wang, J., 2012. Extreme climate events in China: IPCC-AR4model evaluation and projection. Climatic Change, 110: 385–401. doi:10.1007/s10584-011-0090-0.

Kenyon, J., Hegerl, G.C. 2008. Influence of modes of climate variability on global temperature extremes. J. Clim. 21 (15):3872–3889.

Kishore, P., Basha, G., Venkat Ratnam, M., AghaKouchak, A., Sun, Q., Velicogna, I. and Ouarda, T.B.J.M., 2022. Anthropogenic influence on the changing risk of heat waves over India. *Scientific reports*, *12*(1), p.3337.

Kjellstrom, T., McMichael, A.J., 2013. Climate change threats to population health and well-being: the imperative of protective solutions that will last. Global Health Action, 6.doi: 10.3402/gha.v6i0.20816.

Knowlton, K., Kulkarni, S.P., Azhar, G.S., Mavalankar, D., Jaiswal, A., Connolly, M., Nori-Sarma, A., Rajiva, A., Dutta, P., Deol, B. and Sanchez, L., 2014. Development and implementation of South Asia's first heat-health action plan in Ahmedabad (Gujarat, India). *International journal of environmental research and public health*, *11*(4), pp.3473-3492.

Kripalani, R.H., Kulkarni, Ashwini., 1999. Heat Waves and Floods across Asia: Was El Niño, then La Niña the Cause? Drought Network News (1994-2001). 50.

Lefcourt, A.M., Adams, W., 1996. Radio telemetry measurement of body temperatures of feedlot steers during summer. Journal of animal science, 74:2633-2640.

Lorenz, R., Jaeger, E.B., Seneviratne, S.I., 2010. Persistence of heat waves and its link to soil moisture memory. Geophys Res Lett, 37:L09703. doi:10.1029/2010GL042764.

Luo, M., Lau, N.C., 2019. Amplifying effect of ENSO on heat waves in China. Climate Dynamics, 52:3277–3289.

Lee, W.S., Lee, M.I., 2016, Interannual variability of heat waves in South Korea and their connection with large-scale atmospheric circulation patterns. Int. J. Climatol, 36:4815–4830. doi:10.1002/joc.4671.

Matzarakis, A., Mayer, H., Iziomon, M.G., 1999. Applications of a universal thermal index: physiological equivalent temperature. Int. J. Biometeorol, 43 (2): 76–84.

Mazdiyasni, O., AghaKouchak, A., Davis, S.J., Madadgar, S., Mehran, A., Ragno, E., Sadegh, M., Sengupta, A., Ghosh, S., Dhanya, C.T. and Niknejad, M., 2017. Increasing probability of mortality during Indian heat waves. *Science advances*, *3*(6), p.e1700066.

McGregor, G.R., Markou, M.T., Bartzokas, A., Katsoulis, B.D., 2002. An evaluation of the ature and timing of summer human thermal discomfort in Athens, Greece. Clim. Res, 20 (1): 83–94.

Meehl, G., Tebaldi, C., 2004. More intense, more frequent, and longer lasting heat waves in the 21st century. Science, 305: 994–997. doi:10.1126/science.1098704.

Min, S-K., Cai, W., Whetton, P., 2013. Influence of climate variability on seasonal extremes over Australia. J Geophys Res Atmos, 118: 643–654.

Miralles, D.G., Teuling, A.J., van Heerwaarden, C.C., de Arellano, J.V.G., 2014. Megaheatwave temperatures due to combined soil desiccation and atmospheric heat accumulation. Nat. Geosci., 7 (5): 345–349.

Miralles, D.G., van den Berg, M.J., Teuling, A.J., de Jeu, R.A.M., 2012. Soil moisture-temperature coupling: a multiscale observational analysis. Geophys Res Lett, 39: L21707. doi: 10.1029/2012GL053703.

Mishra, V., Mukherjee, S., Kumar, R. and Stone, D.A., 2017. Heat wave exposure in India in current, 1.5 C, and 2.0 C worlds. *Environmental Research Letters*, *12*(12), p.124012.

Mueller, B, Seneviratne, S.I., 2012. Hot days induced by precipitation deficits at the global scale. Proc. Natl. Acad. Sci, 109 (31): 12398–12403.

Mukherjee, S. and Mishra, V., 2018. A sixfold rise in concurrent day and night-time heatwaves in India under 2 C warming. *Scientific Reports*, *8*(1), pp.1-9.

Murari, K.K., Ghosh, S., Patwardhan, A., Daly, E. and Salvi, K., 2015. Intensification of future severe heat waves in India and their effect on heat stress and mortality. *Regional Environmental Change*, *15*, pp.569-579.

Murari, K.K., Sahana, A.S., Daly. E., Ghosh. S., 2016. The influence of El Nino Southern Oscillation on heat waves in India. Meteorol Appl, 23(4): 705–713.

Nageswararao, M.M., Sinha, P., Mohanty, U.C. and Mishra, S., 2020. Occurrence of more heat waves over the central east coast of India in the recent warming era. *Pure and Applied Geophysics*, *177*, pp.1143-1155.

Nairn, J., Fawcett, R., 2013. Defining Heatwaves: Heatwave Defined as a Heat-Impact Event Servicing. All Community and Business Sectors in Australia.CAWCR technical report ISSN 1835-9884.Available on http://www.bushfirecrc.com/sites/default/fileNicholls and Larsen 2011

Nicholls, N., Lavery, B., Frederiksen, C., Drosdowsky, W., Torok, S., 1996. Recent apparent changes in relationships between the El Niño-Southern Oscillation and Australian rainfall and temperature. Geophys Res Lett, 23:3357–3360. doi:10.1029/96GL03166

Nicholls, N., 2012. Is Australia's continued warming caused by drought?. Aust. Meteorol. Oceanogr. J. 62 (2): 93–96.

Narkhede, N., Chattopadhyay, R., Lekshmi, S., Guhathakurta, P., Kumar, N. and Mohapatra, M., 2022. An empirical model-based framework for operational monitoring

and prediction of heatwaves based on temperature data. *Modeling Earth Systems and Environment*, *8*(4), pp.5665-5682.

Nitschke, M., Tucker, G.R. and Bi, P., 2007. Morbidity and mortality during heatwaves in metropolitan Adelaide. Med J Aust, 187: 662-665.

Nori-Sarma, A., Anderson, G.B., Rajiva, A., ShahAzhar, G., Gupta, P., Pednekar, M.S., Son, J.Y., Peng, R.D. and Bell, M.L., 2019. The impact of heat waves on mortality in Northwest India. *Environmental research*, *176*, p.108546.

Oldenborgh, G.J.V., Philip, S., Kew, S., Weele, M.V., Uhe P., Otto, F., Singh, R., Pai, I., Cullen, H,. Achuta Rao, K., (2018) Extreme heat in India and anthropogenic climate change. Nat Hazards Earth Syst Sci, 18: 365–381.

Opitz-Stapleton, S., Sabbag, L., Hawley, K.,Tran, P Hoang, L., Nguyen, P.H. 2016. Heat index trends and climate change implications for occupational heat exposure in Da Nang, Vietnam. Climate Services 2: 41-51.

Pai, D.S, Thapliyal, V., Kokate, P.D, 2004. Decadal variation in the heat and cold waves over India during 1971-2000. Mausam, 55(2): 281-292.

Pai, D.S., Smitha Nair and Ramanathan, A.N., 2013. Long term climatology and trends of heat waves over India during the recent 50 years (1961–2010). Mausam, 64(4): 585–604.

Pai, D.S., Srivastava, A.K. and Smitha Nair, 2017. Heat and cold waves over India. In Observed climate variability and change over the Indian Region (pp. 51-71). Springer, Singapore.

Pai, D.S. and Smitha A Nair., 2022. Impact of El-Niño-Southern Oscillation (ENSO) on extreme temperature events over India. Mausam, *73*(3), pp.597-606.

Parker, T.J., Berry, G.J., Reeder, M.J., Nicholls, N., 2014. Modes of climate variability and heat waves in Victoria, southeastern Australia. Geophys. Res. Lett., 41 (19): 6926–6934.

Patz, J.A., Campbell-Lendrum, D., Holloway, T., Foley, J.A., 2005. Impact of regional climate change on human health. Nature, 438:310–317.

Pantavou, K., Theoharatos, G., Nikolopoulos, G., Katavoutas, G., Asimakopoulos, D., 2008. Evaluation of thermal discomfort in Athens territory and its effect on the daily number of recorded patients at hospitals' emergency rooms. Int. J. Biometeorol., 52 (8): 773–778. http://dx.doi.org/10.1007/s00484-008-0170-7

Pattanaik, D., Mohapatra, M., Srivastava, A.K., Kumar, A., 2017. Heat wave over India during summer 2015:An assessment of real time extended range forecast. Meteor.Atmos.Phys, 129: 375–393. https://doi.org/10.1007/s00703-016-0469-6

Perkins, S.E., Alexander, L.V., 2013. On the measurement of heat waves. J Climate, 26: 4500–4517. http://dx.doi.org/10.1175/JCLI-D-12-00383.1.

Perkins, S.E., 2015. A review on the scientific understanding of heatwaves—Their measurement, driving mechanisms, and changes at the global scale. Atmospheric research, 164-165: 242-267. doi:10.1016/j.atmosres.2015.05.014.

Perkins, S.E., Alexander, L.V., Nairn, J.R., 2012. Increasing frequency, intensity and duration of observed heat waves and warm spells. Geophys Res Lett, 39: L20714. doi:10.1029/2012GL053361.

Raghavan, K., 1967. A climatological study of severe cold waves in India. *Mausam*, *18*(1), pp.91-96.

Rajib, M.A., Mortuza, M.R., Selmi, S., Ankur, A.K., Rahman, M.M., 2011. Increase of heat index over Bangladesh: Impact of Climate Change. World Academy of Science Engineering and Technology 58: 402-405.

Mandal, R., Joseph, S., Sahai, A.K., Phani, R., Dey, A., Chattopadhyay, R. and Pattanaik, D.R., 2019. Real time extended range prediction of heat waves over India. *Scientific Reports*, *9*(1), pp.1-11.

Mandal, R., Joseph, S., Sahai, A.K., Dey, A., Phani, R., Pattanaik, D.R., Kaur, M. and Karmakar, N., 2023. Diagnostics and real-time extended range prediction of cold waves over India. *Climate Dynamics*, pp.1-1.

National Disaster Management Authority (NDMA), 2020. Beating the heat: How India successfully reduced mortality due to heat waves; 2020. Available from: https://ndma.gov.in/sites/default/files/IEC/Booklets/HeatWave%20A5%20BOOK%20Final.pdf.

Rakib, Z.B., 2013. Extreme temperature climatology and evaluation of heat index in Bangladesh during 1981-2010. Journal of Presidency University, Part: B 2: 84-95 ISSN: 2224-7610.

Ratnam, J.V., Behera, S.K., Ratna, S.B., Rajeevan, M., and Yamagata, T., 2016 a. Anatomy of Indian heatwaves Sci. Reports, 6: 24395 doi:10.1038/srep24395 (2016).

Ratnam, J.V., Behera, S.K., Annamalai, H., Ratna, S.B., Rajeevan, M. and Yamagata, T., 2016 b. ENSO's far reaching connection to Indian cold waves. *Scientific Reports*, *6*(1), p.37657.

Rohini, P., Rajeevan, M., Srivastava, A.K. 2016. On the variability and increasing trends of heat waves over India. Sci Reports, 6: 26153.

Rohini, P., Rajeevan, M. and Mukhopadhay, P., 2019. Future projections of heat waves over India from CMIP5 models. *Climate dynamics*, *53*, pp.975-988.

Rohini, P. 2020. *Observational and Modelling Aspects of Heat Waves over India* (Doctoral dissertation), Department of Atmospheric and Space Sciences, Savitribai Phule Pune University, Pune, India.

Rohini, P., Rajeevan, M. and Soni, V.K., 2022 a. Trends in diurnal variation of surface air temperatures over India during hot weather (April–June) season. *Natural Hazards*, *114*(2), pp.1815-1827.

Rohini, P., Rajeevan, M., Rao, S.A. and Pillai, P.A., 2022 b. Assessment of hot weather seasonal temperatures over India using Monsoon Mission Coupled Forecasting System hindcasts. Int.J. Climatology, https://doi.org/10.1002/joc.7866

Rohini, P. and Rajeevan, M., 2023. An analysis of prediction skill of heat waves over India using TIGGE ensemble forecasts. *Earth and Space Science*, *10*(3), p.e2020EA001545.

Rothfusz, LP., 1990. The heat index equation. Technical attachment. Scientific Services Division NWS Southern Region Headquarters, Fort Worth, TX, SR 90-23.

Roxy, M., Rikita, K., Terray, P., Masson, S., 2014. The curious case of Indian Ocean warming. J Clim, 27: 8501–8508. doi: 10.1175/JCLI-D-14-00471.1.

Roxy, M.K., Ritika, K., Terray, P., Murtugudde, R., Ashok, K., Goswami, B., 2015. Drying of Indian subcontinent by rapid Indian Ocean warming and a weakening land-sea thermal gradient. Nature Communications, 6: 7423.

Russo, S., Dosio, A., Graversen, R.G., Sillmann, J., Carrao, H., Dunbar, M.B., Singleton, A., Montagna, P., Barbola, P. and Vogt, J.V., 2014. Magnitude of extreme heat waves in present climate and their projection in a warming world. *Journal of Geophysical Research: Atmospheres*, *119*(22), pp.12-500

Sandeep, A. and Prasad, V.S., 2018. Intra-annual variability of heat wave episodes over the east coast of India. *International Journal of Climatology*, *38*, pp e617-e628.

Sanderson, M.G., Economou, T., Salmon, K.H., Jones, S.E., 2017. Historical trends and variability in heat waves in the United Kingdom. Atmosphere 8(10): 191.

Satyanarayana, G.C. and Rao, D.B., 2020. Phenology of heat waves over India. *Atmospheric research*, *245*, p.105078.

Schlenker, W., Roberts, M. J., 2009. Nonlinear temperature effects indicate severe damages to U.S. crop yields under climate change. Proceedings of the National Academy of Sciences, 106: 15594–15598.

Seneviratne, S.I., Corti, T., Davin, E.L., Hirschi, M., Jaeger, E.B., Lehner, I., Orlowsky, B., Teuling, A.J., 2010. Investigating soil moisture-climate interactions in a changing climate: a review. Earth Sci Rev, 99: 125–161.

Seneviratne, S.I., Donat, M.G., Mueller, B., Alexander, L.V., 2014. No pause in the increase of hot temperature extremes. Nat Clim Change, 4 (3): 161-163.

Seneviratne, S.I., Lüthi, D., Litschi, M., Schär, C., 2006. Land–atmosphere coupling and climatechange in Europe. Nature, 443 (7108): 205–209.

Siebert, S., Ewert, F., Rezaei, E.E., Kage, H., Graß, R., 2014. Impact of heat stress on crop yield - on the importance of considering canopy temperature. Env. Res. Lett, 9: 061002.

Sharma, S. and Mujumdar, P., 2017. Increasing frequency and spatial extent of concurrent meteorological droughts and heatwaves in India. *Scientific reports*, *7*(1), pp.1-9

Sidhu, B.S., 2002. Likely impacts of the 2022 heatwave on India's wheat production, https://www.researchgate.net/ profile /Balsher-Singh-Sidhu/ publication /361376493_2022_heatwave_caused_widespread_wheat_production_losses_across_India/ links/637045792f4bca7fd056fc09/2022-heatwave-caused-widespread-wheat-production-losses-across-India.pdf

Singh, H., Arora, K., Ashrit, R. and Rajagopal, E.N., 2017. Verification of pre-monsoon temperature forecasts over India during 2016 with a focus on heatwave prediction. *Natural Hazards and Earth System Sciences*, *17*(9), pp.1469-1485.

Singh, S., Mall, R.K. and Singh, N., 2021. Changing spatio-temporal trends of heat wave and severe heat wave events over India: An emerging health hazard. *International Journal of Climatology*, *41*, pp.E1831-E1845.

Sharma, S. and Mujumdar, P., 2017. Increasing frequency and spatial extent of concurrent meteorological droughts and heatwaves in India. *Scientific reports*, *7*(1), pp.1-9.

Smitha Anil Nair, Pai, D.S. and Rajeevan, M., 2016, Climatology and trend of cold waves over India during 1971-2010, Mausam, 67, 651-658.

Srivastava, A., Mohapatra, M. and Kumar, N., 2022. Hot weather hazard analysis over India. *Scientific reports*, *12*(1), p.19768.

Srivastava, A.K., Rajeevan, M. and Kshirsagar, S.R., 2009. Development of a high resolution daily gridded temperature data set (1969–2005) for the Indian region. *Atmospheric Science Letters*, *10*(4), pp.249-254.

Steadman, R.G., 1979. The assessment of sultriness. Part I: A temperature humidity index based on human physiology and clothing science. Journal Applied Meteorology, 18:861-873.

Steadman, R.G., 1984. A universal scale of apparent temperature. *Journal of Climate and Applied Meteorology,* **23:** 1674-1687.

Steffen, W., Hughes, L., Perkins, S., 2014. Heatwaves: Hotter, Longer, More Often. Special Report by the Climate Council of Australia, Sydney, Australia.62 pp. [Available online at http://www.climatecouncil.org.au/heatwaves-report].

Subbaramayya, I. and Rao, D.S., 1976. Heat wave and cold wave days in different states of India. MAUSAM, 27(4), pp.436-440.

Sun, C., Li, J., Ding, R., et al, 2016. Strengthening relationship between ENSO and western Russian summer surface temperature. Geophys Res Lett 43: 843–851.

Trenberth, K., Fasullo, J., 2012. Climate extremes and climate change: The Russian heat wave and other climate extremes of 2010. J. Geophys. Res. 117: D17103. doi:10.1029/2012JD018020.

Ullah, I., Saleem, F., Iyakaremye, V., Yin, J., Ma, X., Syed, S., Hina, S., Asfaw, T.G. and Omer, A., 2022. Projected changes in socioeconomic exposure to heatwaves in South Asia under changing climate. *Earth's Future*, *10*(2), p.e2021EF002240

Vautard, C., Gobiet, A., Jacob, D., Belda, M., et al., 2013. The simulation of European heat waves from an ensemble of regional climate models within the EURO-CORDEX project. Clim. Dyn, 41: 2555–2575. http:// dx.doi.org/10.1007/s00382-013-1714-z.

Vautard, R, Yiou P, D'Andrea F, de Noblet, et al., 2007. Summertime European heat and drought waves induced by wintertime Mediterranean rainfall deficit. Geophys. Res, Lett. 34: L07711.

Vittal, H., Villarini, G. and Zhang, W., 2020. On the role of the Atlantic ocean in exacerbating Indian heat waves. *Climate dynamics*, *54*, pp.1887-1896.

Wang, H., Schubert, S., Koster, R., Ham, Y.G., Suarez, M., 2014. On the role of SST forcing in the 2011 and 2012 extreme US heat and drought: a study in contrasts. J Hydrometeorol, 15: 1255–1273. doi:10.1175/JHM-D-13-069.1

White, C.J., Hudson, D., Alves, O., 2014. ENSO, the IOD and the intraseasonal prediction of heat extremes across Australia using POAMA- 2. ClimDyn 43: 1791–1810.

Wilker, E.H., Yeh, G., Wellenius, G.A., Davis, R.B., Phillips, R.S., Mittleman, M.A. 2012 Ambient temperature and biomarkers of heart failure: A repeated measures analysis. Environ.Health Perspect, 120: 1083–1087.

Zachariah, M. *et al*. (2022) Climate Change made devastating early heat in India and Pakistan 30 times more likely, World Weather Attribution, https://www.worldweatherattribution.org/wp-content/uploads/India_Pak-Heatwave-scientific-report.pdf

Zachariah, M., Mondal, A. and AghaKouchak, A., 2021. Probabilistic assessment of extreme heat stress on Indian wheat yields under climate change. *Geophysical Research Letters*, *48*(20), p.e2021GL094702.

Zahid, M., Rasul, G., 2009. Rise in Summer Heat Index over Pakistan. Pakistan Journal of Meteorology, 6: 85-96.

Zuo, J., Pullen, S., Palmer, J., Bennetts, H., Chileshe, N. and Ma, T., 2015. Impacts of heat waves and corresponding measures: a review. *Journal of Cleaner Production*, *92*, pp.1-12.